MODELING OF CONTROLLED-RELEASE DRUG DELIVERY FROM AUTOCATALYTICALLY DEGRADING POLYMER MICROSPHERES

BY

ASHLEE NICOLE FORD VERSYPT

DISSERTATION

Submitted in partial fulfillment of the requirements
for the degree of Doctor of Philosophy in Chemical Engineering
in the Graduate College of the
University of Illinois at Urbana-Champaign, 2012

Urbana, Illinois

Doctoral Committee:

Professor Daniel W. Pack, Chair
Professor Richard D. Braatz, Director of Research
Professor Narayana R. Aluru
Associate Professor Christopher V. Rao

Abstract

A mathematical model is developed for the simultaneous treatment of PLGA degradation and erosion and diffusive drug release with autocatalytic effects and nonconstant effective diffusivity of the drug. A mechanistic reaction-diffusion model with pore evolution coupled to hydrolysis and related to the effective diffusivity through hindered diffusion theory is proposed. Experimental background motivating the attention to the size-dependent effects of autocatalysis on drug release and a brief review of related mathematical models are presented. The model equations are derived, solved numerically with a computational code developed for this work and described in detail, and compared to the analytical solutions to the model in limiting cases. The model performance for the case of drug release from microspheres of different sizes is presented to highlight the capability of the model for predicting size-dependent, autocatalytic effects on the polymer and the release of drug.

Proverbs 3:5-6

Trust in the Lord with all your heart, and lean not on your own understanding.

In all your ways acknowledge Him, and He shall direct your paths.

Acknowledgments

I would like to thank my advisor Professor Richard Braatz, all of my current and former labmates at UIUC and MIT, particularly Michael Rasche, Dr. Masako Kishida, Mo Jiang, Xiaoxiang Zhu, and Lifang Zhou, and my collaborator Professor Daniel Pack and his former students, Dr. Kalena Stovall and Dr. Kara Smith, for all of their guidance during my graduate research and for their feedback on my project. I appreciate Professors Christopher Rao and Narayana Aluru for serving on my doctoral committee in addition to Professors Braatz and Pack. I would also like to acknowledge the undergraduate students, Derek Bradley, Hao Feng, Lisa Hasenberg, Gregory Kutyla, Bhaskar Vaidya, Min Hao Wong, and Zhilong Peter Zhu, who worked with me in developing the Nanoscale Drug Delivery Module: Teacher's Edition [1] and Student's Edition [2]—drug delivery activities and background materials targeted for high school students and teachers. I enjoyed working with and mentoring the students, contributing to the educational outreach project, and gaining experience in managing a research team.

I have been continually motivated by my sweet husband, Joel Versypt. I am so thankful for his encouraging me to "just keep swimming" and for all the countless ways he has contributed to my emotional and physical well-being during this process. Completion of my Ph.D. and my marriage to Joel are two of the most significant achievements of my life! I am very thankful that my graduate school experience has been enriched by my relationship with Joel.

I am extremely grateful for the loving support of my dear friends and family

who have encouraged me throughout the research and dissertation writing process and throughout my entire academic career. My friends have helped to fill my life full of adventures and laughter. I am especially appreciative for my classmates for their friendships and for the countless hours spent doing homework, sharing meals, and discussing research and graduate school concerns. My wonderful teachers and professors at Snyder Public Schools, the University of Oklahoma, and the University of Illinois at Urbana-Champaign, particularly my mentors Mrs. Dianne Atchley, Professor Dimitrios Papavassiliou, and Professor Richard Braatz, have inspired my love for learning. My church families in Snyder and Champaign have supported me consistently through their friendships and prayers. My family members have always believed in me and have encouraged me to reach for the stars. I am so thankful for my entire extended family, especially my parents Pam and Allen Ford, my mother-in-law Jan Versypt, my grandparents Bill and Edith Ford and Ken and Shirley Holder, my sisters Haley Ford, Kelsey Ford, and Jen Wakefield, and their significant others Reggie Copeland and Ben Wakefield. I am truly blessed to have such a strong network of support!

This work was made possible through the support of the National Institutes of Health (NIBIB 5RO1EB005181) and the National Science Foundation (Grant #0426328). This work used the Extreme Science and Engineering Discovery Environment (XSEDE), which is supported by the National Science Foundation (Grant #OCI-1053575). This work was supported by the Department of Energy Computational Science Graduate Fellowship Program of the Office of Science and National Nuclear Security Administration in the Department of Energy under contract DE-FG02-97ER25308.

Table of Contents

Chapter 1

Introduction

1.1 Motivation

Controlled-release drug delivery systems are being developed as alternatives to conventional medical drug therapy regimens for pharmaceuticals that require frequent administrations. The types of drugs of particular interest are deactivated quickly due to short *in vivo* half-life or eliminated from the body before the active agent can be completely utilized. Traditional drug regimens include oral, inhalation, topical, and injection dosage forms. Figure 1.1 illustrates the differences between concentration profiles for controlled-release and traditional drug delivery systems. For traditional drug delivery, the concentration increases, peaks, and decays for some period of time after the dose is administered. To prevent peaks of high toxic concentration, traditional therapies must use sufficiently small dosages. The concentration diminishes over time as the drug is used by or expelled from the body. The drug must be re-administered to maintain the concentration in the therapeutic region and to minimize the time elapsed at low, ineffective concentrations while the therapy is needed. Controlled-release drug delivery enables drug concentrations to be sustained at desired levels within the therapeutic regime for extended periods of time.

By releasing drug molecules in a controlled manner over time from a single administration, controlled-release systems have the potential to provide better management of drug concentrations, reduce side effects caused by concentration extremes and repeated administrations, and improve patient compliance as

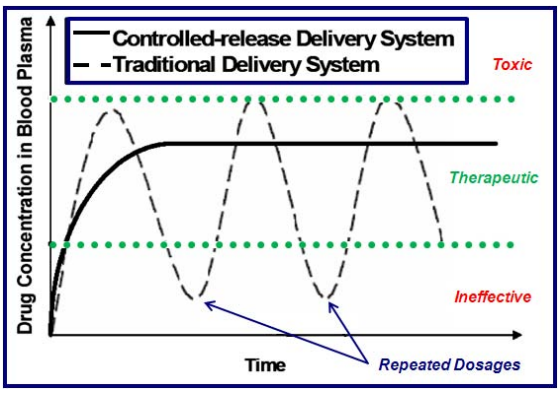

Figure 1.1: Typical release profiles for controlled-release and traditional drug delivery systems.

compared to conventional regimens [3–6]. Despite these advantages, the implementation of controlled-release drug delivery devices for human patients has been gradual as the design of controlled-release devices depends heavily on trial-and-error experiments.

Models are commonly used for understanding, prediction, and design [7]. This dissertation is primarily focused on utilizing models for understanding with attention to their predictive capability for further design work. First-principles modeling is used to develop a deeper understanding of the underlying mechanisms of controlled-release drug delivery, which is needed for the prediction of drug release profiles over a wide range of conditions to be used in the model-based design of microparticles to produce a desired release profile. Empirical and semi-empirical models as commonly applied in the drug delivery field have very limited predictive ability outside of the specific experiments used to fit parameters in the models. First-principles models have the potential for prediction for large changes in the microparticle design, such as designing microparticles with multiple polymer phases, which can be useful for achieving long-term constant dosage rates or pulsatile vaccine administrations.

Bulk-eroding, aliphatic polyesters such as poly(D,L-lactic-co-glycolic acid) (PLGA) formulated as microparticles have been extensively studied for

controlled-release drug delivery mainly because of the biodegradable and bioabsorbable qualities that allow for the passive degradation of the polymer in aqueous environments such as living tissues and for the harmless incorporation of degradation products into the surrounding media [8–10]. Many experimental studies have been conducted to characterize the polymer microparticle degradation and erosion processes and the release of drug molecules from the microparticles [11–27].

1.2 Scope of Research

1.2.1 Research Objectives

The research objectives for this dissertation concern the modeling of drug release from PLGA microspheres.

1. Develop a mechanistic model for reaction and diffusion in PLGA microspheres.
   (a) Consider alternative kinetic models for autocatalytic polymer hydrolysis.
   (b) Couple pore growth to hydrolysis reaction kinetics.
   (c) Treat effective diffusivity as a variable in space and time dependent on pore growth using hindered diffusion.
2. Verify model performance for limiting cases with analytical solutions.
3. Explore effects of physically relevant parameters on the model.

1.2.2 Unique Aspects

The dissertation is focused on the development and use of a mechanistic model for polymer degradation and diffusive drug release from PLGA microspheres that treats the autocatalytic hydrolysis reaction, diffusive transport with a variable effective drug diffusivity, and mass erosion through the developing pore network. The components of the model are coupled, are functions of radial position and time, and are considered simultaneously.

Four different elementary kinetic rate laws for hydrolysis of PLGA by uncatalyzed and catalyzed mechanisms are given as options in the model to account for different possible chemical reactions in the system. The carboxylic acid end groups, the ester bonds, the soluble small polymer oligomers, and the insoluble large polymer oligomers are considered as reactive species in the system. The net rates of generation of each of the reactive species for the four kinetic rate laws are derived. The use of multiple rate laws in the model allows for improving the understanding of the kinetic behavior in the microsphere system with simultaneous reaction and diffusion. The limits of the assumptions of each rate law can be assessed when the model is implemented. The rate laws used here are the first-order rate law for uncatalyzed hydrolysis and the pseudo-first-order rate law, the quadratic-order rate law, and the 1.5th-order rate law for autocatalytic hydrolysis.

Transport effects through porous networks and through the polymer bulk are taken into account by the model. Both hydrolytic degradation and diffusive erosion of the polymer are used to determine the effective diffusivity of the drug for diffusion through the pores in the polymer. The effective diffusivities of the water-soluble polymer oligomers and monomers and the drug species increase as the hydrolytic degradation proceeds due to enhanced porous diffusion pathways through the evolving pore network. In order to account for this effect in the model, the effective diffusivities of the drug and soluble oligomers can be varied using hindered diffusion through the aqueous pores that grow with the progression of the polymer degradation reaction and subsequent dissolution of soluble oligomers. The model has options to consider constant effective diffusivities, a combination of constant and variable effective diffusivities for different species, or variable effective diffusivities for all diffusing species. The hindered diffusion theory is applied to the dynamic systems with growing distributions of pores rather than the traditional static, uniform pore size.

The numerical methods to solve the partial differential equations (PDEs) of

the model include the finite difference discretization scheme for the spatial derivatives of the diffusion term with effective diffusivity as a function of the radius and time. Effective diffusivity is almost always treated as a constant or a function of the concentration or the time. The discretization scheme for the general case of effective diffusivity as a function of position and time is presented.

This dissertation work features a well-commented computational code (available in Appendix B) that can be used to consider the model components independently or in a coupled fashion and to switch between different kinetic rate laws and different definitions of the effective diffusivity for the diffusing species. Overviews of the subroutines of the code and diagrams of the interactions between the subroutines are provided. A sample batch file for running the code and defining the input parameters and options at run time for each simulation with a common executable is also included.

The computational code is thoroughly verified to assess the numerical model performance compared to analytical solutions for limiting cases. The first limiting case, the reaction-dominant limit where no diffusion is observed, is used for verification of the reaction components of the model for the four hydrolysis reaction rate laws. The analytical solutions for the carboxylic acid end group and ester bond concentrations are derived for each of the rate laws. The analysis draws on several references but is more thoroughly presented than in the previously published works. The second limiting case, the diffusion-dominant limit where no reaction is observed, is used for verification of the diffusion component of the model with constant effective diffusivity. The third limiting case, the single-component limit for the reaction-diffusion of COOH independent of other species, is used with the pseudo-first-order rate law for the autocatalytic hydrolysis reaction with constant diffusivity for verification of the reaction and diffusion components acting simultaneously. The derivation of the analytical expression for the concentration profile differs from the traditional treatment of reaction and diffusion within porous

catalysts in that the hydrolysis reaction results in net generation rather than net consumption as in the catalysis literature. This leads to a different eigenfunction based on the sign of the eigenvalues due to the reaction rate. Also, the dynamic concentration profile is derived using the method of eigenfunction expansions rather than simply determining the steady-state concentration profile.

Towards the aim of investigating the size-dependent autocatalytic effects on diffusive drug release, the model predictions are highlighted for the case of varying microsphere sizes with variable effective diffusivity coupled to the hydrolysis of the eroding polymer. The most significant finding is that the model can predict size-dependent drug release that is consistent with expectations from autocatalytic considerations—larger microspheres release drugs faster than smaller microspheres—rather than the size-dependent behavior for diffusion-controlled systems (the model is capable of capturing this behavior as well).

1.2.3 Potential Impact of Study

Polymer microparticles have been fabricated with a variety of configurations including solid microspheres composed of a single type of polymer, thin-shelled microcapsules with aqueous interiors, and core-shell microspheres with solid cores of one polymer surrounded by outer shells of another polymer [27–31]. The model developed in this dissertation could be used in the design of distributions of polymer microparticles of different configurations composed of bulk-eroding, aliphatic polyesters.

Mixing uniform distributions of microspheres of different sizes yields release profiles that are mass-weighted averages of the release profiles for the individual sizes [32]. Lee et al. [33] applied a linear summation of individually measured release profiles to tune release profiles for arrays of PLGA microspheres. The release profiles for a variety of types of microspheres were known experimentally. A matrix was used to predict the relative amounts of each known sample to produce the best

fit for the targeted profile. Then a mixture of the samples was studied experimentally to validate the predictions. Lee et al. [33] were able to produce constant and pulsatile release rates from this procedure. To improve upon this technique, the model developed in the present work could be used to computationally explore a larger span of basis sample sets to allow for finer tuning of microsphere mixtures to attain desired release profiles with greater accuracy. The potential impact of this is a reduction in the number of experiments needed to optimize the controlled release microparticles. Berchane, Jebrail, and Andrews [34] also optimized populations of microspheres to achieve desired drug release profiles. They utilized microsphere samples that differed in size, polydispersity, and polymer molecular weight. They used a model to predict the release profiles from optimized linear combinations of samples, and the results were validated using *in vitro* release experiments. Berchane et al. [34] presented a good strategy for using simulations to optimize drug release profiles from PLGA microspheres, but the model implemented was semi-empirical and did not account for autocatalysis. The model developed in this dissertation could be incorporated in a similar optimization strategy for tailoring drug release profiles for specific drug delivery applications.

1.3 Organization

This dissertation is organized as follows. In Chapter 2 the background concepts of the polymer autocatalytic degradation mechanism, polymer microsphere erosion, and drug release are described. A brief review of published models is presented in Chapter 3. The model framework is introduced in Chapter 4. The components of the model for fulfilling Objective 1 are derived in the next two chapters: the reaction component of the model is detailed in Chapter 5 for Objective 1.a and the pore growth and diffusion components of the model are detailed in Chapter 6 for Objective 1.b and Objective 1.c. The full set of model equations are summarized in

Chapter 7. In Chapter 8 the numerical methods used to solve the model equations numerically are highlighted. The Fortran implementation of the model equations is described in Chapter 9. The verification of the model satisfying Objective 2 is presented in Chapter 10. The model predictions to satisfy Objective 3 are discussed in Chapter 11. Conclusions are presented in Chapter 12. The peer-reviewed conference proceedings paper [35] associated with this dissertation work is reproduced in Appendix A. The Fortran code used for solving the model equations numerically is included as Appendix B.

Chapter 2

Background Concepts

This chapter provides an overview of the phenomena related to the controlled-release drug delivery from bulk-eroding, aliphatic polyesters. Acid-catalyzed polyester hydrolysis is described in Section 2.1. Polymer erosion is detailed in Section 2.2. The coupling between degradation and erosion is explained in Section 2.3, and the overall drug release process is outlined in Section 2.4.

Several synthetic, biodegradable polyesters have been extensively studied for drug delivery applications. These include polymers and copolymers derived from lactic acid and glycolic acid (structure shown in Figure 2.1): poly(D,L-lactic acid) (PLA), poly(glycolic acid) (PGA), poly(D,L-lactic-co-glycolic acid) (PLGA) [3, 36]. Other aliphatic polyesters such as poly(hydroxy butyrate) (PHB) and poly(ϵ-caprolactone) (PCL) have more limited applicability for drug delivery as these polymers have high hydrophobicity [37] and do not readily degrade in aqueous media.

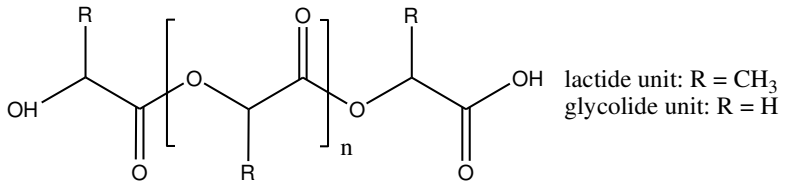

Figure 2.1: Structure of PLA (all R's replaced by methyl groups), PGA (all R's replaced by hydrogen atoms), or PLGA (some fraction of R's replaced by methyl groups and the remaining fraction replaced by hydrogen atoms). n is the number of interior glycolide and/or lactide monomeric units.

Several processes contribute to the overall rate of drug release from polyester microparticles including chemical degradation of the polymer by the autocatalytic

ester hydrolysis reaction, polymer erosion, pore structure evolution as a result of mass erosion, and drug release by diffusion through the polymer matrix and the aqueous pore structure. In the present work, the term *degradation* refers to the process through which the polymer chain bonds are hydrolyzed to form oligomers and monomers. The term *erosion* refers to the loss of mass due to diffusion of water-soluble, small oligomers and monomers, along with the drug compound, out of the polymer matrix. These definitions are the same as those given by Gopferich [8] and have been widely adopted in the literature.

2.1 Acid-Catalyzed, Hydrolytic Degradation

Polyesters are depolymerized in the presence of water. The hydrolysis reaction cleaves the ester bonds of polymer chains. The reaction can be catalyzed by acids or bases, but experimental data on the acidic local pH within PLGA particles [18, 38–41] suggest that only the acid-catalyzed reaction mechanism is relevant for polyester microparticles. The acid-catalyzed mechanism is the bimolecular, acyl-oxygen cleavage $A_{AC}2$ mechanism for ester hydrolysis [42, 43]. The acid catalyst source can be external from strong acid in the medium (non-autocatalytic reaction) or internal from the carboxylic acid end groups of the polymer chains (autocatalytic reaction).

The $A_{AC}2$ mechanism for polyester hydrolysis consists of the following reactions (see Figure 2.2) [42]:

- the carbonyl oxygen is protonated and forms a resonance structure,
- water adds to the electrophilic carbonyl carbon,
- a proton on the OH_2^+ group is transferred to the R′O group,
- the bond between carbon and the R′OH group is cleaved, and
- the carboxyl product is deprotonated.

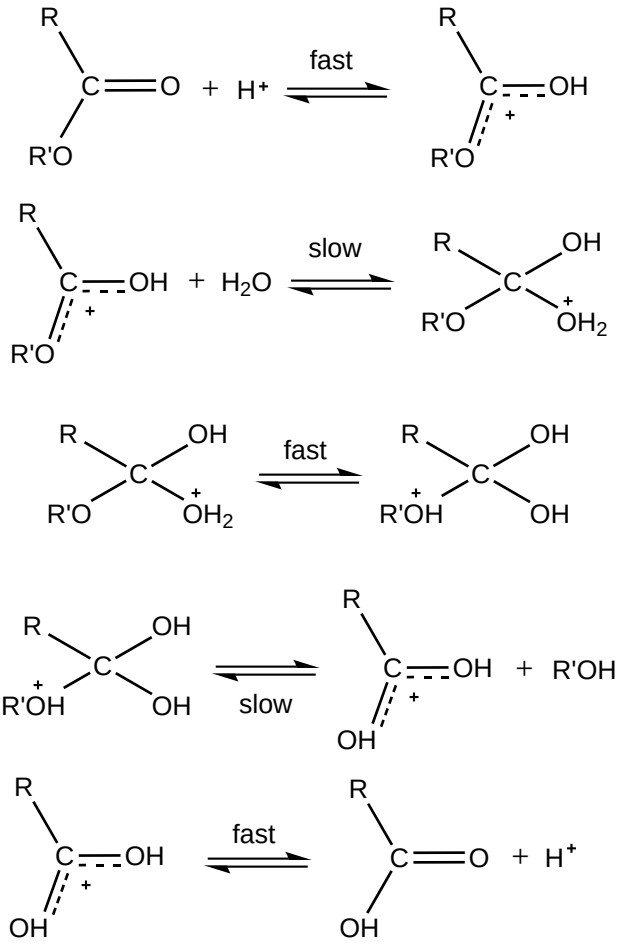

Figure 2.2: $A_{AC}2$ mechanism for acid-catalyzed ester hydrolysis.

The addition of water to the protonated ester is the rate-determining step. While the concentration of acidic carboxyl end groups is low and the total number of ester linkages is high, all ester bonds have equal probability of cleavage with random chain scission as the dominant mode for depolymerization. As the concentration of end groups increases, the autocatalytic effect becomes more pronounced, and cleavage by chain-end scission where ester bonds near the ends of polymer chains are preferentially hydrolyzed can become significant [44, 45]. The chain scission is specific to glycolic linkages as the more hydrophilic glycolic units are hydrolyzed faster than lactic units [11]. The glycolic and lactic monomer units are randomly dispersed throughout the polymer chains, so there is an average chain cleavage probability for any given copolymer ratio. In the present work, PLGA composed of a 50:50 ratio of lactic acid to glycolic acid is the primary focus. This work can be extended to other copolymer ratios by considering the appropriate rate constants for the hydrolytic cleavage of those polymers along with the appropriate materials properties for the polymers. The carboxylic acid end group for a specific reacting polymer chain may be protonated or deprotonated; the local acid concentrations from all sources including other polymer chains and the medium can catalyze the reaction. The reaction is autocatalytic if the dominant acid catalyst source is the dissociated proton from the carboxyl end groups of the PLGA polymer chains in the vicinity of the reacting polymer rather than from an external source [46].

The acid-catalyzed, ester hydrolysis mechanism is summarized by

$$\mathrm{P}_n + \mathrm{H_2O} + \mathrm{H}^+ \rightleftharpoons \mathrm{P}_m + \mathrm{P}_{n-m} + \mathrm{H}^+, \quad n = 2,\, 3,\, \ldots \text{ and } m = 1,\, 2,\, \ldots,\, n-1, \tag{2.1}$$

where P_n denotes polymer chains with degree of polymerization n and H^+ is the acid catalyst. The reaction has the rate constants k_{fwd} and k_{rev} for the forward and reverse reactions, respectively. The hydration is a relatively fast process compared with the timescales for polymer degradation and erosion—on the order of a few

minutes compared to weeks or months—so PLGA, PLA, and PGA are classified as bulk-eroding polymers [47–49]. Since the hydration of the matrix is much faster than the rate of hydrolysis, it is assumed that there is an excess of water in the polymer matrix. The forward hydrolysis reaction in aqueous solutions is kinetically favored to go to completion [50], thus the reverse reaction can be considered to be negligible. The reverse esterification reaction is favored in alcoholic solutions [50], which are not considered in the present work. In subsequent consideration of the mechanism, the reverse reaction is assumed to be negligible.

2.2 Erosion

Biodegradable polymers erode as a result of the hydrolysis reaction; the polymers lose mass due to transport of soluble degradation products and the drug compound out of the microparticles. Polymer erosion is classified as surface-eroding or bulk-eroding [4, 8, 11, 36]. With surface-eroding polymers like polyanhydrides, the rate of penetration of water from bodily fluids *in vivo* or from the buffer medium *in vitro* into the polymer bulk is slower than the rate of polymer degradation at the surface. Surface-eroding polymers react from the surface inward. Bulk-eroding polymers are polymers in which the rate of water penetration is faster than the polymer degradation rate. Generally, the reaction in bulk-eroding polymers is homogenous throughout the polymer bulk. PLGA is a bulk-eroding polymer [47–49].

The erosion depends on the degradation, dissolution, and diffusion processes [51]. The degradation process is treated by the hydrolysis reaction. In the present work, the dissolution of water-soluble oligomers and drug molecules are assumed to occur on faster time scales than diffusion and degradation. This is a suitable assumption for drug compounds that are water-soluble. For drug compounds with low water solubility, the drug dissolution rate could be included in the model as in [52]. Drugs with different chemical properties—solubility, molecular

weight, and OH group density—have been shown to have different release behavior from PLGA pellets; however, the absence of strong correlations between the properties and the release behavior indicate that release behavior is not easily mapped to drug type [53]. In the present work, the drug compounds are assumed to be water-soluble.

According to Kulkarni et al. [54] and van Nostrum et al. [44], poly(D,L-lactic acid) oligomers with degrees of polymerization less than 10 are water soluble. Batycky et al. [45] report that PLGA oligomers of the same range of degrees of polymerization as PLA water-soluble oligomers, up to and including nonamers, are water soluble. Zhao, Hunter, and Rodgers [55] also use nonamers as the largest soluble oligomers in their modeling work. In the present work, the oligomers from monomers to nonamers are considered as completely soluble and are referred to as *small* oligomers for PLGA. Larger oligomers are assumed to be insoluble. Only water-soluble oligomers and monomers, their attached COOH end groups and interior ester bonds, and drugs are transported by diffusion.

PLA, PGA, and PLGA can sometimes exhibit heterogeneous erosion behavior where the interior degrades faster than the polymer surface. This phenomenon is size-dependent; larger microspheres have been observed to experience faster erosion in their centers than smaller microspheres [22–25, 41, 56]. The effective diffusivity has been observed to increase with increasing microsphere diameter [25]. The cause of the heterogeneous mass loss in bulk-eroding polymers is generally attributed to the autocatalytic hydrolysis reaction by which the polymer chemically degrades [25, 26, 41, 57].

The drug compound in a drug delivery polymer particles may be released by diffusion through the polymer matrix, diffusion through aqueous pores, dissolution coincident with polymer dissolution, or osmotic pumping [58]. Diffusion through the dense polymer matrix is possible [59] but is limited to small, hydrophobic molecules [58]. Macromolecular drugs are the most common type of encapsulated

drugs, so diffusion through the aqueous pores is an important mode of transport [60]. Dissolution of the polymer matrix to release the drug without mass transport is typical of surface-eroding polymers rather than bulk-eroding polymers so is not considered here. Osmotic pumping is also not commonly used for PLGA [58]. Thus, in this dissertation, drug diffusion through the polymer matrix and through the aqueous pores are considered as the parallel modes of release from the polymer particle to treat small and large drug molecules and to account for transport prior to significant development of the pore network. The dynamics of pore growth due to hydrolytic degradation and the dependence of effective diffusivity on the average pore size in hindered diffusion are discussed in detail in Chapter 6.

The drug may be loaded in the polymer in a number of ways. A reservoir system refers to a bolus of drug surrounded by a release rate controlling membrane, and monolithic systems are those with drug dispersed continuously throughout a release rate controlling material [61]. Here only monolithic systems are considered with drug loading below the drug solubility limit such that the drug is dissolved in the polymer matrix.

2.3 Coupling Between Autocatalytic Degradation and Erosion

Figure 2.3 illustrates the size-dependent effects of autocatalysis. At the onset of degradation, all particle sizes hydrolyze polyesters at similar rates while generating acidic byproducts. Hydrolysis eventually leads to erosion when sufficiently small water-soluble oligomer fragments from degraded polyesters are transported away from the reaction site. If the diffusion process controlled the drug release without influence by polymer degradation, larger microparticle sizes would be expected to have smaller relative release rates than smaller particles as the diffusion pathways

would be longer and the concentration gradients would be smaller. Contrary to this intuitive diffusion-controlled behavior, polymer degradation does influence the drug release rates for different sized particles.

In domains close to the external surfaces of microparticles (such as those indicated with arrows in Figure 2.3, the diffusion lengths are sufficiently small for the acidic oligomer hydrolysis byproducts to diffuse out of the particles; in smaller microparticles, the entire volume can have short diffusion lengths. Acidic polymer fragments that remain in the microparticles have hindered mobility in regions farther from the external surfaces where transport is limited by greater diffusion lengths. This leads to an accumulation of acidic degradation byproducts in the interior of larger microparticles, which results in a decrease in the microenvironment pH. The acidic end groups further catalyze the hydrolysis reaction leading to accelerated degradation particularly in the interior of large microparticles due to the limited acid transport out of the center. Over time, the autocatalytic effect becomes more pronounced, and microspheres can form heterogeneous, hollow interiors [26]. Small microspheres without long diffusion lengths are less susceptible to acidic buildup and heterogeneous degradation. Experimentalists have reported evidence of local pH drop due to the accumulation of the acidic byproducts of the polymer hydrolysis and have detected degradation rates that increase with polymer particle size as a result of autocatalysis [12, 17–20, 25–27, 38, 41, 62–64]. This provides very strong evidence that the drug release profile is a consequence of the coupling between the autocatalytic reactions and diffusion of acidic reaction products out of the microparticle [12].

2.4 Overall Drug Release Process

Figure 2.4 shows a schematic for the steps related to the morphology and transport in the overall drug release process from microspheres made of bulk-eroding polymers

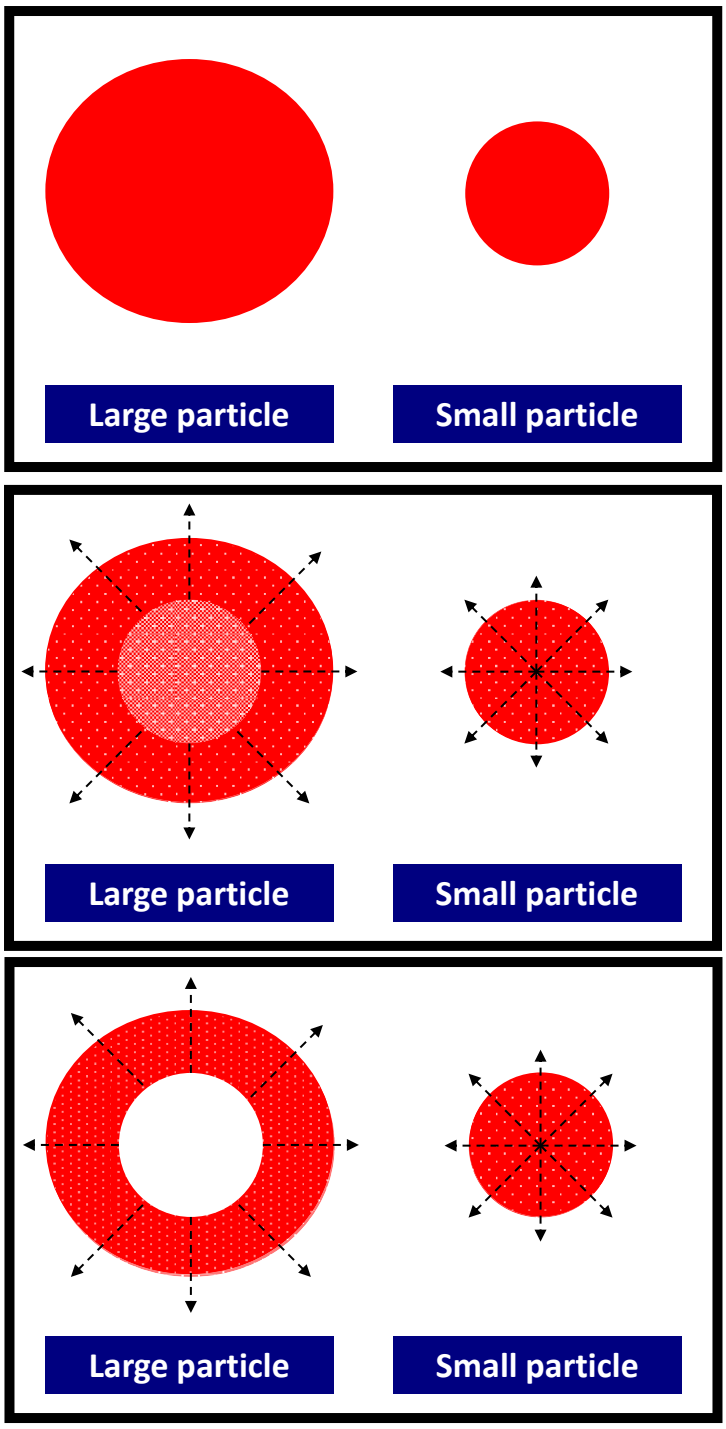

Figure 2.3: Size-dependent autocatalysis in PLGA Microspheres. Lighter colors indicate more accelerated autocatalysis. Arrows indicate regions were diffusion lengths are not prohibitive for reaction products to diffuse out of the microsphere before leading to enhanced autocatalysis. Time progresses from the top panel to the bottom panel with autocatalysis becoming more significant in the interior of the large particle.

such as PLGA. Figure 2.5 shows the phases of drug release process with respect to the relative time scales. The overall drug release process has been described in the literature [36, 58, 65]. The drug molecules are initially distributed throughout the polymer matrix in a manner dependent on the microparticle fabrication technique. Before the drug release is initiated, water from bodily fluids *in vivo* or from the buffer medium *in vitro* must hydrate the polymer matrix of the microspheres. The hydration is a relatively fast process compared to the timescales for polymer degradation and erosion. The water in the polymer matrix can hydrolyze the polymer chains to break them into smaller fragments. Small oligomers are capable of diffusing out of the bulk leaving void volumes in the polymer due to the oligomer mass loss. The void volumes can be connected as pores. The drug is transported through the polymer matrix and through pores due to a concentration gradient. The drug diffuses more readily in aqueous pores than in the polymer matrix, so the effective drug diffusivity increases as the pore network develops due to the hydrolysis of the polymer. Significant mass loss of the polymer occurs as oligomers are solubilized into the pores and the medium, and the pores grow larger than the size of the drug and oligomer molecules. Figure 2.4 illustrates how the polymer degrades hydrolytically, the pore network develops, and the drug is transported out of the microsphere—all of these processes occur in concert for the duration of the drug release process.

An initial burst effect can occur where a significant percentage of the drug is released during the early stage of the release process. This effect has been reported for some formulations of PLGA microspheres; this initial burst can be diminished or eliminated by adjusting the fabrication technique [27, 66]. In the present work, any initial burst is assumed to occur on a time scale much faster than that of drug release by diffusion through the polymer matrix or aqueous pores. The model uses the drug distribution after burst as the initial condition. If experimental evidence for burst is available, the cumulative release profile for the drug can be adjusted to

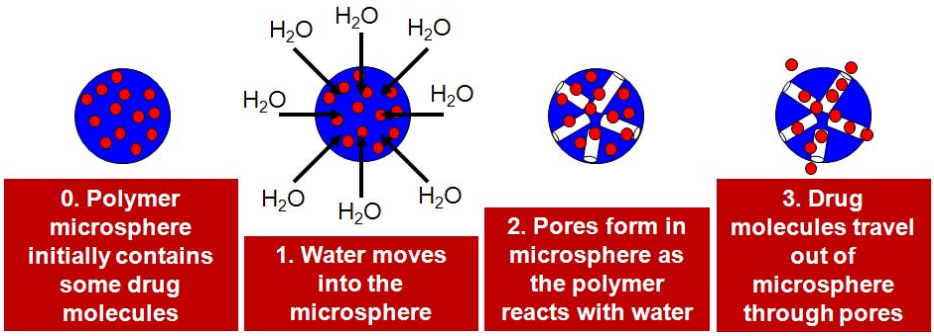

Figure 2.4: Morphology and transport stages of the drug release process for bulk-eroding biodegradable polymer microspheres.

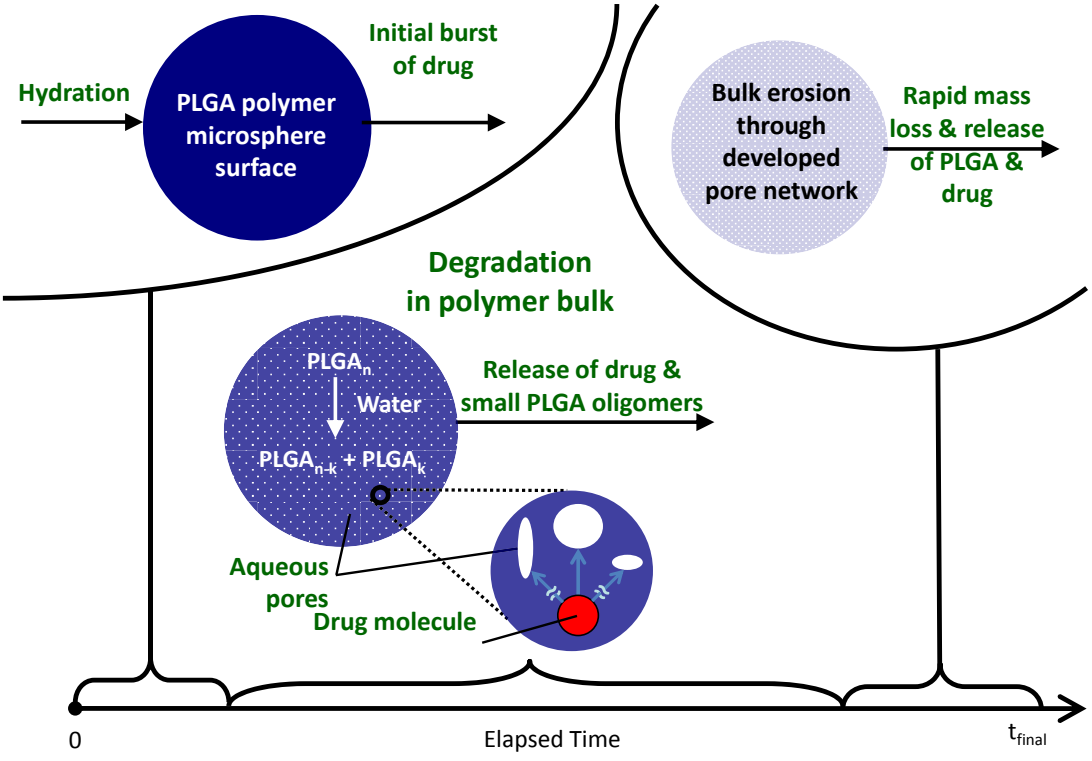

Figure 2.5: Relative time scales for the drug release process for PLGA microspheres.

include the amount of drug released through the initial burst.

The degradation of the polymer bulk constitutes a dominant fraction of the overall time for the drug release process. After the pore network is sufficiently developed, the drug transport increases rapidly and bulk mass loss occurs relatively quickly.

Chapter 3

Literature Review of Modeling Efforts

Over the past few decades, many mathematical models have been developed for polymeric drug delivery devices and comprehensive reviews of the modeling efforts have been published [36, 67, 68]. These models can be distributed among three categories based on the mechanisms of drug release [67]: diffusion-controlled systems (diffusion from non-degrading polymers), swelling-controlled systems (enhanced diffusion from polymers that swell in aqueous media), and erosion-controlled systems (release as a result of degradation and erosion of polymers). For biodegradable polyesters such as PLGA, PLA, and PGA, the drug release occurs through a combination of polymer degradation and erosion, which is classified as being erosion-controlled. Only models developed for erosion-controlled systems are discussed here as they are the most relevant for the bulk-eroding polymers of interest. The focus of this brief review is on how models treat the chemical degradation of the polymer and the diffusion of the drug and reaction products. Some components of previously published models are utilized in subsequent chapters on the components of the proposed model; these aspects are highlighted in the reviews of the literature models.

3.1 Empirical vs. Mechanistic Models for Erosion-Controlled Systems

Both empirical and mechanistic models have been developed for drug release from erosion-controlled systems. A semi-empirical model for drug release from bioerodible

polymer microspheres and disks has been proposed that uses an approximate solution to the Fickian diffusion equation for time-dependent, exponentially-growing diffusivity and a correlation for the matrix erosion process [69]. The autocatalytic effects in [69] were considered by allowing the diffusivity to increase exponentially with time, and several sets of experimental data were fit to the model. A common approach is to use an exponentially decreasing molecular weight or increasing diffusivity based on an empirical fit to data in coordination with an analytical solution to a special case of the Fickian diffusion equation [59, 70, 71]. Empirical or correlative models generally only apply to a specific set of experimental conditions and are not useful for predicting drug release behavior outside of the conditions of the experiments used to construct the models [68]. In contrast, mechanistic models have the capability to apply generally to multiple data sets and can be used to simulate behavior for varied physical conditions. Mechanistic models for erosion-controlled polymer microspheres aim to account for the mass transport and chemical reactions that contribute to the overall drug release process [67].

3.2 Reaction-Diffusion Models and Cellular Automata Models

Mechanistic erosion-controlled models have been characterized as being in one of two categories [67]: reaction-diffusion models and cellular automata models. The first category considers the overall polymer erosion process as a combination of transport and chemical reactions through use of deterministic equations, while the second category treats erosion as a random process using Monte Carlo simulations. The cellular automata models have been applied to surface-eroding and to bulk-eroding systems [72–76]. Cellular automata models can represent the evolution of pores but have the drawback of not being able to explicitly account for autocatalysis in a mechanistic manner. As autocatalysis is important for the

size-dependent degradation heterogeneities for bulk-eroding polyesters, cellular automata models are not considered as candidate models in the present work.

3.3 Coupling Between Reaction and Diffusion

Many mathematical models have been developed to predict degradation, erosion, and drug release from erosion-controlled polymer microparticles [45, 49, 67, 69, 72, 77–82]. Researchers have proposed drug diffusion and dissolution models based on Fickian diffusion and solubility effects [25, 83–87], microstructural models involving degradation leading to erosion in pore networks [45, 55, 88, 89], and polymer degradation models which consider the kinetics of random and chain-end scission mechanisms or intermediate combinations of the two mechanisms for PLGA in solution [45, 90]. Often the models focus on only one of the processes involved in the drug release or treat the processes independently rather than in a coupled manner [45, 72, 79]. The few models that have included autocatalytic effects have not addressed all of the processes involved in the overall drug release mechanism for the PLGA microsphere system [49, 69, 77, 78, 80, 81, 91]. The nonlinearity, tight coupling, and dynamics of the drug delivery processes makes it critical to model the effects in a coupled manner rather than independently to obtain models that are predictive rather than merely correlative [8]. Zilberman and Malka [82] developed a semi-empirical model with a time-dependent diffusion coefficient as a function of changes to the polymer weight loss and degree of crystallinity. They found that the degradation of the polymer has a greater effect on the drug release profile than the change in polymer crystallinity. Zhao, Hunter, and Rodgers [55] presented a mechanistic method for coupling reaction to variable effective diffusivity through hindered diffusion and pore evolution. This method can be applied to autocatalytic hydrolysis coupled to erosion and drug diffusion and release with spatial dependences.

3.4 The Reaction Component of Reaction-Diffusion Models

Autocatalytic hydrolysis kinetics have been modeled for autocatalytic reactions in solution [92, 93] and for the hydrolytic degradation of solid PLGA microspheres without drug diffusion [80, 94, 95]. Often polymer degradation is assumed to follow well-mixed pseudo-first-order kinetics even in models that aim to include autocatalytic effects [17, 25, 34, 53, 59, 96]. The discrepancy between theoretical predictions made from existing models considering uncatalyzed depolymerization kinetics and actual drug release experimental data has been attributed to the models' failure to adequately treat autocatalysis [25]. For PLA, Siparsky et al. [93] have shown that pseudo-first-order kinetics are a good approximation for hydrolysis catalyzed by an external strong acid but are insufficient for modeling autocatalysis where the catalyst is the internal weak carboxylic acid from the polymer end groups. Quadratic, autocatalytic hydrolysis kinetics have been treated in several reports [81, 92–94]. The limitation of quadratic kinetics for autocatalysis is the inability to capture the effects of partial dissociation of the carboxylic acid end groups. A kinetic expression has been derived to include partial dissociation effects with half-order dependence on carboxylic acid [93]. This model fit the kinetic data very well except near the extrema of the data set. We believe that the agreement can be improved by including the diffusion of drug molecules and oligomers of the degrading polymer.

3.5 The Diffusion Component of Reaction-Diffusion Models

Batycky, Hanes, Langer, and Edwards [45] proposed a model that calculated the amount of initial drug burst via a desorption mechanism, accounted for non-catalytic degradation kinetics using a combined random and chain-end scission mechanism, and modeled pore creation mechanistically. In their model, the drug diffused out of a particle with a constant effective diffusivity after the pores were

formed. The model treated each of the processes as independent. As a result, there was no explicit coupling between the polymer degradation and the drug release. Additionally, there was no dependence on the intraparticle pH since the reactions were simulated based on discrete kinetic equations developed by Ziff and McGrady [97] for generic polymer degradation kinetics in the absence of a catalyst. Another disadvantage to Batycky et al. [45] model is its use of formulation-specific parameters that had to be observed from experimental data. The model in the present work uses readily available parameters and couples polymer degradation and drug diffusion through the drug diffusivity.

J. Siepmann et al. [72] fit drug release from PLGA microspheres to the analytical solution of the equation for Fickian diffusion towards a perfect sink medium with a finite mass transfer coefficient at the external particle surface and a constant effective diffusivity. The effective diffusivity and mass transfer coefficients were determined for different size particles by a fitting procedure. The effective diffusivity was observed to vary significantly with the size of the microspheres. When a constant value for the effective diffusivity was used in the Fickian diffusion equation to determine the theoretical release behavior without autocatalytic effects, the simulation results disagreed with the experimental data. This failure to predict the drug release profiles was used as evidence for the need to incorporate autocatalytic effects into models to explain drug release behavior from bulk-eroding, polyester microspheres. Thombre and Himmelstein [77] developed a model for simultaneous transport and reaction from surface-eroding poly(orthoester) that included autocatalytic effects, complete ionization of acidic species, and an effective diffusivity dependent on the extent of polymer degradation in a slab geometry. Ding, Shenderova, and Schwendeman [83] derived a model based on dissolution theory for the acidic PLGA degradation products into aqueous pores; their model did not include drug release and depended on experimentally determined parameters. The model in this dissertation includes the autocatalytic effects that

the model of Siepmann et al. lacks by modifying Thombre and Himmelstein's model to allow for partial or full dissociation of the catalyst and to apply to bulk-eroding spherical PLGA while capturing microclimate pH variations throughout microspheres along with drug release in a more thorough manner than the model proposed by Ding et al. [83].

Mollica et al. [78] presented a model that described the time-dependent radial drug concentration profiles in a PLGA microsphere using a degradation front that extended with time from the particle center to the surface and that allowed for the progressive opening of pores for drug diffusion. The model assumed that the degradation followed first-order reaction kinetics within the front boundary and that no reaction occurred outside the boundary. The model closely fit experimental data for short times. Rothstein, Federspiel, and Little [79] developed a model to simulate the development of the polymer matrix porosity using a first-order degradation rate expression and the diffusion of the drug through the pore structure of the polymer. The results were compared to experimental release studies for a wide variety of drugs. The authors acknowledged that their correlation of effective drug diffusivity to particle size lacked a physically relevant expression to accurately incorporate size-dependent autocatalytic effects. Wang et al. [80] modeled the degradation of biodegradable polymers without drug release. In their model, monomer diffusivity was coupled to the porosity, which depended on the variable concentrations of the ester and monomer. The hydrolysis reaction in their model proceeded both with and without a catalyst. The model in the dissertation uses kinetics similar to the expressions in the Wang et al. [80] model, while also considering simultaneous drug diffusion. Wang et al. [80] also constructed a biodegradation map for planar and cylindrical geometries to quantitatively show the zones where diffusion and reaction each have strong or weak influences.

Arosio et al. [49] developed a model for cylindrical wires that included autocatalytic effects on the diffusion and the molecular weight distribution of the

polymer. The diffusion process was not accounted for explicitly but was approximated by a shrinking core model where the reactions only took place at a moving boundary front within the wires. The model failed to predict published data well, but the authors encouraged comparison to multiple data sources in order to validate models for broad applicability. An objective of this thesis is to develop a model that is useful for predicting drug release for many different drug compounds and a variety of bulk-eroding polymers. These aims are shared by Mollica et al., Rothstein et al., Wang et al., and Arosio et al. [49, 78–80].

Chapter 4

Model Framework

This chapter overviews the equations for a mechanistic model for polymer degradation and diffusive drug release from PLGA microspheres that treats the autocatalytic hydrolysis reaction, diffusive transport having a variable effective drug diffusivity, and mass erosion through the developing pore network. In this chapter, the general conservation equation for the species in the system and the expression for the cumulative fraction of drug released as a function of time are derived. The components of the model for reaction, diffusion, and the coupling between these phenomena are detailed in subsequent chapters. Chapter 5 contains the details of the model associated with the chemical reactions in the system. Chapter 6 contains the model equations for pore growth and variable effective diffusivity. In Chapter 7 the model equations are summarized for the spatially distributed, reacting and diffusing system with spherical symmetry with the effective diffusivity of drug coupled to the evolution of the pore network.

4.1 General Conservation Equation for Reaction and Diffusion

The conservation equation for species i in molar units of concentration (c_i) is [98]

$$\frac{\partial c_i}{\partial t} = -\nabla \cdot \mathbf{N}_i + R_{Vi}, \tag{4.1}$$

where $\mathbf{N}_i$ is the molar flux of i relative to fixed coordinates and R_{Vi} is the net rate of formation of species i by chemical reaction, per unit volume. The sign convention is positive for net generation and negative for net consumption of species i. Assuming the mass-average velocity is zero, the density of the aqueous medium is constant, and the dilute, multicomponent solution can be treated as a pseudobinary solution (interactions between minor components are negligible compared to the binary diffusivity of each minor component i with water) [98], the total molar flux is

$$\mathbf{N}_i = \mathbf{J}_i, \tag{4.2}$$

where $\mathbf{J}_i$ is the molar flux of i relative to the mass-average velocity, and the molar flux for each component in the absence of convection is given by Fick's second law for non-steady-state diffusion in a pseudobinary dilute solution at constant density,

$$\mathbf{J}_i = -D_i \nabla c_i, \tag{4.3}$$

where D_i is the pseudobinary diffusivity of species i in aqueous solution. The conservation equation for species i may be written as

$$\frac{\partial c_i}{\partial t} = \nabla \cdot (D_i \nabla c_i) + R_{Vi}, \tag{4.4}$$

where the reactions occur throughout the polymer microsphere volume, and the species concentrations are radially distributed and transport dependent. The overall microsphere volume is assumed to be constant as the polyesters considered in this work undergo bulk erosion rather than surface erosion.

In spherical coordinates with spherical symmetry, $c_i = c_i(\hat{r}, \theta, \phi, t) = c_i(\hat{r}, t)$, $D_i = D_i(\hat{r}, \theta, \phi, t) = D_i(\hat{r}, t)$, and $R_{Vi} = R_{Vi}(\hat{r}, \theta, \phi, t) = R_{Vi}(\hat{r}, t)$. In general the net rate of formation of species i by chemical reaction, R_{Vi}, depends on c_i as well as on c_j for $j \neq i$ [99]. Let $\hat{r}$ denote the radial distance from the center of the sphere, and

let R denote the radius of the sphere, both in units of length. The conservation equation for species i with spherical symmetry and diffusion only in the radial direction is

$$\frac{\partial c_i(\hat{r},t)}{\partial t} = \frac{1}{\hat{r}^2}\frac{\partial}{\partial \hat{r}}\left(\hat{r}^2 D_i(\hat{r},t)\frac{\partial c_i(\hat{r},t)}{\partial \hat{r}}\right) + R_{Vi}(\hat{r},t). \tag{4.5}$$

The radial position inside the sphere can be normalized by $r = \hat{r}/R$, where r is the dimensionless radial position within the sphere. With normalized radius, (4.5) becomes

$$\frac{\partial c_i(Rr,t)}{\partial t} = \frac{1}{(Rr)^2}\frac{\partial}{\partial (Rr)}\left((Rr)^2 D_i(Rr,t)\frac{\partial c_i(Rr,t)}{\partial (Rr)}\right) + R_{Vi}(Rr,t). \tag{4.6}$$

$$\frac{\partial c_i(r,t)}{\partial t} = \frac{1}{R^3}\frac{1}{r^2}\frac{\partial}{\partial r}\left(R^2 r^2 D_i(r,t)\frac{1}{R}\frac{\partial c_i(r,t)}{\partial r}\right) + R_{Vi}(r,t). \tag{4.7}$$

$$\frac{\partial c_i(r,t)}{\partial t} = \frac{1}{r^2}\frac{\partial}{\partial r}\left(r^2\frac{D_i(r,t)}{R^2}\frac{\partial c_i(r,t)}{\partial r}\right) + R_{Vi}(r,t). \tag{4.8}$$

The initial condition

$$c_i(r,0) = c_{i,t0}(r), \quad 0 \le r < 1 \tag{4.9}$$

and boundary conditions

$$\frac{\partial c_i(0,t)}{\partial r} = 0, \quad t \ge 0 \tag{4.10}$$

and

$$c_i(1,t) = c_{i,r1}, \quad t \ge 0 \tag{4.11}$$

are applied to (4.8), where $c_i(r,t)$ is the molar concentration of species i, $0 \le r \le 1$ is the normalized radial position, $t \ge 0$ is time, $D_i(r,t)$ is the effective diffusivity of species i in the polymer matrix and aqueous pores, $R_{Vi}(r,t)$ is the net rate of generation of species i from the hydrolysis reaction, $c_{i,t0}(r)$ is the initial concentration distribution of species i within the sphere, and $c_{i,r1}$ is the constant surface concentration of species i. The term $R_{Vi}(r,t)$ is a function of the concentrations of some or all of the species at the same position and time,

depending on the stoichiometry of the chemical reactions. Unless otherwise indicated, the initial concentration is uniformly distributed ($c_{i,t0}(r) = c_{i,t0}$). Uniform initial conditions and perfect sink boundary conditions are common assumptions for diffusion-controlled drug release [61, 100].

The species are the carboxylic acid end groups of the polymer chains (COOH), the ester bonds in the polymer chains (E), drug molecules dispersed throughout the microspheres (drug), and PLGA polymer chains of length n (P_n). For the acid-catalyzed reaction kinetics, the H^+ concentration is related to the concentration of COOH with assumptions about the source of the protons and the extent of dissociation of the carboxylic acid. Following the common convention in the chemistry and chemical engineering literature, no distinction is made between H_3O^+ and H^+ when in aqueous solution. The transport of each small oligomer with $n = 1, 2, \ldots, s$, where s is the integer length of the longest soluble oligomer, is individually modeled and the concentrations of insoluble large PLGA polymer chains of length $n = s + 1, s + 2, \ldots$ are tracked as a lumped sum as described in Chapter 7. Note that the bracketed notation for concentrations of specific species (i.e., $[i](r, t)$) is used throughout the dissertation in place of $c_i(r, t)$ for compactness.

The drug is assumed to be non-reactive while in the polymer matrix and aqueous pores, eliminating the net rate of generation term in the conservation equation for the drug giving

$$\frac{\partial[\text{drug}](r,t)}{\partial t} = \frac{1}{r^2}\frac{\partial}{\partial r}\left(r^2 \frac{D_{\text{drug}}(r,t)}{R^2}\frac{\partial[\text{drug}](r,t)}{\partial r}\right). \tag{4.12}$$

The concentrations of the drug at time $t = 0$ and at the surface $r = 1$ must not be the same because their difference is the driving force for the diffusion process without a generation term. The surface concentration must be less than the initial concentration for a net flux out of the sphere: $[\text{drug}]_{r1} < [\text{drug}]_{t0}(r)$. The generation terms for the other species are derived for different kinetic rate laws in Chapter 5.

4.2 Cumulative Release of Drug

The amount of drug remaining in a sphere as a function of time, $m(t)$, is the volume integral of the radial concentration with spherical symmetry:

$$m(t) := \int_0^{\pi} \int_0^{2\pi} \int_0^1 [\text{drug}](r,t)\, r^2 \sin\phi \, dr \, d\theta \, d\phi = \int_0^1 4\pi [\text{drug}](r,t)\, r^2 \, dr. \tag{4.13}$$

The cumulative amount of drug released as a function of time, $M(t)$, is the difference between the initial amount of the drug in the sphere and the amount remaining in the sphere as a function of time, $m(t)$:

$$M(t) := m(0) - m(t). \tag{4.14}$$

Alternatively, $M(t)$ can be determined by integrating the release rate over time. With constant effective diffusivity of drug, D_{drug}, [101],

$$M(t) = \int_0^t 4\pi R^2 \left(-D_{\text{drug}} \frac{\partial [\text{drug}](R,t')}{\partial \hat{r}} \right) dt', \tag{4.15}$$

where the release rate is the product of the surface area and the total molar flux given by (4.3) evaluated at the surface. In terms of dimensionless radius $r = \hat{r}/R$,

$$M(t) = -\int_0^t 4\pi R D_{\text{drug}} \frac{\partial [\text{drug}](1,t')}{\partial r} \, dt', \tag{4.16}$$

The surface flux is not known explicitly at each time when the effective diffusivity of the drug is variable, so this definition is not as practical as (4.14) based on the volume integrals and is not used for numerical determination of the cumulative release of drug.

The cumulative normalized fraction of drug released as a function of time, $Q(t)$, is the ratio of the cumulative amount of drug released as a function of time,

$M(t)$, to the cumulative amount of drug released as $t \to \infty$, M_∞:

$$Q(t) := \frac{M(t)}{M_\infty} = \frac{m(0) - m(t)}{m(0) - \lim_{t\to\infty} m(t)}. \tag{4.17}$$

Using the definition of $m(t)$, $Q(t)$ can be expressed as

$$Q(t) = \frac{\int_0^1 4\pi[\text{drug}](r,0)r^2\,dr - \int_0^1 4\pi[\text{drug}](r,t)r^2\,dr}{\int_0^1 4\pi[\text{drug}](r,0)r^2\,dr - \lim_{t\to\infty}\int_0^1 4\pi[\text{drug}](r,t)r^2\,dr}. \tag{4.18}$$

Taking the limit into the integral in the final term in the denominator, $\lim_{t\to\infty}[\text{drug}](r,t)$ is determined by the boundary condition on the surface of the microparticle. Here, a constant surface concentration is assumed as the boundary condition. As $t \to \infty$ the driving force for diffusion is eliminated, so the limit of the drug concentration is

$$\lim_{t\to\infty}[\text{drug}](r,t) \to [\text{drug}](1,t) = [\text{drug}]_{r1}, \tag{4.19}$$

With the limit evaluated, (4.18) can be simplified to

$$Q(t) = \frac{\int_0^1 \left([\text{drug}]_{t0}(r) - [\text{drug}](r,t)\right) r^2\,dr}{\int_0^1 \left([\text{drug}]_{t0}(r) - [\text{drug}]_{r1}\right) r^2\,dr}. \tag{4.20}$$

The values of $[\text{drug}](r,t)$ are determined from the numerical solution to the PDE for drug concentration, (4.12), coupled to the polymer degradation through the variable effective drug diffusivity. The calculation of $Q(t)$ uses the initial distribution $[\text{drug}](r,0) := [\text{drug}]_{t0}(r)$, the constant surface concentration $[\text{drug}](1,t) := [\text{drug}]_{r1}$, the discrete values of r along the radius, and the numerically-determined $[\text{drug}](r,t)$ values to perform the numerical integrations of the numerator and denominator of (4.20) by the adaptive Simpson's rule implemented by the *quad* intrinsic function in MATLAB.

Chapter 5

Reaction Component of the Model

Elementary rate laws for the hydrolysis reaction are used to derive the net rate of generation terms, $R_{Vi}(r,t)$, in the respective reaction-diffusion equations for the polymer chains, P_n, carboxylic acid end groups, COOH, and ester bonds, E, of the polymer. Here, four rate laws are presented as options for the model for treatment of polyester hydrolysis in different ways. The use of multiple rate laws in the model allows for improving the understanding of the kinetic behavior in the microsphere system with simultaneous reaction and diffusion. The limits of the assumptions of each rate law can be assessed when the model is implemented. The rate laws used here are the first-order rate law for uncatalyzed hydrolysis and the pseudo-first-order rate law, the quadratic-order rate law, and the 1.5th-order rate law for autocatalytic hydrolysis. Note: the reaction orders are all with respect to the overall order for the net rate of generation of carboxylic acid end groups.

The uncatalyzed hydrolysis reaction is

$$\begin{gathered} P_n + H_2O \xrightarrow{k_u} P_m + P_{n-m}, \\ n = 2,\, 3,\, \ldots \text{ and } m = 1,\, 2,\, \ldots,\, n-1, \end{gathered} \tag{5.1}$$

where P_n denotes polymer chains with degree of polymerization n and k_u is the rate constant for the uncatalyzed reaction. The acid-catalyzed hydrolysis reaction is

$$\begin{gathered} P_n + H_2O + H^+ \xrightarrow{k_c} P_m + P_{n-m} + H^+, \\ n = 2,\, 3,\, \ldots \text{ and } m = 1,\, 2,\, \ldots,\, n-1, \end{gathered} \tag{5.2}$$

where H^+ is the acid catalyst that can be from an external source such as a strongly acidic medium or an internal source such as the carboxylic acid end groups, COOH, of the polymer chains and k_c is the rate constant for the catalyzed reaction. If the catalyst is only from an external source of strong acid, the net rate of generation of acid is zero as the catalytic terms cancel. Polyester microparticles for drug delivery applications are typically degraded in aqueous media *in vivo* or *in vitro* at physiological conditions with pH 7.4, so strong acid external catalyst sources are not considered here. With autocatalysis, the carboxylic acid end groups accelerate the reaction by serving as proton donors enabling the acid-catalyzed reaction mechanism.

A variety of kinetic rate laws have been proposed for polyester hydrolysis, including the first-order rate law for uncatalyzed hydrolysis [102] and the pseudo-first-order rate law [103], the quadratic-order rate law [91, 92], and the 1.5th-order rate law with partial dissociation of COOH [93, 104] for acid-catalyzed hydrolysis that can be autocatalytic. The rate laws either consider the uncatalyzed hydrolysis reaction (5.1) or the catalyzed hydrolysis reaction (5.2). The rate laws for the autocatalytic hydrolysis reaction treat the carboxylic acid end groups as the catalyst source but differ by the terms that are considered constant and by the extent of dissociation of the end groups. The experimental studies on the kinetics of polyester hydrolysis treated systems assumed to be well-mixed, ignoring any spatial variations due to diffusion. Convective mass transfer is assumed to be negligible.

5.1 First-Order Rate Law for Uncatalyzed Hydrolysis

The first-order rate law for uncatalyzed hydrolysis uses the uncatalyzed hydrolysis reaction in (5.1) with the assumption of constant concentration of water.

5.1.1 Net Rate of Generation of Polymer Chains

For the random chain scission mechanism of polyester hydrolysis, each ester bond has the same probability of being cleaved. Polymer chains having n monomeric subunits are said to have "length n." Chains of length n are cleaved by hydrolysis into $n-1$ different combinations of chain fragments. A chain of length n can be cleaved from one or the other to produce any specific smaller chain fragments. If the rate constant for hydrolysis of all ester bonds is the same, the probabilities of consuming or producing P_n can be used to determine the rate law for P_n with $n = 2, 3, \ldots$ under isothermal conditions [45, 102]:

$$R_{V\mathrm{P}_n}(r,t) = 2k_u[\mathrm{H_2O}](r,t) \sum_{m=n+1}^{\infty} [\mathrm{P}_m](r,t) - (n-1)\, k_u[\mathrm{H_2O}](r,t)[\mathrm{P}_n](r,t). \quad (5.3)$$

For $n = 1$ no consumption term is needed, and the rate law becomes

$$R_{V\mathrm{P}_1}(r,t) = 2k_u[\mathrm{H_2O}](r,t) \sum_{m=2}^{\infty} [\mathrm{P}_m](r,t), \quad (5.4)$$

where $[\mathrm{P}_1](r,t)$ is the concentration of monomeric chain fragments and $R_{V\mathrm{P}_1}(r,t)$ is the net rate of generation of species P_1. The net rate of generation given by (5.4) is the same as (5.3) with $n = 1$, so the $R_{V\mathrm{P}_1}(r,t)$ term can be included in the general expression for $R_{V\mathrm{P}_n}(r,t)$ for $n = 1, 2, \ldots$.

In aqueous media, the hydration rate of the polymer matrix is fast—on the order of seconds or minutes for a microparticle compared to days or weeks for drug release from a microparticle [48]. The concentration of water is assumed to be constant, $[\mathrm{H_2O}](r,t) = [\mathrm{H_2O}]$. Define

$$k_u' := k_u[\mathrm{H_2O}] \quad (5.5)$$

as the rate constant for uncatalyzed hydrolysis with constant water concentration.

Substituting k'_u into (5.3) and (5.4) and combining the results gives

$$R_{VP_n}(r,t) = 2k'_u \sum_{m=n+1}^{\infty} [P_m](r,t) - (n-1)\, k'_u [P_n](r,t), \qquad n = 1,\, 2,\, \ldots. \tag{5.6}$$

5.1.2 Net Rate of Generation of Carboxylic Acid End Groups

Define the total concentration of polymer chains, [P], as

$$[P](r,t) := \sum_{n=1}^{\infty} [P_n](r,t). \tag{5.7}$$

Summing (5.6) for all $n = 1,\, 2,\, \ldots$ gives [102]

$$R_{VP}(r,t) = 2k'_u \sum_{n=2}^{\infty} \sum_{m=n+1}^{\infty} [P_m](r,t) - \sum_{n=2}^{\infty} (n-1)\, k'_u [P_n](r,t) + 2k'_u \sum_{m=2}^{\infty} [P_m](r,t), \tag{5.8}$$

where $R_{VP}(r,t)$ is the sum of the formation of polymer chains with

$$R_{VP}(r,t) := \sum_{n=1}^{\infty} R_{VP_n}(r,t). \tag{5.9}$$

The double summation in the net rate of generation of polymer chains given by (5.8) can be simplified as [102]

$$\sum_{n=2}^{\infty} \sum_{m=n+1}^{\infty} [P_m](r,t) = \sum_{n=2}^{\infty} (n-1)\, [P_n](r,t) - \sum_{n=2}^{\infty} [P_n](r,t). \tag{5.10}$$

Substituting (5.10) into (5.8) results in

$$\begin{aligned} R_{VP}(r,t) = {} & 2k'_u \sum_{n=2}^{\infty} \left([P_n](r,t) + (n-1)\, [P_n](r,t) - [P_n](r,t) \right) \\ & - \sum_{n=2}^{\infty} (n-1)\, k'_u [P_n](r,t). \end{aligned} \tag{5.11}$$

Canceling terms, combining the summations, and using the fact that $n - 1 = 0$ for

$n = 1$ to change the lower limit of the summation, (5.11) becomes

$$R_{V\mathrm{P}}(r,t) = k'_u \sum_{n=1}^{\infty} (n-1)\,[\mathrm{P}_n](r,t). \tag{5.12}$$

For a linear aliphatic polyester, each polymer chain has one carboxylic acid end group, so

$$[\mathrm{COOH}](r,t) := [\mathrm{P}](r,t) = \sum_{n=1}^{\infty} [\mathrm{P}_n](r,t). \tag{5.13}$$

The concentration of ester bonds is related to the polymer chain concentration as each polymer chain has $n-1$ ester bonds:

$$[\mathrm{E}](r,t) := \sum_{n=1}^{\infty} (n-1)\,[\mathrm{P}_n](r,t). \tag{5.14}$$

Substituting the definitions for $[\mathrm{COOH}](r,t)$ and $[\mathrm{E}](r,t)$ into (5.12) gives [94]

$$R_{V\mathrm{COOH}}(r,t) = k'_u [\mathrm{E}](r,t). \tag{5.15}$$

5.1.3 Net Rate of Generation of Ester Bonds

When an ester bond is broken, a carboxylic acid end group is formed:

$$-R_{V\mathrm{E}}(r,t) = R_{V\mathrm{COOH}}(r,t). \tag{5.16}$$

The net rate of generation of carboxylic acid end groups is given by (5.15), thus

$$R_{V\mathrm{E}}(r,t) = -k'_u [\mathrm{E}](r,t). \tag{5.17}$$

5.2 Pseudo-First-Order Rate Law for Autocatalytic Hydrolysis

The pseudo-first-order rate law for autocatalytic hydrolysis uses the catalyzed hydrolysis reaction (5.2) with the assumptions of constant concentrations of water

and ester bonds and fully dissociated carboxylic acid end groups. The carboxylic acid end groups are treated as the only source of the protons used for the catalytic reaction giving

$$\begin{gathered} \mathrm{P}_n + \mathrm{H_2O} + \mathrm{COOH} \xrightarrow{k_c} \mathrm{P}_m + \mathrm{P}_{n-m} + \mathrm{COOH}, \\ n = 2,\, 3,\, \ldots \text{ and } m = 1,\, 2,\, \ldots,\, n-1. \end{gathered} \tag{5.18}$$

5.2.1 Net Rate of Generation of Carboxylic Acid End Groups

The net rate of generation of carboxylic acid end groups for random chain scission in autocatalyzed polyester hydrolysis is simply the product of the end group concentration and the net rate of generation for uncatalyzed hydrolysis [103]:

$$R_{V\mathrm{COOH}}(r,t) = k_c[\mathrm{COOH}](r,t)[\mathrm{H_2O}](r,t)[\mathrm{E}](r,t). \tag{5.19}$$

Assuming constant concentrations of water and ester bonds before the hydrolysis reaction has progressed to a significant extent, $[\mathrm{H_2O}](r,t) = [\mathrm{H_2O}]$ and $[\mathrm{E}](r,t) = [\mathrm{E}]$. $[\mathrm{H_2O}]$ and $[\mathrm{E}]$ can be combined as part of the rate constant k_1' defined as

$$k_1' := k_c[\mathrm{H_2O}][\mathrm{E}]. \tag{5.20}$$

Substituting the rate constant given by (5.20) into (5.19) gives the pseudo-first-order rate law [103]:

$$R_{V\mathrm{COOH}}(r,t) = k_1'[\mathrm{COOH}](r,t). \tag{5.21}$$

5.2.2 Net Rate of Generation of Polymer Chains

All generation and consumption terms for P_n are the same as in the uncatalyzed case, except multiplied by the COOH catalyst concentration. COOH is responsible for the autocatalysis as the acidic end groups on each polymer chain catalyze the

hydrolysis reaction. The net rate of generation of P_n for $n = 1, 2, \ldots$ is

$$R_{VP_n}(r,t) = k_c[H_2O](r,t)[COOH](r,t) \times \left(2 \sum_{m=n+1}^{\infty} [P_m](r,t) - (n-1)\,[P_n](r,t) \right). \tag{5.22}$$

Assuming constant water concentration, $[H_2O](r,t) = [H_2O]$, and substituting k_1' into (5.22) gives

$$R_{VP_n}(r,t) = \frac{k_1'[COOH](r,t)}{[E]} \left(2 \sum_{m=n+1}^{\infty} [P_m](r,t) - (n-1)\,[P_n](r,t) \right), \quad n = 1, 2, \ldots. \tag{5.23}$$

5.2.3 Net Rate of Generation of Ester Bonds

The key assumption for the pseudo-first-order rate law for autocatalytic hydrolysis is that the ester concentration is constant. Thus,

$$R_{VE}(r,t) \equiv 0. \tag{5.24}$$

5.3 Quadratic-Order Rate Law for Autocatalytic Hydrolysis

The quadratic-order rate law for autocatalytic hydrolysis uses the autocatalyzed hydrolysis reaction in (5.18) with the assumptions of constant concentration of water and fully dissociated carboxylic acid end groups.

5.3.1 Net Rate of Generation of Polymer Chains

All generation and consumption terms for P_n are the same as in the general catalyzed case given by (5.22). The net rate of generation of P_n for $n = 1, 2, \ldots$

is [92]

$$R_{V\mathrm{P}_n}(r,t) = k_c[\mathrm{H_2O}](r,t)[\mathrm{COOH}](r,t) \times \left(2\sum_{m=n+1}^{\infty}[\mathrm{P}_m](r,t) - (n-1)\,[\mathrm{P}_n](r,t)\right). \tag{5.25}$$

Assuming constant concentration of water, $[\mathrm{H_2O}](r,t) = [\mathrm{H_2O}]$, the rate constant k_2' is defined as

$$k_2' := k_c[\mathrm{H_2O}]. \tag{5.26}$$

Substituting k_2' in (5.25) gives

$$R_{V\mathrm{P}_n}(r,t) = k_2'[\mathrm{COOH}](r,t)\left(2\sum_{m=n+1}^{\infty}[\mathrm{P}_m](r,t) - (n-1)\,[\mathrm{P}_n](r,t)\right), \quad n = 1,\, 2,\, \ldots. \tag{5.27}$$

5.3.2 Net Rate of Generation of Carboxylic Acid End Groups

Starting with the rate equation for random chain scission in autocatalyzed polyester hydrolysis given by (5.19) with the assumption of constant water concentration but without making Pitt et al.'s [103] assumption of constant ester concentration, the quadratic rate equation for autocatalysis is [91, 93]

$$R_{V\mathrm{COOH}}(r,t) = k_2'[\mathrm{COOH}](r,t)[\mathrm{E}](r,t). \tag{5.28}$$

5.3.3 Net Rate of Generation of Ester Bonds

The relationship between the net rate of generation of ester bonds and carboxylic acid end groups is given by (5.16). Substituting $R_{V\mathrm{COOH}}(r,t)$ from (5.28) gives

$$R_{V\mathrm{E}}(r,t) = -k_2'[\mathrm{COOH}](r,t)[\mathrm{E}](r,t). \tag{5.29}$$

5.4 1.5th-Order Rate Law for Autocatalytic Hydrolysis

The 1.5th-order rate law for autocatalytic hydrolysis uses the catalyzed hydrolysis reaction in (5.2) with the assumptions of constant concentration of water and partially dissociated carboxylic acid end groups as the only catalyst. The pseudo-first-order and quadratic-order rate laws assume that all COOH groups are completely available for catalytic reactions or can be derived by the alternative assumption that all of the COOH end groups undergo complete dissociation and all of the resulting H^+ ions are available for catalysis. While the 1.5th-order rate law assumes that the COOH end groups serve as the only catalysts for the hydrolysis reaction, the model does not assume full dissociation in the reaction

$$\mathrm{COOH}^* \leftrightharpoons \mathrm{COO}^- + \mathrm{H}^+, \tag{5.30}$$

where COOH^* and COO^- denote undissociated and dissociated carboxylic acid end groups, respectively. Rather, the acid concentration depends on the partial dissociation of the COOH end groups. The concentrations are related by the acid dissociation constant for COOH:

$$K_a := \frac{[\mathrm{H}^+][\mathrm{COO}^-]}{[\mathrm{COOH}]^*}. \tag{5.31}$$

For the dissociation of water,

$$\mathrm{H_2O} \leftrightharpoons \mathrm{H}^+ + \mathrm{OH}^-, \tag{5.32}$$

the dissociation constant is

$$K_w = [\mathrm{H}^+][\mathrm{OH}^-]. \tag{5.33}$$

The mass balance for carboxylic acid end groups is

$$[\mathrm{COOH}] = [\mathrm{COOH}]^* + [\mathrm{COO}^-], \tag{5.34}$$

where [COOH] is the total concentration of carboxylic acid end groups. The charge balance is

$$[\mathrm{H}^+] = [\mathrm{COO}^-] + [\mathrm{OH}^-]. \tag{5.35}$$

Substituting (5.31) into (5.34) for $[\mathrm{COOH}]^*$ gives

$$[\mathrm{COOH}] = \frac{[\mathrm{H}^+][\mathrm{COO}^-]}{K_a} + [\mathrm{COO}^-]. \tag{5.36}$$

Rearranging gives

$$[\mathrm{COO}^-] = \frac{K_a[\mathrm{COOH}]}{K_a + [\mathrm{H}^+]}. \tag{5.37}$$

Substituting (5.33) for $[\mathrm{OH}^-]$ and (5.37) into (5.35) gives

$$[\mathrm{H}^+] = \frac{K_a[\mathrm{COOH}]}{K_a + [\mathrm{H}^+]} + \frac{K_w}{[\mathrm{H}^+]}. \tag{5.38}$$

The assumption of a weak acid implies that $K_a << [\mathrm{H}^+]$, leading to

$$[\mathrm{H}^+] = \sqrt{K_a[\mathrm{COOH}] + K_w}. \tag{5.39}$$

Combining this with the assumption that [COOH] is large gives [104]

$$[\mathrm{H}^+] = \sqrt{K_a[\mathrm{COOH}]}. \tag{5.40}$$

The K_a value for different copolymer ratios of PLGA is determined by taking a weighted average of the K_a values for lactic acid and glycolic acid based on the copolymer composition.

5.4.1 Net Rate of Generation of Polymer Chains

All generation and consumption terms for P_n are the same as in the pseudo-first-order rate law, except with the catalyst concentration given by (5.40), the expression relating $[\mathrm{H}^+]$ to [COOH] to account for partial dissociation. The net

rate of generation of P_n for $n = 1, 2, \ldots$ is

$$R_{V\mathrm{P}_n}(r,t) = k_c[\mathrm{H_2O}](r,t)\sqrt{K_a[\mathrm{COOH}](r,t)} \times \left(2\sum_{m=n+1}^{\infty}[\mathrm{P}_m](r,t) - (n-1)\,[\mathrm{P}_n](r,t)\right). \tag{5.41}$$

Assuming constant concentration of water $[\mathrm{H_2O}](r,t) = [\mathrm{H_2O}]$, the rate constant $k'_{1.5}$ is defined as

$$k'_{1.5} := k_c[\mathrm{H_2O}]. \tag{5.42}$$

Substituting $k'_{1.5}$ into (5.41) gives

$$R_{V\mathrm{P}_n}(r,t) = k'_{1.5}\sqrt{K_a[\mathrm{COOH}](r,t)}\left(2\sum_{m=n+1}^{\infty}[\mathrm{P}_m](r,t) - (n-1)\,[\mathrm{P}_n](r,t)\right), \tag{5.43}$$

$n = 1, 2, \ldots.$

5.4.2 Net Rate of Generation of Carboxylic Acid End Groups

Assuming constant water concentration, the chemical rate expression for acid-catalyzed hydrolysis is

$$R_{V\mathrm{COOH}}(r,t) = k'_{1.5}[\mathrm{H^+}](r,t)[\mathrm{E}](r,t). \tag{5.44}$$

Inserting the expression relating $[\mathrm{H^+}]$ to [COOH] given by (5.40) to account for partial dissociation into (5.44) [93, 104]:

$$R_{V\mathrm{COOH}}(r,t) = k'_{1.5}\sqrt{K_a[\mathrm{COOH}](r,t)}[\mathrm{E}](r,t). \tag{5.45}$$

5.4.3 Net Rate of Generation of Ester Bonds

The relationship between the net rate of generation of ester bonds and carboxylic acid end groups is given by (5.16). Substituting $R_{V\mathrm{COOH}}(r,t)$ from (5.45) gives

$$R_{V\mathrm{E}}(r,t) = -k'_{1.5}\sqrt{K_a[\mathrm{COOH}](r,t)}[\mathrm{E}](r,t). \tag{5.46}$$

Chapter 6

Diffusion Component of the Model

Transport effects through porous networks that are created initially by fabrication methods and grow by polymer degradation are covered in this chapter. Drug diffusion through PLGA microspheres has been observed to be much slower than the rate of diffusion through water [27, 45, 60, 105] and to be dependent on drug molecule size, allowing smaller molecules to diffuse more readily than larger molecules [105]. Insufficient pore size in high molecular weight PLGA until degradation has progressed to yield pores sufficiently large for drug transport has been attributed as a reason for lowered effective diffusivity compared to that in water or in filter media [60], suggesting that drug diffusion is hindered until the pores are large enough to accommodate the drug molecules of different sizes. Drug diffusivity has been observed to increase with time, increasing porosity, and decreasing molecular weight [106], indicating that the effective diffusivity should be transient and dependent on the dynamic polymer morphology.

The model has an option to treat the effective diffusivity of the small oligomers either as a constant or as a variable in the same manner as the drug effective diffusivity. Polymer mass loss is generally not observed in the initial stage after the polymer microsphere is placed in an aqueous medium *in vivo* or *in vitro* [58], which has been attributed to soluble oligomers and monomers having smaller diffusion rate than rate of formation [107], despite the time scale for diffusion with the diffusivity at infinite dilution for lactic acid or glycolic acid being several orders of magnitude faster than the reaction time scale, suggesting that the

soluble oligomers are subject to hindered diffusion or slow diffusion through the polymer matrix.

A sufficiently developed porous structure in more slowly degrading PLA microspheres can offset the faster degradation speed of PLGA microspheres to allow for faster release of proteins from the more porous microspheres [108]. Therefore, both degradation of the polymer and diffusion through pores must be considered simultaneously. Solute transport in porous media can be described by Fickian diffusion if the effective diffusivity is used instead of the binary diffusivity to account for reductions in the diffusivity compared to that in free solution due to diffusion-path, the volume fraction available to the solvent, and hydrodynamic interactions between the solute and the porous solid [109]. The average pore radii start very small in dense, hydrophobic polymer microspheres and are larger in microspheres with a porous internal morphology. The effective diffusivities of the water-soluble polymer oligomers and monomers and the drug compound increase as the hydrolytic degradation proceeds due to enhanced porous diffusion pathways through the evolving pore network. In order to account for this effect in the model, the effective diffusivities of the drug and soluble oligomers are varied using hindered diffusion through aqueous pores that grow with the progression of the polymer degradation reaction and subsequent dissolution of soluble oligomers. The hindered diffusion theory is applied to a dynamic systems with growing pores rather than the traditional static pore size. The porous microspheres are treated with the continuum approach with the average of the pore radii much smaller than the microsphere radii. Each differential volume of the microsphere is considered a representative elementary volume with the details of the pore structures neglected and each symmetric radial point containing two phases: liquid-filled void phase and solid phase [109]. The representative pore radius at each point along the microsphere radius grows as the polymer is hydrolyzed, generating a larger void phase.

6.1 Pore Evolution Dependence on Reaction Kinetics

The microsphere morphology is assumed to contain tortuous cylindrical pores with some distribution of pore radii and some interconnection. The pore evolution is assumed to occur symmetrically throughout the microsphere dependent on the reaction kinetics in the radial direction. This is a simplification of the actual physical process, but the assumption allows for the radius of connecting pores averaged over a shell of radius r, $R_p(r,t)$, to be coupled to the spatially-varying reaction kinetics. $R_p(r,t)$ represents the average pore radius of pores connecting to the exterior of the particle at radial position r within the microsphere [55].

The drug compound is assumed to be distributed through the polymer in a dissolved and not conglomerated state and physically, not chemically, bound to the polymer [88]. For dense polymers, small cavities called micropores are assumed to exist between the chains of the polymer for holding the drug molecules and for saturation by water molecules. The initial porosity is reflected by the initial average pore radius, $R_p(r,0)$, determined from polymer morphology data or based on the space needed for saturation by water molecules throughout the microsphere. For hindered diffusion theory, the pore radius is comparable to the radius of the solute but much larger than that of the solvent [98]. With water as the solvent having a molecular diameter of ≈ 2.75 Å, the initial pore radius, in the absence of microsphere morphology data, is assumed to be ≈ 10 times larger than the diameter of water with $R_p(r,0) = 3$ nm. This minimum pore radius satisfies the 3 nm estimate of minimum system dimensions for continuum transport models using bulk fluid properties of a liquid as calculated by Deen [98]. The minimum initial pore radius is consistent with the value of 3.57 nm used by Lemaire, Belair, and Hildgen [88] in their model of drug release from degradable porous microspheres with diffusion within cylindrical pores of linearly growing pore radii depending on the erosion rate constant.

Drug and small oligomers are assumed to diffuse through two parallel paths: through the dense polymer matrix at a constant diffusivity and through the aqueous pores in the polymer matrix. Also, drug and small oligomers are assumed to have purely steric partition coefficients and to dissolve from the polymer matrix to the aqueous pores on a time scale much faster than the those for degradation or diffusion. Hydrophilic, macromolecular drugs generally do not diffuse through the solid polymer phase [65, 110]. Mao et al. showed that the internal morphology and porosity of PLGA microspheres influenced the release of dextran but had negligible influence on the PLGA degradation [111]. Any drug concentration variation caused by denaturation is neglected. The effects of the dynamic mechanisms of pore coalescence and pore closing, recently observed experimentally [112], are assumed to be negligible.

In the Lemaire [88] and Batycky [45] models for pore erosion, the erosion rate constants depend on experimentally observed quantities. Zhao, Hunter, and Rodgers [55] proposed linking the transient pore radius to molecular properties, initial conditions, and theoretical kinetics rather than empirical data. Their approach is used in the present work with the three significant modifications: (1) reaction kinetics for the four kinetic cases presented in Chapter 5 are used instead of a statistical formulation for pseudo-first-order hydrolysis only, (2) reaction kinetics are coupled to the diffusion of soluble, small oligomers, and (3) pore growth is a function of local position and not averaged over the entire microsphere.

The average monomer size, l_{ave}, is determined by a weighted average of the composite bond lengths for the lactide and glycolide monomers of the PLGA copolymer, designated as l_L and l_G, respectively. If G denotes the fraction of glycolide in the copolymer,

$$l_{\text{ave}} = G l_G + (1 - G) l_L, \tag{6.1}$$

where $l_G = 3.510$ Å and $l_L = 3.517$ Å [55]. The length of a soluble oligomer is nl_{ave} for $n = 1, 2, \ldots, s$ where s is the number of repeat units in the largest soluble oligomer.

The mechanism of pore formation growth is the cleavage and dissolution of a soluble monomer or oligomer from the polymer matrix. The dissolution time scale for the hydrophilic, small oligomers is assumed to be much faster than those for the reaction and for the diffusion.

The transient probability of generating a specific n-mer that contributes to the pore growth at time t and microsphere radial position r is denoted by $f(n)$. The exact probabilities for end scission and random internal bond scission for all n-mers are not known explicitly. To approximate $f(n)$, it is assumed that all bonds are equally reactive and the probabilities for generation of all n-mers by end scission and internal scission are equal. Therefore,

$$f(n) \approx X(r,t), \tag{6.2}$$

where $X(r,t)$ is the probability of random bond cleavages. $X(r,t)$ is proportional to the rate of consumption of ester bonds, which is equal to the rate of generation of new polymer chains or carboxylic acid end groups:

$$\begin{aligned} X(r,t) &\propto -R_{V\text{E}}(r,t) \\ &\propto R_{V\text{COOH}}(r,t), \end{aligned} \tag{6.3}$$

where $R_{V\text{E}}(r,t)$ and $R_{V\text{COOH}}(r,t)$ are the net rates of generation of ester bonds and carboxylic acid end groups, respectively.

To relate the probability of bond cleavages to the rate of bond cleavages, the rate must be normalized to give probability in the range [0,1]. The rate of chain production, $R_{V\text{COOH}}(r,t)$, is scaled by the maximum number of chains that can be

produced or the total number of repeat units that can be converted to monomers:

$$X(r,t) = \frac{R_{V\mathrm{COOH}}(r,t)}{[\mathrm{E}]_{t0}(r) + [\mathrm{COOH}]_{t0}(r)}. \tag{6.4}$$

The transient average number of bonds, $\dot{n}_{\mathrm{ave}}(r,t)$, for all soluble monomers and oligomers generated through bond cleavage per unit time at each microsphere radial position is [55]

$$\dot{n}_{\mathrm{ave}}(r,t) = \sum_{n=1}^{s} n f(n), \tag{6.5}$$

where s is the number of repeat units in the largest soluble oligomer.
Substituting (6.4) for $f(n)$ gives

$$\dot{n}_{\mathrm{ave}}(r,t) = \sum_{n=1}^{s} n \frac{R_{V\mathrm{COOH}}(r,t)}{[\mathrm{E}]_{t0}(r) + [\mathrm{COOH}]_{t0}(r)}. \tag{6.6}$$

As the transient probability of generating a specific n-mer that contributes to the pore growth is independent of n, the summation can be evaluated to give

$$\dot{n}_{\mathrm{ave}}(r,t) = \frac{s(s+1)}{2} \frac{R_{V\mathrm{COOH}}(r,t)}{[\mathrm{E}]_{t0}(r) + [\mathrm{COOH}]_{t0}(r)}. \tag{6.7}$$

The pore radius, $R_p(r,t)$, grows with time along the microsphere radius as soluble monomers and oligomers are produced from polymer degradation [55]:

$$\frac{\partial R_p(r,t)}{\partial t} = l_{\mathrm{ave}} \dot{n}_{\mathrm{ave}}(r,t). \tag{6.8}$$

Substituting (6.7) gives

$$\frac{\partial R_p(r,t)}{\partial t} = \frac{l_{\mathrm{ave}} s(s+1)}{2} \frac{R_{V\mathrm{COOH}}(r,t)}{[\mathrm{E}]_{t0}(r) + [\mathrm{COOH}]_{t0}(r)}. \tag{6.9}$$

Define $\bar{l}_{\mathrm{P}_{n \le s}}$ as the average length of a water-soluble, small oligomer that

contributes to pore growth:

$$\bar{l}_{\mathrm{P}_{n\leq s}} := \frac{l_{\mathrm{ave}} s(s+1)}{2}. \tag{6.10}$$

Therefore, [55]

$$\frac{\partial R_p(r,t)}{\partial t} = \frac{\bar{l}_{\mathrm{P}_{n\leq s}} R_{V\mathrm{COOH}}(r,t)}{[\mathrm{E}]_{t0}(r) + [\mathrm{COOH}]_{t0}(r)}, \tag{6.11}$$

where $\bar{l}_{\mathrm{P}_{n\leq s}}$ is the average length of a water-soluble, small oligomer, $R_{V\mathrm{COOH}}(r,t)$ is the net rate of generation of carboxylic acid end groups, and $[\mathrm{E}]_{t0}(r)$ and $[\mathrm{COOH}]_{t0}(r)$ are the initial concentration distributions of ester bonds and carboxylic acid end groups, respectively.

In their model, Zhao, Hunter, and Rodgers [55] used $\bar{l}_{\mathrm{P}_{n\leq s}} = \frac{(s+1)l_{ave}}{2}$. The missing factor of s seems to be due to a mistake in their evaluation of $\sum_{n=1}^{s} n$. They determined $R_p(t)$ for spatially-uniform, pseudo-first-order kinetics without diffusion of the small oligomers as [55]

$$R_p(t) = \frac{\bar{l}_{\mathrm{P}_{n\leq s}}}{N}\left(\frac{M_n^t}{M_n^0} - 1\right) + R_p(0), \tag{6.12}$$

where M_n^t and M_n^0 are the number-average molecular weight of the polymer at time t and zero, respectively, and N is the initial number-average degree of polymerization. For comparison to their result, using $R_{V\mathrm{COOH}}(r,t)$ for the pseudo-first-order rate law for autocatalytic hydrolysis derived in Chapter 5 given by (5.21) with the assumption of spatially-uniform reaction with no transport yields

$$\frac{dR_p}{dt} = \frac{\bar{l}_{\mathrm{P}_{n\leq s}} k_1' [\mathrm{COOH}](t)}{[\mathrm{E}]_{t0} + [\mathrm{COOH}]_{t0}}. \tag{6.13}$$

Integrating,

$$\int_0^t \frac{dR_p}{dt} dt = \int_0^t \frac{\bar{l}_{\mathrm{P}_{n\leq s}} k_1' [\mathrm{COOH}](t)}{[\mathrm{E}]_{t0} + [\mathrm{COOH}]_{t0}} dt. \tag{6.14}$$

Substituting the profile for $[\mathrm{COOH}](t)$ derived for the reaction-dominant limit in

Chapter 10 given by (10.69),

$$R_p(t) - R_p(0) = \int_0^t \frac{\bar{l}_{\mathrm{P}_{n\leq s}} k_1' [\mathrm{COOH}]_{t0} \exp(k_1' t)}{[\mathrm{E}]_{t0} + [\mathrm{COOH}]_{t0}} dt. \tag{6.15}$$

Evaluating the integral gives

$$\begin{aligned} R_p(t) - R_p(0) &= \frac{\bar{l}_{\mathrm{P}_{n\leq s}} [\mathrm{COOH}]_{t0} (\exp(k_1' t) - 1)}{[\mathrm{E}]_{t0} + [\mathrm{COOH}]_{t0}} \\ &= \frac{\bar{l}_{\mathrm{P}_{n\leq s}} ([\mathrm{COOH}](t) - [\mathrm{COOH}]_{t0})}{[\mathrm{E}]_{t0} + [\mathrm{COOH}]_{t0}}. \end{aligned} \tag{6.16}$$

The number-average molecular weight is inversely proportional to the carboxylic acid end group concentration:

$$\frac{[\mathrm{COOH}](t)}{[\mathrm{COOH}]_{t0}} = \frac{M_n^0}{M_n^t}. \tag{6.17}$$

The initial number-average degree of polymerization is equivalent to the ratio of the total number of repeat units in the polymer to the initial number of polymer chains:

$$N = \frac{[\mathrm{E}]_{t0} + [\mathrm{COOH}]_{t0}}{[\mathrm{COOH}]_{t0}}. \tag{6.18}$$

Substituting (6.17) and (6.18) into (6.16) gives

$$\begin{aligned} R_p(t) - R_p(0) &= \frac{\bar{l}_{\mathrm{P}_{n\leq s}} \left([\mathrm{COOH}]_{t0} \dfrac{M_n^0}{M_n^t} - [\mathrm{COOH}]_{t0} \right)}{[\mathrm{E}]_{t0} + [\mathrm{COOH}]_{t0}} \\ &= \frac{\bar{l}_{\mathrm{P}_{n\leq s}}}{N} \left(\frac{M_n^t}{M_n^0} - 1 \right), \end{aligned} \tag{6.19}$$

which matches (6.12). The equation for the pore radius derived here gives more flexibility for use with different kinetic models and for spatially-dependent reactions coupled to transport.

6.2 Variable Effective Diffusivity

To account for the two parallel modes of diffusion through pores, the effective diffusivity for species i is the sum of the contributions for diffusion through the dense polymer matrix and through the aqueous pores,

$$D_i(r,t) = D_{i,b} + D_{i,p}(r,t), \tag{6.20}$$

where $D_{i,b}$ denotes the effective diffusivity of species i in the bulk polymer and $D_{i,p}(r,t)$ denotes the variable effective diffusivity through the growing aqueous pores.

6.3 Hindered Diffusion through Aqueous Pores

The effective diffusivity, D_i, to describe the average diffusion at any position r for a gas diffusing through a macroporous spherical pellet considering tortuous pores of varying cross-sectional areas and accounting for the fact that not all of the area normal to flux is porous and available for molecules to diffuse [113] is given by [113, 114]

$$D_i = \frac{D_{i,\infty}\epsilon\delta}{\hat{\tau}}, \tag{6.21}$$

where $D_{i,\infty}$ is the molecular diffusion coefficient of species i in bulk solution at infinite dilution at 25°C, ϵ is the porosity defined as the ratio of the volume of void space or pore volume to the total volume of voids and solids, δ is the constrictivity accounting for the variation in the cross-sectional area normal to diffusion, and $\hat{\tau}$ is the length factor of the pores defined as the ratio of the actual distance a molecule travels by diffusion between two points to the shortest distance between those two points. The use of the effective diffusivity avoids the need to consider explicitly the complex three-dimensional particle internal pore structure [115]. Infinite dilution refers to the case where each solute molecule is surrounded by solvent molecules and

has no interactions with other solute molecules [109]. In physical systems, it is difficult to separate δ and $\hat{\tau}$ in experimental measurements, and the terms are often lumped together as a single tortuosity term τ [16, 116] that is generally used as a fudge factor [115]. The porosity, ϵ, represents the uniform mean-free-cross-section in any plane of the porous mass with random pore orientation [116]. Porosity does not give information about the connectedness or number of pores [109].

For liquid solutions in fine pores, additional terms are considered in the effective diffusivity [16, 117, 118]:

$$D_{i,p} = \frac{D_{i,\infty}\epsilon K_p K_r}{\tau}, \tag{6.22}$$

where $D_{i,p}$ is the effective diffusivity in the pores, $D_{i,\infty}$ is the molecular diffusion coefficient of solute species i in bulk solution at infinite dilution; ϵ is the porosity; K_p is the equilibrium partition coefficient defined as the ratio of concentration inside the pore to the concentration outside the pore at equilibrium and accounting for the steric, chemical, and electrostatic interactions between the solute, the solvent, and the pore walls; K_r is the fractional reduction in diffusivity within the pore resulting from hydrodynamic interactions between solutes of comparable magnitude to the pore size and the solvent molecules within the pore [109]; and τ is the tortuosity of the pores. In (6.22) the δ term from (6.21) is incorporated into τ to account for variations in pore length and shape from the ideal array of cylindrical pores oriented parallel to the diffusion path.

In the present work, the intraparticle concentrations, not just cumulative release, are of interest and the pore structure develops with time, so the effective diffusivity is determined as a function of radial position and time. The effective diffusivity within the aqueous pores, $D_{i,p}(r,t)$, for a diffusing species i—the drug or small polyester oligomers and monomers—within a microsphere with evolving

porous microstructure in an aqueous medium can be calculated using [55]

$$D_{i,p}(r,t) = \frac{D_{i,\infty} H(\lambda_i(r,t))}{\tau}, \tag{6.23}$$

where $D_{i,\infty}$ is the molecular diffusion coefficient of species i in water at infinite dilution; $H(\lambda_i(r,t))$ is the hindrance factor accounting for porosity, equilibrium partitioning, and hydrodynamic restrictions on the diffusion of solute species i in fine, liquid-filled pores; $\lambda_i(r,t)$ is the ratio of the solute radius to the dynamic pore radius; and τ is the average tortuosity of the pores. The following subsections explain each of the terms and how they are determined in the present work.

6.3.1 Diffusion Coefficients at Infinite Dilution

The values of the molecular diffusion coefficients at infinite dilution in water, $D_{i,\infty}$, for many drug compounds, lactic acid, and glycolic acid are reported in the literature. Polymers of lactic and glycolic acid are hydrophobic with lactic moieties being more hydrophobic than glycolic moieties because of the presence of a methyl group rather than a hydrogen atom in the lactic monomeric unit [65]. The monomers and small oligomers of lactic and glycolic acid are hydrophilic, so they favor dissolution into the aqueous pores over staying in the polymer bulk after their formation from ester bond cleavage. The diffusion coefficients at infinite dilution for all the small oligomers and monomers are assumed to be equal to the weighted-average of the diffusion coefficients at infinite dilution for lactic acid and glycolic acid. Table 6.1 lists the diffusion coefficients at infinite dilution for several small molecules and proteins.

6.3.2 Tortuosity

Pores are general treated as straight cylinders of uniform diameter with axes parallel to the direction of mean diffusive transport. The tortuosity accounts for

Table 6.1: Diffusion coefficients at infinite dilution in water.

Chemical	$D_{i,\infty}(10^7 \mathrm{cm}^2/\mathrm{s})$	Reference
H^+	931	[119]
Lactic Acid	104	[120]
Glycolic Acid	98.0	[121]
[a]Glucose	69.0	[122]
Lysozyme	11.3	[109]
Ovalbumin	7.76	[123]
Hemoglobin	6.9	[123]
Human Serum Albumin	6.10	[124]
Bovine Serum Albumin	5.94	[123]
Fibronogen	2.0	[109]

Reference temperature: [a]25°C, all others 20°C.

deviations in shape and length of the pores that have varying cross-sections and axes not strictly aligned with the mean direction of diffusion from the porous medium. An isotropic, constant tortuosity is assumed, and typical values of τ are 2-4 [125]. The τ value of 3 is used here as it facilitates comparison to the growth of effective diffusivity predicted by [55] and is adequate for predicting effective diffusivity from macroporous catalysts [16].

6.3.3 Hindrance Factor

$H(\lambda_i)$ is the diffusional hindrance factor for solutes in pores filled with liquid solvent where the size of the solute molecules is comparable to the size of the pores and the solvent is treated as a continuum. The molecular diffusion coefficient of the solute at infinite dilution in the solvent is reduced by factors that account for steric partitioning and hydrodynamic hindrances that result from diffusive flow through fine pores [101]. Large molecules are known to experience hindered diffusion in aqueous pores of molecular dimensions [126]. Steric, chemical, and electrostatic equilibrium partitioning between the pores, solute, and solvent and the hydrodynamics effects on the Brownian motion of the solute within the solvent-filled pore contribute to $H(\lambda_i(r,t))$ [101].

The hindrance factor for diffusion of a rigid, spherical molecule of solute i in

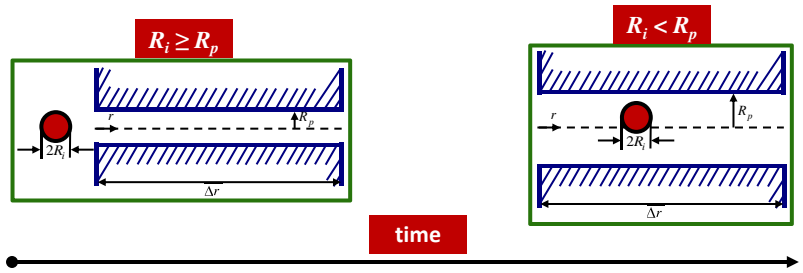

Figure 6.1: Pore evolution with growing pore radius, R_p, compared to solute radius, R_i.

a straight cylindrical pore is given by [126, 127]

$$H(\lambda_i(r,t)) = \Phi_i(\lambda_i(r,t))K_{d_i}(\lambda_i(r,t)), \quad 0 \leq \lambda_i(r,t) \leq 1, \tag{6.24}$$

where

$$\lambda_i(r,t) := \frac{R_i}{R_p(r,t)}, \tag{6.25}$$

R_i and $R_p(r,t)$ are the radii of the diffusing species i and the growing pore, respectively, as illustrated in Figure 6.1, $\Phi(\lambda_i(r,t))$ is the partition coefficient, and $K_d(\lambda_i(r,t))$ is the local hindrance factor for diffusion with [127]

$$K_d(\lambda_i(r,t)) = \frac{2}{(1-\lambda_i(r,t))^2}\int_0^{1-\lambda_i(r,t)} \frac{\beta d\beta}{K(\lambda_i(r,t),\beta)}, \tag{6.26}$$

where β is the dimensionless coordinate normal to the axis of the cylindrical pore scaled by the pore radius and $K(\lambda_i(r,t),\beta)$ is the enhanced drag coefficient relative to the unbounded fluid determined from the solution for the Stokes flow case of continuum hydrodynamics for a spherical solute with size ratio $\lambda_i(r,t)$ located at distance β relative to the centerline of the pore.

When the diameter of the solute is larger than the diameter of the pore, the solute is too large to enter the pore, and the diffusion is completely hindered so $H(\lambda_i(r,t)) = 0$ when $\lambda_i(r,t) > 1$. When the diameter of the solute is smaller than the diameter of the pore, only a portion of the cross-sectional area of the pore is

accessible to the center of the sphere as steric exclusion of the sphere occurs near the pore walls. The partition coefficient is defined as the ratio of the average intrapore concentration to that in bulk solution at equilibrium. For purely steric interactions between solute i and the pore walls [126],

$$\Phi(\lambda_i(r,t)) = (1-\lambda_i(r,t))^2 . \tag{6.27}$$

The use of the purely steric $\Phi(\lambda_i(r,t))$ is a reasonable assumption for molecules that favor partitioning into the aqueous porous phase over the polymeric phase, such as the hydrophilic small oligomers and monomers and hydrophilic drug compounds.

The diffusivity of a solid sphere of radius R_i in a dilute solution with no bulk motion is given by the Stokes-Einstein equation [98]:

$$D_{i,\infty} = \frac{k_B T}{f_S} = \frac{k_B T}{6\pi\eta R_i}, \tag{6.28}$$

where k_B is Boltzmann's constant, T is the absolute temperature, f_S is the drag coefficient from Stokes' law, η is the solvent viscosity, and R_i is the effective radius of solute i. The drug molecular radius is approximated by the radius of a sphere that would have the same value of the binary diffusivity of the drug in water at infinite dilution as calculated by the Stokes-Einstein equation (6.28). This is a common approximation for the radius of the solute [45, 55, 128]. The small oligomer and monomer radii are taken to be their linear polymer chain length, nl_{ave}, where n is the number of repeat units in the oligomer P_n and l_{ave} is the length of the average of the monomers in the polymer or copolymer. The radius of gyration for flexible polymers could be used instead for the soluble oligomers and macromolecular drugs as the steric partitioning coefficients for flexible polymers differ from those for spherical molecules [109]. However, closed-form, nonempirical expressions are not available for the hydrodynamic terms for flexible polymers in cylindrical pores. All diffusing species are treated as spherical solutes due to the availability of

expressions for hindered diffusion for spheres diffusing in liquid-filled cylinders.

Many derivations of $K(\lambda_i(r,t),\beta)$ have been presented and reviewed in the literature for the hydrodynamic drag on a sphere moving parallel to the axis of a cylindrical pore with constant values of $\lambda_i(r,t)$ [101, 126, 127, 129, 130]. Functions are available for both quiescent and flowing fluid solvents in the pore. The axisymmetric case with the solute positioned along the centerline of the pore as it translates is the most well-understood. Assuming all spheres are distributed along the centerline position in the pore allows for the centerline approximation: $K(\lambda_i(r,t),\beta) \approx K(\lambda_i(r,t),0)$ [109, 126].

Stokes' law gives the drag force, F_{D_i}, on a sphere of solute i in an unbounded fluid creeping at a constant velocity [98]:

$$F_{D_i} = 6\pi\eta R_i U = f_S U, \tag{6.29}$$

where η is the viscosity of the fluid, R_i is the solute radius, U is the velocity, and f_S is the drag coefficient. Faxen [131] solved the hydrodynamic equations with the influence of a solid wall near the sphere to give the enhanced drag force at the centerline of a cylindrical tube [129, 132]:

$$F_{D_i} = \frac{6\pi\eta R_i U}{f_F} = \frac{f_S U}{f_F}, \tag{6.30}$$

where $\dfrac{1}{f_F}$ is the centerline enhanced drag coefficient, $K(\lambda_i(r,t),0)$, with f_F given by

$$f_F(\lambda_i(r,t)) \approx 1 - 2.104\lambda_i(r,t) + 2.09\lambda_i(r,t)^3 - 0.95\lambda_i(r,t). \tag{6.31}$$

Renkin [128] used Faxen's $\dfrac{1}{f_F} = K(\lambda_i(r,t),0)$ in (6.26) with the centerline approximation to determine $K_d(\lambda_i(r,t)) = f_F$ as the local hindrance factor for diffusion. The partition coefficient due to purely steric interactions given by (6.27) was combined with f_F to obtain the popular Renkin equation for hindered diffusion

valid for $0 < \lambda_i(r,t) < 0.4$ [128]:

$$H(\lambda_i(r,t)) = (1-\lambda_i(r,t))^2\left(1 - 2.104\lambda_i(r,t) + 2.09\lambda_i(r,t)^3 - 0.95\lambda_i(r,t)^5\right). \quad (6.32)$$

The limited validity of the Renkin equation is suitable when studying solutes in pores of constant radii within the range of $\lambda_i(r,t)$ values.

In the present work, the entire range of $0 \leq \lambda_i(r,t) \leq 1$ is needed to characterize the pore growth with polymer degradation. Bungay and Brenner developed an enhanced drag coefficient accurate within 1% for the full $\lambda_i(r,t)$ range using the centerline approximation [133]:

$$K(\lambda_i(r,t),0) = \frac{K_t(\lambda_i(r,t))}{6\pi}, \quad (6.33)$$

where $K_t(\lambda_i(r,t))$ is the resistance coefficient for a sphere translating through a quiescent fluid along the centerline of a cylindrical pore. Integrating (6.26) gives

$$K_d(\lambda_i(r,t)) = \frac{6\pi}{K_t(\lambda_i(r,t))} \quad (6.34)$$

and using the partition coefficient due to purely steric interactions given by (6.27),

$$H(\lambda_i(r,t)) = \frac{6\pi\left(1-\lambda_i(r,t)\right)^2}{K_t(\lambda_i(r,t))}, \quad 0 \leq \lambda_i(r,t) \leq 1, \quad (6.35)$$

where the hydrodynamic coefficient $K_t(\lambda_i(r,t)))$ derived by Bungay and Brenner is [126, 133]

$$\begin{aligned} K_t(\lambda_i(r,t)) = {} & \frac{9\pi^2\sqrt{2}}{4}\left(1-\lambda_i(r,t)\right)^{-5/2}\left(1 + \sum_{j=1}^{2} a_j\left(1-\lambda_i(r,t)\right)^j\right) \\ & + \sum_{j=0}^{4} a_{j+3}\lambda_i(r,t)^j, \end{aligned} \quad (6.36)$$

where the coefficients a_j are $a_1 = -73/60$, $a_2 = 77293/50400$, $a_3 = -22.5083$,

$a_4 = -5.6117$, $a_5 = -0.3363$, $a_6 = -1.216$, and $a_7 = 1.647$.

Equations for the hindrance factor including radial dependence on the enhanced drag without using the centerline approximation are available [127]. The equation with the widest range of λ was developed by Dechadilok and Deen [127] by taking a least-squares fit to the hydrodynamic results from Mavrovounitis and Brenner [134] as $\lambda \to 1$ and the off-axis hydrodynamic numerical results for $K_i(\lambda, \beta)$ over all radial positions for $0 \leq \lambda \leq 0.9$ developed by Higdon and Muldowney [135]. The resulting expression is recommended by Dechadilok and Deen for use for a wide range of relative particle sizes for diffusion in cylindrical pores [127]; however, the Bungay and Brenner expression [133] given by (6.35) is used in the present work as it is derived from the numerical approximation to an analytical solution rather than a least-squares fit to multiple numerical solutions. Also, the Bungay and Brenner hindrance factor is reported to have 1% accuracy [133], while the Dechadilok and Deen hindrance factor is reported to have only 2% accuracy [127].

Chapter 7

Partial Differential Equations of the Model

In this chapter, the reaction and diffusion contributions to the model developed in Chapters 4, 5, and 6 are combined, and the system of partial differential equations (PDEs) constituting the model are delineated. The system of PDEs is numerically solved using the numerical methods described in Chapter 8 to model controlled-release drug delivery from polyester microspheres that are known to exhibit autocatalytic, size-dependent degradation behavior.

Species concentrations as functions of position and time with spatial variation can be determined using the general form of the conservation equation in Chapter 4 with the net generation terms derived in Chapter 5 for the four kinetic rate laws for hydrolysis and the diffusion contribution from the transport of soluble species with the effective diffusivities of soluble oligomers, monomers, and drug derived in Chapter 6. The PDE for updating the average pore radius, $R_p(r,t)$, in the equation for the effective diffusivity is given in Section 7.1, and the PDE for updating the variable effective diffusivity, $D_i(r,t)$, in the conservation equation is given in Section 7.2. The conservation equations for the drug; the carboxylic acid end groups, COOH; the ester bonds, E; the small polymer chains, P_n, for $n = 1, 2, \ldots, s$; and the sum of the large oligomers, $\mathrm{P}_{n>s}$, are presented as PDEs in Sections 7.3–7.7. The net rates of generation of each of the reacting species derived in Chapter 5 for the four hydrolysis rate laws are summarized in Section 7.8.

Small oligomers are those polymer chains, P_n, with $n \leq s$ for integer values of n, and large oligomers are those with $n \geq s+1$. In the present work, the

oligomers from monomers to nonamers ($s = 9$) are considered as soluble, small oligomers for PLGA. s is an adjustable parameter in the simulation code and can be modified according to the solubility information available. It is assumed that the soluble polymers are completely soluble and that the insoluble polymer chains are not at all soluble. The large oligomers are treated as a lumped sum as discussed in Section 7.7. By eliminating the need to solve the conservation equations explicitly for each polymer chains with $n > s$, the number of PDEs in the system is reduced from order N, where N is a very large number representing the maximum degree of polymerization for truncating the infinite sum to $2NS + 1$, where NS is the number of species equal to $s + 4$ for the s small oligomers and the lumped sum of the concentrations of the large oligomers, COOH, E, and drug. Each species has a corresponding PDE for updating the value of $D_i(r, t)$. A single PDE is used to update $R_p(r, t)$.

Recall the conservation equation for species i from (4.8),

$$\frac{\partial c_i(r,t)}{\partial t} = \frac{1}{r^2}\frac{\partial}{\partial r}\left(r^2 \frac{D_i(r,t)}{R^2}\frac{\partial c_i(r,t)}{\partial r}\right) + R_{Vi}(r,t) \tag{7.1}$$

with initial condition

$$c_i(r,0) = c_{i,t0}(r), \quad 0 \le r < 1 \tag{7.2}$$

and boundary conditions

$$\frac{\partial c_i(0,t)}{\partial r} = 0, \quad t \ge 0 \tag{7.3}$$

and

$$c_i(1,t) = c_{i,r1}, \quad t \ge 0. \tag{7.4}$$

7.1 Pore Radius

Recall (6.11),

$$\boxed{\frac{\partial R_p(r,t)}{\partial t} = \frac{\bar{l}_{\mathrm{P}_{n\leq s}} R_{V\mathrm{COOH}}(r,t)}{[\mathrm{E}]_{t0}(r) + [\mathrm{COOH}]_{t0}(r)},} \tag{7.5}$$

with initial condition

$$R_p(r,0) = R_{p,t0}, \quad 0 \leq r < 1 \tag{7.6}$$

and boundary conditions

$$\frac{\partial R_p(0,t)}{\partial r} = 0, \quad t \geq 0 \tag{7.7}$$

and

$$R_p(1,t) = 0, \quad t \geq 0, \tag{7.8}$$

where $\bar{l}_{\mathrm{P}_{n\leq s}}$ is the average length of a water-soluble, small oligomer given by

$$\bar{l}_{\mathrm{P}_{n\leq s}} = \frac{l_{\mathrm{ave}} s(s+1)}{2}, \tag{7.9}$$

$l_{\mathrm{ave}} = G l_G + (1-G) l_L$, G is the fraction of glycolide in the copolymer, $l_G = 3.510$ Å and $l_L = 3.517$ Å, s is the number of repeat units in the largest soluble oligomer, $R_{V\mathrm{COOH}}(r,t)$ is the net rate of generation of carboxylic acid end groups listed for four hydrolysis rate laws in Section 7.8, and $[\mathrm{E}]_{t0}(r)$ and $[\mathrm{COOH}]_{t0}(r)$ are the initial concentration distributions of ester bonds and carboxylic acid end groups, respectively.

7.2 Effective Diffusivity

Recall (6.20),

$$D_i(r,t) = D_{i,b} + D_{i,p}(r,t), \tag{7.10}$$

where $D_{i,b}$ denotes the effective diffusivity of species i in the bulk polymer and $D_{i,p}(r,t)$ denotes the variable effective diffusivity through the growing aqueous

pores.

Recall (6.23),

$$D_{i,p}(r,t) = \frac{D_{i,\infty} H(\lambda_i(r,t))}{\tau}, \tag{7.11}$$

where $D_{i,\infty}$ is the molecular diffusion coefficient of species i in water at infinite dilution; $H(\lambda_i(r,t))$ is the hindrance factor accounting for porosity, equilibrium partitioning, and hydrodynamic restrictions on the diffusion of solute species i in fine, liquid-filled pores; $\lambda_i(r,t)$ is the ratio of the solute radius to the dynamic pore radius; and τ is the average tortuosity of the pores, assumed to be 3.

Recall (6.35),

$$H(\lambda_i(r,t)) = \frac{6\pi \left(1-\lambda_i(r,t)\right)^2}{K_t(\lambda_i(r,t))}, \quad 0 \le \lambda_i(r,t) \le 1, \tag{7.12}$$

where

$$\lambda_i(r,t) := \frac{R_i}{R_p(r,t)}, \tag{7.13}$$

R_i and $R_p(r,t)$ are the radii of the diffusing species i and the growing pore, respectively, and the hydrodynamic coefficient $K_t(\lambda_i(r,t))$ is given by (6.36),

$$\begin{aligned} K_t(\lambda_i(r,t)) = \frac{9\pi^2\sqrt{2}}{4} \left(1-\lambda_i(r,t)\right)^{-5/2} \left(1 + \sum_{j=1}^{2} a_j \left(1-\lambda_i(r,t)\right)^j\right) \\ + \sum_{j=0}^{4} a_{j+3} \lambda_i(r,t)^j, \end{aligned} \tag{7.14}$$

with the coefficients a_j: $a_1 = -73/60$, $a_2 = 77293/50400$, $a_3 = -22.5083$, $a_4 = -5.6117$, $a_5 = -0.3363$, $a_6 = -1.216$, and $a_7 = 1.647$.

To update the effective diffusivity during calls to the numerical solver, the effective diffusivity must be formulated as a PDE with respect to time. The first partial derivative of $D_i(r,t)$ with respect to t is

$$\boxed{\frac{\partial D_i(r,t)}{\partial t} = \frac{\partial D_{i,p}(r,t)}{\partial t} = \frac{D_{i,\infty}}{\tau} \frac{dH}{d\lambda_i} \frac{\partial \lambda_i(r,t)}{\partial t},} \tag{7.15}$$

with initial condition

$$D_i(r,0) = D_{i,b}, \quad 0 \leq r < 1 \tag{7.16}$$

and boundary conditions

$$\frac{\partial D_i(0,t)}{\partial r} = 0, \quad t \geq 0 \tag{7.17}$$

and

$$D_i(1,t) = 0, \quad t \geq 0, \tag{7.18}$$

where $D_{i,b}$ is the effective diffusivity of species i in the bulk polymer, $D_{i,\infty}$ is the molecular diffusion coefficient of species i in water at infinite dilution, $\tau = 3$ is the average tortuosity of the pores, $\lambda_i(r,t)$ is the ratio of the solute radius to the pore radius and is defined by (7.13), the partial derivative of $\lambda_i(r,t)$ with respect to t is

$$\frac{\partial \lambda_i(r,t)}{\partial t} = \frac{-R_i}{R_p(r,t)^2} \frac{\partial R_p(r,t)}{\partial t}, \tag{7.19}$$

the partial derivative of $R_p(r,t)$ with respect to t is given by (7.5), the derivative of $H(\lambda_i)$ is

$$\frac{dH}{d\lambda_i} = \frac{-12\pi(1-\lambda_i(r,t))K_t(\lambda_i(r,t)) - 6\pi\left(1-\lambda_i(r,t)\right)^2 \frac{dK_t}{d\lambda_i}}{\left(\frac{dK_t}{d\lambda_i}\right)^2}, \tag{7.20}$$

the hydrodynamic coefficient $K_t(\lambda_i(r,t))$ is given by (7.14), and the derivative of $K_t(\lambda_i)$ is

$$\begin{aligned} \frac{dK_t}{d\lambda_i} = {} & \frac{-45\pi^2\sqrt{2}}{8}\left(1-\lambda_i(r,t)\right)^{-7/2}\left(1+\sum_{j=1}^{2} a_j\left(1-\lambda_i(r,t)\right)^j\right) \\ & - \frac{9\pi^2\sqrt{2}}{4}\left(1-\lambda_i(r,t)\right)^{-5/2}\sum_{j=1}^{2} j a_j\left(1-\lambda_i(r,t)\right)^{j-1} \\ & + \sum_{j=1}^{4} j a_{j+3}\lambda_i(r,t)^{j-1}. \end{aligned} \tag{7.21}$$

7.3 Drug Concentration

The conservation equation for the drug, $[\text{drug}](r,t)$, with no net generation term ($R_{V\,\text{drug}}(r,t) \equiv 0$) is given by (4.12),

$$\boxed{\frac{\partial[\text{drug}](r,t)}{\partial t} = \frac{1}{r^2}\frac{\partial}{\partial r}\left(r^2 \frac{D_{\text{drug}}(r,t)}{R^2}\frac{\partial[\text{drug}](r,t)}{\partial r}\right),} \tag{7.22}$$

with initial condition

$$[\text{drug}](r,0) = [\text{drug}]_{t0}(r), \quad 0 \le r < 1 \tag{7.23}$$

and boundary conditions

$$\frac{\partial[\text{drug}](0,t)}{\partial r} = 0, \quad t \ge 0 \tag{7.24}$$

and

$$[\text{drug}](1,t) = [\text{drug}]_{r1}, \quad t \ge 0 \tag{7.25}$$

and the constraint

$$[\text{drug}]_{r1} < [\text{drug}]_{t0}(r), \tag{7.26}$$

where the effective diffusivity of the drug, $D_{\text{drug}}(r,t)$, is calculated using the equations of Section 7.2. The concentrations of the drug at time $t = 0$ must not be the same as the concentration at the surface $r = 1$ for all interior radial points because the concentration difference is the driving force for the diffusion process without a generation term. The surface concentration must be less than the initial concentration for net flux in the direction of increasing r toward the exterior of the sphere: $[\text{drug}]_{r1} < [\text{drug}]_{t0}(r)$.

7.4 Carboxylic Acid End Group Concentration

The carboxylic acid end group concentration, $[\mathrm{COOH}](r,t)$, can be tracked using the conservation equation with the net rate of generation term, $R_{V\mathrm{COOH}}(r,t)$, for the appropriate kinetic rate law summarized in Section 7.8. Recall that each polymer chain has one carboxylic acid end group, so the relationship between the polymer chain concentration and the carboxylic acid end group concentration is

$$[\mathrm{COOH}](t) = \sum_{n=1}^{\infty} [\mathrm{P}_n](t). \tag{7.27}$$

With stationary, insoluble, large oligomers, the effective diffusivity for P_n for integers $n > s$ is assumed to be zero. In the conservation equations for each of the large oligomers, the accumulation term is equal to the net rate of generation term. The transport of carboxylic acid end groups is only due to transport of small oligomers. The diffusion term of the conservation equation for COOH is equivalent to the sum of the diffusion terms for the small oligomers:

$$\frac{1}{r^2}\frac{\partial}{\partial r}\left(r^2 \frac{D_{\mathrm{COOH}}(r,t)}{R^2}\frac{\partial [\mathrm{COOH}](r,t)}{\partial r}\right) = \sum_{n=1}^{s} \frac{1}{r^2}\frac{\partial}{\partial r}\left(r^2 \frac{D_{\mathrm{P}_n}(r,t)}{R^2}\frac{\partial [\mathrm{P}_n](r,t)}{\partial r}\right). \tag{7.28}$$

The conservation equation for COOH is

$$\boxed{\frac{\partial [\mathrm{COOH}](r,t)}{\partial t} = \sum_{n=1}^{s} \frac{1}{r^2}\frac{\partial}{\partial r}\left(r^2 \frac{D_{\mathrm{P}_n}(r,t)}{R^2}\frac{\partial [\mathrm{P}_n](r,t)}{\partial r}\right) + R_{V\mathrm{COOH}}(r,t),} \tag{7.29}$$

with initial condition

$$[\mathrm{COOH}](r,0) = [\mathrm{COOH}]_{t0}(r), \quad 0 \le r < 1 \tag{7.30}$$

and boundary conditions

$$\frac{\partial [\mathrm{COOH}](0,t)}{\partial r} = 0, \quad t \ge 0 \tag{7.31}$$

and

$$[\mathrm{COOH}](1,t) = [\mathrm{COOH}]_{r1}, \quad t \geq 0 \tag{7.32}$$

with $D_{\mathrm{P}_n}(r,t)$, the effective diffusivity of the small oligomers of length n, calculated using the equations of Section 7.2 and $R_{V\mathrm{COOH}}(r,t)$, the net rate of generation of carboxylic acid end groups from the hydrolysis reaction, given by (5.15), (5.21), (5.28), and (5.45) for the four hydrolysis rate laws.

7.5 Ester Bond Concentration

The ester bond concentration, $[\mathrm{E}](r,t)$, can be tracked using the conservation equation with the net rate of generation term, $R_{V\mathrm{E}}(r,t)$, for the appropriate kinetic rate law summarized in Section 7.8. Recall that each polymer chain of length n has $n-1$ ester bonds, so the relationship between the polymer chain concentration and the ester bond concentration is

$$[\mathrm{E}](t) = \sum_{n=1}^{\infty}(n-1)[\mathrm{P}_n](t). \tag{7.33}$$

With stationary, insoluble, large oligomers, the effective diffusivity for P_n for integers $n > s$ is assumed to be zero. In the conservation equations for each of the large oligomers, the accumulation term is equal to the net rate of generation term. The transport of ester bonds is only due to transport of small oligomers. The diffusion term of the conservation equation for E is equivalent to the sum of the diffusion terms for the small oligomers multiplied by the factor $n-1$:

$$\frac{1}{r^2}\frac{\partial}{\partial r}\left(r^2\frac{D_{\mathrm{E}}(r,t)}{R^2}\frac{\partial[\mathrm{COOH}](r,t)}{\partial r}\right) = \sum_{n=1}^{s}(n-1)\frac{1}{r^2}\frac{\partial}{\partial r}\left(r^2\frac{D_{\mathrm{P}_n}(r,t)}{R^2}\frac{\partial[\mathrm{P}_n](r,t)}{\partial r}\right). \tag{7.34}$$

The conservation equation for E is

$$\boxed{\frac{\partial[\mathrm{E}](r,t)}{\partial t} = \sum_{n=1}^{s}(n-1)\frac{1}{r^2}\frac{\partial}{\partial r}\left(r^2\frac{D_{\mathrm{P}_n}(r,t)}{R^2}\frac{\partial[\mathrm{P}_n](r,t)}{\partial r}\right) + R_{V\mathrm{E}}(r,t),} \tag{7.35}$$

with initial condition

$$[\mathrm{E}](r,0) = [\mathrm{E}]_{t0}(r), \quad 0 \le r < 1 \tag{7.36}$$

and boundary conditions

$$\frac{\partial[\mathrm{E}](0,t)}{\partial r} = 0, \quad t \ge 0 \tag{7.37}$$

and

$$[\mathrm{E}](1,t) = [\mathrm{E}]_{r1}, \quad t \ge 0 \tag{7.38}$$

with $D_{\mathrm{P}_n}(r,t)$, the effective diffusivity of the small oligomers of length n, calculated using the equations of Section 7.2 and $R_{V\mathrm{E}}(r,t)$, the net rate of generation of ester bonds from the hydrolysis reaction, given by (5.17), (5.24), (5.29), and (5.46) for the four hydrolysis rate laws.

7.6 Small Oligomer Concentration

The small oligomer concentration, $[\mathrm{P}_n](r,t)$, can be tracked using the conservation equation with the net rate of generation term, $R_{V\mathrm{P}_n}(r,t)$, for the appropriate kinetic rate law summarized in Section 7.8. The conservation equation for each water-soluble, small oligomer, $\mathrm{P_n}$, for $n = 1, 2, \ldots, s$ is

$$\boxed{\frac{\partial[\mathrm{P}_n](r,t)}{\partial t} = \frac{1}{r^2}\frac{\partial}{\partial r}\left(r^2\frac{D_{\mathrm{P}_n}(r,t)}{R^2}\frac{\partial[\mathrm{P}_n](r,t)}{\partial r}\right) + R_{V\mathrm{P}_n}(r,t),} \tag{7.39}$$

with initial condition

$$[\mathrm{P}_n](r,0) = 0, \quad 0 \le r < 1 \tag{7.40}$$

and boundary conditions

$$\frac{\partial[\mathrm{P}_n](0,t)}{\partial r} = 0, \quad t \geq 0 \tag{7.41}$$

and

$$[\mathrm{P}_n](1,t) = [\mathrm{P}_n]_{r1}, \quad t \geq 0, \tag{7.42}$$

with $D_{\mathrm{P}_n}(r,t)$, the effective diffusivity of the small oligomers of length n, calculated using the equations of Section 7.2 and $R_{V\mathrm{P}_n}(r,t)$, the net rate of generation of polymer chains from the hydrolysis reaction, given by (5.6), (5.23), (5.27), and (5.43) for the four hydrolysis rate laws.

7.7 Large Oligomer Concentration

To save computations for explicitly calculating the full distribution of P_n for $n = 1, 2, \ldots$, a method has been developed to explicitly track only the small oligomer concentrations and a lumped sum of large oligomer concentrations. The full distribution of P_n is not of particular interest in the present work as the drug cumulative release profile is the quantity that can be validated with experimental results. The carboxylic acid end group and small oligomer concentrations are needed to determine the evolution of the pore network in the microparticle to determine the effective diffusivities of the drug and small oligomers, as discussed in Chapter 6 and summarized in Section 7.2.

For all of the kinetic mechanisms presented in Chapter 5 and summarized in Section 7.8, the net rate of generation term for each polymer chain, $R_{V\mathrm{P}_n}(r,t)$, depends on the concentration of the polymer chain of length n, $[\mathrm{P}_n](r,t)$, and the sum of the concentrations of all polymer chains longer than n, $\sum_{i=n+1}^{\infty} [\mathrm{P}_i](r,t)$. The summation can be divided into the contribution from small oligomers, with the

longest soluble oligomer having length s, and large oligomers:

$$\sum_{i=n+1}^{\infty} [\mathrm{P}_i](r,t) = \sum_{i=n+1}^{s} [\mathrm{P}_i](r,t) + \sum_{i=s+1}^{\infty} [\mathrm{P}_i](r,t). \tag{7.43}$$

The net rate of generation term for each of the small oligomers depends on a subset of the concentrations of the other small oligomers and the sum of the concentrations of the large oligomers. The sum of the concentrations of the large oligomers is denoted by

$$[\mathrm{P}_{n>s}](r,t) := \sum_{i=s+1}^{\infty} [\mathrm{P}_i](r,t). \tag{7.44}$$

An alternate PDE for the carboxylic acid end group concentration can be formulated as

$$\frac{\partial [\mathrm{COOH}](r,t)}{\partial t} = \frac{\partial}{\partial t} \sum_{n=1}^{\infty} [\mathrm{P}_n](r,t). \tag{7.45}$$

Splitting the summation into small and large oligomers and using the notation for the sum of the concentrations of large oligomers gives

$$\begin{aligned} \frac{\partial [\mathrm{COOH}](r,t)}{\partial t} &= \frac{\partial}{\partial t} \sum_{n=1}^{s} [\mathrm{P}_n](r,t) + \frac{\partial}{\partial t} \sum_{n=s+1}^{\infty} [\mathrm{P}_n](r,t) \\ &= \sum_{n=1}^{s} \frac{\partial [\mathrm{P}_n](r,t)}{\partial t} + \frac{\partial [\mathrm{P}_{n>s}](r,t)}{\partial t}. \end{aligned} \tag{7.46}$$

Solving for the change in the sum of the concentrations of the large oligomers gives

$$\frac{\partial [\mathrm{P}_{n>s}](r,t)}{\partial t} = \frac{\partial [\mathrm{COOH}](r,t)}{\partial t} - \sum_{n=1}^{s} \frac{\partial [\mathrm{P}_n](r,t)}{\partial t}. \tag{7.47}$$

The COOH and P_n accumulation terms are known from the conservation equations, (7.29) and (7.39), respectively. The diffusion terms for the carboxylic acid end groups and the small oligomers cancel using (7.28), so the conservation

equation for $\mathrm{P}_{n>s}$ is

$$\boxed{\frac{\partial[\mathrm{P}_{n>s}](r,t)}{\partial t} = R_{V\mathrm{COOH}}(r,t) - \sum_{n=1}^{s} R_{V\mathrm{P}_n}(r,t).} \tag{7.48}$$

Assuming that the initial concentrations of all the small oligomers are zero, the initial condition for (7.48) is

$$[\mathrm{P}_{n>s}](r,0) = [\mathrm{COOH}](r,0), \quad 0 \leq r < 1. \tag{7.49}$$

The assumption is reasonable for polymers with moderate to high molecular weight. The boundary conditions are

$$\frac{\partial[\mathrm{P}_{n>s}](0,t)}{\partial r} = 0, \quad t \geq 0 \tag{7.50}$$

and

$$[\mathrm{P}_{n>s}](1,t) = [\mathrm{P}_{n>s}]_{r1}, \quad t \geq 0. \tag{7.51}$$

The net rate of generation of carboxylic acid end groups from the hydrolysis reaction, $R_{V\mathrm{COOH}}(r,t)$, is given by (5.15), (5.21), (5.28), and (5.45) and the net rate of generation of small oligomers of length n from the hydrolysis reaction, $R_{V\mathrm{P}_n}(r,t)$, is given by (5.6), (5.23), (5.27), and (5.43) for the four hydrolysis rate laws.

7.8 Summary of Net Rate of Generation Terms

The net rate of generation terms for the polymer chains, $R_{V\mathrm{P}_n}(r,t)$, the carboxylic acid end groups, $R_{V\mathrm{COOH}}(r,t)$, and the ester bonds, $R_{V\mathrm{E}}(r,t)$, derived in Chapter 5 for each of the four polymer hydrolysis rate laws are summarized here.

- First-Order Rate Law for Uncatalyzed Hydrolysis

  - Net Rate of Generation of Polymer Chains: $R_{V\mathrm{P}_n}(r,t)$

    Recall (5.6),

$$R_{V\mathrm{P}_n}(r,t) = 2k'_u \sum_{m=n+1}^{\infty} [\mathrm{P}_m](r,t) - (n-1)\, k'_u [\mathrm{P}_n](r,t), \qquad n = 1,\, 2,\, \ldots, \tag{7.52}$$

    where $k'_u := k_u[\mathrm{H_2O}]$, k_u is the rate constant for the uncatalyzed hydrolysis reaction, $[\mathrm{H_2O}]$ is the constant concentration of water, and $[\mathrm{P}_n](r,t)$ is the concentration of polymer chains with a number-average degree of polymerization n.

  - Net Rate of Generation of Carboxylic Acid End Groups: $R_{V\mathrm{COOH}}(r,t)$

    Recall (5.15),

$$R_{V\mathrm{COOH}}(r,t) = k'_u[\mathrm{E}](r,t), \tag{7.53}$$

    where $k'_u := k_u[\mathrm{H_2O}]$, k_u is the rate constant for the uncatalyzed hydrolysis reaction, $[\mathrm{H_2O}]$ is the constant concentration of water, and $[\mathrm{E}](r,t)$ is the total ester bond concentration of the polymer.

  - Net Rate of Generation of Ester Bonds: $R_{V\mathrm{E}}(r,t)$

    Recall (5.17),

$$R_{V\mathrm{E}}(r,t) = -k'_u[\mathrm{E}](r,t), \tag{7.54}$$

    where $k'_u := k_u[\mathrm{H_2O}]$, k_u is the rate constant for the uncatalyzed hydrolysis reaction, $[\mathrm{H_2O}]$ is the constant concentration of water, and $[\mathrm{E}](r,t)$ is the total ester bond concentration of the polymer.

- Pseudo-First-Order Rate Law for Autocatalytic Hydrolysis

  - Net Rate of Generation of Polymer Chains: $R_{V\mathrm{P}_n}(r,t)$

    Recall (5.23),

$$R_{V\mathrm{P}_n}(r,t) = \frac{k_1'[\mathrm{COOH}](r,t)}{[\mathrm{E}]} \times \left(2 \sum_{m=n+1}^{\infty} [\mathrm{P}_m](r,t) - (n-1)\,[\mathrm{P}_n](r,t) \right), \qquad (7.55)$$

$$n = 1,\, 2,\, \ldots,$$

    where $k_1' := k_c[\mathrm{H_2O}][\mathrm{E}]$, k_c is the rate constant for the autocatalytic hydrolysis reaction, $[\mathrm{H_2O}]$ is the constant concentration of water, $[\mathrm{E}]$ is the constant total ester bond concentration of the polymer, $[\mathrm{COOH}](r,t)$ is the concentration of carboxylic acid end groups, and $[\mathrm{P}_n](r,t)$ is the concentration of polymer chains with a number-average degree of polymerization n.

  - Net Rate of Generation of Carboxylic Acid End Groups: $R_{V\mathrm{COOH}}(r,t)$

    Recall (5.21),

$$R_{V\mathrm{COOH}}(r,t) = k_1'[\mathrm{COOH}](r,t) \qquad (7.56)$$

    where $k_1' := k_c[\mathrm{H_2O}][\mathrm{E}]$, k_c is the rate constant for the autocatalytic hydrolysis reaction, $[\mathrm{H_2O}]$ is the constant concentration of water, $[\mathrm{E}]$ is the constant total ester bond concentration of the polymer, $[\mathrm{COOH}](r,t)$ is the concentration of carboxylic acid end groups.

  - Net Rate of Generation of Ester Bonds: $R_{V\mathrm{E}}(r,t)$

    Recall (5.24),

$$R_{V\mathrm{E}}(r,t) \equiv 0. \qquad (7.57)$$

- Quadratic-Order Rate Law for Autocatalytic Hydrolysis

  - Net Rate of Generation of Polymer Chains: $R_{V\mathrm{P}_n}(r,t)$

    Recall (5.27),

$$R_{V\mathrm{P}_n}(r,t) = k_2'[\mathrm{COOH}](r,t) \times \left(2\sum_{m=n+1}^{\infty}[\mathrm{P}_m](r,t) - (n-1)\,[\mathrm{P}_n](r,t)\right), \qquad (7.58)$$
$$n = 1,\, 2,\, \ldots,$$

    where $k_2' := k_c[\mathrm{H_2O}]$, k_c is the rate constant for the autocatalytic hydrolysis reaction, $[\mathrm{H_2O}]$ is the constant concentration of water, $[\mathrm{COOH}](r,t)$ is the concentration of carboxylic acid end groups, and $[\mathrm{P}_n](r,t)$ is the concentration of polymer chains with a number-average degree of polymerization n.

  - Net Rate of Generation of Carboxylic Acid End Groups: $R_{V\mathrm{COOH}}(r,t)$

    Recall (5.28),

$$R_{V\mathrm{COOH}}(r,t) = k_2'[\mathrm{COOH}](r,t)[\mathrm{E}](r,t), \qquad (7.59)$$

    where $k_2' := k_c[\mathrm{H_2O}]$, k_c is the rate constant for the autocatalytic hydrolysis reaction, $[\mathrm{H_2O}]$ is the constant concentration of water, $[\mathrm{COOH}](r,t)$ is the concentration of carboxylic acid end groups, and $[\mathrm{E}](r,t)$ is the total ester bond concentration of polymer.

  - Net rate of generation of ester bonds, $R_{V\mathrm{E}}(r,t)$

    Recall (5.29),

$$R_{V\mathrm{E}}(r,t) = -k_2'[\mathrm{COOH}](r,t)[\mathrm{E}](r,t), \qquad (7.60)$$

    where $k_2' := k_c[\mathrm{H_2O}]$, k_c is the rate constant for the autocatalytic hydrolysis reaction, $[\mathrm{H_2O}]$ is the constant concentration of water, $[\mathrm{COOH}](r,t)$ is the concentration of carboxylic acid end groups, and

$[\mathrm{E}](r,t)$ is the total ester bond concentration of polymer.

- 1.5th-Order Rate Law for Autocatalytic Hydrolysis
  - Net Rate of Generation of Polymer Chains: $R_{V\mathrm{P}_n}(r,t)$

    Recall (5.43),

$$R_{V\mathrm{P}_n}(r,t) = k'_{1.5}\sqrt{K_a[\mathrm{COOH}](r,t)} \times \left(2\sum_{m=n+1}^{\infty}[\mathrm{P}_m](r,t) - (n-1)\,[\mathrm{P}_n](r,t)\right), \quad n = 1,\,2,\,\ldots, \tag{7.61}$$

    where $k'_{1.5} := k_c[\mathrm{H_2O}]$, k_c is the rate constant for the autocatalytic hydrolysis reaction, $[\mathrm{H_2O}]$ is the constant concentration of water, K_a is the acid dissociation constant for COOH, $[\mathrm{COOH}](r,t)$ is the concentration of carboxylic acid end groups, and $[\mathrm{P}_n](r,t)$ is the concentration of polymer chains with a number-average degree of polymerization n.
  - Net Rate of Generation of Carboxylic Acid End Groups: $R_{V\mathrm{COOH}}(r,t)$

    Recall (5.45),

$$R_{V\mathrm{COOH}}(r,t) = k'_{1.5}\sqrt{K_a[\mathrm{COOH}](r,t)}[\mathrm{E}](r,t), \tag{7.62}$$

    where $k'_{1.5} := k_c[\mathrm{H_2O}]$, k_c is the rate constant for the autocatalytic hydrolysis reaction, $[\mathrm{H_2O}]$ is the constant concentration of water, K_a is the acid dissociation constant for COOH, $[\mathrm{COOH}](r,t)$ is the concentration of carboxylic acid end groups, and $[\mathrm{E}](r,t)$ is the total ester bond concentration of the polymer.
  - Net Rate of Generation of Ester Bonds: $R_{V\mathrm{E}}(r,t)$

    Recall (5.46),

$$R_{V\mathrm{E}}(r,t) = -k'_{1.5}\sqrt{K_a[\mathrm{COOH}](r,t)}[\mathrm{E}](r,t), \tag{7.63}$$

where $k'_{1.5} := k_c[\mathrm{H_2O}]$, k_c is the rate constant for the autocatalytic hydrolysis reaction, $[\mathrm{H_2O}]$ is the constant concentration of water, K_a is the acid dissociation constant for COOH, $[\mathrm{COOH}](r,t)$ is the concentration of carboxylic acid end groups, and $[\mathrm{E}](r,t)$ is the total ester bond concentration of the polymer.

Chapter 8

Numerical Methods

This chapter presents the numerical methods used to solve the partial differential equations (PDEs) of the model for drug delivery from PLGA microspheres given in Chapter 7. First, a brief overview of numerical methods for PDEs is presented, and the finite difference operators are derived. Next, the discretizations of the reaction term, the spatial derivatives of the diffusion term, and the temporal derivative of the accumulation term are discussed. The diffusion term includes variable effective diffusivity as a function of the radius and time, so the diffusivity must be included in the spatial derivatives. The implicit ordinary differential equation (ODE) solver utilized for solving the model equations is discussed.

As summarized in Chapter 7, the conservation equations consist of nonlinear, parabolic PDEs in spherical coordinates with radial symmetry to describe the reaction-diffusion conservation of the chemical species in PLGA microspheres undergoing polymer degradation and diffusive drug release. The system of PDEs of the model must be solved numerically because the effective diffusivities for some of the species are not constant and the equations are nonlinear and coupled. For each set of parameter values, a new numerical solution must be determined.

The primary methods for numerically solving PDEs are the finite difference method, the finite element method, and the finite volume method. Each of these methods encompasses many numerical schemes. In schemes of the finite difference method, the differential operators and the domain of a PDE are discretized to obtain a system of equations that can be solved more easily than the

PDE [136, 137]. In schemes of the finite element method, the solution space is discretized with basis functions to determine a solution that is a weighted combination of the basis functions [136]. In schemes of the finite volume method, the spatial domain is discretized into finite-sized volume elements, and the fluxes through volume elements are computed using surface integrals based on the current average values across each volume element [138].

The finite element and finite volume methods have more flexibility in the geometry that they can handle as these methods do not depend on the structure of the grid points as the finite difference method does [139], but they are not as straightforward to implement as the finite difference method. As the boundary conditions and geometry for the model are simple (a one-dimensional sphere with symmetry at the origin and constant concentration Dirichlet boundary condition at the surface), the finite difference method is used for numerically solving the model PDEs in this dissertation. For further comparisons between the finite difference, finite element, and finite volume methods and details of their implementation, refer to [136] and [139]. Only the finite difference method is discussed further here.

In the finite difference method, derivatives are approximated using finite, small intervals rather than infinitely small intervals as in the definitions of the derivatives. The domain for the differential equation is discretized into a finite number of grid points. The approximations to the derivatives are evaluated at the discretized points in one or multiple dimensions to obtain a system of algebraic or ordinary differential equations, depending on the number of dimensions discretized. Numerical solvers can be used to solve the system of algebraic or ordinary differential equations for the numerical solution to the PDE at each discretized grid point. Taylor series expansions can be used to determine the order of the truncation error—the difference between the numerical solution obtained using the finite difference method and the exact solution to a differential equation.

The method of lines is a semidiscrete method where a PDE first is

discretized in space and then the resulting system of time-dependent ordinary differential equations (ODEs) at each grid point is solved using any of the numerical solvers for ODEs [138, 139]. Many software packages are available for solving systems of ODEs. The method of lines approach is used here.

In the following subsections, a few sample finite difference schemes are presented for approximating first and second derivatives. Then, the methods used for this dissertation for time- and space-differencing are detailed, and the general form of the differential-difference equation used for the method of lines is given.

8.1 Finite Difference Method

Several finite difference operators exist to discretize derivatives. The most common difference operators (forward, backward, and central) are presented below and applied to the general form of the PDEs of the model in subsequent sections. The finite difference operators are usually defined on an grid with intervals of Δx between grid points $x_i = (i-1)\Delta x$, where the index i has integer values. The index i is chosen to start from 1 rather than 0 for consistency with array indexing in Fortran and MATLAB software. The operators also can be defined on smaller or larger intervals, such as $\frac{1}{2}\Delta x$ or $2\Delta x$. Let $F_i \approx f(x_i)$ represent the numerical approximation at x_i. The interval sizes should match in the numerator and the denominator to approximate a derivative, and the index should scale with the interval size (i.e., $F_{i+\frac{1}{2}}$ for $f(x_i + \frac{1}{2}\Delta x)$).

8.1.1 Definitions of the First Derivative

The derivative of a function $f(x)$ at the point x_i is typically defined by

$$\frac{df(x_i)}{dx} := \lim_{\Delta x \to 0} \frac{f(x_i + \Delta x) - f(x_i)}{\Delta x}. \tag{8.1}$$

The standard definition of the derivative of $f(x)$ uses forward intervals for the numerator. In the limit that the interval size goes to zero and if the derivative is continuous at (x_i), mathematically equivalent forms for the definitions of the derivative of $f(x)$ at the point (x_i) can be defined using backward intervals [137, 139],

$$\frac{df(x_i)}{dx} := \lim_{\Delta x \to 0} \frac{f(x_i) - f(x_i - \Delta x)}{\Delta x}, \tag{8.2}$$

and centered intervals [137, 139],

$$\frac{df(x_i)}{dx} := \lim_{\Delta x \to 0} \frac{f(x_i + \frac{1}{2}\Delta x) - f(x_i - \frac{1}{2}\Delta x)}{\Delta x}. \tag{8.3}$$

8.1.2 Definitions of Taylor Series Expansions

The Taylor series expansion of the function $f(x)$ about x_i is

$$f(x) = \sum_{n=0}^{\infty} \frac{\frac{d^n}{dx^n} f(x_i)}{n!} (x - x_i)^n. \tag{8.4}$$

The function values $f(x_i + \Delta x)$ and $f(x_i - \Delta x)$ are expanded in Taylor series about x_i as

$$\begin{aligned} f(x_i + \Delta x) &= \sum_{n=0}^{\infty} \frac{\frac{d^n}{dx^n} f(x_i)}{n!} (\Delta x)^n \\ &= f(x_i) + \Delta x \frac{df(x_i)}{dx} + \frac{(\Delta x)^2}{2} \frac{d^2 f(x_i)}{dx^2} + \frac{(\Delta x)^3}{6} \frac{d^3 f(x_i)}{dx^3} + \dots \end{aligned} \tag{8.5}$$

and

$$\begin{aligned} f(x_i - \Delta x) &= \sum_{n=0}^{\infty} \frac{\frac{d^n}{dx^n} f(x_i)}{n!} (-\Delta x)^n \\ &= f(x_i) - \Delta x \frac{df(x_i)}{dx} + \frac{(\Delta x)^2}{2} \frac{d^2 f(x_i)}{dx^2} - \frac{(\Delta x)^3}{6} \frac{d^3 f(x_i)}{dx^3} + \dots . \end{aligned} \tag{8.6}$$

8.1.3 Forward Difference Operator

The forward difference operator, Δ_+, applied to a function $f(x)$ is defined by [140]

$$\Delta_+ f(x) := f(x + \Delta x) - f(x). \tag{8.7}$$

The scheme for approximating the first derivative of $f(x)$ at the point x_i using the forward difference operator and the definition of the derivative given by (8.1) is

$$\begin{aligned} \frac{df(x_i)}{dr} &= \lim_{\Delta x \to 0} \frac{f(x_i + \Delta x) - f(x_i)}{\Delta x} \\ &= \lim_{\Delta x \to 0} \frac{\Delta_+ f(x_i)}{\Delta x} \\ &\approx \frac{\Delta_+ F_i}{\Delta x} \\ &\approx \frac{F_{i+1} - F_i}{\Delta x}. \end{aligned} \tag{8.8}$$

The truncation error, $T(x_i)$, for a numerical method is equal to the difference between the numerical scheme, evaluated by replacing the numerical approximation F_i with the exact solution $f(x_i)$, and the differential equation. $T(x_i)$ for the scheme for approximating the first derivative using the forward difference operator can be determined by subtracting the left-hand-side of (8.8) from the right-hand-side, substituting $f(x_i + \Delta x)$ for F_{i+1} and $f(x_i)$ for F_i, and using the Taylor series expansion for $f(x_i + \Delta x)$ given by (8.5), [138]:

$$\begin{aligned} T(x_i) &= \frac{f(x_i + \Delta x) - f(x_i)}{\Delta x} - \frac{df(x_i)}{dx} \\ &= \frac{\left(f(x_i) + \Delta x \dfrac{df(x_i)}{dx} + \dfrac{(\Delta x)^2}{2} \dfrac{d^2 f(x_i)}{dx^2} + \dots \right) - f(x_i)}{\Delta x} - \frac{df(x_i)}{dx} \\ &= \frac{\Delta x}{2} \frac{d^2 f(x_i)}{dx^2} + \dots . \end{aligned} \tag{8.9}$$

The order of accuracy is determined by the lowest power of Δx in the truncation error [137]. The scheme for approximating the first derivative using the forward

difference operator is first-order accurate in Δx.

8.1.4 Backward Difference Operator

The backward difference operator, Δ_-, applied to a function $f(x)$ is defined by [140]

$$\Delta_- f(x) := f(x) - f(x - \Delta x). \tag{8.10}$$

The scheme for approximating the first derivative of $f(x)$ at the point x_i using the backward difference operator and the definition of the derivative given by (8.2) is

$$\begin{aligned} \frac{df(x_i)}{dx} &= \lim_{\Delta x \to 0} \frac{f(x_i) - f(x_i - \Delta x)}{\Delta x} \\ &= \lim_{\Delta x \to 0} \frac{\Delta_- f(x_i)}{\Delta x} \\ &\approx \frac{\Delta_- F_j}{\Delta x} \\ &\approx \frac{F_i - F_{i-1}}{\Delta x}. \end{aligned} \tag{8.11}$$

$T(x_i)$ for the scheme for approximating the first derivative using the backward difference operator can be determined by subtracting the left-hand-side of (8.11) from the right-hand-side, substituting $f(x_i)$ for F_j and $f(x_i - \Delta x)$ for F_{i-1}, and using the Taylor series expansion for $f(x_i - \Delta x)$ given by (8.6), [138]:

$$\begin{aligned} T(x_i) &= \frac{f(x_i) - f(x_i - \Delta x)}{\Delta x} - \frac{df(x_i)}{dr} \\ &= \frac{f(x_i) - \left(f(x_i) - \Delta x \dfrac{df(x_i)}{dx} + \dfrac{(\Delta x)^2}{2} \dfrac{d^2 f(x_i)}{dx^2} - \cdots \right)}{\Delta x} - \frac{df(x_i)}{dx} \\ &= -\frac{\Delta x}{2} \frac{d^2 f(x_i)}{dx^2} + \ldots . \end{aligned} \tag{8.12}$$

The scheme for approximating the first derivative using the backward difference operator is first-order accurate in the Δx.

8.1.5 Central Difference Operator

The central difference operator, δ, applied to a function $f(x)$ is defined by [140]

$$\delta f(x) := f(x + \frac{1}{2}\Delta x) - f(x - \frac{1}{2}\Delta x). \tag{8.13}$$

The scheme for approximating the first derivative of $f(x)$ at the point x_i using the central difference operator and the definition of the derivative given by (8.3) is

$$\begin{aligned} \frac{df(x_i)}{dx} &= \lim_{\Delta x \to 0} \frac{f(x_i + \frac{1}{2}\Delta x) - f(x_i - \frac{1}{2}\Delta x)}{\Delta x} \\ &= \lim_{\Delta x \to 0} \frac{\delta f(x_i)}{\Delta x} \\ &\approx \frac{\delta F_i}{\Delta x} \\ &\approx \frac{F_{i+\frac{1}{2}} - F_{i-\frac{1}{2}}}{\Delta x}. \end{aligned} \tag{8.14}$$

Alternatively, the central difference operator can be defined over the interval of $2\Delta x$ by

$$\delta_2 f(x) := f(x + \Delta x, t) - f(x - \Delta x) \tag{8.15}$$

and can be used to approximate the first derivative of $f(x)$ at the point x_i by

$$\begin{aligned} \frac{df(x_i)}{dx} &= \lim_{\Delta x \to 0} \frac{f(x_i + \Delta x) - f(x_i - \Delta x)}{2\Delta x} \\ &= \lim_{\Delta x \to 0} \frac{\delta_2 f(x_i)}{2\Delta x} \\ &\approx \frac{\delta_2 F_i}{2\Delta x} \\ &\approx \frac{F_{i+1} - F_{i-1}}{2\Delta x}. \end{aligned} \tag{8.16}$$

The truncation errors for δ and δ_2 have the same order as they only differ by a constant due to the interval spacing. The truncation error is derived for the interval size of $2\Delta x$ as the Taylor series expansions have been shown for $f(x_i + \Delta x)$ and $f(x_i - \Delta x)$ in (8.5) and (8.6). $T(x_i)$ for the scheme for approximating the first

derivative using the central difference operator can be determined by subtracting the left-hand-side of (8.16) from the right-hand-side, substituting $f(x_i - \Delta x)$ for F_{i-1} and $f(x_i + \Delta x)$ for F_{i+1}, and using the Taylor series expansions for the grid points $f(x_i + \Delta x)$ and $f(x_i - \Delta x)$, [138]:

$$\begin{aligned} T(x_i) &= \frac{f(x_i + \Delta x) - f(x_i - \Delta x)}{2\Delta x} - \frac{df(x_i)}{dx} \\ &= \frac{f(x_i) + \Delta x \dfrac{df(x_i)}{dx} + \dfrac{(\Delta x)^2}{2}\dfrac{d^2 f(x_i)}{dx^2} + \dfrac{(\Delta x)^3}{6}\dfrac{d^3 f(x_i)}{dx^3} + \ldots}{2\Delta x} \\ &\quad - \frac{f(x_i) - \Delta x \dfrac{df(x_i)}{dx} + \dfrac{(\Delta x)^2}{2}\dfrac{d^2 f(x_i)}{dx^2} - \dfrac{(\Delta x)^3}{6}\dfrac{d^3 f(x_i)}{dx^3} + \ldots}{2\Delta x} \\ &\quad - \frac{df(x_i)}{dx} \\ &= \frac{(\Delta x)^2}{6}\frac{d^3 f(x_i)}{dx^3} + \ldots . \end{aligned} \tag{8.17}$$

The scheme for approximating the first derivative using the central difference operator is second-order accurate in Δx.

8.2 Time-Differencing

It is a common practice to consider time- and space-differencing independently, although they are not completely independent, to treat the issues that arise from the choices of finite difference operators [137, 139]. For the numerical integration of a PDE, the initial and boundary conditions give the starting values at all spatial grid points, and the values for the entire spatial mesh are updated for each time step. Generally, only occasional time points are written to output files for storage and analysis, and as few time points as possible are kept in memory [137]. Intermediate values between output times can be discarded after the updates are completed for each time step. Future time points are not available. The current time point may be calculated explicitly using previous time points, implicitly as a function of the current time point, or a combination of implicitly and explicitly.

With the ODEs in time that result from discretization of the PDEs in space, approximating the derivative of $f_j(t)$ with the first-order accurate forward difference operator given by (8.8) gives the explicit forward Euler scheme at the point $(r_j, t_k) = ((j-1)\Delta r, (k-1)\Delta t)$:

$$\frac{df_j(t_k)}{dt} \approx \frac{F_j^{k+1} - F_j^k}{\Delta t}, \tag{8.18}$$

where $f_j(t)$ is a continuous function of time at r_j, F_j^k is the numerical approximation to $f_j(t)$ at the discrete point (r_j, t_k), and Δt is the time step.

With this scheme values at the current time point t_k are used to update the next time point t_{k+1}:

$$C_j^{k+1} \approx C_j^k + \Delta t \frac{df_j(t_k)}{dt}. \tag{8.19}$$

The forward Euler scheme, along with other higher-order explicit methods, has severe stability requirements restricting the size of the time step relative to the spatial mesh size [141]. For the diffusion equation in polar coordinates with spherical symmetry, the explicit scheme is stable only if [140]

$$\Delta t \leq \frac{(\Delta r)^2}{6 \max \alpha_i(r,t)}, \tag{8.20}$$

where $\alpha_i(r,t)$ is the variable diffusion coefficient divided by the square of the particle radius.

Explicit methods are not suitable for stiff ODEs, which involve slow smooth transients and much faster transients that need to be fully resolved to give the correct behavior of the slow transients. Small time steps must be taken for accurate solutions in the interval when the fast transient is significant [141]. A problem is considered stiff if the time scales for the slow and fast transients are widely separated (examples: fast reaction and slow diffusion or vice versa). Stiff problems require many time steps small in comparison to the time scale of the rapid transient

to maintain stability of the numerical integration, making the computational time required to produce a complete solution for the entire time frame of the slow transient prohibitive in many cases. Failure to resolve or damp rapid transients introduces local truncation errors that perturb the system from accurately computing the desired solution [138]. Chemical reaction systems and the translation of diffusion terms by finite differences to a large system of ODES in the method of lines are sources of stiffness [142].

Approximating the derivative of $f_j(t)$ with the first-order accurate backward difference operator given by (8.11) gives the implicit backward Euler scheme at the point $(r_j, t_k) = ((j-1)\Delta r, (k-1)\Delta t)$:

$$\frac{df_j(t_k)}{dt} \approx \frac{F_j^k - F_j^{k-1}}{\Delta t}. \tag{8.21}$$

Add 1 to each index gives the equivalent form in terms of k and $k+1$:

$$\frac{df_j(t_{k+1})}{dt} \approx \frac{F_j^{k+1} - F_j^k}{\Delta t}. \tag{8.22}$$

With this scheme values at the current time point t_k and the next time point t_{k+1} are used to update the next time point:

$$F_j^{k+1} \approx F_j^k + \Delta t \frac{df_j(t_{k+1})}{dt}. \tag{8.23}$$

The backward Euler scheme, along with other implicit methods, is more computationally expensive than the corresponding explicit method. However, the stability restriction of the explicit method is circumvented by the implicit scheme being unconditionally stable, allowing for larger time steps to be taken to satisfy accuracy considerations for maintaining an acceptably small truncation error rather than numerical stability requirements [140].

Many more sophisticated ODE solvers are available that have higher orders

of accuracy and have been designed for specific types of problems [137]. MATLAB has a suite of built-in ODE solvers, including some designed for stiff problems. The limitation of these solvers is that they save all the intermediate times in memory even when a coarse distribution of time step values is specified for output. This becomes restrictive when a large system of PDEs is discretized in space, creating an even larger system of ODEs.

The ODE solver used here is RADAU5 [142], which uses a 5th order implicit Runge-Kutta method with step-size control implemented in Fortran. Briefly, the method is based on a Radau quadrature method (3-stage Radau IIA) that is L-stable [143] meaning that its region of absolute stability contains the entire left half-plane and rapid transient deviations from the smooth solution are damped quickly [138]. The method is detailed in [142], and [143] provides a thorough description of numerical methods for stiff ODE initial value problems. The solver uses a variable step-size method to handle stiff problems. When the dynamics of fast and slow phenomena begin at the start of the simulation, the time step size is initially small to capture the dynamics of the fast transient. It is inefficient to maintain this step size after the fast dynamics have decayed. The solver increases the step size incrementally using error estimates to maintain the local error per step below a specified tolerance.

8.3 Space-Differencing

Numerical schemes may use multiple spatial grid point values for the approximation of spatial derivatives. Schemes that are second-order accurate in Δr using the central difference operator are used here for approximating the first derivatives with respect to r using the grid point r_j and its two adjacent neighbors, r_{j-1} and r_{j+1}. The effects of the boundary conditions on evaluating the approximations to the derivatives are discussed in relation to the discretization of the spatial derivatives of

the diffusion term.

The parameter $\alpha_i(r,t)$ simplifies the diffusion term of the general conservation equation and is defined as

$$\alpha_i(r,t) := \frac{D_i(r,t)}{R^2}. \tag{8.24}$$

The outer derivative of the diffusion term can be distributed as

$$\begin{aligned}\frac{1}{r^2}\frac{\partial}{\partial r}\left(r^2\alpha_i(r,t)\frac{\partial c_i(r,t)}{\partial r}\right) = &\frac{2\alpha_i(r,t)}{r}\frac{\partial c_i(r,t)}{\partial r} \\ &+ \frac{\partial}{\partial r}\left(\alpha_i(r,t)\frac{\partial c_i(r,t)}{\partial r}\right).\end{aligned} \tag{8.25}$$

It is possible to write the second term as

$$\frac{\partial}{\partial r}\left(\alpha_i(r,t)\frac{\partial c_i(r,t)}{\partial r}\right) = \frac{\partial \alpha_i(r,t)}{\partial r}\frac{\partial c_i(r,t)}{\partial r} + \alpha_i(r,t)\frac{\partial^2 c_i(r,t)}{\partial r^2}, \tag{8.26}$$

but the standard procedure is to use a difference operator to approximate the term in its original form [140]. The numerical approximations to $\alpha_i(r,t)$ and $c_i(r,t)$ at $((j-1)\Delta r, t)$ are denoted as $A_{i_j}(t)$ and $C_{i_j}(t)$, respectively, with time as a continuous variable.

8.3.1 Numerical Approximation in the Range $0 < r < 1$

The interior portion of the spatial domain discretized by Δr into NR discretizations is considered first. The schemes for approximating first derivatives derived with the central difference operator over intervals of Δr and $2\Delta r$ in the spatial dimension are given by (8.14) and (8.16), respectively. The numerical approximation to the diffusion term given by (8.25) at $(r_j, t) = ((j-1)\Delta r, t)$ for $0 < r_j < 1$ and $t > 0$

is [140]

$$\begin{aligned}
\frac{1}{r_j^2}\frac{\partial}{\partial r}\left(r_j^2\alpha_i(r_j,t)\frac{\partial c_i(r_j,t)}{\partial r}\right) &\approx \frac{2A_{i_j}(t)}{(j-1)\Delta r}\frac{\delta_2 C_{i_j}(t)}{2\Delta r} + \frac{\delta\left(A_i(r_j,t)\dfrac{\partial C_i(r_j,t)}{\partial r}\right)}{\Delta r} \\
&\approx \frac{A_{i_j}(t)\left(C_{i_{j+1}}(t) - C_{i_{j-1}}(t)\right)}{(j-1)(\Delta r)^2} \\
&\quad + \frac{A_{i_{j+\frac{1}{2}}}(t)\delta C_{i_{j+\frac{1}{2}}}(t) - A_{i_{j-\frac{1}{2}}}(t)\delta C_{i_{j-\frac{1}{2}}}(t)}{(\Delta r)^2} \\
&\approx \frac{A_{i_j}(t)\left(C_{i_{j+1}}(t) - C_{i_{j-1}}(t)\right)}{(j-1)(\Delta r)^2} \\
&\quad + \frac{A_{i_{j+\frac{1}{2}}}(t)\left(C_{i_{j+1}}(t) - C_{i_j}(t)\right)}{(\Delta r)^2} \\
&\quad - \frac{A_{i_{j-\frac{1}{2}}}(t)\left(C_{i_j}(t) - C_{i_{j-1}}(t)\right)}{(\Delta r)^2}, \\
j &= 2,\, 3,\, \ldots,\, NR-1.
\end{aligned} \tag{8.27}$$

The values of A_i at the intermediate grid points $r_{j+\frac{1}{2}}$ and $r_{j-\frac{1}{2}}$ can be approximated using the known values at the adjacent grid points:

$$A_{i_{j+\frac{1}{2}}}(t) \approx \frac{A_{i_{j+1}}(t) + A_{i_j}(t)}{2} \tag{8.28}$$

and

$$A_{i_{j-\frac{1}{2}}}(t) \approx \frac{A_{i_j}(t) + A_{i_{j-1}}(t)}{2}. \tag{8.29}$$

Substituting the expressions given by (8.28) and (8.29) into (8.27) and simplifying yields

$$\begin{aligned}
&\frac{1}{r_j^2}\frac{\partial}{\partial r}\left(r_j^2\alpha_i(r_j,t)\frac{\partial c_i(r_j,t)}{\partial r}\right) \\
&\approx \frac{A_{i_j}(t)\big((j+1)C_{i_{j+1}}(t)-2(j-1)C_{i_j}(t)+(j-3)C_{i_{j-1}}(t)\big)}{2(j-1)(\Delta r)^2} \\
&\quad+\frac{A_{i_{j+1}}(t)\left(C_{i_{j+1}}(t)-C_{i_j}(t)\right)}{2(\Delta r)^2} \\
&\quad+\frac{A_{i_{j-1}}(t)\left(C_{i_{j-1}}(t)-C_{i_j}(t)\right)}{2(\Delta r)^2}, \\
&j=2,\,3,\,\ldots,\,NR-1.
\end{aligned} \tag{8.30}$$

In the limit that $A_{i_j} = A_{i_{j+1}} = A_{i_{j-1}}$, the general expression given by (8.30) becomes the more common spherical discretization scheme for diffusion with diffusivity independent of r [100, 144]:

$$\begin{aligned}
&\frac{1}{r_j^2}\frac{\partial}{\partial r}\left(r_j^2\alpha_i(t)\frac{\partial c_i(r_j,t)}{\partial r}\right) \\
&\approx \frac{A_i(t)\left(jC_{i_{j+1}}(t)-2(j-1)C_{i_j}(t)+(j-2)\,C_{i_{j-1}}(t)\right)}{(j-1)(\Delta r)^2}, \\
&j=2,\,3,\,\ldots,\,NR-1.
\end{aligned} \tag{8.31}$$

Note that the index used here is different than that in the references to account for MATLAB and Fortran indexing starting with 1 instead of 0 as in [100, 144].

8.3.2 Numerical Approximation at $r = 0$

The numerical scheme given by (8.30) is valid for integers $1 < j < NR$. At the $r = 1$ boundary, the concentration of species i is known explicitly by the constant surface boundary condition given by (4.11), so it is unnecessary to calculate updated values for $c_{i,r1} \approx C_{i_{NR}}$. At the origin, the index is $j = 1$, the scheme (8.30) has a singularity, and the $j = 0$ index lies outside the boundary of the one-dimensional sphere. At the center of the sphere, the boundary condition given

by (4.10) enforces radial symmetry about the origin. The numerical approximation to the boundary condition is

$$\frac{\partial c_i(0,t)}{\partial r} \approx \frac{\delta_2 C_{i_1}(t)}{2\Delta r} = \frac{C_{i_2}(t) - C_{i_0}(t)}{2\Delta r} = 0. \tag{8.32}$$

The concentration at the grid point outside the boundary, $C_{i_0}(t)$, is

$$C_{i_0}(t) = C_{i_2}(t). \tag{8.33}$$

With points at $j = 0$ and $j = 2$ being symmetric, $A_{i_0}(t) = A_{i_2}(t)$.

The diffusion term given by (8.25) evaluated in the limit as $r \to 0$ with the boundary condition $\dfrac{\partial c_i(0,t)}{\partial r} = 0$ is

$$\begin{aligned}
&\lim_{r\to 0}\left(\frac{1}{r^2}\frac{\partial}{\partial r}\left(r^2\alpha_i(r,t)\frac{\partial c_i(r,t)}{\partial r}\right)\right) \\
&= \lim_{r\to 0}\left(\frac{2\alpha_i(r,t)}{r}\frac{\partial c_i(r,t)}{\partial r} + \frac{\partial}{\partial r}\left(\alpha_i(r,t)\frac{\partial c_i(r,t)}{\partial r}\right)\right) \\
&= \lim_{r\to 0}\left(\frac{2\alpha_i(r,t)\dfrac{\partial c_i(r,t)}{\partial r}}{r}\right) + \frac{\partial}{\partial r}\left(\alpha_i(r,t)\frac{\partial c_i(r,t)}{\partial r}\right).
\end{aligned} \tag{8.34}$$

The first term gives an indeterminate form of $0/0$ that can be resolved using l'Hospital's Rule:

$$\begin{aligned}
\lim_{r\to 0}\left(\frac{2\alpha_i(r,t)\dfrac{\partial c_i(r,t)}{\partial r}}{r}\right) &= \lim_{r\to 0}\left(\frac{\dfrac{\partial}{\partial r}\left(2\alpha_i(r,t)\dfrac{\partial c_i(r,t)}{\partial r}\right)}{\dfrac{\partial}{\partial r}r}\right) \\
&= 2\frac{\partial}{\partial r}\left(\alpha_i(r,t)\frac{\partial c_i(r,t)}{\partial r}\right).
\end{aligned} \tag{8.35}$$

The result substituted into (8.34) yields

$$\lim_{r\to 0}\left(\frac{1}{r^2}\frac{\partial}{\partial r}\left(r^2\alpha_i(r,t)\frac{\partial c_i(r,t)}{\partial r}\right)\right) = 3\frac{\partial}{\partial r}\left(\alpha_i(r,t)\frac{\partial c_i(r,t)}{\partial r}\right). \tag{8.36}$$

As in (8.27), the partial derivative term may be approximated by

$$\begin{aligned}\frac{\partial}{\partial r}\left(\alpha_i(r_j,t)\frac{\partial c_i(r_j,t)}{\partial r}\right) &\approx \frac{A_{i_{j+\frac{1}{2}}}(t)\left(C_{i_{j+1}}(t)-C_{i_j}(t)\right)}{(\Delta r)^2} \\ &\quad - \frac{A_{i_{j-\frac{1}{2}}}(t)\left(C_{i_j}(t)-C_{i_{j-1}}(t)\right)}{(\Delta r)^2} \\ &\approx \frac{A_{i_j}(t)\left(C_{i_{j+1}}(t)-2C_{i_j}(t)+C_{i_{j-1}}\right)}{2(\Delta r)^2} \\ &\quad + \frac{A_{i_{j+1}}(t)\left(C_{i_{j+1}}(t)-C_{i_j}(t)\right)}{2(\Delta r)^2} \\ &\quad + \frac{A_{i_{j-1}}(t)\left(C_{i_{j-1}}(t)-C_{i_j}(t)\right)}{2(\Delta r)^2}.\end{aligned} \tag{8.37}$$

Using the symmetry boundary condition at $j = 1$, $C_{i_0}(t) = C_{i_2}(t)$ and $A_{i_0}(t) = A_{i_2}(t)$. Therefore,

$$\lim_{r\to 0}\left(\frac{1}{r^2}\frac{\partial}{\partial r}\left(r^2\alpha_i(r,t)\frac{\partial c_i(r,t)}{\partial r}\right)\right) \approx \frac{3\left(A_{i_1}(t)+A_{i_2}(t)\right)\left(C_{i_2}(t)-C_{i_1}(t)\right)}{(\Delta r)^2}. \tag{8.38}$$

In the limit that $A_{i_1} = A_{i_2}$, the general expression given by (8.38) becomes the more common spherical discretization scheme for diffusion at $r = 0$ with diffusivity independent of r [100, 144]:

$$\lim_{r\to 0}\left(\frac{1}{r^2}\frac{\partial}{\partial r}\left(r^2\alpha_i(t)\frac{\partial c_i(r,t)}{\partial r}\right)\right) \approx \frac{6A_i(t)}{(\Delta r)^2}\left(C_{i_2}(t)-C_{i_1}(t)\right). \tag{8.39}$$

8.4 General Form for Model Differential-Difference Equations

Terms which are not functions of spatial derivatives may be discretized in space by evaluating at the discrete points $r_j = (j-1)\Delta r$ for $j = 1, 2, \ldots, NR$, where NR is the number of evenly-spaced radial discretizations, resulting in functions of time at each grid point. The reaction term, $R_{Vi}(r,t)$, of the conservation terms is nonlinear but is only a function of the concentrations of the species in the system and not a

function of any derivatives. Therefore, the reaction term can be approximated numerically at the point (r_j, t) by

$$R_{Vi}(r_j, t) \approx R_{Vi_j}(t). \tag{8.40}$$

Likewise, the average pore radius, $R_p(r, t)$, and the effective diffusivity of species i, $D_i(r, t)$, are nonlinear but not functions of any spatial derivatives, so they may be approximated numerically at the point (r_j, t) by

$$R_p(r_j, t) \approx R_{p_j}(t). \tag{8.41}$$

and

$$D_i(r_j, t) \approx D_{i_j}(t), \tag{8.42}$$

respectively.

By approximating the spatial derivatives with central differences as described in Section 8.3 and evaluating all functions of r at the discrete spatial point $r_j = (j-1)\Delta r$ with continuous time, the system of PDEs for updating $R_p(r, t)$ and $D_i(r, t)$ and the conservation equations in Chapter 7 becomes a system of differential-difference equations in time:

$$\frac{dR_{p_j}(t)}{dt} = f\left(R_{Vi_j}(t)\right), \quad j = 1, 2, \ldots, NR-1, \tag{8.43}$$

$$\frac{dR_{p_{NR}}(t)}{dt} = 0, \tag{8.44}$$

$$\frac{dD_{i_j}(t)}{dt} = f\left(R_{p_j}(t), \frac{dR_{p_j}(t)}{dt}\right), \quad j = 1, 2, \ldots, NR-1, \tag{8.45}$$

$$\frac{dD_{i_{NR}}(t)}{dt} = 0, \tag{8.46}$$

$$\frac{dC_{i_1}(t)}{dt} = \frac{3\left(A_{i_1}(t) + A_{i_2}(t)\right)\left(C_{i_2}(t) - C_{i_1}(t)\right)}{(\Delta r)^2} + R_{Vi_1}(t), \tag{8.47}$$

$$\frac{dC_{i_j}(t)}{dt} = \frac{A_{i_j}(t)\left((j+1)\,C_{i_{j+1}}(t) - 2(j-1)C_{i_j}(t) + (j-3)\,C_{i_{j-1}}(t)\right)}{2(j-1)(\Delta r)^2} + \frac{A_{i_{j+1}}(t)\left(C_{i_{j+1}}(t) - C_{i_j}(t)\right) + A_{i_{j-1}}(t)\left(C_{i_{j-1}}(t) - C_{i_j}(t)\right)}{2(\Delta r)^2} + R_{Vi_j}(t), \quad j = 2,\, 3,\, \ldots,\, NR-1, \tag{8.48}$$

and

$$\frac{dC_{i_{NR}}(t)}{dt} = 0, \tag{8.49}$$

with initial conditions for $j = 1,\, 2,\, \ldots,\, NR$

$$\begin{aligned} R_{p_j}(0) &= R_{p,t0}, \\ D_{i_j}(0) &= D_{i,b}, \\ C_{i_j}(0) &= C_{i_j,t0}. \end{aligned} \tag{8.50}$$

where $R_{p_j}(t)$ is the numerical approximation to the average pore radius at (r_j, t), $D_{i_j}(t)$ is the numerical approximation to the effective diffusivity of species i at (r_j, t), $C_{i_j}(t)$ is the numerical approximation to the molar concentration of species i at (r_j, t), Δr is the spatial discretization size, $t \geq 0$ is time, $A_{i_j}(t)$ is the numerical approximation to the ratio of the effective diffusivity of species i to the particle radius at (r_j, t), $R_{Vi_j}(t)$ is the numerical approximation to the net generation of species i from the hydrolysis reaction at (r_j, t), $R_{p,t0}$ is the numerical approximation to the initial average pore size, $D_{i,b}$ is the effective diffusivity of species i in the polymer bulk, and $C_{i_j,t0}$ is the numerical approximation to the initial concentration distribution of species i at $(r_j, 0)$.

Chapter 9

Computational Implementation of Model Equations

This chapter provides details for the implementation of the numerical methods for determining solutions to the model equations in the Fortran programming language and for processing the solution data. The same code is used for considering limiting cases and the full model. Options can be specified to turn on or off certain portions of the code to investigate the effects of the coupling between the model components. Switching between reaction rate laws and constant and variable effective diffusivity are possible through the use of the options. The codes developed for the defining and solving the model equations are provided in Appendix B, excluding the RADAU5 ODE solver routine developed by [142] and the linear algebra routines the solver uses, which were not modified in the present work.

A batch file, *kraken.deck*, is modified for each simulation specifying the parameters and options for that case to be read by the executable at run time. The batch files are submitted to the batch job queue on a remote computational cluster for simultaneous running of many jobs. The same executable can be used while many variables and simulation options are explored. This reduces potential errors involved with entering variables accurately in the code or on the command line and reduces time spent on compilation of the executable. A sample batch file is included in Appendix B.17. The *makefile* for compiling the code into an executable, *radau*, is included in Appendix B.18. The output can be directed to save in different subfolders from the same executable. This saves memory and allows for an organized system for storing run data. The jobs are run in series on single

processors on the Kraken Cray XT5 supercomputer at the National Institute for Computational Resources through allocations with the Extreme Science and Engineering Discovery Environment (XSEDE). Typical full model run times, with error tolerance of 10^{-6} with 100 calls to the ODE solver and 101 spatial discretization points, are on the order of 1 hour with very fast queue times, so parallelization of the code was not pursued.

Overviews of the subroutines developed in this work and the options specified for the RADAU5 solver are provided in the following sections.

9.1 Fortran Driver Routine *driver_radau5*

The Fortran driver routine *driver_radau5* is the driver for calling the RADAU5 subroutine and its subsidiary subroutines, which are used directly from [142], to solve the system of ODEs defined in the subroutine *deriv* for the spatially discretized system of PDEs given in Chapter 7 for drug delivery from spherical polymer particles. The code for the driver is in Appendix B.1.

Figure 9.1 shows the calling hierarchy for the Fortran routine driver_radau5 and its external subroutines. To initialize the system variables, the driver calls two subroutines *intpar* and *initial*. The initial parameters, time, and solution vector are written to output: *simulation.out* if the run begins at $t = 0$ with uniform initial drug concentration or *simulation_restart.out* if the run begins at a later time or with a prescribed initial drug concentration profile. The parameters for RADAU5 are initialized, and the ODE solver is called $NT - 1$ times. At the end of each call, the status of the solver call is written to the standard output stream, and the current simulation time and the solution vector and written to the same output file where the initial conditions were written (*simulation.out* or *simulation_restart.out*). The solution vector consists of the concentration profiles of the species, the average pore radius, and the effective diffusivities of the species at each radial position.

MATLAB is used to create visualizations from the output data and for calculation of the profiles of pH and cumulative release of drug with and without burst effects.

9.2 Subroutine *intpar*

The subroutine *intpar* reads input tokens and parameters from the command line or the script file *kraken,deck* and calculates constant quantities. Table 9.1 defines the input for the executable read by *intpar*. The code for *intpar* is in Appendix B.2.

intpar calculates the initial ester bond concentration relative to the carboxylic acid end group concentration, assuming that both are uniformly distributed. Let $[\mathrm{B}](r,t)$ denote the total concentration of monomers (constant without transport effect) and $N(r,t)$ denote the average number of monomers per chain. Then,

$$[\mathrm{B}](r,t) = [\mathrm{COOH}](r,t) + [\mathrm{E}](r,t) \tag{9.1}$$

and

$$N(r,t) = \frac{M_n(r,t)}{M_1}, \tag{9.2}$$

where $[\mathrm{COOH}](r,t)$ is the concentration of COOH end groups, $[\mathrm{E}](r,t)$ is the concentration of ester bonds, $M_n(r,t)$ is the number average molecular weight of the polymer (small and large oligomers), and M_1 is the monomer molecular weight. Each chain has one COOH end group, so

$$[\mathrm{COOH}](r,t) = \frac{[\mathrm{B}](r,t)}{N(r,t)}. \tag{9.3}$$

Substituting (9.1) and (9.2) into (9.3) and solving for $[\mathrm{E}](r,t)$ gives

$$[\mathrm{E}](r,t) = [\mathrm{COOH}](r,t)\left(\frac{M_n(r,t)}{M_1} - 1\right). \tag{9.4}$$

This only holds for all t without transport effects. It is true at $t = 0$ even with

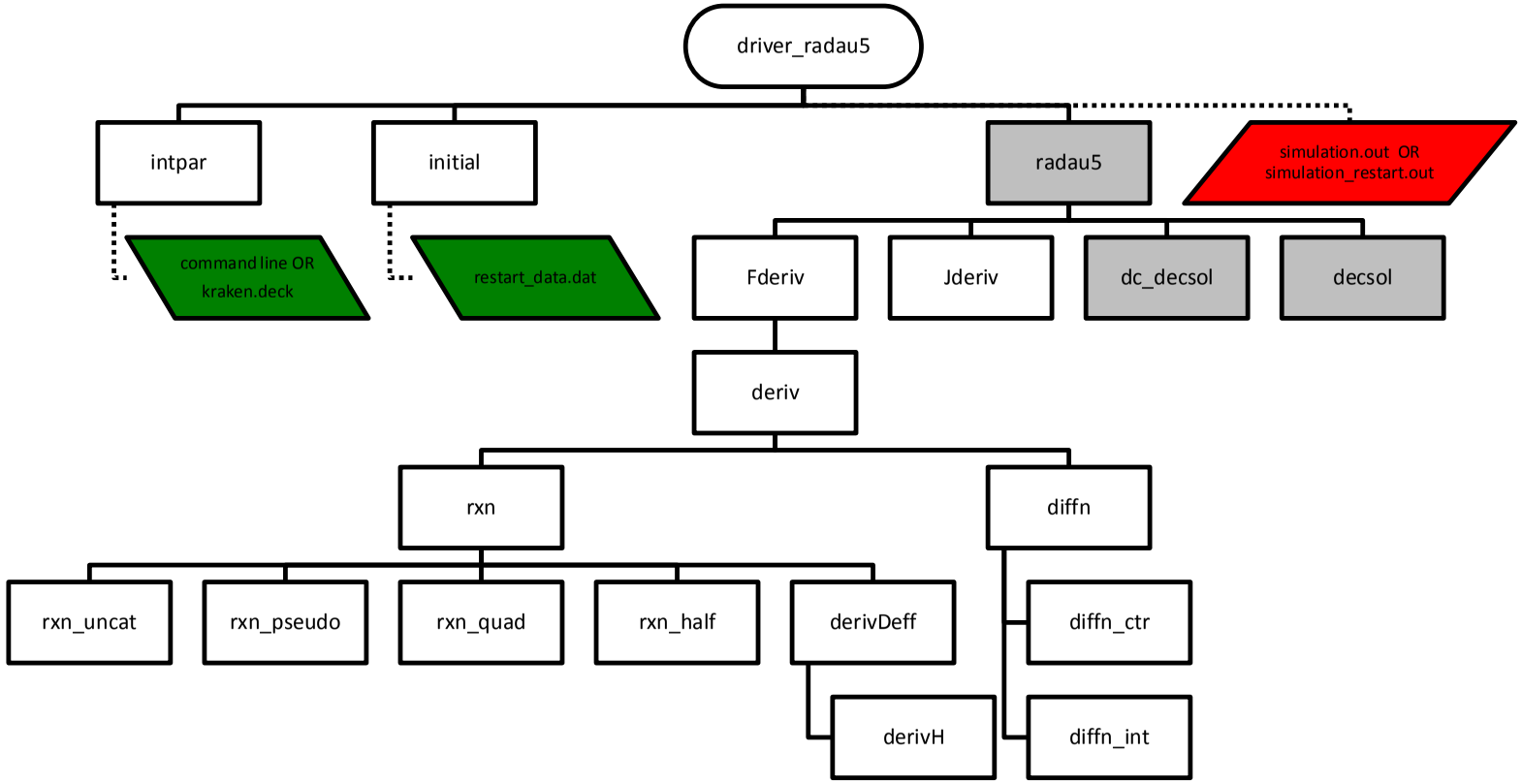

Figure 9.1: Call graph for the Fortran routine *driver_radau5* and its external subroutines. Shaded rectangles indicate reference subroutines from [142]. Green trapezoids that lean towards the left indicate input that is read, and the red trapezoid that leans toward the right indicates output that is written. Dashed lines indicate data transfer to and from disk.

Table 9.1: Input tokens and parameters read by Fortran subroutine *intpar*.

Tokens		
Name	Value	Interpretation
restart	0	Start from $t = 0$
	1	Finish an incomplete run
	2	Refine an interval
diffn_on	0	No diffusion
	1	Diffusivity: constant for all species
	2	Diffusivity: constant for small oligomers and variable for drug
	3	Diffusivity: variable for all species
rxn_on	0	No reaction
	1	First-order rate law for uncatalyzed hydrolysis
	2	Pseudo-first-order rate law for autocatalytic hydrolysis
	3	Quadratic-order rate law for autocatalytic hydrolysis
	4	1.5th-order rate law for autocatalytic hydrolysis
kscale_on	0	Use supplied k parameter as rate constant
	1	Use supplied k parameter as k_1' and convert to rate constant

Parameters	
Name	Definition
NR	Number of spatial discretizations including the boundaries
NS	Number of species
R	Polymer particle radius in cm
tau	Tortuosity, τ
DD	Diffusivity at infinite dilution of the drug, $D_{\mathrm{drug},\infty}$, in cm^2/s
DH	Diffusivity at infinite dilution of the monomers, $D_{\mathrm{P}_1,\infty}$, in cm^2/s
k	Reaction rate constant in units of days^{-1}, $\mathrm{M}^{-1}\mathrm{days}^{-1}$ or $\mathrm{M}^{-1/2}\mathrm{days}^{-1}$
PDI	Polymer polydispersity index
Mw	Polymer weight-average molecular weight
$drug0$	Initial drug concentration
$COOH0$	Initial COOH concentration
$Xrxn$	Extent of reaction in reaction-dominant limit
NT	Number of time points including $t = 0$ for output;
	$NT - 1$ is number of calls to RADAU5
$Rp0$	Initial uniform pore radius of polymer, $R_p(r, 0) = R_{p,t0}g$
$tfinal\_override$	Optional override for final time in days
G	Glycolic acid fraction of the polymer
TOL	Error tolerance TOL=RTOL=ATOL
$DD0$	Diffusivity of drug in the bulk polymer, $D_{\mathrm{drug},b}$
$DH0$	Diffusivity of small oligomers in the bulk polymer, $D_{\mathrm{P}_n,b}$

transport effects. Assuming uniformly distributions polymer throughout the particle,

$$[\mathrm{E}]_{t0} = [\mathrm{COOH}]_{t0} \left(\frac{M_{n,t0}}{M_1} - 1 \right). \tag{9.5}$$

The PDEs may be calculated with dimensionless concentrations. For the drug, the concentrations are scaled by the initial drug concentration at the center, $[\mathrm{drug}](0,0)$. For the polymeric species, the concentrations are scaled by the initial carboxylic acid end group concentration, $[\mathrm{COOH}]_{t0}$. The small oligomers are assumed to have zero initial concentration, so the initial large oligomer sum is equivalent to $[\mathrm{COOH}]_{t0}$. The scaled concentrations factor out of the accumulation terms and the diffusion terms. The scaled terms cancel for the net rates of generation for all species for the first-order rate law for uncatalyzed hydrolysis and the pseudo-first-order rate law for autocatalytic hydrolysis. The other two rate laws can be made dimensionless by modifying their rate constants to include the scaled $[\mathrm{COOH}]_{t0}$ concentration (a factor of $[\mathrm{COOH}]_{t0}$ for the quadratic-order rate law and of $\sqrt{[\mathrm{COOH}]_{t0}}$ for the 1.5th-order rate law). These modifications are reflected in the calculations of the rate constants when $kscale\_on = 1$. The most commonly reported degradation rate in the literature for PLGA is the rate constant for the pseudo-first order rate law for autocatalytic hydrolysis, k_1'. With *kscale_on* and dimensionless concentration terms, the rate constants for each of the four rate laws can be related to k_1' by equating $R_{V\mathrm{COOH}}(0)$ for the catalyzed and uncatalyzed cases to relate k_u and k_c:

$$R_{V\mathrm{COOH}}(0) = k_u'[\mathrm{E}]_{t0} = k_1'[\mathrm{COOH}]_{t0}. \tag{9.6}$$

- First-Order Rate Law for Uncatalyzed Hydrolysis

$$k_u' = k_u[\mathrm{H_2O}] = \frac{k_1'[\mathrm{COOH}]_{t0}}{[\mathrm{E}]_{t0}} \tag{9.7}$$

- Pseudo-First-Order Rate Law for Autocatalytic Hydrolysis

$$k_1' = k_c[\mathrm{H_2O}][\mathrm{E}] \tag{9.8}$$

- Quadratic-Order Rate Law for Autocatalytic Hydrolysis

$$k_2' = k_c[\mathrm{H_2O}] = \frac{k_1'[\mathrm{COOH}]_{t0}}{[\mathrm{E}]_{t0}} \tag{9.9}$$

- 1.5th-Order Rate Law for Autocatalytic Hydrolysis

$$k_{1.5}' = k_c[\mathrm{H_2O}] = \frac{k_1'\sqrt{[\mathrm{COOH}]_{t0}}}{[\mathrm{E}]_{t0}} \tag{9.10}$$

9.3 Subroutine *initial*

The subroutine *initial* sets the initial conditions for $Ri(NS)$, the solute radius of each species, and $u(NE)$, the solution vector for the system of ODEs, where $NE = NR(2NS + 1)$ is the number of ODEs in the system. Figure 9.2 shows the algorithm flow chart for *initial*. The code for *initial* is in Appendix B.3.

If *restart*=0, the values of $Rp0$, $drug0$, and $COOH0$ from *intpar* are used to initialize the solution vector with uniform concentration profiles. The vector of solute radii, Ri, consists of the average monomer length, l_{ave} (denoted as $lave$), multiplied by the number of monomeric units in the small oligomers; 0 for large oligomers, ester bonds, and carboxylic acid end groups; and the value Rd for the drug radius estimated from the Stokes-Einstein equation (6.28) with the diffusion coefficient at infinite dilution at 37°C. The initial vector of effective diffusivity values is populated by adding $D_{i,b}$ (given as $DH0$ and $DD0$ in *intpar* for the oligomers and the drug, respectively) to the calculated value for hindered diffusion, $D_{i,p}$, using $\lambda_i(r,t)$ denoted as the local variable $lambda = Ri/Rp0$ for each species.

For $restart > 0$, the initial time and solution vector are read from

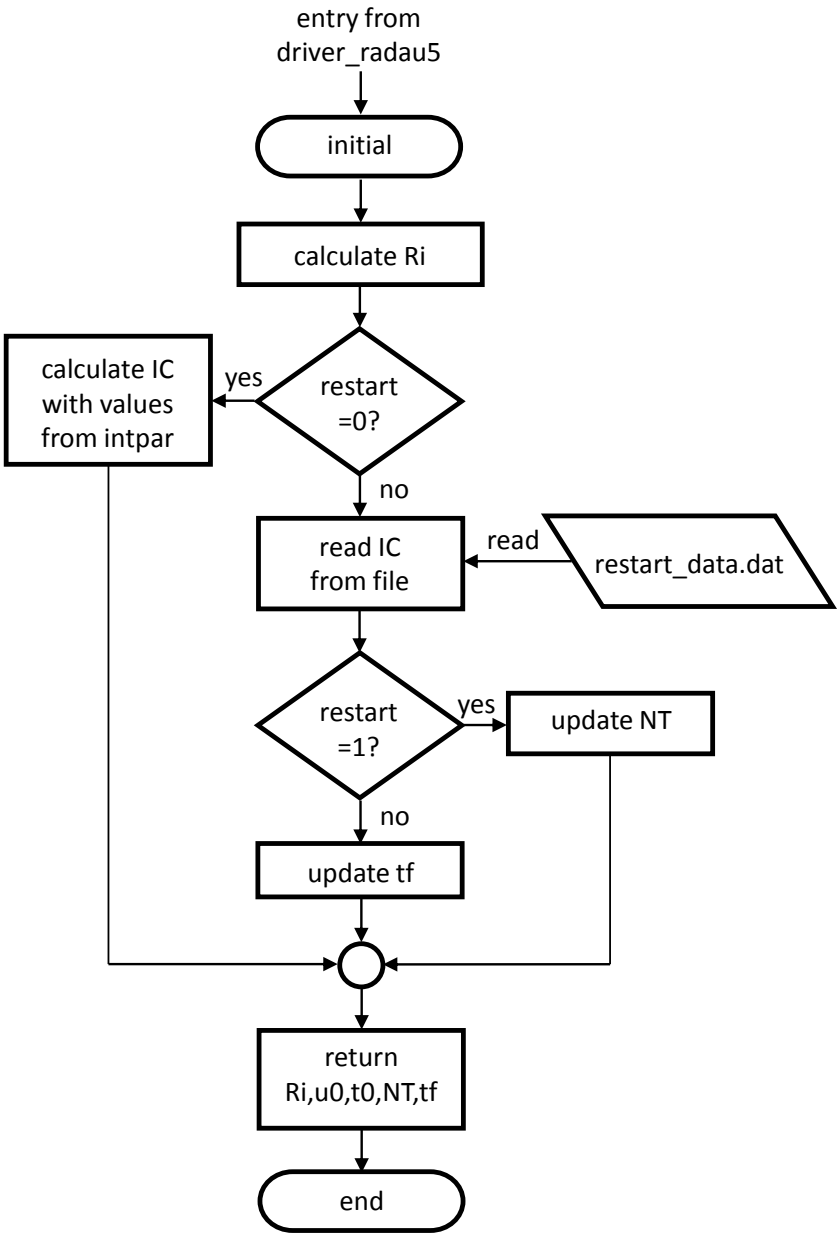

Figure 9.2: Flow chart for Fortran subroutine *initial*. Ri is the vector of solute radii for each species, *restart* is the token determining how the initial conditions are specified, and IC are the initial conditions $u0$ at $t0$ for the differential-difference equations in the system of ODEs, $NT-1$ is the number of calls to RADAU5, and tf is the time interval covered by each call to RADAU5. *intpar* is the subroutine that reads input data from the command line or a script file, and *restart_data.dat* is an optional file that contains the time and solution vector for initializing the current simulation at the end point of a previous simulation.

restart_data.dat. This option can be used to prescribe a nonuniform initial drug concentration profile at $t = 0$. For *restart*=1, the time intervals for calls to RADAU5 are kept the same as the interval size calculated in *intpar* based on the input parameters. The number of calls to the solver is adjusted if $t0 > 0$. For *restart*=2, the number of calls to the solver is kept at the valued specified in the script file, and the time intervals for the solver calls are adjusted.

9.4 RADAU5 Options and Subroutines *Fderiv* and *Jderiv*

The solver RADAU5 has a number of options to be specified. See the header of the *driver_radau5* routine in Appendix B.1 for a more complete description of the options. The values used for all the results presented in this dissertation are summarized here.

An external routine can be specified to compute the Jacobian matrix. Deriving the explicit analytical expressions for the partial derivatives with respect to each species concentration at each radial position is very time intensive. Evaluation of the analytical Jacobian is also computationally expensive. Alternatively, the option $IJAC$ is specified as zero, and the Jacobian is computed internally by finite differences. The subroutine *Jderiv* is simply a dummy routine. The numerical Jacobian does not have a banded structure, so the $MLJAC$ option is equal to NE to indicate that the Jacobian is a full matrix. The option $MUJAC$ need not be defined if $MLJAC$ is equal to the system size. The RADAU5 routine solves linearly implicit or explicit systems of first order ODEs of the form $MY' = F(X, Y)$ where M is the mass matrix. M is assumed to be the identity matrix if the parameter $IMAS$ is set to zero for a linearly explicit system as in the system described in this dissertation. The options $MLMAS$ and $MUMAS$ need not be specified for the structure of M in this case. The internal subroutine $SOLOUT$ is never called (option IOUT = 0) as the species of interest are explicitly

written to file at the end of each call to the integrator in the *driver_radau5* routine. The tolerance is specified as a scalar value, so $ITOL = 0$. The RADAU5 parameter vectors $WORK$ and $IWORK$ are initialized to zero to set the default values.

$RPAR$ and $IPAR$ are populated in *driver_radau5* with parameter values needed by the *deriv* subroutine and are passed into Fderiv, where the values are translated back into their respective variable names for local use within *deriv* and its subsidiary subroutines. The system of ODEs defined in subroutine *deriv* is called by *Fderiv*. The codes for *Fderiv* and *Jderiv* are given in Appendix B.5 and Appendix B.4, respectively.

9.5 Subroutine *deriv*

The PDEs for the concentrations of the drug, carboxylic acid end groups, ester bonds, small soluble polymer oligomers, and large polymer oligomers; average pore radius; and effective diffusivities of species within a sphere as functions of radial position and time comprise the system of PDEs. The PDEs are discretized radially to form a system of ODEs solved by the numerical integrator RADAU5. Figure 9.3 shows the algorithm flow chart for *deriv*. The code for *deriv* is in Appendix B.6.

9.6 Subroutine *rxn* and Subsidiary Subroutines

The subroutine *rxn* computes the reaction dependent-terms when $rxn\_on > 0$. If $rxn\_on = 0$ this subroutine is bypassed. The code for *rxn* is in Appendix B.7.

The net rate of generation, R_{Vi}, for carboxylic acid end groups, ester bonds, and small oligomers are updated using the net rates of generation for the species derived in Chapter 5. Each rate law has its own subroutine that is called based on the value of *rxn_on*. $rxn\_on = 1$ uses the subroutine *rxn_uncat* with code in Appendix B.8. $rxn\_on = 2$ uses the subroutine *rxn_pseudo* with code in Appendix B.9. $rxn\_on = 3$ uses the subroutine *rxn_quad* with code in

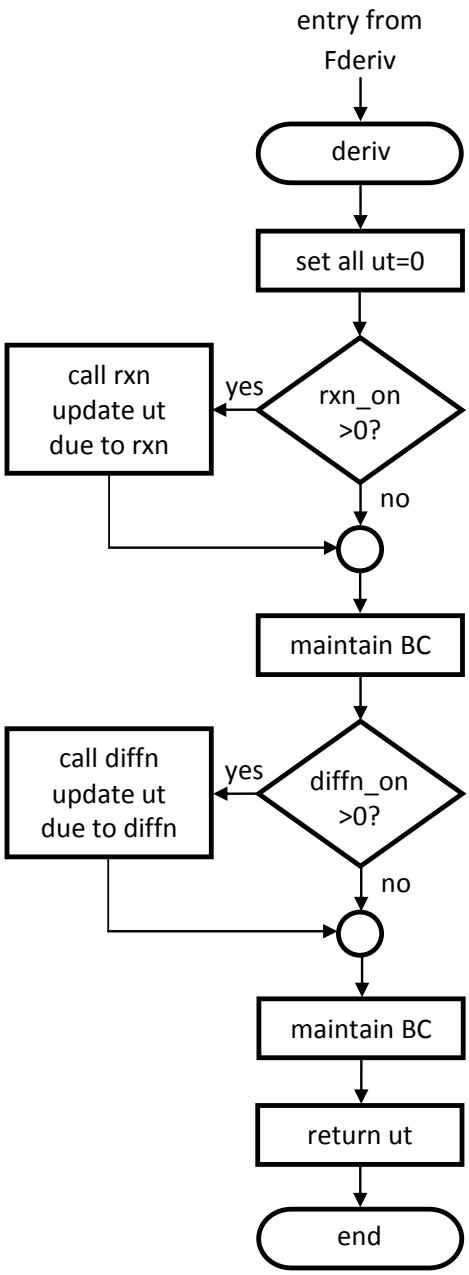

Figure 9.3: Flow chart for Fortran subroutine *deriv*. $ut(NE)$ is the derivative vector for the system of ODEs, *rxn_on* is the token determining which, if any, of the reaction rate laws to use, *diffn_on* is the token determining whether diffusion occurs and which of the constant or variable effective diffusivity options to implement, and BC are the surface boundary conditions. *diffn* is the subroutine that updates the diffusion contribution to the derivative vector, and *rxn* is the subroutine that updates the reaction contribution to the derivative vector.

Appendix B.10. $rxn\_on = 4$ uses the subroutine *rxn_half* with code in Appendix B.11.

The net rate of generation of the sum of the large oligomers and the differential equations for the average pore radius and the variable effective diffusivity of each species are updated using the R_{Vi} terms for the polymeric species. $\lambda_i(r,t)$ is calculated locally as *lambda* at the current value of R_p for each species and radial position. If $0 < lambda < 1$, the variable effective diffusivity of species is updated using the subroutine *derivDeff*, which computes the derivative of the effective diffusivity. The subroutine calls *derivH* to compute the derivative of the hindrance factor as given in Chapter 7. The codes for *derivDeff* and *derivH* are in Appendix B.12 and Appendix B.13, respectively.

9.7 Subroutine *diffn* and Subsidiary Subroutines

The subroutine *diffn* computes the diffusion dependent-terms when $diffn\_on > 0$. If $diffn\_on = 0$, this subroutine is bypassed. The code for *diffn* is in Appendix B.14.

A local vector of effective diffusivity for a single species at each position is passed to the subroutines that compute the diffusion terms. The local vector contains values of $\alpha_i(r,t_k) = D_i(r,t_k)/R^2$. If $diffn\_on = 1$, $D_i(r,t_k)$ for the small oligomers and the drug at every time step are set to the maximum values specified by DH and DD, respectively, as converted to units of days^{-1} by *intpar*. The global updated vector of effective diffusivity is ignored completely, and the effective diffusivity is treated as a constant for all species. If $diffn\_on = 2$, $D_i(r,t_k)$ for the small oligomers is set to the maximum values specified by DH. The updated vector of effective diffusivity is ignored for the small oligomers giving constant effective diffusivity of the polymeric species. The value of $D_i(r,t_k)$ for the drug is updated using the global vector of effective diffusivity, coupling the effective diffusivity of the drug to the reaction dynamics. If $diffn\_on = 3$, $D_i(r,t_k)$ for the small oligomers and

the drug are updated using the global vector of effective diffusivity.

The subroutine *diffn_ctr* computes the diffusion terms at r=0 , and the subroutine *diffn_int* computes the diffusion terms at $0 < r < 1$. Both subroutines update the diffusion contribution to the conservation equations for a single species with the local vector of effective diffusivity. The finite difference discretization schemes for these subroutines are described in Chapter 8. The codes for *diffn_ctr* and *diffn_int* are in Appendix B.15 and Appendix B.16, respectively.

The diffusion contributions to the conservation equations for carboxylic acid end groups and ester bonds by the transport of the soluble, small oligomers are updated in the *diffn* subroutine.

Chapter 10

Verification of the Computational Code

After the model equations are selected, discretized by a numerical method, and solved computationally, the code used to solve the model equations must be verified and validated to assess the quality of the code. Verification is the process of checking that the model equations are solved correctly using a particular code. Validation is the process of determining whether the equations chosen for the model are appropriate for the physical system being modeled [145]. This chapter assesses the convergence of the discrete, numerical approximations calculated by the code to the continuous equations of the model.

Beyond assessing the errors between the values of numerical approximations and analytical solutions, it is important to verify that the numerical approximations to the reaction-diffusion conservation equations converge to the exact solutions of the continuous equations at the theoretical rate-of-convergence for the numerical method. The verification of the rate-of-convergence ensures that the numerical methods have been implemented properly and the approximations depend on the spatial and temporal resolution in a known way.

Code verification involves using a known analytical solution to a limiting case in comparison to numerical approximations on discrete grids with successively refined grid spacing to verify the rate-of-convergence to the analytical, continuous solution. Section 10.1 describes the metrics used for code verification in the subsequent sections. Sections 10.2–10.4 present comparisons between the numerical and analytical solutions for some limiting cases of the reaction-diffusion model. In

Section 10.2 the reaction-dominant limit is used for verification of the reaction components of the model for the four hydrolysis reaction rate laws detailed in Chapter 5. In Section 10.3 the diffusion-dominant limit is used for verification of the diffusion component of the model with constant effective diffusivity. In Section 10.4 the single-component limit for the reaction-diffusion of COOH is used for the pseudo-first-order rate law for the autocatalytic hydrolysis reaction with constant diffusivity for verification of the reaction and diffusion components acting simultaneously.

10.1 Metrics for Code Verification

Three metrics are used in this section to quantify the error between the numerical approximations to the model equations and the analytical solutions of limiting cases: percent error, root-mean-square error, and rate-of-convergence.

Percent error is used to quantify the relative error between numerical and analytical values. The percent error, PE, between an analytical value, v_{an}, and an approximate numerical value, v_{num}, is defined as

$$PE(v) := \left| \frac{v_{an} - v_{num}}{v_{an}} \right| \times 100\%. \tag{10.1}$$

The global truncation error, e_N, is the accumulation of the local error due to a single iteration of the numerical method after N iterations and is defined by

$$e_N = |y(t_N) - y^N|, \tag{10.2}$$

where $y(t_N)$ is the continuous analytical solution at the Nth discrete time point and y^N is the approximate numerical solution at the Nth discrete time point.

The root-mean-square error, $RMSE$, is a scalar value with the same units as the data that is the square root of the mean of the errors between the numerical

and analytical values. For a 1-dimensional model with m discrete values, let the vector $\mathbf{x}$ be composed of the differences between the analytical solution and the model numerical approximation at the discrete points, that is, $x_j = x_{j_{an}} - x_{j_{num}}$ for $j = 1, 2, \ldots, m$. The $RMSE$ of a vector is defined as

$$RMSE(\mathbf{x}) := \sqrt{\frac{\sum_{j=1}^{m} |x_j|^2}{m}} = \sqrt{\frac{\sum_{j=1}^{m} (x_{j_{an}} - x_{j_{num}})^2}{m}} = \frac{|\mathbf{x}|_2}{\sqrt{m}}, \tag{10.3}$$

where the l^2-norm, $|\mathbf{x}|_2$, of a vector $\mathbf{x}$ with m elements is defined as

$$|\mathbf{x}|_2 := \sqrt{\sum_{j=1}^{m} |x_j|^2}. \tag{10.4}$$

For a 2-dimensional model with $m \times n$ discrete values, let the matrix $\mathbf{X}$ be composed of the differences between the analytical solution and the model numerical approximation at discrete points, that is, $x_{j,k} = x_{j,k_{an}} - x_{j,k_{num}}$ for $j = 1, 2, \ldots, m$ and $k = 1, 2, \ldots, n$. The $RMSE$ of a matrix is defined as

$$RMSE(\mathbf{X}) := \sqrt{\frac{\sum_{j=1}^{m}\sum_{k=1}^{n} |x_{j,k}|^2}{mn}} = \sqrt{\frac{\sum_{j=1}^{m}\sum_{k=1}^{n} (x_{j,k_{an}} - x_{j,k_{num}})^2}{mn}} = \frac{||\mathbf{X}||_F}{\sqrt{mn}}, \tag{10.5}$$

where the Frobenius norm, $||\mathbf{X}||_F$, of an $m \times n$ matrix $\mathbf{X}$ is defined as

$$||\mathbf{X}||_F := \sqrt{\sum_{j=1}^{m}\sum_{k=1}^{n} |x_{j,k}|^2}. \tag{10.6}$$

The rate-of-convergence is a measure of how quickly discrete solutions converge to continuous solutions as the grid size is reduced, i.e., $\Delta r, \Delta t \to 0$. The truncation error for a numerical method is the theoretical benchmark for the expected rate-of-convergence. If the numerical method is correctly implemented in the code, the numerical solution should match or exceed the theoretical

rate-of-convergence. Let Δx be the grid size for a computational grid. The rate-of-convergence is determined by comparing the error between exact solutions, y^{Exact}, and discrete solutions, $y(\Delta x)$, of scalar quantities or multi-dimensional quantities for successive *coarse* and *fine* grids with grid sizes Δx_C and Δx_F, respectively. The error between the exact and discrete solutions is

$$\epsilon_y(\Delta x) = ||y^{\text{Exact}} - y(\Delta x)|| = \beta(\Delta x)^p + O(\Delta x^p), \tag{10.7}$$

where the norm is user-defined, β is a regression coefficient, and p is the rate-of-convergence or the rate at which the error ϵ_y is reduced as the grid size decreases, $\Delta x \to 0$ [146]. The values of p and β can be determined if the error is known for two grid sizes. The two error equations are [146]

$$\begin{aligned} \epsilon_y(\Delta x_C) &= ||y^{\text{Exact}} - y(\Delta x_C)|| \approx \beta \Delta x_C^p \\ \epsilon_y(\Delta x_F) &= ||y^{\text{Exact}} - y(\Delta x_F)|| \approx \beta \Delta x_F^p. \end{aligned} \tag{10.8}$$

Solving (10.8) for p and β gives

$$p = \frac{\log \dfrac{\epsilon_y(\Delta x_C)}{\epsilon_y(\Delta x_F)}}{\log \dfrac{\Delta x_C}{\Delta x_F}} \tag{10.9}$$

and

$$\beta = \frac{\epsilon_y(\Delta x_C)}{\Delta x_C} = \frac{\epsilon_y(\Delta x_F)}{\Delta x_F}, \tag{10.10}$$

where the refinement ratio is $R_{CF} = \Delta x_C / \Delta x_F > 1$.

For each of the limiting cases (reaction-dominant limit, diffusion-dominant limit, and single-component limit), the percent error and the root-mean-square error are reported for quantities calculated by the numerical approximations and the analytical solutions. The rate-of-convergence is determined by comparing the root-mean-square error of certain quantities at different levels of grid refinement in

the r- and t-dimensions, independently.

10.2 Reaction-Dominant Limit

To verify that the numerical methods for the reaction component of the model have been implemented correctly, the numerical results for the reaction-dominant limit are compared to the analytical solution for the hydrolysis reaction rate laws for the case of well-mixed reactions (spatially uniform) in a constant volume, closed system.

The reaction-dominant limit of the reaction-diffusion equation for the conservation of species i given by (4.8) is approached as the effective diffusivity goes to zero and only reactions are observed. In a reacting system with spatial uniformity, the net amount of diffusion of any species is negligible. To approach the condition of well-mixedness, the effective diffusivities are assumed to be zero. The reaction-dominant limit is obtained by adding the following assumptions to those used to derive (4.8):

- The effective diffusivity is zero: $D_i(r,t) = 0$.
- The species concentration is well-mixed: $c_i(r,t) = c_i(t)$.
- The reactions are well-mixed without radial dependence: $\dfrac{\partial c_i(r,t)}{\partial t} = \dfrac{dc_i(t)}{dt}$ and $R_{Vi}(r,t) = R_{Vi}(t)$.
- The initial condition for each species i is $c_i(0) = c_{i,t0}$.

Without diffusion the net rates of generation derived in Chapter 5 are equal to the accumulation terms in the conservation equations for the appropriate species,

$$\frac{dc_i(t)}{dt} = R_{Vi}(t), \tag{10.11}$$

with initial condition

$$c_i(0) = c_{i,t0}. \tag{10.12}$$

10.2.1 Analytical Solutions for the Species Concentration, $c_i(t)$, in the Reaction-Dominant Limit

The analytical solutions for the carboxylic acid end group concentration, [COOH](t), and the ester bond concentration, [E](t), for the four hydrolysis kinetic rate laws derived in Chapter 5 are derived by solving ordinary differential equations (ODEs) of the form

$$\frac{d[\mathrm{COOH}](t)}{dt} = R_{V\mathrm{COOH}}(t) \tag{10.13}$$

and

$$\frac{d[\mathrm{E}](t)}{dt} = R_{V\mathrm{E}}(t), \tag{10.14}$$

respectively, where the reactions are assumed to be well-mixed. The differential equations in (10.13) and (10.14) are equivalent to the conservation equations for the COOH and E species, respectively, in the reaction-dominant limit given by (10.11). The analytical solutions are derived below for each rate law for hydrolysis.

10.2.1.1 First-Order Rate Law for Uncatalyzed Hydrolysis

The analytical expression for the concentration profile of carboxylic acid end groups for the first-order rate law for uncatalyzed hydrolysis is derived using two alternative methods: polymer chain concentration with moment analysis and ester bond concentration analysis. Expressions for the concentration profile of ester bonds, the time, t_X, required for the reaction to reach extent of reaction X, and the extrema of $R_{V\mathrm{COOH}}(t)$ and [COOH](t) are also derived.

Moment Analysis Recall (5.12) and assume that the system is well-mixed,

$$R_{V\mathrm{P}}(t) = k_u' \sum_{n=1}^{\infty} (n-1)\,[\mathrm{P}_n](t), \tag{10.15}$$

where $[\mathrm{P}](t) := \sum_{n=1}^{\infty}[\mathrm{P}_n](t)$. Moments are defined for each integer j as

$$\mu_j(t) := \sum_{n=1}^{\infty} n^j [\mathrm{P}_n](t). \tag{10.16}$$

For a linear aliphatic polyester, each polymer chain has one carboxylic acid end group, so

$$[\mathrm{COOH}](t) := [\mathrm{P}](t) = \sum_{n=1}^{\infty}[\mathrm{P}_n](t) = \mu_0(t). \tag{10.17}$$

(10.15) can be rewritten as [102]

$$R_{V\mathrm{COOH}}(t) = \frac{d\mu_0(t)}{dt} = k'_u \left(\mu_1(t) - \mu_0(t)\right), \tag{10.18}$$

with initial condition

$$\mu_0(0) = \mu_{0,t0}. \tag{10.19}$$

The initial concentration of monomer units among all polymer chains is by definition equivalent to μ_1. In a closed system, the total monomer concentration is constant, therefore

$$\frac{d\mu_1(t)}{dt} = 0. \tag{10.20}$$

The integration of (10.18) with μ_1 as a constant gives

$$\int_{\mu_{0,t0}}^{\mu_0(t)} \frac{1}{\mu_1 - \mu'_0} d\mu'_0 = \int_{t0}^{t} k'_u dt' \tag{10.21}$$

and

$$-\ln\left(\mu_1 - \mu_0(t)\right) + \ln\left(\mu_1 - \mu_{0,t0}\right) = k'_u t. \tag{10.22}$$

Multiplying through by -1 and taking the exponential to eliminate the logarithms yields

$$\frac{\mu_1 - \mu_0(t)}{\mu_1 - \mu_{0,t0}} = \exp\left(-k'_u t\right). \tag{10.23}$$

Solving for $\mu_0(t)$ yields

$$\mu_0(t) = \mu_1 - (\mu_1 - \mu_{0,t0}) \exp(-k_u' t). \tag{10.24}$$

Using the definitions of [COOH](t) and $\mu_j(t)$, the concentration of [COOH](t) as a function of time is

$$[\text{COOH}](t) = \sum_{n=1}^{\infty} n[\text{P}_n]_{t0} - \left(\sum_{n=1}^{\infty} n[\text{P}_n]_{t0} - [\text{COOH}]_{t0} \right) \exp(-k_u' t), \tag{10.25}$$

where

$$[\text{COOH}]_{t0} := [\text{COOH}](0). \tag{10.26}$$

The carboxylic acid end group and ester concentrations can be related by considering the amount of reacted ester. For every ester bond that is cleaved, one new carboxylic acid group is formed. For the spatially-uniform system with no transport effects, the relation is given by

$$[\text{E}]_{t0} - [\text{E}](t) = [\text{COOH}](t) - [\text{COOH}]_{t0}, \tag{10.27}$$

where

$$[\text{E}]_{t0} := [\text{E}](0). \tag{10.28}$$

Evaluating the definition of ester bonds in relation to the polymer chain concentration given by (5.14) at $t = 0$ gives

$$[\text{E}]_{t0} = \sum_{n=1}^{\infty} (n-1)[\text{P}_n]_{t0} = \sum_{n=1}^{\infty} n[\text{P}_n]_{t0} - \sum_{n=1}^{\infty} [\text{P}_n]_{t0}. \tag{10.29}$$

Rearranging and substituting $[\text{COOH}]_{t0}$ for the final term in (10.29) yields

$$\sum_{n=1}^{\infty} n[\text{P}_n]_{t0} = [\text{E}]_{t0} + [\text{COOH}]_{t0}. \tag{10.30}$$

Substituting (10.30) into (10.25) gives

$$[\text{COOH}](t) = [\text{COOH}]_{t0} + [\text{E}]_{t0}\left(1 - \exp\left(-k'_u t\right)\right). \tag{10.31}$$

Substituting (10.27) into (10.31) gives

$$[\text{E}](t) = [\text{E}]_{t0} \exp\left(-k'_u t\right). \tag{10.32}$$

Ester Bond Concentration Analysis Recall (5.15) and assume that the system is well-mixed,

$$R_{V\text{COOH}}(t) = k'_u[\text{E}](t). \tag{10.33}$$

Combining the net rate of generation of COOH with (10.13) and the expression relating [E](t) and [COOH](t) given by (10.27) gives

$$R_{V\text{COOH}}(t) = \frac{d[\text{COOH}](t)}{dt} = k'_u\left([\text{E}]_{t0} + [\text{COOH}]_{t0} - [\text{COOH}](t)\right). \tag{10.34}$$

Integrating yields

$$\int_{[\text{COOH}]_{t0}}^{[\text{COOH}](t)} \frac{1}{[\text{E}]_{t0} + [\text{COOH}]_{t0} - [\text{COOH}]'} d[\text{COOH}]' = \int_{t0}^{t} k'_u dt' \tag{10.35}$$

and

$$-\ln\left([\text{E}]_{t0} + [\text{COOH}]_{t0} - [\text{COOH}](t)\right) + \ln[\text{E}]_{t0} = k'_u t. \tag{10.36}$$

Multiplying through by -1 and taking the exponential to eliminate the logarithms yields

$$\frac{[\text{E}]_{t0} + [\text{COOH}]_{t0} - [\text{COOH}](t)}{[\text{E}]_{t0}} = \exp\left(-k'_u t\right). \tag{10.37}$$

Solving for [COOH](t) yields

$$[\text{COOH}](t) = [\text{COOH}]_{t0} + [\text{E}]_{t0}\left(1 - \exp\left(-k'_u t\right)\right). \tag{10.38}$$

This equation is equivalent to (10.31), the expression derived using moment analysis, showing that the moment analysis and the ester bond concentration analysis produce the same results.

Derivation of t_X A rearranged version of (10.32) useful for estimating k'_u from experimental data is [94]

$$\ln[\mathrm{E}](t) = -k'_u t + \ln[\mathrm{E}]_{t0}. \tag{10.39}$$

This equation can be written in terms of the extent of reaction X relative to the ester bonds, which is the proportion of ester bonds that have reacted in the system at time t_X:

$$[\mathrm{E}](t_X) = (1 - X)[\mathrm{E}]_{t0}. \tag{10.40}$$

Substituting (10.40) into (10.39) gives

$$\ln\left((1 - X)[\mathrm{E}]_{t0}\right) = -k'_u t_X + \ln[\mathrm{E}]_{t0}. \tag{10.41}$$

Solving for t_X yields

$$t_X = \frac{1}{k'_u} \ln \frac{1}{1 - X}. \tag{10.42}$$

Derivation of Extrema of $R_{V\mathrm{COOH}}(t)$ The extrema of $R_{V\mathrm{COOH}}(t)$ on a closed time interval $[0, t_f]$ are located at the endpoints of the interval or the critical points in the interval where $\dfrac{dR_{V\mathrm{COOH}}(t)}{dt} = 0$ or $\dfrac{dR_{V\mathrm{COOH}}(t)}{dt}$ does not exist. The largest of the values of $R_{V\mathrm{COOH}}(t)$ evaluated at the endpoints and critical points is the absolute maximum value, and the smallest of these values is the absolute minimum value. The interval endpoint t_f is taken to the be time when the extent of reaction X approaches 100%.

The rate of generation of carboxylic acid end groups is given by (10.33)

and (10.34) for the first-order rate law for uncatalyzed hydrolysis:

$$R_{V\mathrm{COOH}}(t) = k'_u[\mathrm{E}](t) = k'_u\left([\mathrm{E}]_{t0} + [\mathrm{COOH}]_{t0} - [\mathrm{COOH}](t)\right). \tag{10.43}$$

Endpoints Evaluating (10.43) at time $t = 0$,

$$R_{V\mathrm{COOH}}(0) = k'_u[\mathrm{E}]_{t0}. \tag{10.44}$$

Using the equation for t_X given by (10.42) and the definition of t_f,

$$t_f = \lim_{X\to 1} \frac{1}{k'_u} \ln \frac{1}{1-X} \to \infty \tag{10.45}$$

The carboxylic acid concentration given by (10.38) in the limit of $t_f \to \infty$ is

$$\lim_{t_f\to\infty} [\mathrm{COOH}](t_f) = [\mathrm{COOH}]_{t0} + [\mathrm{E}]_{t0}\left(1 - \exp\left(-k'_u t_f\right)\right) = [\mathrm{COOH}]_{t0} + [\mathrm{E}]_{t0}. \tag{10.46}$$

Evaluating (10.43) at time $t = t_f \to \infty$,

$$\lim_{t_f\to\infty} R_{V\mathrm{COOH}}(t_f) = k'_u\left([\mathrm{E}]_{t0} + [\mathrm{COOH}]_{t0} - \left([\mathrm{COOH}]_{t0} + [\mathrm{E}]_{t0}\right)\right) = 0. \tag{10.47}$$

Critical Points The critical points of $R_{V\mathrm{COOH}}(t)$ are located where $\dfrac{dR_{V\mathrm{COOH}}(t)}{dt} = 0$ or $\dfrac{dR_{V\mathrm{COOH}}(t)}{dt}$ does not exist.

$$\begin{aligned}
\frac{dR_{V\mathrm{COOH}}(t)}{dt} &= \frac{d\left(k'_u\left([\mathrm{E}]_{t0} + [\mathrm{COOH}]_{t0} - [\mathrm{COOH}](t)\right)\right)}{dt} \\
&= -k'_0 \frac{d[\mathrm{COOH}](t)}{dt} \\
&= -k'_0 R_{V\mathrm{COOH}}(t).
\end{aligned} \tag{10.48}$$

As $k'_0 > 0$ and the derivative is smooth and continuous in the interval, the only critical point of $R_{V\mathrm{COOH}}(t)$ occurs when $R_{V\mathrm{COOH}}(t) = 0$. This critical point coincides with the endpoint t_f.

Absolute Maximum and Minimum Values The absolute minimum value of the rate of generation of COOH in the interval $[0, t_f]$ is $R_{V\mathrm{COOH}}(t_f) = 0$ as $t_f \to \infty$ with COOH at its maximum value, $[\mathrm{COOH}](t_f) \to [\mathrm{E}]_{t0} + [\mathrm{COOH}]_{t0}$. The absolute maximum value of the rate of generation of COOH in the interval $[0, t_f]$ is $R_{V\mathrm{COOH}}(0) = k'_u[\mathrm{E}]_{t0}$ with COOH at its minimum value, $[\mathrm{COOH}](0) = [\mathrm{COOH}]_{t0}$.

Summary For the first-order rate law for uncatalyzed hydrolysis, the analytical solutions to the conservation equations for COOH and E in the reaction-dominant limit are

$$[\mathrm{COOH}](t) = [\mathrm{COOH}]_{t0} + [\mathrm{E}]_{t0}\left(1 - \exp\left(-k'_u t\right)\right). \tag{10.49}$$

and

$$[\mathrm{E}](t) = [\mathrm{E}]_{t0} \exp\left(-k'_u t\right), \tag{10.50}$$

where $[\mathrm{COOH}]_{t0}$ and $[\mathrm{E}]_{t0}$ are the initial concentrations of carboxylic acid end groups and ester bonds, respectively, $k'_u := k_u[\mathrm{H_2O}]$, k_u is the rate constant for the uncatalyzed hydrolysis reaction, and $[\mathrm{H_2O}]$ is the constant concentration of water.

The time when the extent of reaction reaches 99%, $t_{0.99}$, is given by (10.42) with $X = 0.99$,

$$t_{0.99} = \frac{1}{k'_{t0}} \ln \frac{1}{1 - 0.99} = \frac{\ln 100}{k'_{t0}}. \tag{10.51}$$

10.2.1.2 Pseudo-First-Order Rate Law for Autocatalytic Hydrolysis

The analytical expression for the concentration profile of carboxylic acid end groups for the pseudo-first-order rate law for autocatalytic hydrolysis is derived using ester bond concentration analysis. Expressions for the concentration profile of ester bonds, the time, t_X, required for the reaction to reach extent of reaction X, and the extrema of $R_{V\mathrm{COOH}}(t)$ and $[\mathrm{COOH}](t)$ are also derived.

Ester Bond Concentration Analysis Since each polymer chain one carboxylic acid end group, $[\mathrm{COOH}](t)$ is not completely independent of the concentrations of the

other species. If the hydrolysis reaction progresses to a significant extent, the assumption of constant ester bond concentration is no longer valid. At the time, t_f, when the extent of reaction approaches 100%, all the ester bonds have been cleaved, $E = 0$, and the monomers are the only remaining polymeric species as

$$\sum_{n=2}^{\infty} [\mathrm{P}_n](t_f) = 0. \tag{10.52}$$

The hydrolysis reaction stops, and the rate of generation of new carboxylic acid end groups is zero,

$$R_{V\mathrm{COOH}}(t) = 0, \quad t \geq t_f, \tag{10.53}$$

so

$$[\mathrm{COOH}](t) = [\mathrm{COOH}](t_f), \quad t \geq t_f. \tag{10.54}$$

It is assumed that the ester bond concentration is constant at the initial value unless t_f is reached. The values of t_f and $[\mathrm{COOH}](t_f)$ are derived later in this section.

If the reaction reaches completion at t_f, the assumption of constant ester concentration is violated. The ester concentration is assumed to have a constant value of zero from t_f onward. The rate of generation of ester bonds is still zero but has a discontinuity at t_f. The ester bond concentration is

$$[\mathrm{E}](t) = \begin{cases} [\mathrm{E}]_{t0}, & \text{if } 0 \leq t < t_f; \\ 0, & \text{if } t \geq t_f, \end{cases} \tag{10.55}$$

where t_f is the time when the extent of reaction approaches 100%.

With consideration of t_f and assuming that the system is well-mixed, (5.21) becomes

$$R_{V\mathrm{COOH}}(t) = \begin{cases} k_1'[\mathrm{COOH}](t), & \text{if } 0 \leq t < t_f; \\ 0, & \text{if } t \geq t_f. \end{cases} \tag{10.56}$$

The integration of (10.56) for $t < t_f$ gives

$$\int_{[\mathrm{COOH}]_{t0}}^{[\mathrm{COOH}](t)} \frac{1}{[\mathrm{COOH}]'} d[\mathrm{COOH}]' = \int_{t0}^{t} k_1' dt' \tag{10.57}$$

and

$$\ln \frac{[\mathrm{COOH}](t)}{[\mathrm{COOH}]_{t0}} = k_1' t. \tag{10.58}$$

Solving for [COOH](t) for $t < t_f$ yields [103]

$$[\mathrm{COOH}](t) = [\mathrm{COOH}]_{t0} \exp(k_1' t), \quad t < t_f. \tag{10.59}$$

Derivation of t_X A rearranged version of (10.59) useful for estimating k_1' from experimental data is

$$\ln[\mathrm{COOH}](t) = k_1' t + \ln[\mathrm{COOH}]_{t0}. \tag{10.60}$$

Even though [E] is assumed constant in the pseudo-first-order rate law for the autocatalytic hydrolysis reaction, the extent of reaction completion relative to [COOH] is of interest. The expressions relating [E](t) and [COOH](t) given by (10.27) and relating [E](t) to the extent of reaction given by (10.40) can be substituted into (10.60) to determine the time when the extent of reaction X has been reached,

$$\ln\left([\mathrm{E}]_{t0} + [\mathrm{COOH}]_{t0} - (1 - X)[\mathrm{E}]_{t0}\right) = k_1' t_X + \ln[\mathrm{COOH}]_{t0}. \tag{10.61}$$

Solving for t_X yields

$$t_X = \frac{1}{k_1'} \ln \frac{[\mathrm{COOH}]_{t0} + X[\mathrm{E}]_{t0}}{[\mathrm{COOH}]_{t0}}. \tag{10.62}$$

Derivation of Extrema of $R_{V\mathrm{COOH}}(t)$ The extrema of $R_{V\mathrm{COOH}}(t)$ on a closed time interval $[0, t_f]$ are located at the endpoints of the interval or the critical points in the interval where $\dfrac{dR_{V\mathrm{COOH}}(t)}{dt} = 0$ or $\dfrac{dR_{V\mathrm{COOH}}(t)}{dt}$ does not exist. The largest of the values of $R_{V\mathrm{COOH}}(t)$ evaluated at the endpoints and critical points is the

absolute maximum value, and the smallest of these values is the absolute minimum value. The interval endpoint t_f is taken to the be time when the extent of reaction X approaches 100%.

The rate of generation of carboxylic acid end groups is given by (10.56) for the pseudo-first-order rate law for autocatalytic hydrolysis:

$$R_{V\mathrm{COOH}}(t) = \begin{cases} k_1'[\mathrm{COOH}](t), & \text{if } 0 \leq t < t_f; \\ 0, & \text{if } t \geq t_f. \end{cases} \tag{10.63}$$

Endpoints Evaluating (10.63) at time $t = 0$,

$$R_{V\mathrm{COOH}}(0) = k_1'[\mathrm{COOH}]_{t0}. \tag{10.64}$$

Using the equation for t_X given by (10.62) and the definition of t_f,

$$t_f = \lim_{X \to 1} \frac{1}{k_1'} \ln \frac{[\mathrm{COOH}]_{t0} + X[\mathrm{E}]_{t0}}{[\mathrm{COOH}]_{t0}} = \frac{1}{k_1'} \ln \frac{[\mathrm{COOH}]_{t0} + [\mathrm{E}]_{t0}}{[\mathrm{COOH}]_{t0}} \tag{10.65}$$

The carboxylic acid concentration given by (10.59) at t_f is

$$[\mathrm{COOH}](t_f) = [\mathrm{COOH}]_{t0} \exp(k_1' t_f) = [\mathrm{COOH}]_{t0} + [\mathrm{E}]_{t0}. \tag{10.66}$$

Evaluating (10.63) as time approaches t_f from the left,

$$\lim_{t \to {t_f}^-} R_{V\mathrm{COOH}}(t) = k_1' \left([\mathrm{COOH}]_{t0} + [\mathrm{E}]_{t0} \right). \tag{10.67}$$

Critical Points The critical points of $R_{V\mathrm{COOH}}(t)$ are located where $\dfrac{dR_{V\mathrm{COOH}}(t)}{dt} = 0$ or $\dfrac{dR_{V\mathrm{COOH}}(t)}{dt}$ does not exist. For $0 \leq t < t_f$,

$$\begin{aligned}\frac{dR_{V\mathrm{COOH}}(t)}{dt} &= \frac{d\left(k_1'[\mathrm{COOH}](t)\right)}{dt} \\ &= k_1' \frac{d[\mathrm{COOH}](t)}{dt} \\ &= k_1' R_{V\mathrm{COOH}}(t).\end{aligned} \tag{10.68}$$

As $k_1' > 0$ and the derivative is smooth and continuous in the interval, the only critical point of $R_{V\mathrm{COOH}}(t)$ occurs when $R_{V\mathrm{COOH}}(t) = 0$. This critical point can only occur if $[\mathrm{COOH}](t) = 0$, which is only possible if $[\mathrm{COOH}]_{t0} = 0$ or transport effects are considered. If $[\mathrm{COOH}]_{t0} = 0$, then $[\mathrm{COOH}](t) \equiv 0$. For nontrivial initial conditions and without transport effects, no critical points exist in the interval $[0, t_f)$. At t_f the derivative does not exist because of the discontinuity of (10.63). $R_{V\mathrm{COOH}}(t_f)$ is a critical point.

Absolute Maximum and Minimum Values The absolute minimum value of the net rate of generation of COOH in the interval $[0, t_f)$ is $R_{V\mathrm{COOH}}(0) = 0$ with COOH at its minimum value, $[\mathrm{COOH}](0) = [\mathrm{COOH}]_{t0}$. The absolute maximum value of the net rate of generation of COOH in the interval $[0, t_f)$ is $\lim\limits_{t \to {t_f}^-} R_{V\mathrm{COOH}}(t) = k_1' \left([\mathrm{COOH}]_{t0} + [\mathrm{E}]_{t0}\right)$ with $t_f = \dfrac{1}{k_1'} \ln \dfrac{[\mathrm{COOH}]_{t0} + [\mathrm{E}]_{t0}}{[\mathrm{COOH}]_{t0}}$ with COOH at its maximum value, $[\mathrm{COOH}](t_f) = [\mathrm{E}]_{t0} + [\mathrm{COOH}]_{t0}$.

Summary For the pseudo-first-order rate law for autocatalytic hydrolysis, the analytical solutions to the conservation equations for COOH and E in the reaction-dominant limit are

$$[\mathrm{COOH}](t) = \begin{cases} [\mathrm{COOH}]_{t0} \exp(k_1' t), & \text{if } 0 \leq t \leq t_f; \\ [\mathrm{COOH}]_{t0} + [\mathrm{E}]_{t0}, & \text{if } t \geq t_f. \end{cases} \tag{10.69}$$

and

$$[\mathrm{E}](t) = \begin{cases} [\mathrm{E}]_{t0}, & \text{if } 0 \leq t < t_f; \\ 0, & \text{if } t \geq t_f, \end{cases} \tag{10.70}$$

where $[\mathrm{COOH}]_{t0}$ is the initial concentration of carboxylic acid end groups, $k_1' := k_c[\mathrm{H_2O}][\mathrm{E}]$, $[\mathrm{H_2O}]$ and $[\mathrm{E}] = [\mathrm{E}]_{t0}$ are the constant concentrations of water and ester bonds, respectively, k_c is the rate constant for the autocatalytic hydrolysis reaction, $t_f = \dfrac{1}{k_1'} \ln \dfrac{[\mathrm{COOH}]_{t0} + [\mathrm{E}]_{t0}}{[\mathrm{COOH}]_{t0}}$, and t_f is the time required for the reaction to reach completion.

For the reaction-dominant limit plots shown in Section 10.2.2, the final time is chosen to be the time for 99% release, so the reaction time is always less than t_f. The time when the extent of reaction reaches 99%, $t_{0.99}$, is given by (10.62) with $X = 0.99$,

$$t_{0.99} = \frac{1}{k_1'} \ln \frac{[\mathrm{COOH}]_{t0} + 0.99[\mathrm{E}]_{t0}}{[\mathrm{COOH}]_{t0}}. \tag{10.71}$$

10.2.1.3 Quadratic-Order Rate Law for Autocatalytic Hydrolysis

The analytical expression for the concentration profile of carboxylic acid end groups for the quadratic-order rate law for autocatalytic hydrolysis is derived using two alternative methods: polymer chain concentration with moment analysis and ester bond concentration analysis. Expressions for the concentration profile of ester bonds, the time required, t_X, for the reaction to reach extent of reaction X, and the extrema of $R_{V\mathrm{COOH}}(t)$ and $[\mathrm{COOH}](t)$ are also derived.

Moment Analysis Nishida et al. [92] added the autocatalytic contribution of the carboxylic acid end groups to the model by Yoon et al. [102] for polyester hydrolysis by multiplying the net rate of generation of the sum of the polymer chains for uncatalyzed hydrolysis, (5.12), by the carboxylic acid end group concentration to

obtain

$$R_{VP}(t) = k_2' \sum_{n=1}^{\infty} (n-1)[\mathrm{P}_n](t)[\mathrm{COOH}](t), \tag{10.72}$$

with initial condition

$$[\mathrm{P}](0) = [\mathrm{P}]_{t0}. \tag{10.73}$$

Using the definition of $[\mathrm{E}](t)$ related to the polymer chain concentration given by (5.14) and the fact that $[\mathrm{COOH}](t) = [\mathrm{P}](t)$, (10.72) is equivalent to (5.28),

$$R_{V\mathrm{COOH}}(t) = k_2'[\mathrm{COOH}](t)[\mathrm{E}](t). \tag{10.74}$$

Using moments as defined in (10.16), (10.72) can be rewritten as [92]

$$R_{V\mathrm{COOH}}(t) = \frac{d\mu_0(t)}{dt} = k_2'\mu_0(t)(\mu_1(t) - \mu_0(t)), \tag{10.75}$$

with initial condition

$$\mu_0(0) = \mu_{0,t0}. \tag{10.76}$$

With constant μ_1, the integration of (10.75) is

$$\int_{\mu_{0,t0}}^{\mu_0(t)} \frac{1}{\mu_0' \left(\mu_1 - \mu_0'\right)} d\mu_0' = \int_{t0}^{t} k_2' dt'. \tag{10.77}$$

The integral can be solved using a partial fractions expansion.

$$\int_{\mu_{0,t0}}^{\mu_0(t)} \frac{1}{\mu_0'(\mu_1 - \mu_0')} d\mu_0' = \frac{1}{\mu_1} \int_{\mu_{0,t0}}^{\mu_0(t)} \left(\frac{1}{\mu_0'} + \frac{1}{\mu_1 - \mu_0'} \right) d\mu_0' = k_2' t'. \tag{10.78}$$

$$\int_{\mu_{0,t0}}^{\mu_0(t)} \frac{1}{\mu_0'} d\mu_0' + \int_{\mu_{0,t0}}^{\mu_0(t)} \frac{1}{\mu_1 - \mu_0'} d\mu_0' = \mu_1 k_2' t'. \tag{10.79}$$

$$\ln \frac{\mu_0(t)}{\mu_{0,t0}} - \ln \frac{\mu_1 - \mu_0(t)}{\mu_1 - \mu_{0,t0}} = \mu_1 k_2' t. \tag{10.80}$$

$$\frac{\mu_0(t)(\mu_1 - \mu_{0,t0})}{\mu_{0,t0}(\mu_1 - \mu_0(t))} = \exp(\mu_1 k_2' t). \tag{10.81}$$

Solving for $\mu_0(t)$ yields

$$\mu_0(t)(\mu_1 - \mu_{0,t0}) = \mu_{0,t0}(\mu_1 - \mu_0(t))\exp(\mu_1 k_2' t). \tag{10.82}$$

$$\mu_0(t) = \frac{\mu_1 \mu_{0,t0}\exp(\mu_1 k_2' t)}{\mu_{0,t0}\exp(\mu_1 k_2' t) + \mu_1 - \mu_{0,t0}}. \tag{10.83}$$

$$\mu_0(t) = \frac{\mu_1 \mu_{0,t0}}{\mu_{0,t0} + (\mu_1 - \mu_{0,t0})\exp(-\mu_1 k_2' t)}. \tag{10.84}$$

Using the relationship between the ester concentration and the concentration of polymer chains from (5.14) along with the definitions of $\mu_0(t)$ and μ_1,

$$[\mathrm{E}](t) = \mu_1 - \mu_0(t). \tag{10.85}$$

Substituting (10.85) into (10.84) gives

$$[\mathrm{COOH}](t) = \frac{[\mathrm{COOH}]_{t0}([\mathrm{E}]_{t0} + [\mathrm{COOH}]_{t0})}{[\mathrm{COOH}]_{t0} + [\mathrm{E}]_{t0}\exp(-([\mathrm{E}]_{t0} + [\mathrm{COOH}]_{t0})k_2' t)}. \tag{10.86}$$

Ester Bond Concentration Analysis Recall (5.28) and assume that the system is well-mixed,

$$R_{V\mathrm{COOH}}(t) = k_2'[\mathrm{COOH}](t)[\mathrm{E}](t). \tag{10.87}$$

Considering $u(t)$, the number of carboxylic acid end groups generated by hydrolysis after time t,

$$u(t) := [\mathrm{COOH}](t) - [\mathrm{COOH}]_{t0} = [\mathrm{E}]_{t0} - [\mathrm{E}](t), \tag{10.88}$$

the net rate of generation of $[\mathrm{COOH}](t)$ given by (10.87) can be rewritten in terms of the single variable $u(t)$ as [91, 93]

$$\frac{du(t)}{dt} = k_2'([\mathrm{COOH}]_{t0} + u(t))([\mathrm{E}]_{t0} - u(t)), \tag{10.89}$$

with initial condition

$$u(0) = 0. \tag{10.90}$$

Integration of the differential equation gives

$$\int_0^{u(t)} \frac{1}{([\mathrm{E}]_{t0} - u')([\mathrm{COOH}]_{t0} + u')} du' = \int_{t0}^{t} k_2' dt'. \tag{10.91}$$

This integral can be solved by a partial fractions expansion [91, 93]:

$$\frac{1}{[\mathrm{E}]_{t0} + [\mathrm{COOH}]_{t0}} \int_{t0}^{u(t)} \left(\frac{1}{[\mathrm{E}]_{t0} - u'} + \frac{1}{[\mathrm{COOH}]_{t0} + u'} \right) du' = k_2' t. \tag{10.92}$$

$$\frac{1}{[\mathrm{E}]_{t0} + [\mathrm{COOH}]_{t0}} \left(\int_0^{u(t)} \frac{1}{[\mathrm{E}]_{t0} - u'} du' + \int_{t0}^{u(t)} \frac{1}{[\mathrm{COOH}]_{t0} + u'} du' \right) = k_2' t. \tag{10.93}$$

$$\frac{1}{[\mathrm{E}]_{t0} + [\mathrm{COOH}]_{t0}} \left(\ln \frac{[\mathrm{E}]_{t0}}{[\mathrm{E}]_{t0} - u(t)} + \ln \frac{[\mathrm{COOH}]_{t0} + u(t)}{[\mathrm{COOH}]_{t0}} \right) = k_2' t. \tag{10.94}$$

$$\frac{[\mathrm{E}]_{t0}([\mathrm{COOH}]_{t0} + u(t))}{([\mathrm{E}]_{t0} - u(t))[\mathrm{COOH}]_{t0}} = \exp(([\mathrm{E}]_{t0} + [\mathrm{COOH}]_{t0}) k_2' t). \tag{10.95}$$

Solving for $u(t)$ yields [91]

$$u(t) = \frac{[\mathrm{COOH}]_{t0}(\exp(([\mathrm{E}]_{t0} + [\mathrm{COOH}]_{t0}) k_2' t) - 1)}{1 + \frac{[\mathrm{COOH}]_{t0}}{[\mathrm{E}]_{t0}} \exp(([\mathrm{E}]_{t0} + [\mathrm{COOH}]_{t0}) k_2' t)}. \tag{10.96}$$

$$u(t) = \frac{[\mathrm{COOH}]_{t0}(1 - \exp(-([\mathrm{E}]_{t0} + [\mathrm{COOH}]_{t0}) k_2' t))}{\frac{[\mathrm{COOH}]_{t0}}{[\mathrm{E}]_{t0}} + \exp(-([\mathrm{E}]_{t0} + [\mathrm{COOH}]_{t0}) k_2' t)}. \tag{10.97}$$

Inserting (10.97) into $[\mathrm{COOH}](t) = u(t) + [\mathrm{COOH}]_{t0}$ yields

$$[\mathrm{COOH}](t) = [\mathrm{COOH}]_{t0} \left(\frac{(1 - \exp(-([\mathrm{E}]_{t0} + [\mathrm{COOH}]_{t0}) k_2' t))}{\frac{[\mathrm{COOH}]_{t0}}{[\mathrm{E}]_{t0}} + \exp(-([\mathrm{E}]_{t0} + [\mathrm{COOH}]_{t0}) k_2' t)} + 1 \right). \tag{10.98}$$

$$[\mathrm{COOH}](t) = \frac{[\mathrm{COOH}]_{t0} \left([\mathrm{E}]_{t0} + [\mathrm{COOH}]_{t0} \right)}{[\mathrm{COOH}]_{t0} + [\mathrm{E}]_{t0} \exp\left(- \left([\mathrm{E}]_{t0} + [\mathrm{COOH}]_{t0} \right) k_2' t \right)}. \tag{10.99}$$

(10.99) is equivalent to (10.86), the expression derived using moment analysis, showing that the moment analysis and the ester bond concentration analysis produce the same results.

Inserting (10.97) into $[\mathrm{E}](t) = [\mathrm{E}]_{t0} - u(t)$ yields

$$[\mathrm{E}](t) = [\mathrm{E}]_{t0}\left(1 - \frac{[\mathrm{COOH}]_{t0}(1 - \exp(-([\mathrm{E}]_{t0} + [\mathrm{COOH}]_{t0})k_2' t))}{[\mathrm{COOH}]_{t0} + [\mathrm{E}]_{t0}\exp(-([\mathrm{E}]_{t0} + [\mathrm{COOH}]_{t0})k_2' t)}\right). \tag{10.100}$$

$$[\mathrm{E}](t) = \frac{[\mathrm{E}]_{t0}\left([\mathrm{E}]_{t0} + [\mathrm{COOH}]_{t0}\right)\exp\left(-\left([\mathrm{E}]_{t0} + [\mathrm{COOH}]_{t0}\right)k_2' t\right)}{[\mathrm{COOH}]_{t0} + [\mathrm{E}]_{t0}\exp\left(-\left([\mathrm{E}]_{t0} + [\mathrm{COOH}]_{t0}\right)k_2' t\right)}. \tag{10.101}$$

Derivation of t_X A rearranged version of (10.99) useful for estimating k_2' from experimental data is [93]

$$\ln\frac{[\mathrm{COOH}](t)}{[\mathrm{E}](t)} = ([\mathrm{E}]_{t0} + [\mathrm{COOH}]_{t0})k_2' t + \ln\frac{[\mathrm{COOH}]_{t0}}{[\mathrm{E}]_{t0}}. \tag{10.102}$$

The expression relating $[\mathrm{E}](t)$ to the extent of reaction given by (10.40) can be substituted into (10.102) to determine the time at which X extent of reaction relative to the ester bonds has been reached,

$$\ln\frac{[\mathrm{E}]_{t0} + [\mathrm{COOH}]_{t0} - (1-X)[\mathrm{E}]_{t0}}{(1-X)[\mathrm{E}]_{t0}} = ([\mathrm{E}]_{t0} + [\mathrm{COOH}]_{t0})k_2' t_X + \ln\frac{[\mathrm{COOH}]_{t0}}{[\mathrm{E}]_{t0}}. \tag{10.103}$$

Solving for t_X yields

$$t_X = \frac{1}{k_2'\left([\mathrm{E}]_{t0} + [\mathrm{COOH}]_{t0}\right)}\ln\frac{[\mathrm{COOH}]_{t0} + X[\mathrm{E}]_{t0}}{[\mathrm{COOH}]_{t0}\left(1-X\right)}. \tag{10.104}$$

Derivation of Extrema of $R_{V\mathrm{COOH}}(t)$ The extrema of $R_{V\mathrm{COOH}}(t)$ on a closed time interval $[0, t_f]$ are located at the endpoints of the interval or the critical points in the interval where $\dfrac{dR_{V\mathrm{COOH}}(t)}{dt} = 0$ or $\dfrac{dR_{V\mathrm{COOH}}(t)}{dt}$ does not exist. The largest of the values of $R_{V\mathrm{COOH}}(t)$ evaluated at the endpoints and critical points is the absolute maximum value, and the smallest of these values is the absolute minimum value. The interval endpoint t_f is taken to the be time when the extent of reaction X approaches 100%.

The net rate of generation of carboxylic acid end groups is given by (10.87) for the quadratic-order rate law for autocatalytic hydrolysis. Substituting the

number of carboxylic acid end groups generated by hydrolysis, $u(t)$, given by (10.88),

$$R_{V\mathrm{COOH}}(t) = k_2'[\mathrm{COOH}](t)[\mathrm{E}](t) = k_2'([\mathrm{COOH}]_{t0} + u(t))([\mathrm{E}]_{t0} - u(t)) = \frac{du(t)}{dt}. \tag{10.105}$$

Endpoints Evaluating (10.105) at time $t = 0$,

$$R_{V\mathrm{COOH}}(0) = k_2'[\mathrm{COOH}]_{t0}[\mathrm{E}]_{t0}. \tag{10.106}$$

Using the equation for t_X given by (10.104) and the definition of t_f,

$$t_f = \lim_{X\to 1} \frac{1}{k_2'\left([\mathrm{E}]_{t0} + [\mathrm{COOH}]_{t0}\right)} \ln \frac{[\mathrm{COOH}]_{t0} + X[\mathrm{E}]_{t0}}{[\mathrm{COOH}]_{t0}\left(1 - X\right)} \to \infty \tag{10.107}$$

The carboxylic acid concentration given by (10.99) in the limit of $t_f \to \infty$ is

$$\begin{aligned} \lim_{t_f\to\infty} [\mathrm{COOH}](t_f) &= \frac{[\mathrm{COOH}]_{t0}\left([\mathrm{E}]_{t0} + [\mathrm{COOH}]_{t0}\right)}{[\mathrm{COOH}]_{t0} + [\mathrm{E}]_{t0}\exp\left(-k_2' t_f\left([\mathrm{E}]_{t0} + [\mathrm{COOH}]_{t0}\right)\right)} \\ &= [\mathrm{COOH}]_{t0} + [\mathrm{E}]_{t0}. \end{aligned} \tag{10.108}$$

The corresponding ester concentration is

$$\lim_{t_f\to\infty} [\mathrm{E}](t_f) = [\mathrm{COOH}]_{t0} + [\mathrm{E}]_{t0} - [\mathrm{COOH}](t_f) = 0. \tag{10.109}$$

Evaluating (10.105) at time $t = t_f \to \infty$,

$$\lim_{t_f\to\infty} R_{V\mathrm{COOH}}(t_f) = k_2'\left([\mathrm{COOH}]_{t0} + [\mathrm{E}]_{t0}\right)0 = 0. \tag{10.110}$$

Critical Points The critical points of $R_{V\mathrm{COOH}}(t)$ are located where $\dfrac{dR_{V\mathrm{COOH}}(t)}{dt} = 0$ or $\dfrac{dR_{V\mathrm{COOH}}(t)}{dt}$ does not exist.

$$\begin{aligned}\frac{dR_{V\mathrm{COOH}}(t)}{dt} &= \frac{d\left(k_2'([\mathrm{COOH}]_{t0} + u(t))([\mathrm{E}]_{t0} - u(t))\right)}{dt} \\ &= k_2'\frac{du(t)}{dt}\left([\mathrm{E}]_{t0} - [\mathrm{COOH}]_{t0} - 2u(t)\right) \\ &= k_2' R_{V\mathrm{COOH}}(t)\left([\mathrm{E}]_{t0} - [\mathrm{COOH}]_{t0} - 2u(t)\right).\end{aligned} \tag{10.111}$$

As $k_2' > 0$ and the derivative is smooth and continuous in the interval, the critical points of $R_{V\mathrm{COOH}}(t)$ occur when $R_{V\mathrm{COOH}}(t) = 0$ or $[\mathrm{E}]_{t0} - [\mathrm{COOH}]_{t0} - 2u(t) = 0$. The first critical point coincides with the endpoint t_f. The second critical point at time $t = t_{cp}$ gives

$$u(t_{cp}) = \frac{[\mathrm{E}]_{t0} - [\mathrm{COOH}]_{t0}}{2}. \tag{10.112}$$

Using the definition of $u(t_{cp})$ given by (10.88),

$$\begin{aligned}[\mathrm{COOH}](t_{cp}) &= u(t_{cp}) + [\mathrm{COOH}]_{t0} \\ &= \frac{[\mathrm{E}]_{t0} - [\mathrm{COOH}]_{t0}}{2} + [\mathrm{COOH}]_{t0} \\ &= \frac{[\mathrm{E}]_{t0} + [\mathrm{COOH}]_{t0}}{2},\end{aligned} \tag{10.113}$$

and

$$\begin{aligned}[\mathrm{E}](t_{cp}) &= [\mathrm{E}]_{t0} - u(t_{cp}) \\ &= [\mathrm{E}]_{t0} - \frac{[\mathrm{E}]_{t0} - [\mathrm{COOH}]_{t0}}{2} \\ &= \frac{[\mathrm{E}]_{t0} + [\mathrm{COOH}]_{t0}}{2}.\end{aligned} \tag{10.114}$$

The extent of reaction at time t_{cp}, X_{cp}, is related to the ester concentration by (10.40),

$$[\mathrm{E}](t_{cp}) = (1 - X_{cp})[\mathrm{E}]_{t0}. \tag{10.115}$$

Substituting the value of $u(t_{cp})$ at the critical point,

$$[\mathrm{E}](t_{cp}) = (1 - X_{cp})[\mathrm{E}]_{t0} = [\mathrm{E}]_{t0} - \frac{[\mathrm{E}]_{t0} - [\mathrm{COOH}]_{t0}}{2}. \tag{10.116}$$

Solving for X_{cp},

$$X_{cp} = \frac{[\mathrm{E}]_{t0} - [\mathrm{COOH}]_{t0}}{2[\mathrm{E}]_{t0}}. \tag{10.117}$$

The time for critical point can be determined by (10.104) evaluated at X_{cp}:

$$\begin{aligned} t_{cp} &= \frac{1}{k_2' \left([\mathrm{E}]_{t0} + [\mathrm{COOH}]_{t0}\right)} \ln \frac{[\mathrm{COOH}]_{t0} + X_{cp}[\mathrm{E}]_{t0}}{[\mathrm{COOH}]_{t0}\left(1 - X_{cp}\right)} \\ &= \frac{1}{k_2' \left([\mathrm{E}]_{t0} + [\mathrm{COOH}]_{t0}\right)} \ln \frac{[\mathrm{E}]_{t0}}{[\mathrm{COOH}]_{t0}}. \end{aligned} \tag{10.118}$$

Evaluating (10.105) at the critical point at time $t = t_{cp}$ gives

$$\begin{aligned} R_{V\,\mathrm{COOH}}(t_{cp}) &= k_2' \left(\frac{[\mathrm{E}]_{t0} + [\mathrm{COOH}]_{t0}}{2}\right)\left(\frac{[\mathrm{E}]_{t0} + [\mathrm{COOH}]_{t0}}{2}\right) \\ &= \frac{k_2' \left([\mathrm{E}]_{t0} + [\mathrm{COOH}]_{t0}\right)^2}{4}. \end{aligned} \tag{10.119}$$

Absolute Maximum and Minimum Values The absolute minimum value of the net rate of generation of COOH in the interval $[0, t_f]$ is $R_{V\,\mathrm{COOH}}(t_f) = 0$ as $t_f \to \infty$ with COOH at its maximum value, $[\mathrm{COOH}](t) \to [\mathrm{E}]_{t0} + [\mathrm{COOH}]_{t0}$. The absolute maximum value of the net rate of generation of COOH in the interval $[0, t_f]$ is $R_{V\,\mathrm{COOH}}(t_{cp}) = \dfrac{k_2' \left([\mathrm{E}]_{t0} + [\mathrm{COOH}]_{t0}\right)^2}{4}$ where $X_{cp} = \dfrac{[\mathrm{E}]_{t0} - [\mathrm{COOH}]_{t0}}{2[\mathrm{E}]_{t0}}$, $t_{cp} = \dfrac{1}{k_2' \left([\mathrm{E}]_{t0} + [\mathrm{COOH}]_{t0}\right)} \ln \dfrac{[\mathrm{E}]_{t0}}{[\mathrm{COOH}]_{t0}}$, and $[\mathrm{COOH}](t_{cp}) = [\mathrm{E}](t_{cp}) = \dfrac{[\mathrm{E}]_{t0} + [\mathrm{COOH}]_{t0}}{2}$. COOH has its minimum value at $[\mathrm{COOH}](0) = [\mathrm{COOH}]_{t0}$.

Summary For the quadratic-order rate law for autocatalytic hydrolysis, the analytical solutions to the conservation equations for COOH and E in the

reaction-dominant limit are

$$[\text{COOH}](t) = \frac{[\text{COOH}]_{t0}\left([\text{E}]_{t0} + [\text{COOH}]_{t0}\right)}{[\text{COOH}]_{t0} + [\text{E}]_{t0}\exp\left(-\left([\text{E}]_{t0} + [\text{COOH}]_{t0}\right)k_2' t\right)}. \tag{10.120}$$

and

$$[\text{E}](t) = \frac{[\text{E}]_{t0}\left([\text{E}]_{t0} + [\text{COOH}]_{t0}\right)\exp\left(-\left([\text{E}]_{t0} + [\text{COOH}]_{t0}\right)k_2' t\right)}{[\text{COOH}]_{t0} + [\text{E}]_{t0}\exp\left(-\left([\text{E}]_{t0} + [\text{COOH}]_{t0}\right)k_2' t\right)}. \tag{10.121}$$

where $[\text{COOH}]_{t0}$ and $[\text{E}]_{t0}$ are the initial concentrations of carboxylic acid end groups and ester bonds, respectively, $k_2' := k_c[\text{H}_2\text{O}]$, $[\text{H}_2\text{O}]$ is the constant concentration of water, and k_c is the rate constant for the autocatalytic hydrolysis reaction

The time when the extent of reaction reaches 99%, $t_{0.99}$, is given by (10.104) with $X = 0.99$,

$$t_{0.99} = \frac{1}{k_2'\left([\text{E}]_{t0} + [\text{COOH}]_{t0}\right)} \ln \frac{[\text{COOH}]_{t0} + 0.99[\text{E}]_{t0}}{[\text{COOH}]_{t0}\left(1 - 0.99\right)}. \tag{10.122}$$

10.2.1.4 1.5th-Order Rate Law for Autocatalytic Hydrolysis

The analytical expression for the concentration profile of carboxylic acid end groups for the 1.5th-order rate law for autocatalytic hydrolysis is derived using ester bond concentration analysis. Expressions for the concentration profile of ester bonds, the time, t_X, required for the reaction to reach extent of reaction X, and the extrema of $R_{V\text{COOH}}(t)$ and $[\text{COOH}](t)$ are also derived.

Ester Bond Concentration Analysis Recall (5.46) and assume that the system is well-mixed,

$$R_{V\text{E}}(t) = -k_{1.5}'\sqrt{K_a[\text{COOH}](t)}\,[\text{E}](t). \tag{10.123}$$

Rewriting in terms of the ester bond concentration instead of carboxylic acid end group concentration using the expression relating $[\text{E}](t)$ and $[\text{COOH}](t)$ given

by (10.27) yields

$$R_{VE}(t) = -k'_{1.5}\sqrt{K_a\left([\mathrm{E}]_{t0} + [\mathrm{COOH}]_{t0} - [\mathrm{E}](t)\right)}\,[\mathrm{E}](t), \tag{10.124}$$

with initial condition

$$[\mathrm{E}](0) = [\mathrm{E}]_{t0}. \tag{10.125}$$

(10.124) differs from the expression used by Siparsky, Voorhees, and Miao [93], which was missing the negative sign from the right-hand side of the equation.

Integrating (10.124) gives

$$\int_{[\mathrm{E}]_{t0}}^{[\mathrm{E}](t)} \frac{1}{[\mathrm{E}]'\sqrt{[\mathrm{E}]_{t0} + [\mathrm{COOH}]_{t0} - [\mathrm{E}]'}}\, d[\mathrm{E}]' = \int_{t0}^{t} -k'_{1.5}\sqrt{K_a}\, dt'. \tag{10.126}$$

The solution to the integral of the form of (10.126) is given by

$$\int \frac{1}{y\sqrt{a+by}}\, dy = \frac{1}{\sqrt{a}} \ln\left|\frac{\sqrt{a+by}-\sqrt{a}}{\sqrt{a+by}+\sqrt{a}}\right| + C, \tag{10.127}$$

where a, b, and C are constants, C is the constant of integration, and $a > 0$. Substituting $a := [\mathrm{E}]_{t0} + [\mathrm{COOH}]_{t0}$, $b := -1$, $y := [\mathrm{E}]'$, and the limits of integration, (10.126) becomes [93]

$$\frac{1}{\sqrt{a}}\left(\ln\left|\frac{\sqrt{a-[\mathrm{E}](t)}-\sqrt{a}}{\sqrt{a-[\mathrm{E}](t)}+\sqrt{a}}\right| - \ln\left|\frac{\sqrt{a-[\mathrm{E}]_{t0}}-\sqrt{a}}{\sqrt{a-[\mathrm{E}]_{t0}}+\sqrt{a}}\right|\right) = -k'_{1.5}\sqrt{K_a}\, t. \tag{10.128}$$

Using the definition of a, $a - [\mathrm{E}]_{t0} = [\mathrm{COOH}]_{t0}$. This can be substituted into (10.128), and noting that $a - [\mathrm{E}](t) = [\mathrm{COOH}](t)$, the result can be rearranged to give

$$\ln\left|\frac{\sqrt{[\mathrm{COOH}](t)}-\sqrt{a}}{\sqrt{[\mathrm{COOH}](t)}+\sqrt{a}}\right| - \ln\left|\frac{\sqrt{[\mathrm{COOH}]_{t0}}-\sqrt{a}}{\sqrt{[\mathrm{COOH}]_{t0}}+\sqrt{a}}\right| = -k'_{1.5}\sqrt{aK_a}\, t. \tag{10.129}$$

$a > [\mathrm{COOH}](t)$ and $a > [\mathrm{COOH}]_{t0}$, so $\left|\sqrt{[\mathrm{COOH}](t)}-\sqrt{a}\right| = \sqrt{a} - \sqrt{[\mathrm{COOH}](t)}$ and $\left|\sqrt{[\mathrm{COOH}]_{t0}}-\sqrt{a}\right| = \sqrt{a} - \sqrt{[\mathrm{COOH}]_{t0}}$. The denominators of both

logarithmic terms are positive with $[\mathrm{COOH}](t) > 0$ and $a > 0$. The absolute values in (10.129) can be replaced giving

$$\ln \frac{\sqrt{a} - \sqrt{[\mathrm{COOH}](t)}}{\sqrt{a} + \sqrt{[\mathrm{COOH}](t)}} - \ln \frac{\sqrt{a} - \sqrt{[\mathrm{COOH}]_{t0}}}{\sqrt{a} + \sqrt{[\mathrm{COOH}]_{t0}}} = -k'_{1.5}\sqrt{aK_a}\, t. \tag{10.130}$$

Define $c := \dfrac{\sqrt{a} + \sqrt{[\mathrm{COOH}]_{t0}}}{\sqrt{a} - \sqrt{[\mathrm{COOH}]_{t0}}}$. Taking the exponential of both sides gives

$$c\frac{\sqrt{a} - \sqrt{[\mathrm{COOH}](t)}}{\sqrt{a} + \sqrt{[\mathrm{COOH}](t)}} = \exp\left(-k'_{1.5}\sqrt{aK_a}\, t\right). \tag{10.131}$$

Solving for $[\mathrm{COOH}](t)$ gives

$$[\mathrm{COOH}](t) = a\left(\frac{c - \exp\left(-k'_{1.5}\sqrt{aK_a}\, t\right)}{c + \exp\left(-k'_{1.5}\sqrt{aK_a}\, t\right)}\right)^2, \tag{10.132}$$

where

$$a := [\mathrm{E}]_{t0} + [\mathrm{COOH}]_{t0} \tag{10.133}$$

and

$$c := \frac{\sqrt{a} + \sqrt{[\mathrm{COOH}]_{t0}}}{\sqrt{a} - \sqrt{[\mathrm{COOH}]_{t0}}}. \tag{10.134}$$

Substituting (10.132) into the expression relating $[\mathrm{E}](t)$ and $[\mathrm{COOH}](t)$ given by (10.27) and solving for $[\mathrm{E}](t)$ yields

$$[\mathrm{E}](t) = a\left(1 - \left(\frac{c - \exp\left(-k'_{1.5}\sqrt{aK_a}\, t\right)}{c + \exp\left(-k'_{1.5}\sqrt{aK_a}\, t\right)}\right)^2\right). \tag{10.135}$$

Derivation of t_X A rearranged version of (10.132) useful for estimating $k'_{1.5}$ from experimental data is

$$\ln \frac{\sqrt{a} - \sqrt{[\mathrm{COOH}](t)}}{\sqrt{a} + \sqrt{[\mathrm{COOH}](t)}} = -k'_{1.5}\sqrt{aK_a}\, t - \ln c, \tag{10.136}$$

where a and c are defined by (10.133) and (10.134), respectively.

The expression relating [E](t) to the extent of reaction given by (10.40) can be substituted into (10.136) to determine the time at which X extent of reaction relative to the ester bonds has been reached,

$$\ln \frac{\sqrt{a} - \sqrt{[\mathrm{E}]_{t0} + [\mathrm{COOH}]_{t0} - (1-X)[\mathrm{E}]_{t0}}}{\sqrt{a} + \sqrt{[\mathrm{E}]_{t0} + [\mathrm{COOH}]_{t0} - (1-X)[\mathrm{E}]_{t0}}} = -k'_{1.5}\sqrt{aK_a}\, t_X - \ln c. \tag{10.137}$$

Solving for t_X yields

$$t_X = \frac{1}{k'_{1.5}\sqrt{aK_a}} \ln \frac{\sqrt{a} + \sqrt{[\mathrm{COOH}]_{t0} + X[\mathrm{E}]_{t0}}}{c\left(\sqrt{a} - \sqrt{[\mathrm{COOH}]_{t0} + X[\mathrm{E}]_{t0}}\right)}, \tag{10.138}$$

where a and c are defined by (10.133) and (10.134), respectively.

Derivation of Extrema of $R_{V\mathrm{COOH}}(t)$ The extrema of $R_{V\mathrm{COOH}}(t)$ on a closed time interval $[0, t_f]$ are located at the endpoints of the interval or the critical points in the interval where $\dfrac{dR_{V\mathrm{COOH}}(t)}{dt} = 0$ or $\dfrac{dR_{V\mathrm{COOH}}(t)}{dt}$ does not exist. The largest of the values of $R_{V\mathrm{COOH}}(t)$ evaluated at the endpoints and critical points is the absolute maximum value, and the smallest of these values is the absolute minimum value. The interval endpoint t_f is taken to the be time when the extent of reaction X approaches 100%.

The net rate of generation of carboxylic acid end groups is given by (5.45) for the first-order rate law for uncatalyzed hydrolysis. Substituting (10.27) for the ester concentration,

$$\begin{aligned} R_{V\mathrm{COOH}}(t) &= k'_{1.5}\sqrt{K_a[\mathrm{COOH}](t)}\,[\mathrm{E}](t) \\ &= k'_{1.5}\sqrt{K_a[\mathrm{COOH}](t)}\,([\mathrm{E}]_{t0} + [\mathrm{COOH}]_{t0} - [\mathrm{COOH}](t))\,, \end{aligned} \tag{10.139}$$

where a and c are defined by (10.133) and (10.134), respectively.

Endpoints Evaluating (10.139) at time $t = 0$,

$$R_{V\mathrm{COOH}}(0) = k'_{1.5}\sqrt{K_a[\mathrm{COOH}]_{t0}}\,[\mathrm{E}]_{t0}. \tag{10.140}$$

Using the equation for t_X given by (10.138), the definition of t_f, and the definition for a given by (10.133),

$$t_f = \lim_{X\to 1}\frac{1}{k'_{1.5}\sqrt{aK_a}}\ln\frac{\sqrt{a}+\sqrt{[\mathrm{COOH}]_{t0}+X[\mathrm{E}]_{t0}}}{c\left(\sqrt{a}-\sqrt{[\mathrm{COOH}]_{t0}+X[\mathrm{E}]_{t0}}\right)} \to \infty \tag{10.141}$$

The carboxylic acid concentration given by (10.132) in the limit of $t_f \to \infty$ is

$$\lim_{t_f\to\infty}[\mathrm{COOH}](t_f) = a\left(\frac{c-\exp\left(-k'_{1.5}\sqrt{aK_a}\,t_f\right)}{c+\exp\left(-k'_{1.5}\sqrt{aK_a}\,t_f\right)}\right)^2 = [\mathrm{E}]_{t0}+[\mathrm{COOH}]_{t0}, \tag{10.142}$$

where a and c are defined by (10.133) and (10.134), respectively. The corresponding ester concentration is

$$\lim_{t_f\to\infty}[\mathrm{E}](t_f) = [\mathrm{COOH}]_{t0}+[\mathrm{E}]_{t0}-[\mathrm{COOH}](t_f) = 0. \tag{10.143}$$

Evaluating (10.139) at time $t = t_f \to \infty$,

$$\lim_{t_f\to\infty} R_{V\mathrm{COOH}}(t_f) = k'_{1.5}\sqrt{K_a\left([\mathrm{E}]_{t0}+[\mathrm{COOH}]_{t0}\right)}\,0 = 0. \tag{10.144}$$

Critical Points The critical points of $R_{V\mathrm{COOH}}(t)$ are located where $\dfrac{dR_{V\mathrm{COOH}}(t)}{dt} = 0$ or $\dfrac{dR_{V\mathrm{COOH}}(t)}{dt}$ does not exist.

$$\begin{aligned}\frac{dR_{V\mathrm{COOH}}(t)}{dt} &= \frac{d\left(k'_{1.5}\sqrt{K_a[\mathrm{COOH}](t)}\left([\mathrm{E}]_{t0}+[\mathrm{COOH}]_{t0}-[\mathrm{COOH}](t)\right)\right)}{dt}\\ &= k'_{1.5}\sqrt{K_a}\left(\frac{[\mathrm{E}]_{t0}+[\mathrm{COOH}]_{t0}-[\mathrm{COOH}](t)}{2\sqrt{[\mathrm{COOH}](t)}}-\sqrt{[\mathrm{COOH}](t)}\right)\\ &\quad\times\frac{d[\mathrm{COOH}](t)}{dt}.\end{aligned} \tag{10.145}$$

As $k'_{1.5} > 0$, $\sqrt{K_a} > 0$, and the derivative is smooth and continuous in the interval, the critical points of $R_{V\mathrm{COOH}}(t)$ occur when $R_{V\mathrm{COOH}}(t) = 0$ or $\dfrac{[\mathrm{E}]_{t0} + [\mathrm{COOH}]_{t0} - [\mathrm{COOH}](t)}{2\sqrt{[\mathrm{COOH}](t)}} - \sqrt{[\mathrm{COOH}](t)} = 0$. The first critical point coincides with the endpoint t_f. The second critical point at time $t = t_{cp}$ gives

$$[\mathrm{COOH}](t_{cp}) = \frac{[\mathrm{E}]_{t0} + [\mathrm{COOH}]_{t0}}{3}. \tag{10.146}$$

The corresponding ester concentration is

$$[\mathrm{E}](t_{cp}) = [\mathrm{COOH}]_{t0} + [\mathrm{E}]_{t0} - [\mathrm{COOH}](t_{cp}) = \frac{2\left([\mathrm{E}]_{t0} + [\mathrm{COOH}]_{t0}\right)}{3}. \tag{10.147}$$

The extent of reaction at time t_{cp}, X_{cp}, is related to the ester concentration by (10.40),

$$[\mathrm{E}](t_{cp}) = (1 - X_{cp})[\mathrm{E}]_{t0} = \frac{2\left([\mathrm{E}]_{t0} + [\mathrm{COOH}]_{t0}\right)}{3}. \tag{10.148}$$

Solving for X_{cp},

$$X_{cp} = \frac{[\mathrm{E}]_{t0} - 2[\mathrm{COOH}]_{t0}}{3[\mathrm{E}]_{t0}}. \tag{10.149}$$

The time for critical point can be determined by (10.138) evaluated at X_{cp}:

$$\begin{aligned} t_{cp} &= \frac{1}{k'_{1.5}\sqrt{aK_a}} \ln \frac{\sqrt{a} + \sqrt{[\mathrm{COOH}]_{t0} + X_{cp}[\mathrm{E}]_{t0}}}{c\left(\sqrt{a} - \sqrt{[\mathrm{COOH}]_{t0} + X_{cp}[\mathrm{E}]_{t0}}\right)} \\ &= \frac{1}{k'_{1.5}\sqrt{aK_a}} \ln \frac{\sqrt{a} + \sqrt{([\mathrm{COOH}]_{t0} + [\mathrm{E}]_{t0})/3}}{c\left(\sqrt{a} - \sqrt{([\mathrm{COOH}]_{t0} + [\mathrm{E}]_{t0})/3}\right)}, \end{aligned} \tag{10.150}$$

where a and c are defined by (10.133) and (10.134), respectively.

Evaluating (10.139) at the critical point at time $t = t_{cp}$ gives

$$\begin{aligned} R_{V\mathrm{COOH}}(t_{cp}) &= \frac{2k'_{1.5}}{3}\sqrt{K_a \frac{[\mathrm{E}]_{t0} + [\mathrm{COOH}]_{t0}}{3}}\left([\mathrm{E}]_{t0} + [\mathrm{COOH}]_{t0}\right) \\ &= \frac{2k'_{1.5}\sqrt{K_a}}{3\sqrt{3}}\left([\mathrm{E}]_{t0} + [\mathrm{COOH}]_{t0}\right)^{1.5}. \end{aligned} \tag{10.151}$$

Absolute Maximum and Minimum Values The absolute minimum value of the net rate of generation of COOH in the interval $[0, t_f]$ is $R_{V\mathrm{COOH}}(t_f) = 0$ as $t_f \to \infty$ with COOH at its maximum value, $[\mathrm{COOH}](t) \to [\mathrm{E}]_{t0} + [\mathrm{COOH}]_{t0}$. The absolute maximum value of the net rate of generation of COOH in the interval $[0, t_f]$ is $R_{V\mathrm{COOH}}(t_{cp}) = \dfrac{2k'_{1.5}\sqrt{K_a}}{3\sqrt{3}}\left([\mathrm{E}]_{t0} + [\mathrm{COOH}]_{t0}\right)^{1.5}$ where $X_{cp} = \dfrac{[\mathrm{E}]_{t0} - 2[\mathrm{COOH}]_{t0}}{3[\mathrm{E}]_{t0}}$, $t_{cp} = \dfrac{1}{k'_{1.5}\sqrt{aK_a}} \ln \dfrac{\sqrt{a} + \sqrt{([\mathrm{COOH}]_{t0} + [\mathrm{E}]_{t0})/3}}{c\left(\sqrt{a} - \sqrt{([\mathrm{COOH}]_{t0} + [\mathrm{E}]_{t0})/3}\right)}$, $a = [\mathrm{E}]_{t0} + [\mathrm{COOH}]_{t0}$, $c = \dfrac{\sqrt{a} + \sqrt{[\mathrm{COOH}]_{t0}}}{\sqrt{a} - \sqrt{[\mathrm{COOH}]_{t0}}}$, $[\mathrm{COOH}](t_{cp}) = \dfrac{[\mathrm{E}]_{t0} + [\mathrm{COOH}]_{t0}}{3}$, and $[\mathrm{E}](t_{cp}) = \dfrac{2\left([\mathrm{E}]_{t0} + [\mathrm{COOH}]_{t0}\right)}{3}$. COOH has its minimum value at $[\mathrm{COOH}](0) = [\mathrm{COOH}]_{t0}$.

Summary For the 1.5th-order rate law for autocatalytic hydrolysis, the analytical solutions to the conservation equations for COOH and E in the reaction-dominant limit are

$$[\mathrm{COOH}](t) = a\left(\frac{c - \exp\left(-k'_{1.5}\sqrt{aK_a}\,t\right)}{c + \exp\left(-k'_{1.5}\sqrt{aK_a}\,t\right)}\right)^2 \tag{10.152}$$

and

$$[\mathrm{E}](t) = a\left(1 - \left(\frac{c - \exp\left(-k'_{1.5}\sqrt{aK_a}\,t\right)}{c + \exp\left(-k'_{1.5}\sqrt{aK_a}\,t\right)}\right)^2\right), \tag{10.153}$$

where

$$a := [\mathrm{E}]_{t0} + [\mathrm{COOH}]_{t0} \tag{10.154}$$

and

$$c := \frac{\sqrt{a} + \sqrt{[\mathrm{COOH}]_{t0}}}{\sqrt{a} - \sqrt{[\mathrm{COOH}]_{t0}}}. \tag{10.155}$$

where $[\mathrm{COOH}]_{t0}$ and $[\mathrm{E}]_{t0}$ are the initial concentrations of carboxylic acid end groups and ester bonds, respectively, $k'_{1.5} := k_c[\mathrm{H_2O}]$, $[\mathrm{H_2O}]$ is the constant concentration of water, k_c is the rate constant for the autocatalytic hydrolysis reaction, and K_a is the acid dissociation constant for COOH.

The time when the extent of reaction reaches 99%, $t_{0.99}$, is given by (10.138) with $X = 0.99$,

$$t_{0.99} = \frac{1}{k'_{1.5}\sqrt{aK_a}} \ln \frac{\sqrt{a} + \sqrt{[\text{COOH}]_{t0} + 0.99[\text{E}]_{t0}}}{c\left(\sqrt{a} - \sqrt{[\text{COOH}]_{t0} + 0.99[\text{E}]_{t0}}\right)}. \tag{10.156}$$

10.2.2 Comparison of Numerical and Analytical Solutions for Carboxylic Acid End Group and Ester Bond Concentrations, [COOH](t) and [E](t)

The numerical solutions for the ODEs for [COOH](t) and [E](t) for well-mixed hydrolysis reactions are determined using the model algorithm described in Chapter 8 with the assumptions for the reaction-dominant limit given in Section 10.2. The ODEs are solved using the 5th-order accurate RADAU5 implicit solver with adaptive time stepping. The relative tolerance = absolute tolerance $= TOL = 1 \times 10^{-4}$. The initial time step is set to $t_{0.99}/(NT - 1)$, the maximum allowable time step, where $NT - 1$ is the number of calls to the solver and the number of evenly-spaced time output points after the initial condition and $t_{0.99}$ is the reaction time by the time required for achieving 99% extent of reaction. The numerical results for $NT = 51$, 101, and 201 are compared. The analytical solutions are computed using the equations in Section 10.2.1. Results from the numerical and analytical solutions are compared for the concentrations of carboxylic acid end groups and ester bonds for the four hydrolysis rate laws. The concentrations are normalized by dividing by the sum of the initial ester and carboxylic acid end group concentrations as this quantity represents the total monomer concentration; the normalization is used for visualization, not for calculations of the concentrations in the numerical code. Time is made dimensionless by dividing $t_{0.99}$, which allows for the concentrations at different rate constant values to be represented by a single curve as a function of dimensionless time.

The numerical approximation to $c_{\text{COOH}}(t)$ is denoted as $[\text{COOH}]^k$ in the

following discussion and is evaluated at the discrete points $((k-1)\Delta t) = (t_k)$ for $k = 1, 2, \ldots, NT$, where NT is the number of time discretizations, rather than as a continuous function of t. The analytical solution is evaluated at the same discrete points as the numerical solution for comparison, $[\text{COOH}](t_k)$.

Figure 10.1 shows the analytical and numerical dimensionless carboxylic acid end group and ester bond concentration profiles at each dimensionless time discretization, $t_k/t_{0.99}$, used for the numerical solution with $NT = 101$ and $TOL = 1 \times 10^{-4}$ for the four hydrolysis models in the reaction-dominant limit. The analytical profiles for COOH are given by (10.49), (10.69), (10.120), and (10.152), and the analytical profiles for E are given by (10.50), (10.70), (10.121), and (10.153). The curves for COOH show the proper extrema for $[\text{COOH}](t)$ and $R_{V\text{COOH}}(t)$.

Figure 10.2 shows the numerical dimensionless carboxylic acid end group concentration, sum of the concentrations of large oligomers, and sum of the concentrations of small oligomers at each dimensionless time discretization, $t_k/t_{0.99}$, used for the numerical solution with $NT = 101$ and $TOL = 1 \times 10^{-4}$ for the four hydrolysis rate laws.

The percent error value for the COOH concentration at each discrete value of t_k is given by

$$PE([\text{COOH}](t_k)) = \left| \frac{[\text{COOH}](t_k) - [\text{COOH}]^k}{[\text{COOH}](t_k)} \right| \times 100\%. \tag{10.157}$$

Figure 10.3 shows the percent error between analytical and numerical COOH concentration profiles at each dimensionless time discretization, $t_k/t_{0.99}$, used for the numerical solution with $NT = 101$ and $TOL = 1 \times 10^{-4}$ for the four hydrolysis rate laws.

The rate-of-convergence in the t-dimension cannot be determined accurately as the ODE solver uses adaptive time stepping making the size of Δt variable and independent of NT. Instead, the error is assessed relative to the specified error

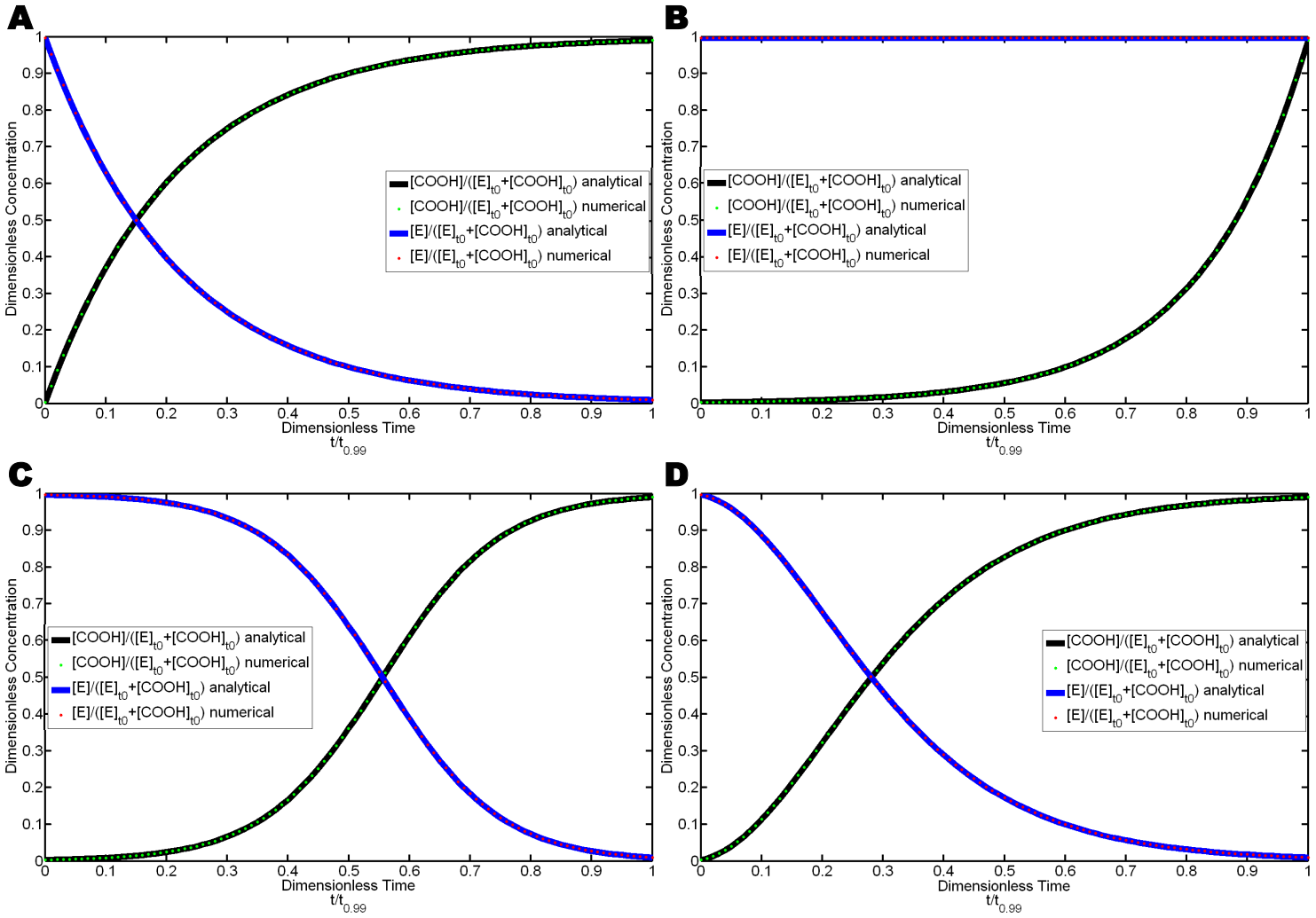

Figure 10.1: Analytical and numerical dimensionless carboxylic acid end group and ester bond concentration profiles as functions of dimensionless time $t/t_{0.99}$ in the reaction-dominant limit with $NT = 101$ and $TOL = 1 \times 10^{-4}$: A) uncatalyzed hydrolysis model, B) pseudo-first-order, autocatalytic hydrolysis model, C) quadratic-order, autocatalytic hydrolysis model, and D) 1.5th-order, autocatalytic hydrolysis model.

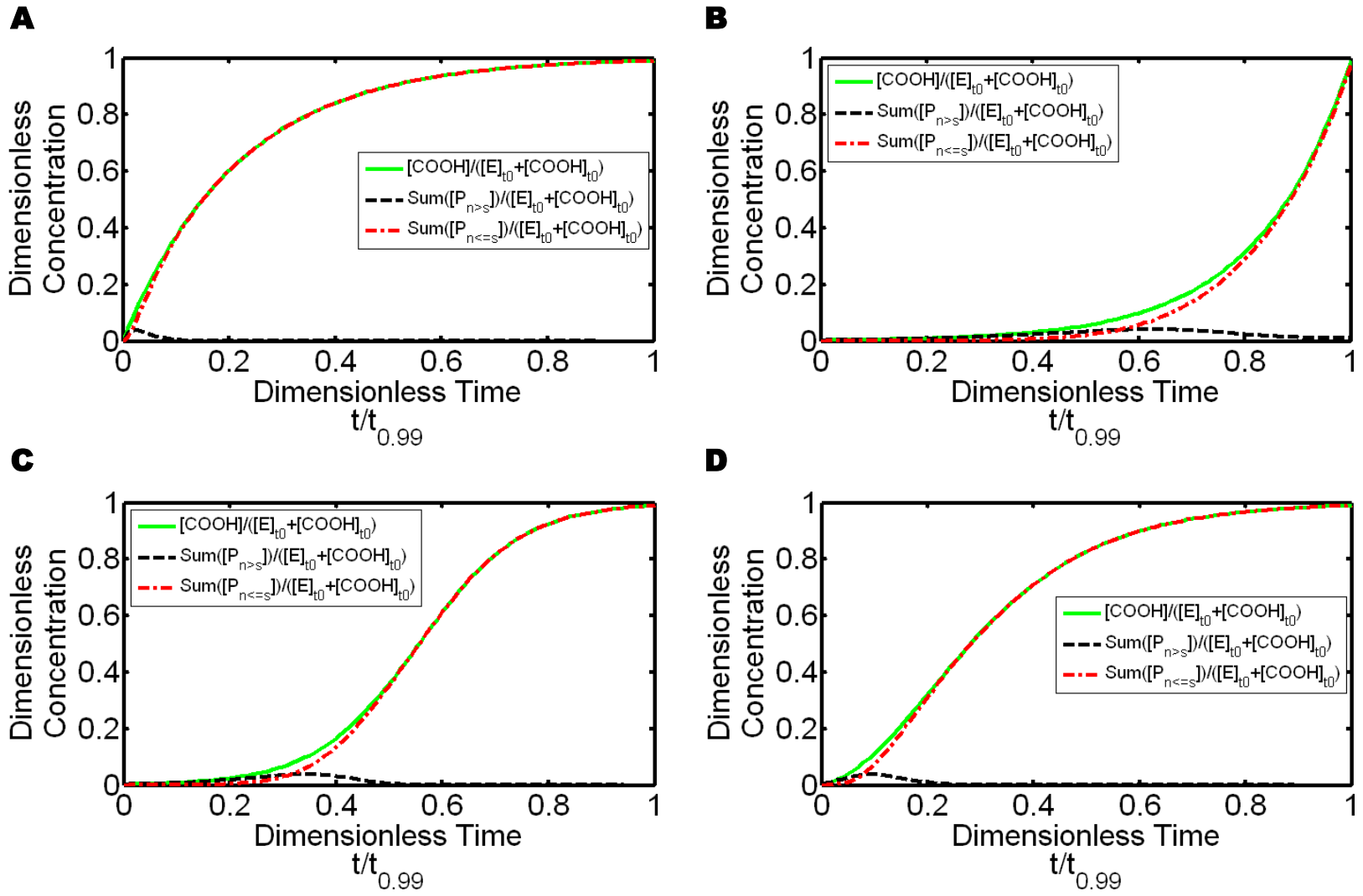

Figure 10.2: Numerical dimensionless carboxylic acid end group concentration, sum of the concentrations of large oligomers, and sum of the concentrations of small oligomers as functions of dimensionless time $t/t_{0.99}$ in the reaction-dominant limit with $NT = 101$ and $TOL = 1 \times 10^{-4}$: A) uncatalyzed hydrolysis model, B) pseudo-first-order, autocatalytic hydrolysis model, C) quadratic-order, autocatalytic hydrolysis model, and D) 1.5th-order, autocatalytic hydrolysis model.

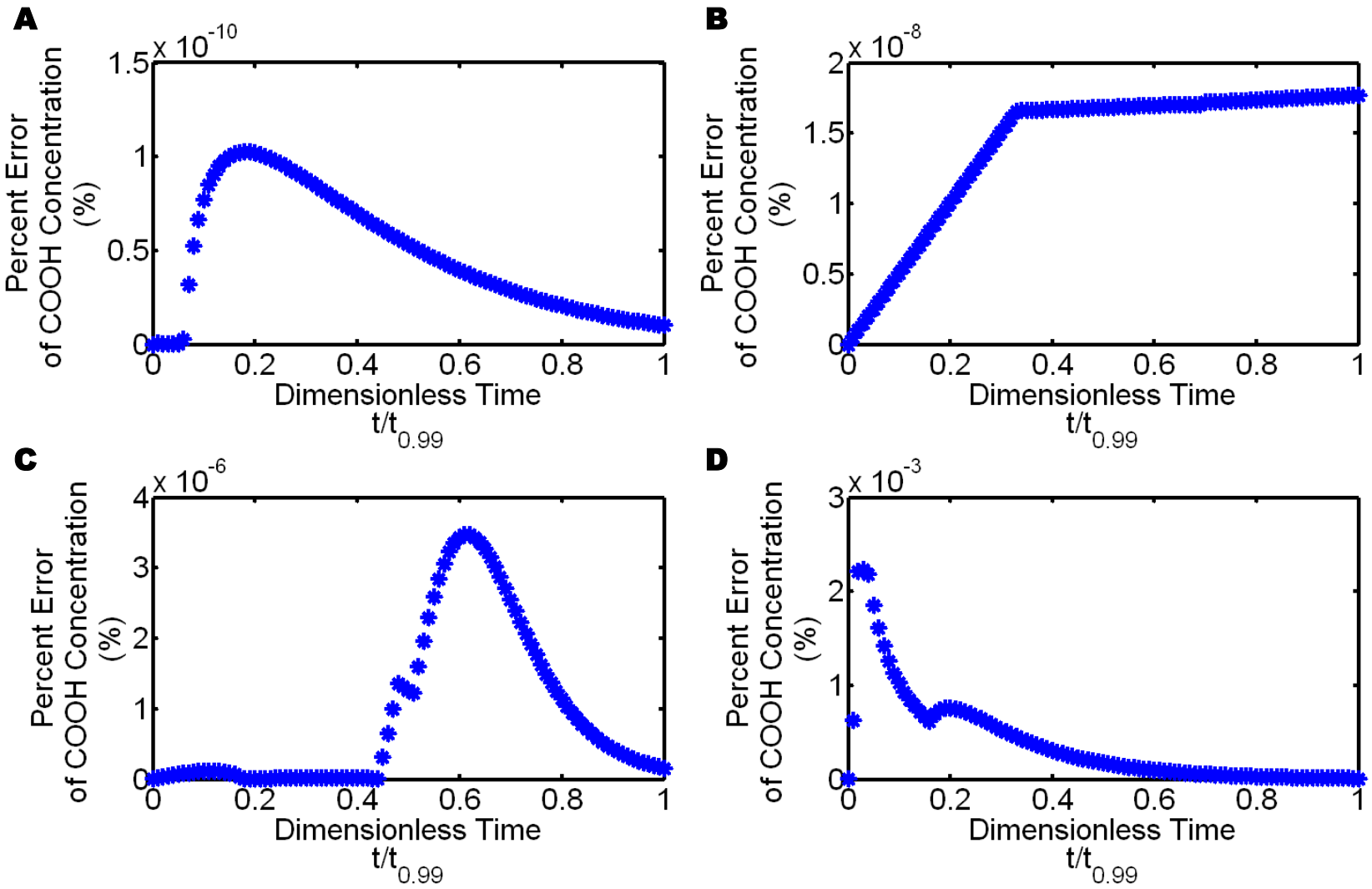

Figure 10.3: Percent error between analytical and numerical carboxylic acid end group concentration profiles as a function of dimensionless time $t/t_{0.99}$ in the reaction-dominant limit with $NT = 101$ and $TOL = 1 \times 10^{-4}$: A) uncatalyzed hydrolysis model, B) pseudo-first-order, autocatalytic hydrolysis model, C) quadratic-order, autocatalytic hydrolysis model, and D) 1.5th-order, autocatalytic hydrolysis model.

tolerance. The solver adjusts the time step size to maintain the estimate of the local error below the tolerance value. The global truncation error at the final time step, $t_{NT} = t_{0.99}$, is used to assess the error between the numerical and analytical COOH concentrations,

$$e_{NT} = |[\text{COOH}](t_{NT}) - [\text{COOH}]^{NT}|. \tag{10.158}$$

The root-mean-square error between the dimensionless numerical and analytical COOH concentration profiles in the t-dimension with values that range between 0 and 1 is calculated by

$$RMSE(\mathbf{x}) = \frac{|\mathbf{x}|_2}{\sqrt{NT}}, \tag{10.159}$$

where the vector $\mathbf{x}$ is composed of elements $x_k = \dfrac{[\text{COOH}](t_k) - [COOH]^k}{[\text{COOH}]_{t0} + [\text{E}]_{t0}}$ for $k = 1, 2, \ldots, NT$. Table 10.1 shows the global truncation error of the numerical COOH concentration at $t_{0.99}$ and the root-mean-square error of the dimensionless COOH concentration profiles for three grids with increasing NT for the four hydrolysis rate laws.

The error tolerances for the data are absolute tolerance = relative tolerance $= TOL = 1 \times 10^{-4} = 0.01\%$. For all four hydrolysis rate laws and for the three temporal resolutions used, the global truncation error values are much smaller than the absolute tolerance, and the percent error and root-mean-square values are smaller than the relative tolerance. Thus, the solver yields accurate solutions for the ODEs in the reaction-dominant limit even without a strict error tolerance value. The results of this section verify the code regarding the reaction equations and the RADAU5 ODE solver.

10.3 Diffusion-Dominant Limit

To verify that the numerical methods for the diffusion component of the model have been implemented correctly, the numerical results for the diffusion-dominant limit

Table 10.1: Global truncation errors of COOH concentration at $t_{0.99}$ and root-mean-square errors between the dimensionless numerical and analytical COOH concentration profiles with different temporal resolution for the uncatalyzed hydrolysis model (Rxn 1), pseudo-first-order, autocatalytic hydrolysis model (Rxn 2), quadratic-order, autocatalytic hydrolysis model (Rxn 3), and 1.5th-order, autocatalytic hydrolysis model (Rxn 4) in the reaction-dominant limit with $TOL = 1 \times 10^{-4}$.

NT	e_{NT} g/cm^3	$RMSE$
	Rxn 1	
51	1.83×10^{-20}	4.90×10^{-12}
101	1.25×10^{-21}	4.17×10^{-13}
201	8.60×10^{-22}	6.18×10^{-14}
	Rxn 2	
51	6.78×10^{-17}	1.66×10^{-9}
101	2.20×10^{-18}	5.25×10^{-11}
201	8.95×10^{-20}	2.10×10^{-12}
	Rxn 3	
51	2.14×10^{-17}	1.17×10^{-8}
101	1.96×10^{-17}	1.01×10^{-8}
201	3.63×10^{-19}	2.14×10^{-10}
	Rxn 4	
51	4.09×10^{-19}	1.54×10^{-6}
101	3.16×10^{-19}	1.51×10^{-6}
201	3.10×10^{-19}	1.66×10^{-6}

are compared to the analytical solution for diffusion for the case of constant effective diffusivity, constant surface concentration, and uniform initial concentration distribution.

The diffusion-dominant limit of the reaction-diffusion equation for the conservation of species i given by (4.8) is approached as the net rate of generation, $R_{Vi}(r,t)$, goes to zero and only diffusion is observed. The net rate of generation can equal or approach zero if the species is inert, the reaction is completed, or the generation and consumption reactions for the species offset each other. For the diffusion-dominant case, diffusivity may be treated as a constant or as a variable quantity. Additionally, the initial concentration may be uniform or may have some prescribed radial distribution. Consideration of constant diffusivity and uniform initial concentration allows for the numerical results to be compared to an analytical solution given by Crank [100], which is derived below. With constant diffusivity, the diffusion-dominant limiting case matches the case of drug diffusion not coupled to the hydrolysis of the polymer. The diffusion-dominant limit for this case is obtained by adding the following assumptions to those used to derive (4.8):

- The effective diffusivity is constant: $D_i(r,t) = D_i$.
- Only diffusion is observable as the net rate of generation of species i is zero: $R_{Vi} = 0$.
- Species i has a uniform initial distribution: $c_{i,t0}(r) = c_{i,t0}$.
- The concentrations of species i at time $t = 0$ must not be the same as the concentration at the surface $r = 1$ for all interior radial points because the concentration difference is the driving force for the diffusion process without a generation term. The surface concentration must be less than the initial concentration for net flux in the direction of increasing r toward the exterior of the sphere: $c_{i,r1} < c_{i,t0}$.

Applying the assumptions, the PDE for radial diffusion of species i from a sphere with constant effective diffusivity, no generation term, surface concentration less than the initial concentration, and dimensionless r is given by

$$\frac{\partial c_i(r,t)}{\partial t} = \frac{D_i}{R^2}\frac{1}{r^2}\frac{\partial}{\partial r}\left(r^2\frac{\partial c_i(r,t)}{\partial r}\right), \tag{10.160}$$

with initial condition

$$c_i(r,0) = c_{i,t0}, \quad 0 \leq r < 1 \tag{10.161}$$

and boundary conditions

$$\frac{\partial c_i(0,t)}{\partial r} = 0, \quad t \geq 0 \tag{10.162}$$

and

$$c_i(1,t) = c_{i,r1}, \quad t \geq 0 \tag{10.163}$$

and the constraint

$$c_{i,r1} < c_{i,t0}, \tag{10.164}$$

where $c_i(r,t)$ is concentration of the species i, D_i is the constant effective diffusivity of the species, R is the radius of the sphere, $0 \leq r \leq 1$ is the normalized radial position, $t \geq 0$ is time, $c_{i,t0}$ is the uniform initial concentration distribution of the species within the sphere, and $c_{i,r1}$ is the constant surface concentration of the species. The conservation equation for the drug species given by (4.12) matches (10.160) when the assumption of constant effective diffusivity is applied.

10.3.1 Analytical Solution for Species Concentration, $c_i(r,t)$, in the Diffusion-Dominant Limit

The technique of linearization can be used to transform (10.160)–(10.163) to the equations of diffusion in a plane sheet with constant concentration at the surfaces.

Let $v_i(r,t) = rc_i(r,t)$. Making the substitution gives

$$\frac{\partial}{\partial t}\left(\frac{v_i(r,t)}{r}\right) = \frac{D_i}{R^2}\frac{1}{r^2}\frac{\partial}{\partial r}\left(r^2\frac{\partial}{\partial r}\left(\frac{v_i(r,t)}{r}\right)\right). \tag{10.165}$$

Evaluation of the first derivatives of $\dfrac{v_i(r,t)}{r}$ gives

$$\frac{1}{r}\frac{\partial v_i(r,t)}{\partial t} = \frac{D_i}{R^2}\frac{1}{r^2}\frac{\partial}{\partial r}\left(r^2\left(\frac{1}{r}\frac{\partial v_i(r,t)}{\partial r} - \frac{1}{r^2}v_i(r,t)\right)\right) \tag{10.166}$$

$$\frac{\partial v_i(r,t)}{\partial t} = \frac{D_i}{R^2}\frac{1}{r}\frac{\partial}{\partial r}\left(r\frac{\partial v_i(r,t)}{\partial r} - v_i(r,t)\right). \tag{10.167}$$

Evaluation of the derivative with respect to r gives

$$\frac{\partial v_i(r,t)}{\partial t} = \frac{D_i}{R^2}\frac{1}{r}\left(\frac{\partial v_i(r,t)}{\partial r} + r\frac{\partial^2 v_i(r,t)}{\partial r^2} - \frac{\partial v_i(r,t)}{\partial r}\right). \tag{10.168}$$

The parameter α_i is defined as

$$\alpha_i := \frac{D_i}{R^2}. \tag{10.169}$$

With substitution of α_i and cancellation of terms, the linearized form is

$$\frac{\partial v_i(r,t)}{\partial t} = \alpha_i\frac{\partial^2 v_i(r,t)}{\partial r^2}, \quad 0 \le r \le 1 \text{ and } t \ge 0, \tag{10.170}$$

with initial condition

$$v_i(r,0) = rc_{i,t0}, \quad 0 \le r < 1 \tag{10.171}$$

and boundary conditions

$$v_i(0,t) = 0, \quad t \ge 0 \tag{10.172}$$

and

$$v_i(1,t) = c_{i,r1}, \quad t \ge 0. \tag{10.173}$$

The analytical solution for the linear PDE in (10.170)–(10.173) in terms of dimensionless r with initial distribution $rc_{i,t0}(r)$ and constant surface concentration

$c_{i,r1}$ is equivalent to that for diffusion in a plane sheet with thickness of 1 and diffusion coefficient α_i and the same initial and boundary conditions for $0 < r < 1$ and $t > 0$ [100]:

$$\begin{aligned} v_i(r,t) &= r c_i(r,t) \\ &= r c_{i,r1} + \frac{2c_{i,r1}}{\pi} \sum_{n=1}^{\infty} \frac{\cos(n\pi)}{n} \sin(n\pi r) \exp\left(-\alpha_i n^2 \pi^2 t\right) \\ &\quad + 2 \sum_{n=1}^{\infty} \sin(n\pi r) \exp\left(-\alpha_i n^2 \pi^2 t\right) \int_0^1 r c_{i,t0}(r) \sin(n\pi r)\, dr. \end{aligned} \tag{10.174}$$

Assuming the initial distribution is a uniform concentration, $c_{i,t0}(r) = c_{i,t0}$, and the surface concentration is maintained at $c_{i,r1}$, the integral in (10.174) can be evaluated as

$$\int_0^1 r c_{i,t0}(r) \sin(n\pi r)\, dr = c_{i,t0} \int_0^1 r \sin(n\pi r)\, dr = \frac{-c_{i,t0} \cos(n\pi)}{n\pi}. \tag{10.175}$$

Substitution of $\cos(n\pi) = (-1)^n$ yields

$$\int_0^1 r c_{i,t0} \sin(n\pi r)\, dr = \frac{-c_{i,t0}(-1)^n}{n\pi}. \tag{10.176}$$

Substitution of the evaluated integral into (10.174) and division by r for $0 < r < 1$ and $t > 0$ yields

$$c_i(r,t) = c_{i,r1} + \frac{2\left(c_{i,r1} - c_{i,t0}\right)}{\pi r} \sum_{n=1}^{\infty} \frac{(-1)^n}{n} \sin(n\pi r) \exp\left(-\alpha_i n^2 \pi^2 t\right). \tag{10.177}$$

The concentration terms can be rearranged to give

$$\frac{c_i(r,t) - c_{i,r1}}{c_{i,r1} - c_{i,t0}} = \frac{2}{\pi r} \sum_{n=1}^{\infty} \frac{(-1)^n}{n} \sin(n\pi r) \exp\left(-\alpha_i n^2 \pi^2 t\right). \tag{10.178}$$

The driving force for diffusion is the difference between the concentration inside the sphere and the surface concentration. Multiplying (10.178) by -1 to rearrange the terms in the denominator gives the fraction of the driving force

remaining as a function of time:

$$\frac{c_i(r,t) - c_{i,r1}}{c_{i,t0} - c_{i,r1}} = -\frac{2}{\pi r}\sum_{n=1}^{\infty}\frac{(-1)^n}{n}\sin(n\pi r)\exp\left(-\alpha_i n^2\pi^2 t\right). \tag{10.179}$$

For calculating the cumulative release profile, it is useful to express the concentration as the fraction of the concentration released as a function of time, which can be obtained by adding 1 to (10.178) [100]:

$$\begin{aligned}\frac{c_i(r,t) - c_{i,r1}}{c_{i,r1} - c_{i,t0}} + \frac{c_{i,r1} - c_{i,t0}}{c_{i,r1} - c_{i,t0}} &= \frac{c_i(r,t) - c_{i,t0}}{c_{i,r1} - c_{i,t0}} \\ &= \frac{c_{i,t0} - c_i(r,t)}{c_{i,t0} - c_{i,r1}} \\ &= 1 + \frac{2}{\pi r}\sum_{n=1}^{\infty}\frac{(-1)^n}{n}\sin(n\pi r)\exp\left(-\alpha_i n^2\pi^2 t\right).\end{aligned} \tag{10.180}$$

The concentration at $r = 0$ for $t > 0$ is given by taking the limit of (10.178) as $r \to 0$:

$$\begin{aligned}\lim_{r\to 0}\frac{c_i(r,t) - c_{i,r1}}{c_{i,r1} - c_{i,t0}} &= \frac{c_i(0,t) - c_{i,r1}}{c_{i,r1} - c_{i,t0}} \\ &= \lim_{r\to 0}\frac{2}{\pi r}\sum_{n=1}^{\infty}\frac{(-1)^n}{n}\sin(n\pi r)\exp\left(-\alpha_i n^2\pi^2 t\right) \\ &= \frac{2}{\pi}\sum_{n=1}^{\infty}\frac{(-1)^n}{n}\exp\left(-\alpha_i n^2\pi^2 t\right)\lim_{r\to 0}\frac{\sin(n\pi r)}{r}.\end{aligned} \tag{10.181}$$

The term $\lim_{r\to 0}\dfrac{\sin(n\pi r)}{r}$ has the indeterminate form of $0/0$. The indeterminate form is resolved using l'Hospital's Rule:

$$\lim_{r\to 0}\frac{\sin(n\pi r)}{r} = \lim_{r\to 0}\frac{n\pi\cos(n\pi r)}{1} = n\pi. \tag{10.182}$$

Substitution of the limit into (10.181) gives the fraction of the concentration released as a function of time for $t > 0$ [100]:

$$\frac{c_i(0,t) - c_{i,r1}}{c_{i,r1} - c_{i,t0}} = 2\sum_{n=1}^{\infty}(-1)^n\exp\left(-\alpha_i n^2\pi^2 t\right). \tag{10.183}$$

The analogous form for the fraction of the driving force remaining as a function of time is

$$\frac{c_i(0,t) - c_{i,r1}}{c_{i,t0} - c_{i,r1}} = -2\sum_{n=1}^{\infty}(-1)^n \exp\left(-\alpha_i n^2 \pi^2 t\right). \tag{10.184}$$

The analogous form for the fraction of the concentration released as a function of time is

$$\frac{c_{i,t0} - c_i(0,t)}{c_{i,t0} - c_{i,r1}} = 1 + 2\sum_{n=1}^{\infty}(-1)^n \exp\left(-\alpha_i n^2 \pi^2 t\right). \tag{10.185}$$

10.3.2 Analytical Solution for Cumulative Release of Drug, $Q(t)$, in the Diffusion-Dominant Limit

The general expression for the cumulative release of drug given by (4.20) derived in Section 4.2 is

$$Q(t) = \frac{\int_0^1 \left([\text{drug}]_{t0}(r) - [\text{drug}](r,t)\right) r^2\, dr}{\int_0^1 \left([\text{drug}]_{t0}(r) - [\text{drug}]_{r1}\right) r^2\, dr}. \tag{10.186}$$

With the same assumptions used in the derivation of (10.180) for the analytical solution of $c_i(r,t)$ for the drug species—the initial distribution is a uniform concentration $[\text{drug}]_{t0}(r) = [\text{drug}]_{t0}$ and the surface concentration is maintained at $[\text{drug}]_{r1}$—the cumulative release profile for the drug is

$$Q(t) = \frac{\int_0^1 \left([\text{drug}]_{t0} - [\text{drug}](r,t)\right) r^2\, dr}{\int_0^1 \left([\text{drug}]_{t0} - [\text{drug}]_{r1}\right) r^2\, dr}. \tag{10.187}$$

The integral in the denominator is evaluated as

$$Q(t) = \frac{\int_0^1 \left([\text{drug}]_{t0} - [\text{drug}](r,t)\right) r^2\, dr}{\frac{1}{3}\left([\text{drug}]_{t0} - [\text{drug}]_{r1}\right)}. \tag{10.188}$$

The result can be simplified as

$$Q(t) = \int_0^1 3r^2 \frac{[\text{drug}]_{t0} - [\text{drug}](r,t)}{[\text{drug}]_{t0} - [\text{drug}]_{r1}}\, dr. \tag{10.189}$$

The quantity $\dfrac{[\text{drug}]_{t0} - [\text{drug}](r,t)}{[\text{drug}]_{t0} - [\text{drug}]_{r1}}$ is equivalent to $\dfrac{c_{i,t0} - c_i(r,t)}{c_{i,t0} - c_{i,r1}}$ for drug species i

given by (10.180), so (10.189) becomes

$$Q(t) = \int_0^1 3r^2 \left(1 + \frac{2}{\pi r} \sum_{n=1}^{\infty} \frac{(-1)^n}{n} \sin(n\pi r) \exp\left(-\alpha_{\text{drug}} n^2 \pi^2 t\right)\right) dr. \tag{10.190}$$

The result can be simplified by integrating the first term and taking the integral of the second term into the summation:

$$Q(t) = 1 + \frac{6}{\pi} \sum_{n=1}^{\infty} \frac{(-1)^n}{n} \exp\left(-\alpha_{\text{drug}} n^2 \pi^2 t\right) \int_0^1 r \sin(n\pi r)\, dr. \tag{10.191}$$

Evaluation of the integral yields [100]

$$Q(t) = 1 - \frac{6}{\pi^2} \sum_{n=1}^{\infty} \frac{1}{n^2} \exp\left(-\alpha_{\text{drug}} n^2 \pi^2 t\right), \tag{10.192}$$

where $\alpha_{\text{drug}} = D_{\text{drug}}/R^2$, D_{drug} is the constant effective diffusivity of the drug, and R is the radius of the sphere.

The analytical solution given by (10.192) can be checked by deriving the expression in a different manner using the alternate expression for the cumulative amount of drug released as a function of time, $M(t)$, given by (4.16),

$$M(t) = -\int_0^t 4\pi R D_{\text{drug}} \frac{\partial [\text{drug}](1, t')}{\partial r}\, dt'. \tag{10.193}$$

With the drug concentration given by (10.177), the partial derivative with respect to r at the surface is

$$\begin{aligned} \frac{\partial [\text{drug}](1,t)}{\partial r} = & \frac{2\left([\text{drug}]_{r1} - [\text{drug}]_{t0}\right)}{\pi} \\ & \times \sum_{n=1}^{\infty} \frac{(-1)^n}{n} \exp\left(-\alpha_{\text{drug}} n^2 \pi^2 t\right) \frac{\partial}{\partial r} \left(\frac{\sin(n\pi r)}{r}\right)\Bigg|_{r=1}. \end{aligned} \tag{10.194}$$

The partial derivative term at $r = 1$ is evaluated as

$$\frac{\partial}{\partial r} \left(\frac{\sin(n\pi r)}{r}\right)\Bigg|_{r=1} = \left(\frac{n\pi \cos(n\pi r)}{r} - \frac{\sin(n\pi r)}{r^2}\right)\Bigg|_{r=1} = n\pi(-1)^n. \tag{10.195}$$

Substitution of (10.195) into the partial derivative of the drug concentration at the surface given by (10.194) and cancellation of terms yields

$$\frac{\partial[\text{drug}](1,t)}{\partial r} = 2\left([\text{drug}]_{r1} - [\text{drug}]_{t0}\right)\sum_{n=1}^{\infty}\exp\left(-\alpha_{\text{drug}}n^2\pi^2 t\right). \tag{10.196}$$

Substitution of (10.196) into the expression for $M(t)$ in (10.193) yields

$$M(t) = 8\pi R D_{\text{drug}}\left([\text{drug}]_{t0} - [\text{drug}]_{r1}\right)\sum_{n=1}^{\infty}\int_0^t \exp\left(-\alpha_{\text{drug}}n^2\pi^2 t'\right)dt'. \tag{10.197}$$

The time integral of the exponential term is evaluated as

$$\int_0^t \exp\left(-\alpha_{\text{drug}}n^2\pi^2 t'\right)dt' = \frac{\exp\left(-\alpha_{\text{drug}}n^2\pi^2 t\right) - 1}{-\alpha_{\text{drug}}n^2\pi^2}. \tag{10.198}$$

Substitution of the integral result gives

$$M(t) = \frac{8R^3\left([\text{drug}]_{t0} - [\text{drug}]_{r1}\right)}{\pi}\sum_{n=1}^{\infty}\frac{1 - \exp\left(-\alpha_{\text{drug}}n^2\pi^2 t\right)}{n^2}. \tag{10.199}$$

The summation term $\displaystyle\sum_{n=1}^{\infty}\frac{1}{n^2} = \frac{\pi^2}{6}$, so

$$\begin{aligned} M(t) = {} & \frac{4}{3}\pi R^3\left([\text{drug}]_{t0} - [\text{drug}]_{r1}\right) \\ & - \frac{8R^3\left([\text{drug}]_{t0} - [\text{drug}]_{r1}\right)}{\pi}\sum_{n=1}^{\infty}\frac{\exp\left(-\alpha_{\text{drug}}n^2\pi^2 t\right)}{n^2}. \end{aligned} \tag{10.200}$$

By an analogous treatment, the cumulative amount of drug released as $t \to \infty$, M_∞, is

$$\begin{aligned} M_\infty &= 8\pi R D_{\text{drug}}\left([\text{drug}]_{t0} - [\text{drug}]_{r1}\right)\sum_{n=1}^{\infty}\lim_{t\to\infty}\int_0^t \exp\left(-\alpha_{\text{drug}}n^2\pi^2 t'\right)dt' \\ &= \frac{8\pi R D_{\text{drug}}\left([\text{drug}]_{t0} - [\text{drug}]_{r1}\right)}{\alpha_{\text{drug}}\pi^2}\sum_{n=1}^{\infty}\frac{1}{n^2} \\ &= \frac{4}{3}\pi R^3\left([\text{drug}]_{t0} - [\text{drug}]_{r1}\right). \end{aligned} \tag{10.201}$$

With substitution of the expressions for $M(t)$ and M_∞ given by (10.200) and (10.201), respectively, into the definition of $Q(t)$ given by (4.17),

$$Q(t) := \frac{M(t)}{M_\infty}, \tag{10.202}$$

the cumulative release is [101]

$$Q(t) = 1 - \frac{6}{\pi^2} \sum_{n=1}^{\infty} \frac{1}{n^2} \exp\left(-\alpha_{\text{drug}} n^2 \pi^2 t\right). \tag{10.203}$$

This expression matches (10.192) derived using volume integrals rather than time integrals.

10.3.3 Comparison of Numerical and Analytical Solutions for Drug Concentration, [drug](r,t), and Cumulative Release of Drug, $Q(t)$

The numerical solution for the conservation equation for [drug](r,t) for the diffusion-dominant limit is determined using the numerical methods algorithm described in Chapter 8 with the assumptions for the diffusion-dominant limit given in Section 10.3 and relative tolerance = absolute tolerance = $TOL = 1 \times 10^{-4}$ unless otherwise indicated. The analytical solution is computed using the equations in Section 10.3.1 for the drug species. The numerical solution for the cumulative release of drug is determined by numerical integration using adaptive Simpson quadrature in MATLAB with the numerical concentration values as described in Section 4.2. The analytical solution for the cumulative release of drug is computed using (10.192). The drug concentration profiles and cumulative release profiles from the numerical and analytical solutions are compared. The concentrations are made dimensionless by expressing as fractions of concentration released. The radius r is defined in dimensionless terms in the formulation of the conservation equation in Chapter 4. Time is made dimensionless by multiplying the diffusion time by the

diffusivity parameter $\alpha_{\text{drug}} = D_{\text{drug}}/R^2$, allowing for the cumulative release at different parameter values to be represented by a single curve as a function of dimensionless time.

The numerical approximation to $c_{\text{drug}}(r,t)$ is denoted as $[\text{drug}]_j^k$ in the following discussion and is evaluated at the discrete points $((j-1)\Delta r, (k-1)\Delta t) = (r_j, t_k)$ for $j = 1, 2, \ldots, NR$ and $k = 1, 2, \ldots, NT$, where NR is the number of evenly-spaced radial discretizations and NT is the number of evenly-spaced time discretizations, rather than as a continuous function of r and t. The analytical solution is evaluated at the same discrete points as the numerical solution for comparison, $[\text{drug}](r_j, t_k)$. Analogously, the numerical and analytical cumulative release of drug profiles are denoted as Q^k and $Q(t_k)$, respectively.

Figure 10.4 shows the analytical drug concentration profiles expressed as fractions of concentration released as functions of dimensionless radial position r for different values of $\alpha_{\text{drug}}t$ in the diffusion-dominant limit using (10.180) for $0 < r < 1$ and (10.185) for $r = 0$ with $NR = 101$.

The percent error value for the drug concentration at each discrete point (r_j, t_k) is given by

$$PE([\text{drug}](r_j,t_k)) = \left| \frac{[\text{drug}](r_j,t_k) - [\text{drug}]_j^k}{[\text{drug}](r_j,t_k)} \right| \times 100\%. \tag{10.204}$$

Figure 10.5 shows the percent error between analytical and numerical drug concentration profiles at each dimensionless radial position r_j and dimensionless time $\alpha_{\text{drug}}t_k = D_{\text{drug}}t_k/R^2$ discretization used for the numerical solution with $NR = 101$ and $NT = 101$.

Figure 10.6 shows the analytical and numerical percentage of cumulative release of drug profiles at each value of dimensionless time $\alpha_{\text{drug}}t_k = D_{\text{drug}}t_k/R^2$ discretization used for the numerical solution with $NR = 101$ and $NT = 101$ and (10.192) for the analytical solution.

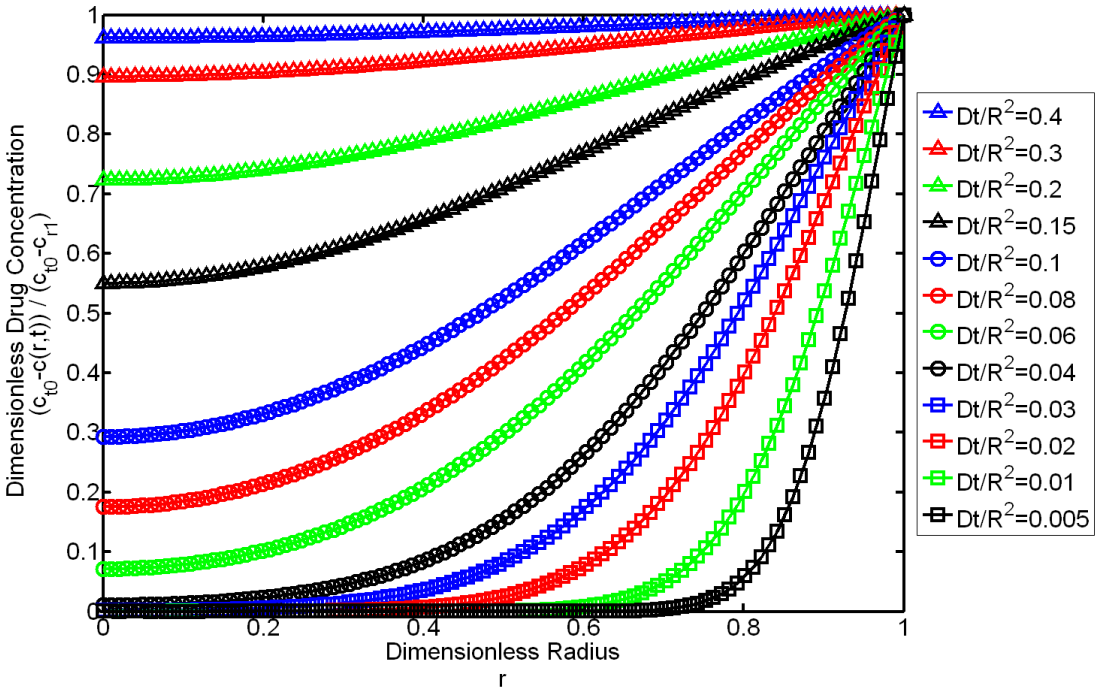

Figure 10.4: Analytical drug concentration profiles as functions of dimensionless radial position r for different values of dimensionless time $\alpha_{\text{drug}}t = D_{\text{drug}}t/R^2$ in the diffusion-dominant limit with $NR = 101$.

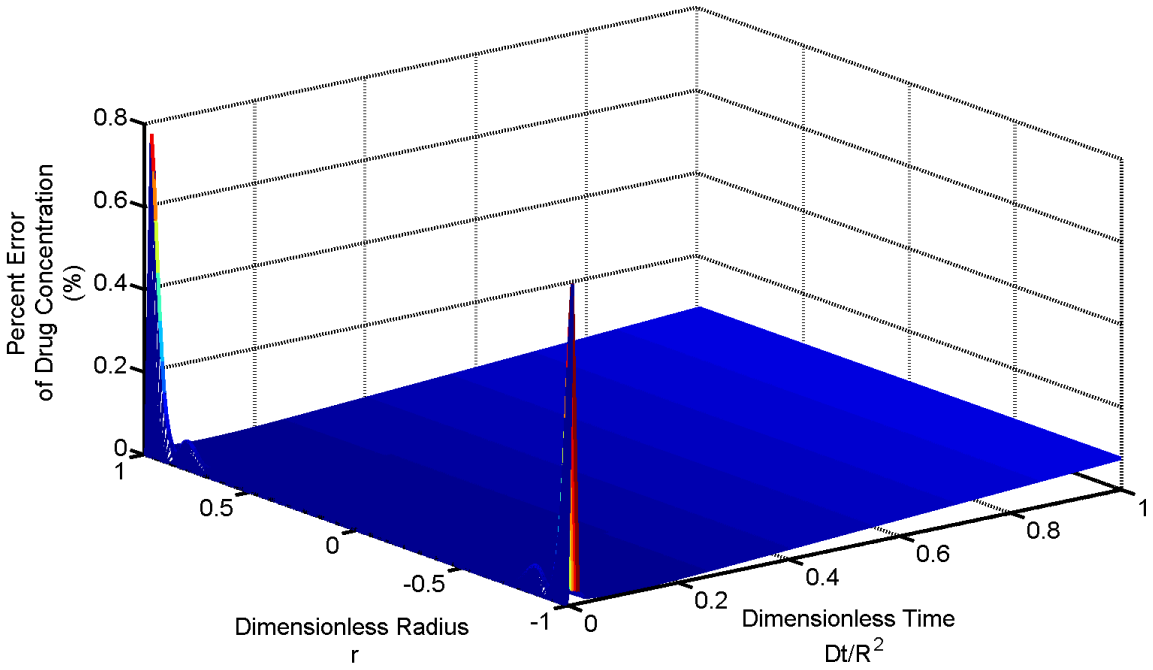

Figure 10.5: Percent error between analytical and numerical drug concentration profiles as a function of dimensionless radial position r and dimensionless time $\alpha_{\text{drug}}t = D_{\text{drug}}t/R^2$ in the diffusion-dominant limit with $NR = 101$ and $NT = 101$.

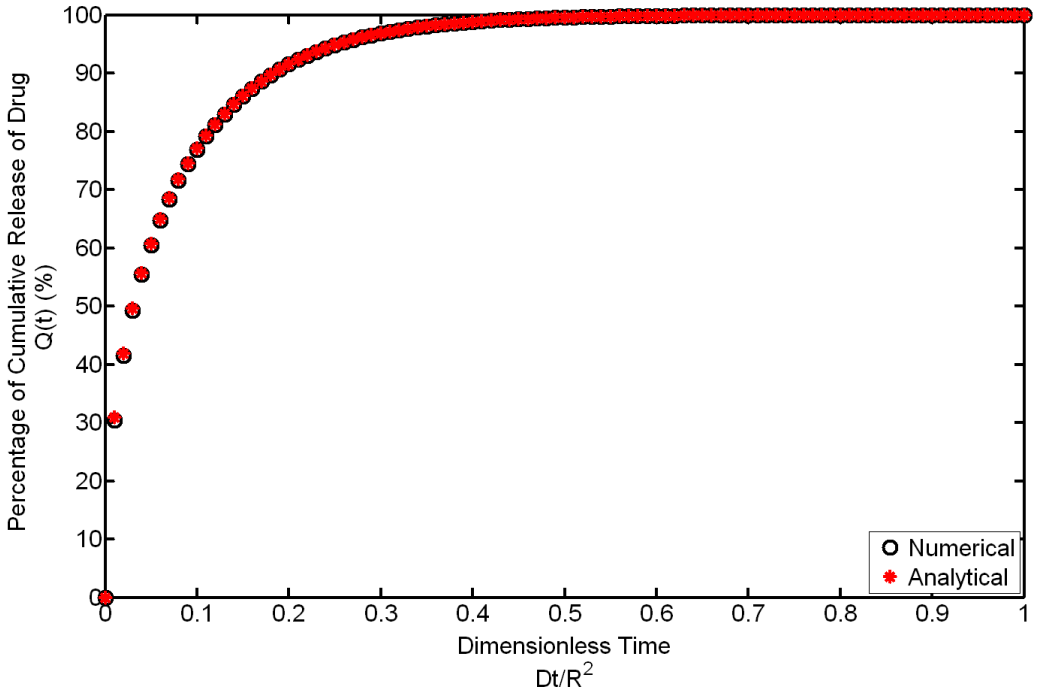

Figure 10.6: Analytical and numerical percentage of cumulative release of drug profiles as functions of dimensionless time $\alpha_{\text{drug}}t = D_{\text{drug}}t/R^2$ in the diffusion-dominant limit with $NR = 101$ and $NT = 101$.

The percent error value for the cumulative release of drug at each discrete value of t_k is given by

$$PE(Q(t_k)) = \left| \frac{Q(t_k) - Q^k}{Q(t_k)} \right| \times 100\%. \tag{10.205}$$

Figure 10.7 shows the percent error between analytical and numerical cumulative release of drug profiles at each dimensionless time $\alpha_{\text{drug}} t_k = D_{\text{drug}} t_k / R^2$ discretization used for the numerical solution. The percent error is greater for the cumulative release profiles than for the drug concentration profiles as the numerical approximations to the cumulative release profiles involve numerical integration of the drug concentration profiles, propagating the error associated with those profiles along with the error inherit to the Simpson quadrature numerical integration scheme. The root-mean-square error between the numerical and analytical cumulative release of drug percentage profiles is 0.11%. The cumulative release percentage values are between 0 and 100%.

The root-mean-square error between the dimensionless numerical and analytical drug concentration profiles with values that range between 0 and 1 is calculated by

$$RMSE(\mathbf{X}) = \frac{||\mathbf{X}||_F}{\sqrt{NR\,NT}}, \tag{10.206}$$

where the matrix $\mathbf{X}$ is composed of elements $x_{j,k} = \dfrac{[\text{drug}](r_j, t_k) - [\text{drug}]_j^k}{[\text{drug}]_{t0} - [\text{drug}]_{r0}}$ for $j = 1, 2, \ldots, NR$ and $k = 1, 2, \ldots, NT$. The root-mean-square error between the dimensionless numerical and analytical drug concentration profiles is 2.73×10^{-5} with $NR = 101$, $NT = 101$, and $TOL = 1 \times 10^{-4}$.

To determine the rate-of-convergence in the r-dimension, the root-mean-square error between the dimensionless numerical and analytical drug concentration profiles at the discrete time $t_k = t_{NT}$ is used as ϵ_y to quantify the error. Recall that the time step size is variable for the ODE solver. The

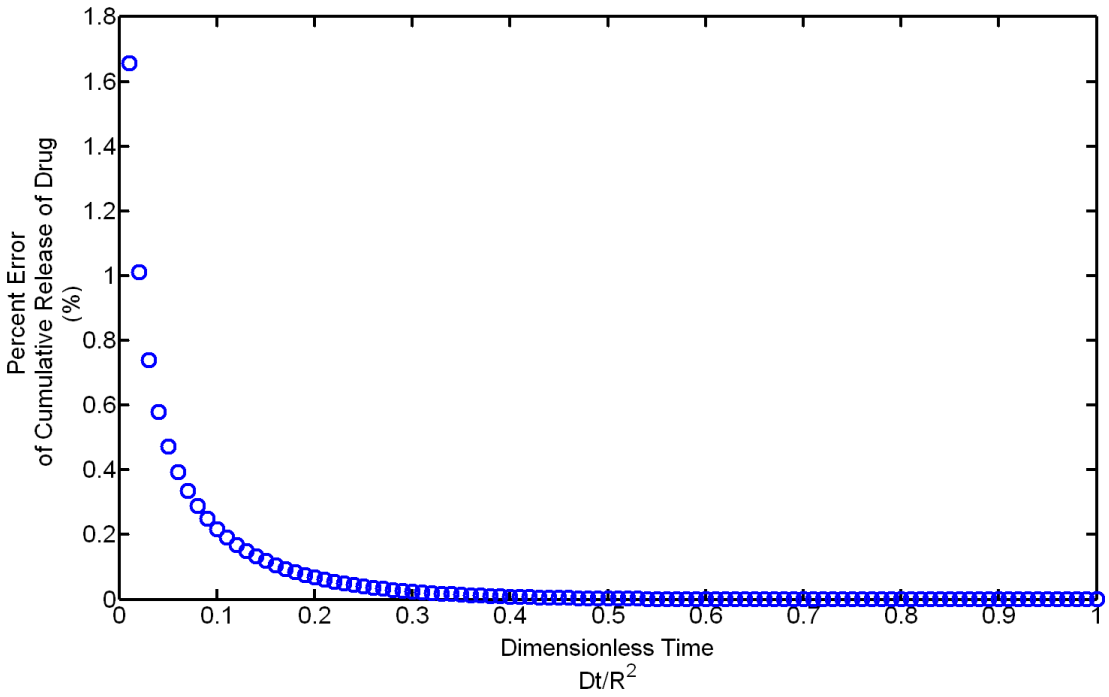

Figure 10.7: Percent error between analytical and numerical cumulative release of drug profiles as functions of dimensionless time $\alpha_{\text{drug}}t = D_{\text{drug}}t/R^2$ in the diffusion-dominant limit with $NR = 101$ and $NT = 101$.

root-mean-square error is calculated along a spatial vector at the final time, $\alpha_{\text{drug}}t = 1$, to eliminate the effects of the time step size on the error in order to determine the spatial contribution to the error independently,

$$RMSE(\mathbf{x}) = \frac{||\mathbf{x}||_2}{\sqrt{NR}}, \tag{10.207}$$

where the vector $\mathbf{x}$ is composed of the elements $x_j = \dfrac{[\text{drug}](r_j, t_{NT}) - [\text{drug}]_j^{NT}}{[\text{drug}]_{t0} - [\text{drug}]_{r0}}$ for $j = 1, 2, \ldots, NR$. The errors for nine grids with increasing NR from 6 to 301 and three error tolerance values from 1×10^{-4} to 1×10^{-12} all with $NT = 101$ are compared in Figure 10.8. The spatial step size is $\Delta r = 1/(NR - 1)$. Table 10.2 shows the rates-of-convergence observed for pairs of the discrete solutions shown in Figure 10.8 with $TOL = 1 \times 10^{-8}$ and $NT = 101$.

The observed rates-of-convergence approach the theoretical

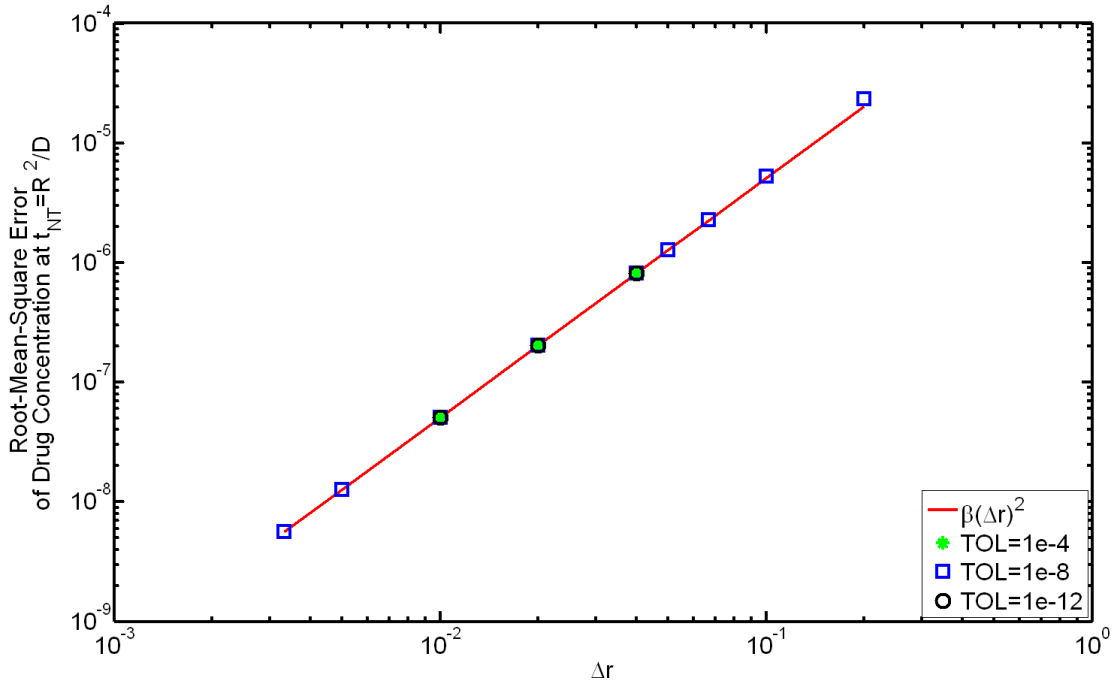

Figure 10.8: Root-mean-square error between dimensionless analytical and numerical drug concentration profiles in the r-dimension at the final time $t_{NT} = R^2/D_{\text{drug}}$ with $NT = 101$ as a function of the spatial discretization size Δr in the diffusion-dominant limit for error tolerance $TOL = 1 \times 10^{-4}$, 1×10^{-8}, and 1×10^{-12}. The solid line shows the expected error with the theoretical rate-of-convergence, $p = 2$, and the observed regression coefficient, $\beta = 5.09 \times 10^{-4}$, for the three smallest Δr values for $TOL = 1 \times 10^{-8}$.

Table 10.2: Rates-of-convergence observed using pairs of discrete solutions in the diffusion-dominant limit. The theoretical rate-of-convergence is 2.

Δr_C	Δr_F	Refinement Ratio	p
0.2	0.1	2	2.14
0.1	0.067	1.5	2.05
0.067	0.05	1.33	2.02
0.05	0.04	1.25	2.02
0.04	0.02	2	2.01
0.02	0.01	2	2.00
0.01	0.005	2	2.00
0.005	0.0033	1.5	2.00

rate-of-convergence for the central difference operator used for approximating the second derivatives in the spatial dimension. The error is reduced slightly by restricting the error tolerance, but shrinking the grid spacing reduces the error more substantially. Solutions with $NR \geq 51$ give acceptable drug concentration percent error values, and those with $NR \geq 101$ give high resolution for visualizations and reach the theoretical rate-of-convergence. The results of this section verify the code regarding the diffusion equations and the spatial discretization scheme.

10.4 Single-Component Limit

To verify that the numerical methods for the reaction and diffusion components of the model have been implemented correctly in tandem, the numerical results for the single-component limit are compared to the analytical solution for reaction and diffusion for a single species in the case of constant effective diffusivity, constant surface concentration, uniform initial concentration distribution, and a first-order generation term. The carboxylic acid end group species with the pseudo-first-order rate law for autocatalytic hydrolysis is treated in this section.

The single-component limit of the reaction-diffusion equation for the conservation of species i, (4.8), is approached when one species does not interact with other species. In the model reaction-diffusion system, the COOH rate of generation for the pseudo-first-order, autocatalytic hydrolysis model does not depend on the concentrations of any other species. If the effective diffusivity of COOH is taken to be a constant independent of the transport of the oligomers, then COOH can be modeled without coupling between other species. An analytical solution for the reaction-diffusion case with constant effective diffusivity, constant surface concentration, uniform initial concentration distribution, homogeneous boundary conditions, and first-order generation can be derived. As only one species is considered in the single-component limit, the subscript i is dropped for

convenience. The single-component limit for this case is obtained adding the following assumptions to those used to derive (4.8):

- The effective diffusivity is constant: $D(r,t) = D$.
- The surface boundary condition is homogeneous with a constant concentration of zero: $c(1,t) = c_{r1} = 0$.
- The initial distribution is uniform: $c(r,t) = c_{t0}$.
- The net rate of generation is first order in the concentration of the species: $R_V(r,t) = kc(r,t)$.

Applying the assumptions, the PDE for radial diffusion and first-order generation of a single component from a sphere with constant effective diffusivity, constant surface concentration of zero, uniform initial condition, and dimensionless r is given by

$$\frac{\partial c(r,t)}{\partial t} = \frac{D}{R^2}\frac{1}{r^2}\frac{\partial}{\partial r}\left(r^2\frac{\partial c(r,t)}{\partial r}\right) + kc(r,t) \tag{10.208}$$

with initial condition

$$c(r,0) = c_{t0}, \quad 0 \leq r < 1 \tag{10.209}$$

and boundary conditions

$$\frac{\partial c(0,t)}{\partial r} = 0, \quad t \geq 0 \tag{10.210}$$

and

$$c(1,t) = c_{r1} = 0, \quad t \geq 0, \tag{10.211}$$

where $c(r,t)$ is concentration of the species i, D is the constant effective diffusivity of the species, R is the radius of the sphere, $0 \leq r \leq 1$ is the normalized radial position, $t \geq 0$ is time, k is the rate constant for the first-order reaction, c_{t0} is the uniform initial concentration distribution of the species within the sphere, c_{r1} is the constant, homogeneous surface concentration of the species, and $k, \alpha > 0$.

10.4.1 Analytical Solution for the Concentration, $c(r,t)$, in the Single-Component Limit

The technique of linearization with the substitution of $v(r,t) = rc(r,t)$ can be used to transform (10.208)–(10.211) to a linear, nonhomogeneous second-order PDE with a source term and homogeneous, time-independent boundary conditions. Following the linearization steps in 10.3.1 and substituting $\alpha = D/R^2$, the linearized form is

$$\frac{\partial v(r,t)}{\partial t} = \alpha \frac{\partial^2 v(r,t)}{\partial r^2} + kv(r,t), \quad 0 \leq r \leq 1 \text{ and } t \geq 0, \tag{10.212}$$

with initial condition

$$v(r,0) = c_{t0} r, \quad 0 < r < 1 \tag{10.213}$$

and boundary conditions

$$v(0,t) = 0, \quad t \geq 0 \tag{10.214}$$

and

$$v(1,t) = 0, \quad t \geq 0. \tag{10.215}$$

The solution can be determined directly from the method of eigenfunction expansions [147],

$$v(r,t) = \sum_{n=1}^{\infty} a_n(t)\phi_n(r), \tag{10.216}$$

where $a_n(t)$ are the time-dependent, generalized Fourier coefficients and $\phi_n(r)$ are the eigenfunctions of the related homogeneous PDE for diffusion of v_h without a source term,

$$\frac{\partial v_h(r,t)}{\partial t} = \alpha \frac{\partial^2 v_h(r,t)}{\partial r^2}. \tag{10.217}$$

The boundary value problem resulting from separation of variables is

$$\frac{d^2\phi_n}{dr^2} = -\lambda_n \phi_n, \quad 0 \leq r \leq 1, \tag{10.218}$$

with boundary conditions

$$\phi_n(0) = 0 \tag{10.219}$$

and

$$\phi_n(1) = 0, \tag{10.220}$$

where λ_n are the eigenvalues. With the homogeneous, Dirichlet boundary conditions, the eigenvalues are

$$\lambda_n = n^2\pi^2, \quad n = 1, 2, \ldots, \tag{10.221}$$

with corresponding eigenfunctions

$$\phi_n(r) = \sin(n\pi r), \quad n = 1, 2, \ldots. \tag{10.222}$$

The Fourier sine series for the eigenfunction expansion for $v(r,t)$ is used because of the eigenfunctions and eigenvalues of the homogeneous PDE; the series can be differentiated term by term since the eigenfunction $\sin(n\pi r)$ and $v(r,t)$ satisfy the same boundary conditions [147].

The eigenfunction expansion of the source term is

$$kv(r,t) = \sum_{n=1}^{\infty} b_n(t)\phi_n(r), \tag{10.223}$$

where $b_n(t)$ are the coefficients of the Fourier sine series. As the source term is first-order in the linearized concentration, $b_n(t) = ka_n(t)$.

Inserting the eigenfunction expansion for $v(r,t)$ given by (10.216) and the eigenfunction expansions for the source term given by (10.223) into the nonhomogeneous PDE in (10.212) yields

$$\sum_{n=1}^{\infty} \frac{\partial a_n(t)\phi_n(r)}{\partial t}\phi_n(r) = \sum_{n=1}^{\infty} \alpha \frac{\partial^2 a_n(t)\phi_n(r)}{\partial r^2} + \sum_{n=1}^{\infty} b_n(t)\phi_n(r). \tag{10.224}$$

With the eigenfunctions for the homogeneous PDE for $v_h(r,t)$ given by (10.222) that satisfy $d^2\phi_n/dr^2 + \lambda_n\phi_n = 0$, the result can be simplified as

$$\sum_{n=1}^{\infty} \frac{da_n(t)}{dt}\phi_n(r) = \sum_{n=1}^{\infty} \left(-\alpha\lambda_n\right) a_n(t)\phi_n(r) + \sum_{n=1}^{\infty} k a_n(t)\phi_n(r). \tag{10.225}$$

Combining the sums,

$$\sum_{n=1}^{\infty} \left(\frac{da_n(t)}{dt} + \left(\alpha\lambda_n - k\right) a_n(t) \right) \phi_n(r) = 0. \tag{10.226}$$

For each $n = 1, 2, \ldots,$

$$\frac{da_n(t)}{dt} + \left(\alpha\lambda_n - k\right) a_n(t) = 0. \tag{10.227}$$

Alternatively, the ODE may be expressed as

$$\frac{da_n(t)}{dt} + \alpha\left(\lambda_n - \Phi_1^2\right) a_n(t) = 0, \tag{10.228}$$

where $k, \alpha > 0$ and $\Phi_1 = \sqrt{k/\alpha}$ is the Thiele modulus quantifying the ratio of the characteristic reaction rate in the absence of mass transfer limitations to the characteristic diffusion rate for the first-order reaction-diffusion system [113].

The solution to the linear, first-order ODE for the Fourier coefficients using the integrating factor $e^{\int \alpha\left(\lambda_n - \Phi_1^2\right)dt}$ is

$$a_n(t) = a_n(0) \exp\left(-\left(\lambda_n - \Phi_1^2\right)\alpha t\right), \quad n = 1, 2, \ldots, \tag{10.229}$$

where [147]

$$a_n(0) = \frac{\int_0^1 v(1,t)\phi_n(r)dr}{\int_0^1 \phi_n^2(r)dr}. \tag{10.230}$$

Substitution of ϕ_n given by (10.222) gives

$$a_n(0) = 2\int_0^1 v(1,t)\sin\left(n\pi r\right)dr. \tag{10.231}$$

With the uniform initial condition, $v(1,t) = c_{t0}r$, the integral is the same as the

integral previously evaluated in (10.176) for the diffusion-dominant limit. Thus,

$$a_n(0) = \frac{-2c_{t0}(-1)^n}{n\pi}, \quad n = 1,\, 2,\, \ldots. \tag{10.232}$$

Substitution of the expression for $a_n(0)$ into (10.229) gives

$$a_n(t) = \frac{-2c_{t0}(-1)^n}{n\pi} \exp\left(-\left(\lambda_n - \Phi_1^2\right)\alpha t\right), \quad n = 1,\, 2,\, \ldots. \tag{10.233}$$

For $0 < r < 1$ and $t > 0$, substitution of the eigenfunctions $\phi_n(r)$ given by (10.222), the eigenvalues $\lambda_n(r)$ given by (10.221), the Fourier coefficients $a_n(t)$ given by (10.233), and $\Phi_1 = \sqrt{k/\alpha}$ into the eigenfunction expansion for $v(r,t)$ given by (10.216) yields

$$v(r,t) = \frac{-2c_{t0}}{\pi} \sum_{n=1}^{\infty} \frac{(-1)^n}{n} \exp\left(-\left(n^2\pi^2 - \Phi_1^2\right)\alpha t\right) \sin\left(n\pi r\right). \tag{10.234}$$

Recall that the transformation from the conservation equation in radial coordinates involved $v(r,t) = c(r,t)r$. Dividing $v(r,t)$ given by (10.234) by r and using l'Hospital's Rule to resolve the indeterminate form at $r = 0$ as shown in (10.182), the concentration profiles for $t > 0$ in the single-component limit are

$$c(r,t) = \frac{-2c_{t0}}{\pi r} \sum_{n=1}^{\infty} \frac{(-1)^n}{n} \exp\left(-\left(n^2\pi^2 - \Phi_1^2\right)\alpha t\right) \sin\left(n\pi r\right), \quad 0 < r < 1 \tag{10.235}$$

and

$$c(0,t) = -2c_{t0} \sum_{n=1}^{\infty} (-1)^n \exp\left(-\left(n^2\pi^2 - \Phi_1^2\right)\alpha t\right), \quad r = 0. \tag{10.236}$$

The profiles in (10.235) and (10.236) are analogous to the concentration profiles in the diffusion-dominant limit given by (10.179) and (10.184) for $r > 0$ and $r = 0$, respectively, for $c_{r1} = 0$. With the homogeneous boundary condition at the surface, the first-order generation simply contributes a temporal exponential growth term to each profile in the single-component limit.

The profile for $c(r,t)$ exhibits exponential growth due to the pseudo-first-order, autocatalytic hydrolysis reaction and exponential decay due to diffusion. For a solution that reaches a steady state, the time derivative of $c(r,t)$ must be zero; either the exponential term must (i) be constant or (ii) approach 0 as $t \to \infty$. For the first case, the exponential term is constant with a value of 1 if $n^2\pi^2 - \Phi_1^2 = 0$, which can only be satisfied for a single value of n when $\Phi_1 = m\pi$. For the second case, for the exponential to approach 0 as $t \to \infty$, the terms inside the exponential must all be positive, so

$$n^2\pi^2 - \Phi_1^2 > 0, \quad n = 1, 2, \ldots. \tag{10.237}$$

In the most restrictive case of $n = 1$,

$$\begin{aligned} \Phi_1^2 &< \pi^2, \\ k &< \pi^2\alpha. \end{aligned} \tag{10.238}$$

If $\Phi_1 = m\pi$, the solution can be stable if

$$\begin{aligned} n^2\pi^2 - m^2\pi^2 \geq 0, \quad n, m = 1, 2, \ldots, \\ n \geq m. \end{aligned} \tag{10.239}$$

Thus, $m = 1$ is the only multiple of π that gives stable solution with $\Phi_1 = m\pi$. Larger values of m have modes that grow with time. Large microspheres, slow diffusion, or fast reaction can give large Thiele modulus. For large values of Φ_1, the first-order reaction generation dominates the conservation equation, so the single component accumulates in the interior faster than it can be transported out of the sphere; no steady state is possible for $\Phi_1 > \pi$. For small values of Φ_1, the diffusion dominates the conservation equation, so any amount of the component generated by the reaction is transported away before it can accumulate and autocatalyze the reaction unboundedly; a steady state can be reached. For $\Phi_1 = \pi$ the reaction and

diffusion phenomena can reach an equilibrium steady state. The Thiele modulus Φ_1 is an indicator of the relative importance of the reaction and diffusion contributions to the conservation of the species.

10.4.2 Comparison of Numerical and Analytical Solutions for COOH Concentration, [COOH](r, t)

The numerical solution for the conservation equation for [COOH](r, t) in the single-component limit for pseudo-first-order, autocatalytic hydrolysis and diffusion is determined using the numerical methods algorithm described in Chapter 8 with the assumptions for the single-component limit given in Section 10.4. The analytical solution is computed using the equations in Section 10.4.1 for the COOH species. The COOH concentration profiles from the numerical and analytical solutions are compared. The radius r is defined in dimensionless terms in the formulation of the conservation equation in Chapter 4. For $\Phi_1 \leq 1$, the COOH concentration is scaled by the uniform initial COOH concentration, and time is made dimensionless with the same term as used in the diffusion-dominant limit, αt. For $\Phi_1 \geq 1$, the COOH concentration is scaled by the sum of the initial concentrations of E and COOH, and time is made dimensionless with the same term as used in the reaction-dominant limit, $t/t_{0.99}$, where $t_{0.99}$ is the time required for 99% conversion of ester bonds to carboxylic acid end groups in the reaction-dominant limit.

The numerical approximation to $c_{\mathrm{COOH}}(r, t)$ is denoted as $[\mathrm{COOH}]_j^k$ in the following discussion and is evaluated at the discrete points $((j-1)\Delta r, (k-1)\Delta t) = (r_j, t_k)$ for $j = 1, 2, \ldots, NR$ and $k = 1, 2, \ldots, NT$, where NR is the number of evenly-spaced radial discretizations and NT is the number of evenly-spaced time discretizations, rather than as a continuous function of r and t. The analytical solution is evaluated at the same discrete points as the numerical solution for comparison, [COOH](r_j, t_k).

Figure 10.9 shows the dimensionless analytical carboxylic acid end group

concentration profiles in the single-component limit using (10.235) for $0 < r < 1$ and (10.236) for $r = 0$ at each dimensionless radial position, r_j, and each dimensionless time discretization, Dt_k/R^2 for $\Phi_1 \leq 1$ or $t_k/t_{0.99}$ for $\Phi_1 \geq 1$, used for the numerical solution with $NR = 101$ and $NT = 101$.

Figures 10.10, 10.11, and 10.12 show the dimensionless numerical COOH concentration profiles at $r = 0$ in the single-component limit as functions of dimensionless time for small, intermediate, and large ranges of Φ_1, respectively. The diffusion-dominant limit and the reaction-dominant limit curves are indicated on the plots. The profiles for different values of Φ_1 fall between these two limits. The profiles show that for a single reacting and diffusing component with constant effective diffusivity D, if the radius R increases, Φ_1 increases, and the acid accumulates in the center of the sphere to a greater extent. For constant R and increasing D, diffusive effects become more significant. These relationships are explored further in Chapter 11 for the full model with multiple components and variable effective diffusivity coupled to the generation of carboxylic acid end groups.

The percent error value for the COOH concentration at each discrete point (r_j, t_k) is given by

$$PE([\text{COOH}](r_j, t_k)) = \left| \frac{[\text{COOH}](r_j, t_k) - [\text{COOH}]_j^k}{[\text{COOH}](r_j, t_k)} \right| \times 100\%. \tag{10.240}$$

Figure 10.13 shows the percent error between analytical and numerical COOH concentration profiles at each dimensionless radial position, r_j, and dimensionless time discretization, Dt_k/R^2 for $\Phi_1 \leq 1$ or $t_k/t_{0.99}$ for $\Phi_1 \geq 1$, used for the numerical solution with $NR = 101$, $NT = 101$, and $TOL = 1 \times 10^{-4}$.

As in the reaction-dominant limit, the global truncation error of the numerical COOH concentration at the final time step is assessed relative to the specified error tolerance. The elements of the global truncation error vector at the

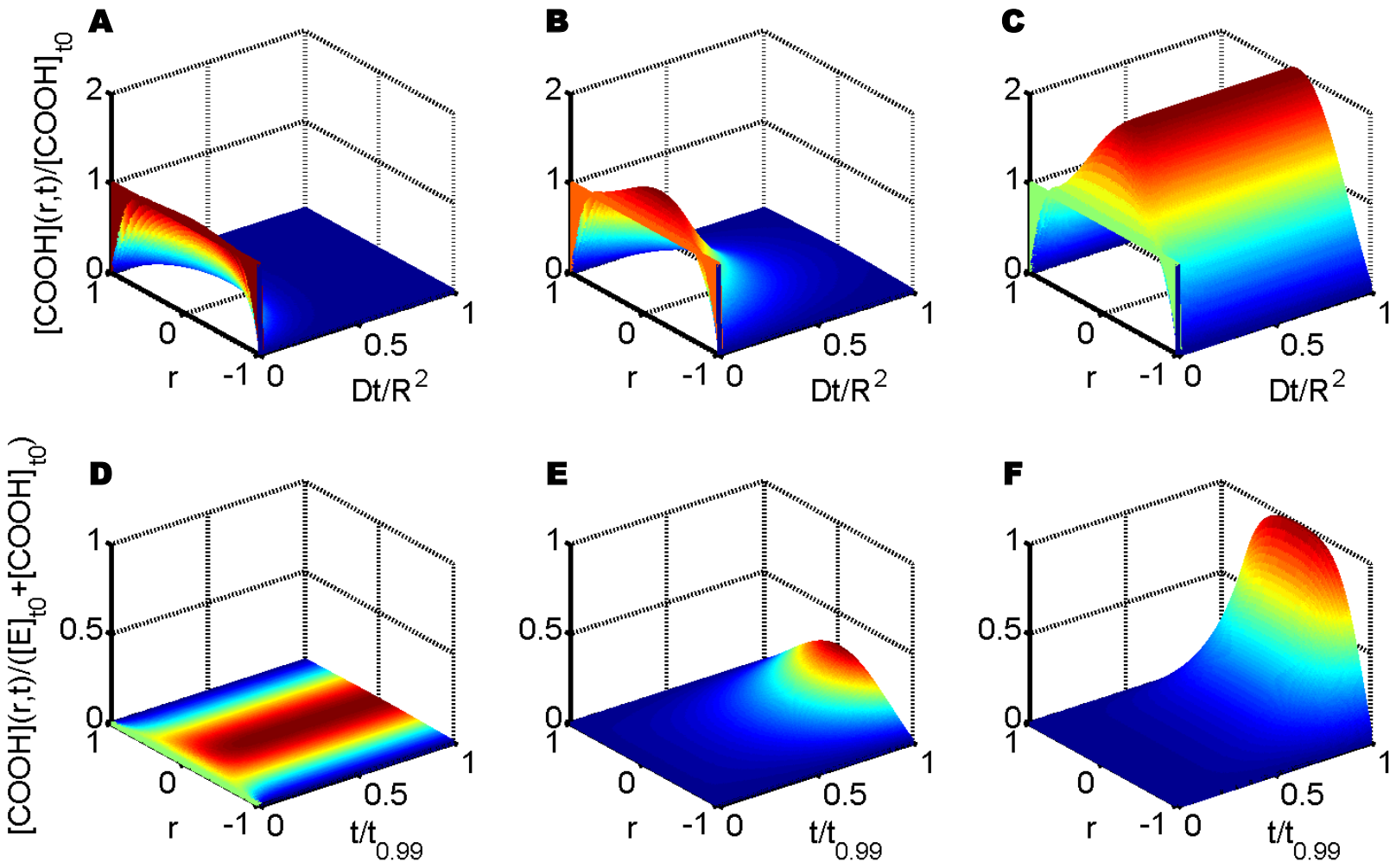

Figure 10.9: Analytical dimensionless carboxylic acid end group concentration profiles as functions of dimensionless radius r and dimensionless time (Dt/R^2 for $\Phi_1 \leq 1$ and $t/t_{0.99}$ for $\Phi_1 \geq 1$) in the single-component limit with $NR = 101$ and $NT = 101$ for A) $\Phi_1 = 1 \times 10^{-5}\pi$, B) $\Phi_1 = 0.75\pi$, C) $\Phi_1 = \pi$, D) $\Phi_1 = \pi$, E) $\Phi_1 = 1.75\pi$, and F) $\Phi_1 = 4\pi$.

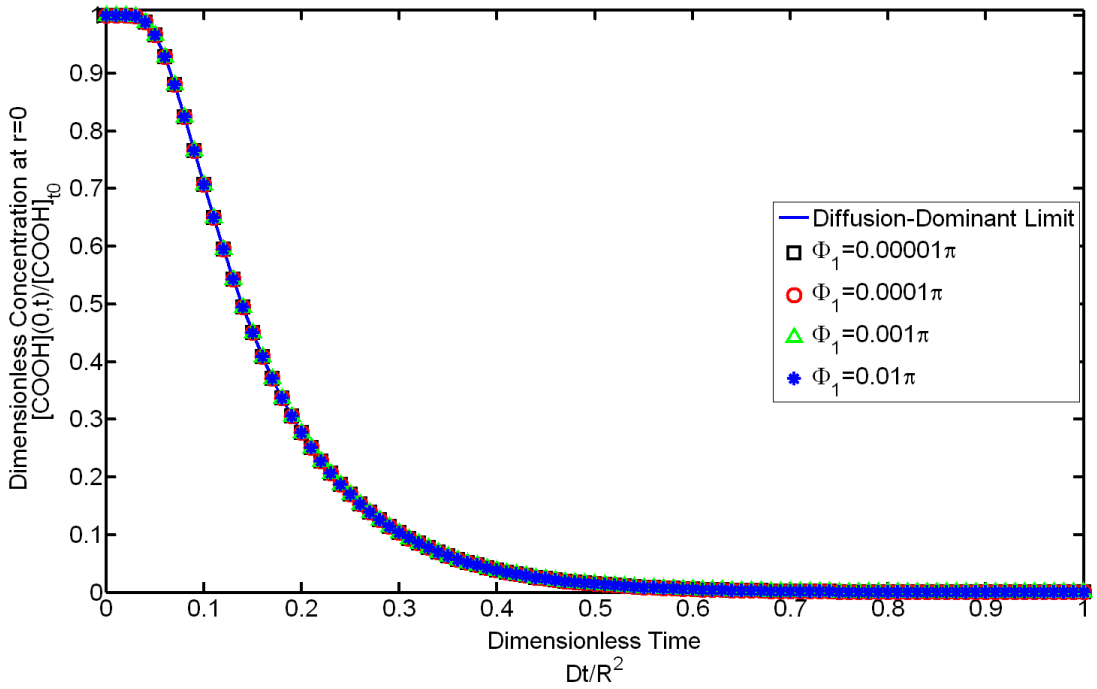

Figure 10.10: Numerical COOH concentration profiles at $r = 0$ scaled by the initial concentration as functions of dimensionless time $\alpha t = Dt/R^2$ for small values of Φ_1 approaching the diffusion-dominant limit with $NR = 101$, $NT = 101$, and $TOL = 1 \times 10^{-4}$ in the single-component limit.

final time step, t_{NT}, are

$$e_{j,NT} = |[\text{COOH}](r_j, t_{NT}) - [\text{COOH}]_j^{NT}|, \quad j = 1, 2, \ldots, NR. \tag{10.241}$$

Figure 10.14 shows the global truncation error of the numerical COOH concentration at the final time step in the single-component at each dimensionless radial position, r_j, used for the numerical solution with $NR = 101$, $NT = 101$, and $TOL = 1 \times 10^{-4}$. For the entire range of the parameter Φ_1, the global truncation error values as a function of radius are much smaller than the absolute tolerance.

The root-mean-square error between the dimensionless numerical and analytical COOH concentration profiles is calculated by

$$RMSE(\mathbf{X}) = \frac{||\mathbf{X}||_F}{\sqrt{(NR)(NT)}}, \tag{10.242}$$

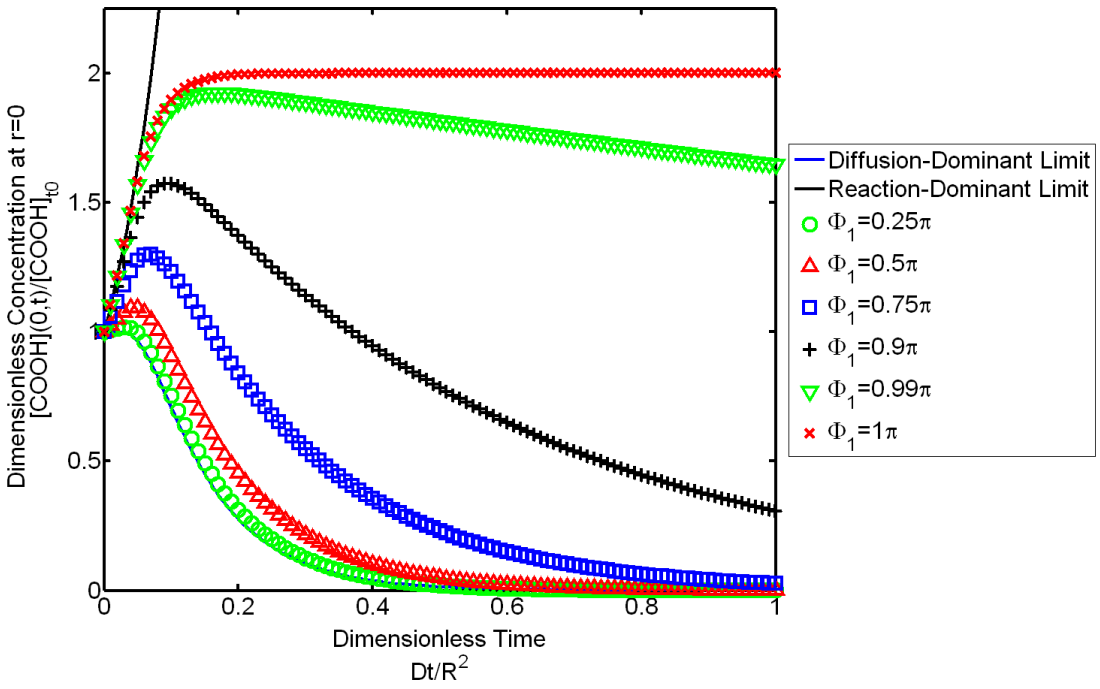

Figure 10.11: Numerical COOH concentration profiles at $r = 0$ scaled by the initial concentration as functions of dimensionless time $\alpha t = Dt/R^2$ for intermediate values of Φ_1 with $NR = 101$, $NT = 101$, and $TOL = 1 \times 10^{-4}$ in the single-component limit.

where the matrix $\mathbf{X}$ is composed of elements $x_{j,k} = \dfrac{[\text{COOH}](r_j, t_k) - [COOH]_j^k}{\max[\text{COOH}](r_j, t_k)}$ for $k = 1, 2, \ldots, NT$. The scaling is relative to the maximum value for each profile as the range for each profile is not strictly between 0 and 1 when scaled by either $[\text{COOH}]_{t0}$ or $[\text{COOH}]_{t0} + [\text{E}]_{t0}$, depending on the value of Φ_1. Table 10.3 shows the root-mean-square error between the numerical and analytical COOH concentration profiles scaled by the maximum concentration with $NR = 101$, $NT = 101$, and $TOL = 1 \times 10^{-4}$ for different values of Φ_1/π.

As in the diffusion-dominant limit, the root-mean-square error between the dimensionless numerical and analytical COOH concentration profiles at the discrete time $t_k = t_{NT}$ is used as ϵ_y to quantify the error to determine the rate-of-convergence in the r-dimension. Recall that the time step size is variable for the ODE solver. The root-mean-square error is calculated along a spatial vector at the final time to eliminate the effects of the time step size on the error in order to

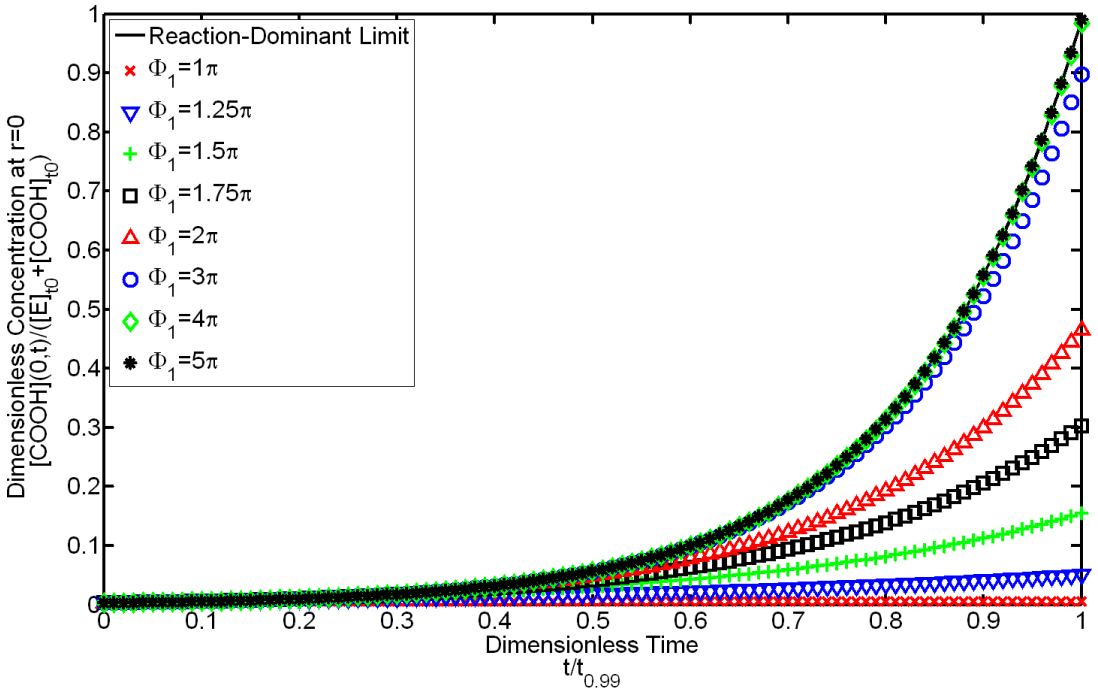

Figure 10.12: Numerical COOH concentration profiles at $r = 0$ scaled by the sum of the initial concentrations of ester bonds and carboxylic acid end groups as functions of dimensionless time $t/t_{0.99}$ for large values of Φ_1 approaching the reaction-dominant limit with $NR = 101$, $NT = 101$, and $TOL = 1 \times 10^{-4}$ in the single-component limit.

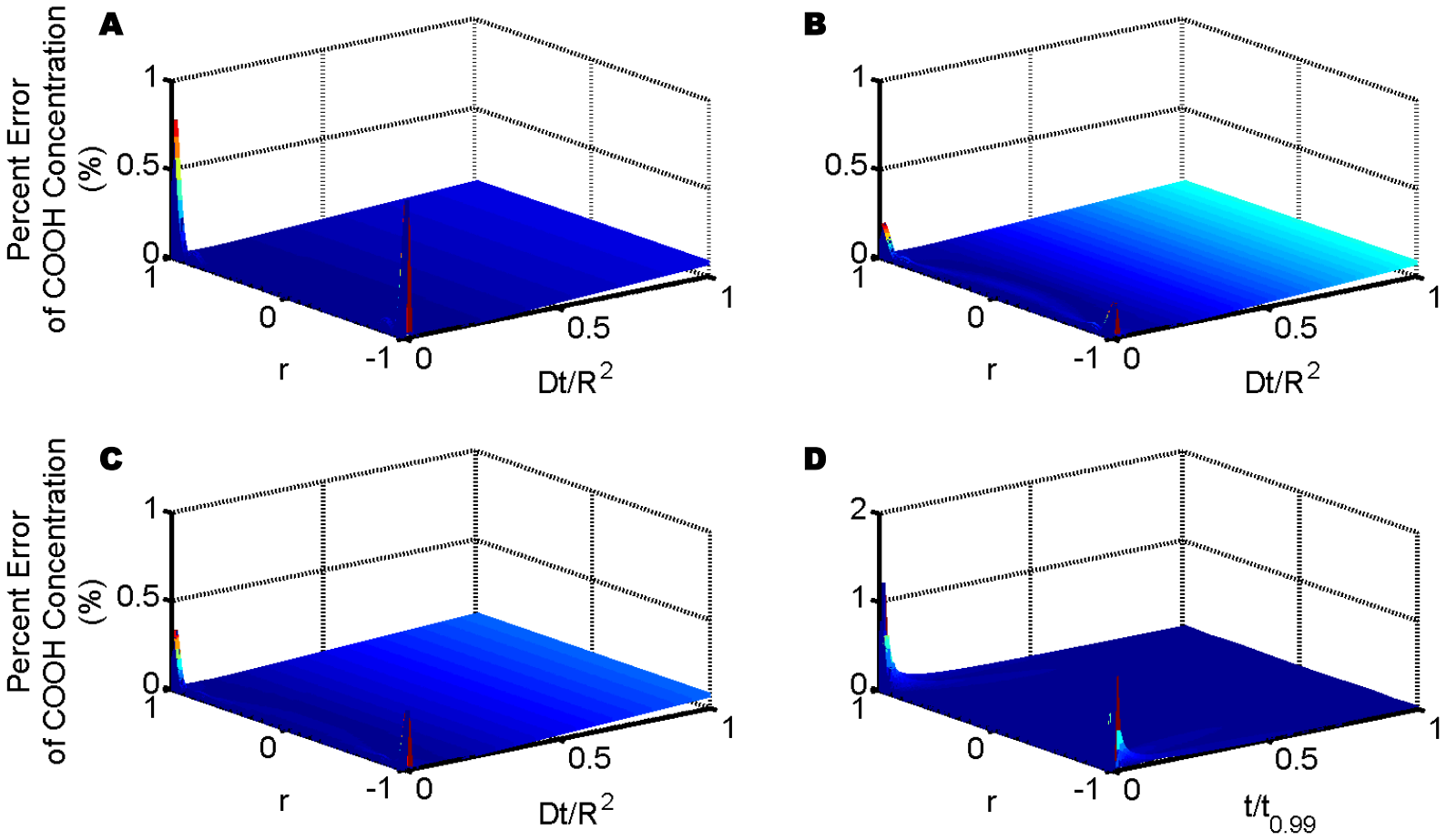

Figure 10.13: Percent error between analytical and numerical carboxylic acid end group concentration profiles as functions of dimensionless radius and dimensionless time (Dt/R^2 for $\Phi_1 \leq 1$ and $t/t_{0.99}$ for $\Phi_1 > 1$) with $NR = 101$, $NT = 101$, and $TOL = 1 \times 10^{-4}$ in the single-component limit for A) $\Phi_1 = 1 \times 10^{-5}\pi$, B) $\Phi_1 = 0.99\pi$, C) $\Phi_1 = \pi$, and D) $\Phi_1 = 5\pi$.

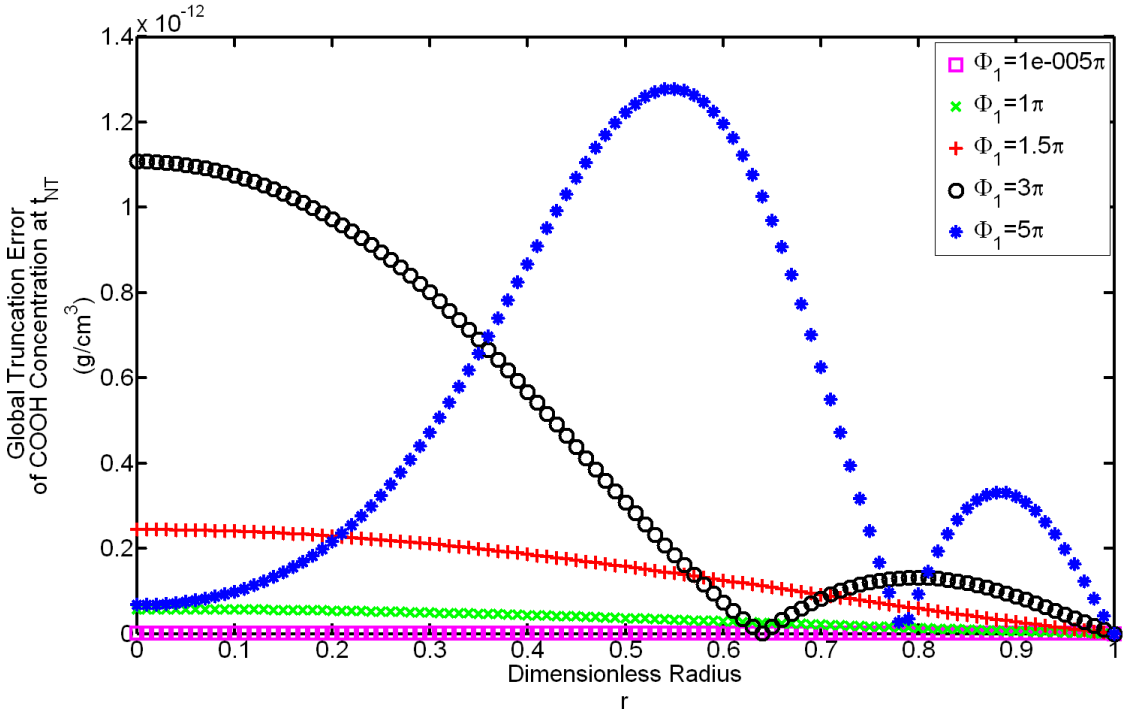

Figure 10.14: Global truncation error of the numerical COOH concentration profiles at t_{NT} with $NR = 101$, $NT = 101$, and $TOL = 1 \times 10^{-4}$ as functions of the dimensionless radius for values of Φ_1 in the full range considered in the single-component limit.

Table 10.3: Root-mean-square errors between the numerical and analytical COOH concentration profiles scaled by the maximum concentration with $NR = 101$, $NT = 101$, and $TOL = 1 \times 10^{-4}$ for different values of Φ_1/π in the single-component limit.

Φ_1/π	$RMSE$	$\max[\text{COOH}](r_j, t_k)/[\text{COOH}]_{t0}$	$\max[\text{COOH}](r_j, t_k)/([\text{COOH}]_{t0} + [\text{E}]_{t0})$
0.00001	2.73×10^{-5}	1.00×10^{0}	3.18×10^{-3}
0.0001	2.73×10^{-5}	1.00×10^{0}	3.18×10^{-3}
0.001	2.73×10^{-5}	1.00×10^{0}	3.18×10^{-3}
0.01	2.73×10^{-5}	1.00×10^{0}	3.18×10^{-3}
0.1	2.73×10^{-5}	1.00×10^{0}	3.19×10^{-3}
0.25	2.73×10^{-5}	1.02×10^{0}	3.23×10^{-3}
0.5	2.77×10^{-5}	1.09×10^{0}	3.47×10^{-3}
0.75	3.72×10^{-5}	1.30×10^{0}	4.13×10^{-3}
0.9	9.23×10^{-5}	1.57×10^{0}	5.00×10^{-3}
0.99	2.41×10^{-4}	1.92×10^{0}	6.11×10^{-3}
1	2.70×10^{-4}	2.00×10^{0}	6.36×10^{-3}
1.01	1.32×10^{-4}	2.24×10^{0}	7.12×10^{-3}
1.1	9.01×10^{-5}	5.42×10^{0}	1.72×10^{-2}
1.25	5.45×10^{-5}	1.58×10^{1}	5.02×10^{-2}
1.5	2.69×10^{-5}	4.85×10^{1}	1.54×10^{-1}
1.75	1.27×10^{-5}	9.52×10^{1}	3.03×10^{-1}
2	5.70×10^{-6}	1.46×10^{2}	4.65×10^{-1}
3	1.76×10^{-5}	2.83×10^{2}	8.98×10^{-1}
4	1.62×10^{-5}	3.10×10^{2}	9.84×10^{-1}
5	1.67×10^{-5}	3.11×10^{2}	9.90×10^{-1}

determine the spatial contribution to the error independently,

$$RMSE(\mathbf{x}) = \frac{||\mathbf{x}||_2}{\sqrt{NR}}, \tag{10.243}$$

where the vector $\mathbf{x}$ is composed of the elements $x_j = \dfrac{[\text{COOH}](r_j, t_{NT}) - [\text{COOH}]_j^{NT}}{\max[\text{COOH}](r_j, t_{NT})}$ for $j = 1, 2, \ldots, NR$. The errors for nine grids with increasing NR from 6 to 301 and three error tolerance values from 1×10^{-4} to 1×10^{-12} all with $NT = 101$ and $\Phi_1 = \pi$ are compared in Figure 10.15. The spatial step size is $\Delta r = 1/(NR - 1)$. Table 10.4 shows the rates-of-convergence observed for pairs of the discrete solutions shown in Figure 10.15 with $TOL = 1 \times 10^{-8}$, $NT = 101$, and $\Phi_1 = \pi$. The observed rates-of-convergence approach the theoretical rate-of-convergence for the central difference operator used for approximating the second derivatives in the spatial dimension.

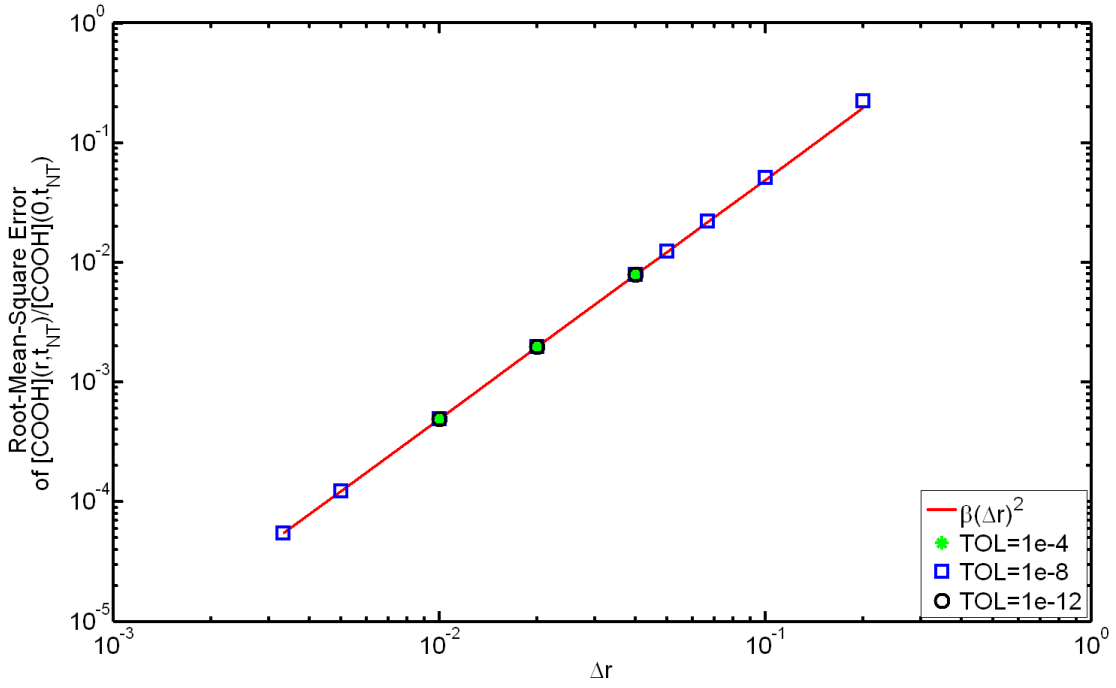

Figure 10.15: Root-mean-square error between dimensionless analytical and numerical COOH concentration profiles at t_{NT} scaled by $COOH(0, t_{NT})$ with $NT = 101$ and $\Phi_1 = \pi$ as a function of the spatial discretization size Δr in the single-component limit for error tolerance $TOL = 1 \times 10^{-4}$, 1×10^{-8}, and 1×10^{-12}. The solid line shows the expected error with the theoretical rate-of-convergence, $p = 2$, and the observed regression coefficient, $\beta = 4.92$, for the three smallest Δr values for $TOL = 1 \times 10^{-8}$.

Table 10.4: Rates-of-convergence, p, observed using pairs of discrete solutions in the single-component limit with $\Phi_1 = \pi$. The theoretical rate-of-convergence is 2.

Δr_C	Δr_F	Refinement Ratio	p
0.2	0.1	2	2.14
0.1	0.067	1.5	2.05
0.067	0.05	1.33	2.02
0.05	0.04	1.25	2.02
0.04	0.02	2	2.01
0.02	0.01	2	2.00
0.01	0.005	2	2.00
0.005	0.0033	1.5	2.00

Solutions with $NR \geq 101$, $NT \geq 101$, and $TOL \leq 1 \times 10^{-4}$ give adequate scaled root-mean-square errors, percent errors, and global truncation errors for the range of Φ_1 values explored indicating that there is good agreement between the numerical and analytical solutions in the single-component limit. The results of this section verify the code regarding the numerical solution of the conservation equation with both reaction and diffusion equations contributions for a single component.

Chapter 11

Model Performance and Discussion

In this chapter, numerical solutions to the full model presented in Chapter 7 solved with the methods of Chapter 8 implemented in the manner described in Chapter 9 are given for a variety of physical parameter values with different configurations of model options. In Chapter 10 the numerical solutions for limiting cases are given, whereas this chapter presents numerical solutions for the case of fully-coupled reaction and diffusion in a multi-component system. It is impossible to show the model performance for every possible case. Instead, the aim of this chapter is to highlight model performance for a set of physically realistic cases to provide insight into the validity of the model and the mechanisms underlying the physical system. The most significant finding of the model regards the predictions of the drug release from microspheres of different sizes and is covered in Section 11.1. Section 11.2 shows the ability of the model to treat nonuniform initial drug distributions. Section 11.3 explains some limitations of the model and potential ways to circumvent the limitations.

If the model is used with the $diffn\_on = 3$ option with the diffusivity at infinite dilution specified for the small oligomers as the weighted-average of the diffusivity at infinite dilute for the lactic acid and glycolic acid monomers, the polymer diffuses away more rapidly than it can react (diffusion-dominant limit), and no drug release is predicted using the model. Therefore, the following results are obtained with $diffn\_on = 2$ with the effective diffusivity of the small oligomers constant.

11.1 Size-Dependent Release Behavior

It is well-known that cumulative release from small particles in the diffusion-dominant limit with constant effective diffusivity is faster than from large particles. The results of the diffusion-dominant limit presented in Section 10.3 show that the concentration and release curves collapse onto a single curve when plotted against the diffusive dimensionless time, Dt/R^2. One of the primary motivations for the present work is to investigate the size-dependent autocatalytic effects on diffusive drug release. Towards this aim, model predictions for different microsphere sizes with variable effective diffusivity coupled to the hydrolysis of the eroding polymer are compared. The diffusion through the bulk polymer is assumed to be negligible for this analysis to isolate the effects of the pore growth on the diffusive drug release. Model predictions of drug release with a simplified expression for the variable effective diffusivity of the drug through the aqueous pores with simultaneous drug diffusion through the polymer bulk are available in Appendix A.

This analysis exclusively uses the quadratic-order rate law for autocatalytic hydrolysis. The ester bond concentration changes significantly throughout the simulation time, violating the primary assumption of the pseudo-first-order rate law. The quadratic-order rate law is used over the 1.5th-order rate law due to the insensitivity of the quadratic-order rate law to the initial carboxylic acid concentration. The first-order rate law for uncatalyzed hydrolysis is not suitable for predicting the behavior of systems known to exhibit autocatalytic degradation. Table 11.1 shows the constant parameters used for the comparison between microspheres of radii $R = 5$, 25, and 50 μm.

11.1.1 Polymer Degradation and Erosion

Figure 11.1 shows the effects of microsphere radius on the concentration profiles for the carboxylic acid end groups and the ester bonds. With the same constant

Table 11.1: Constant parameters for comparison of effects of microsphere radius.

Name	Value
NR	101
NS	13
DD	1×10^{-6} cm^2/s
DH	1.22×10^{-8} cm^2/s
k_1'	0.077 days^{-1}
PDI	1
Mw	20,000
$Xrxn$	0.99
$Rp0$	0
G	0.5
TOL	1×10^{-6}
$DD0$	0
$DH0$	0

effective diffusivity for the small oligomers, the largest microsphere has concentration profiles at $r = 0$ that approach the reaction-dominant limit while the smallest microsphere has concentration profiles that are affected strongly by the diffusion of the small oligomers. These size-dependent diffusive effects are as expected.

11.1.2 Microclimate pH

Figure 11.1 shows the effects of microsphere radius on the intraparticle pH profiles assuming the initial pH is 7.4. The results illustrate the size-dependent microclimate pH behavior observed experimentally [83]. The center of the largest microsphere has the most acidic pH due to the accumulation of acidic reaction products that autocatalyze the hydrolysis reaction.

11.1.3 Pore Growth

Figure 11.3 shows the effects of microsphere radius on the average pore radius. $R_p(r,t)/R_d$ values above the threshold of 1 correspond to $\lambda_{\text{drug}}(r,t) < 1$. With a uniform initial drug concentration throughout the polymer microsphere with a constant surface boundary concentration of zero, the concentration driving force

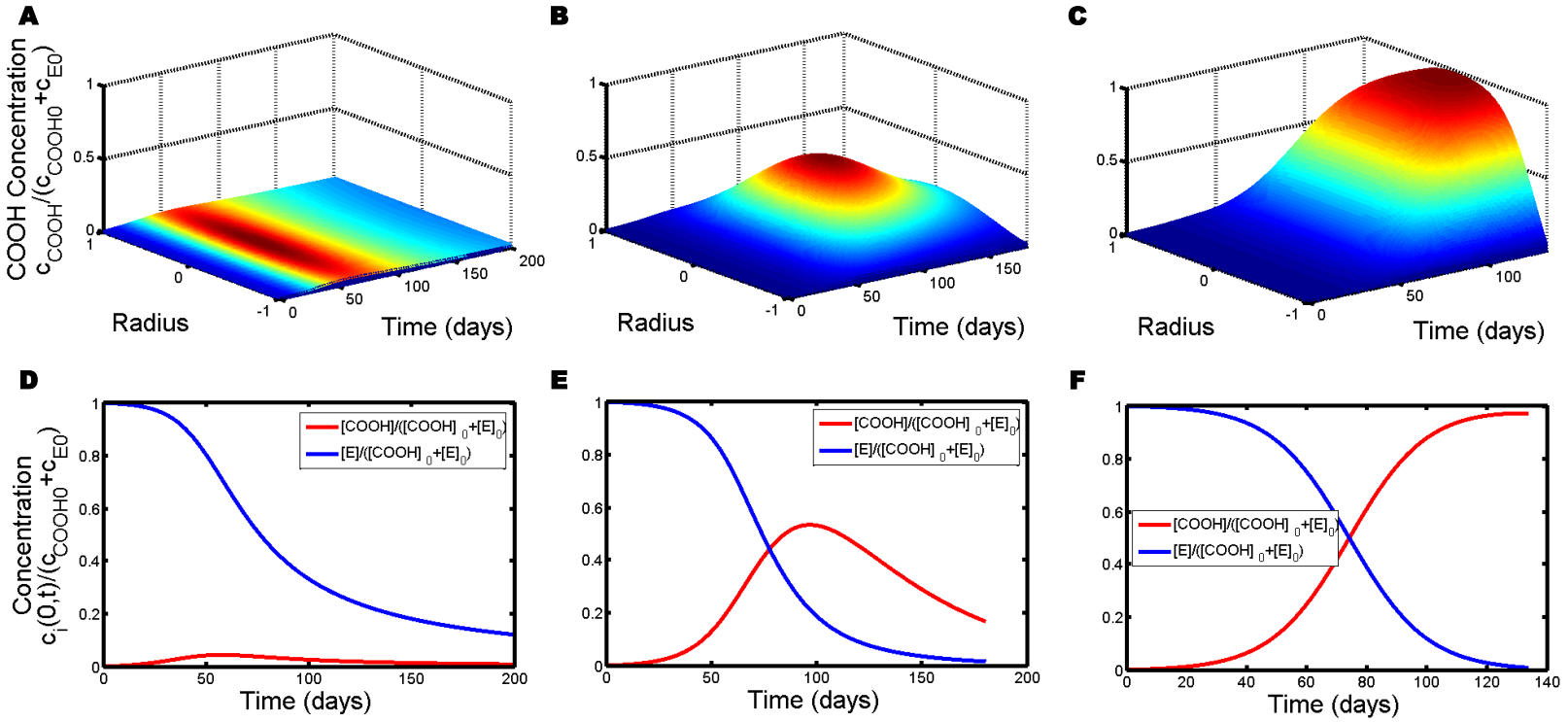

Figure 11.1: Polymer degradation and erosion with microsphere radius $R = 5$ μm (Panels A and D), $R = 25$ μm (Panels B and E) and $R = 50$ μm (Panels C and F). Panels A, B, and C show the carboxylic acid end group concentration profiles, and Panels D, E, and F show the profiles for the carboxylic acid end group and ester bond concentration profiles at $r = 0$.

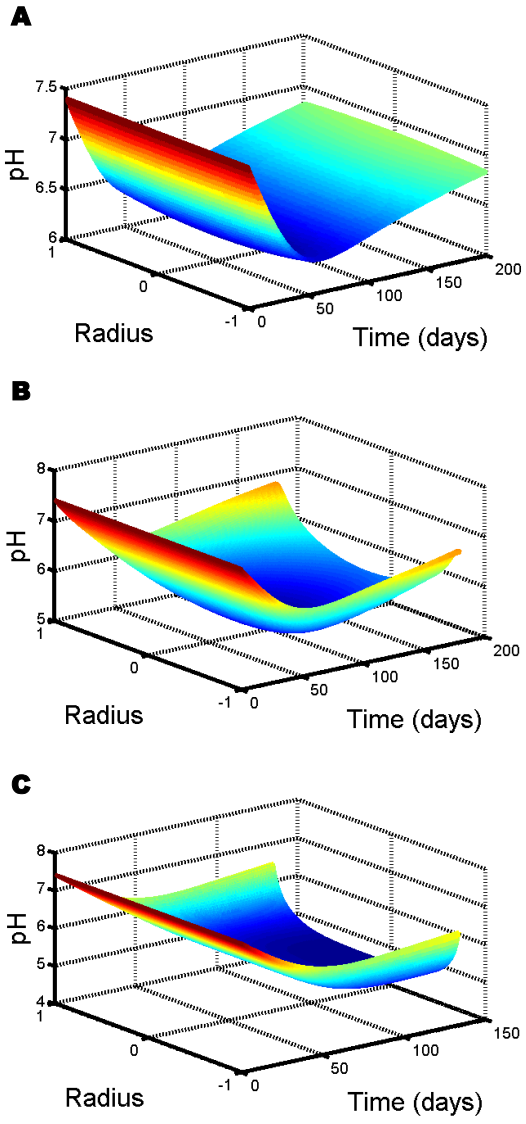

Figure 11.2: Intraparticle pH profiles for microsphere radius A) $R = 5$ μm, B) $R = 25$ μm, and C) $R = 50$ μm.

initially exists only between the boundary at $r = 1$ and the adjacent discretization point inside the microsphere at $r = 1 - \Delta r$. The growth of the effective diffusivity in the interior has no effect on the drug release until $D_{\text{drug}}(r, t) > 0$ coincides with a concentration gradient. Release is delayed until $R_p(1 - \Delta r, t)/R_d > 1$. This occurs at earlier times for larger microspheres.

11.1.4 Variable Effective Diffusivity

Figure 11.4 shows the effects of microsphere radius on the effective diffusivity of the drug within the microsphere. Larger microspheres have larger $D_{\text{drug}}(r, t)$ than small microspheres allowing for faster drug release once release begins. The effective diffusivity in the vicinity of the concentration gradient between the first interior spatial discretization point and the surface grows fastest for the largest microspheres, initiating drug release sooner than for the other microspheres.

11.1.5 Drug Concentration Profiles

Figure 11.6 shows the effects of microsphere radius on the concentration profiles of the drug. The time required for the drug concentration to reach 0 once release begins does not exhibit a clear trend with microsphere size. The smallest microsphere requires about 30 days and has spatial variation in drug concentration with time. The intermediate-sized microsphere has nearly spatially uniform drug concentrations over time and the time required for the total change in drug concentration is about 40 days. For the time required for release to be greater for the intermediate-sized microsphere than for the smallest microsphere is consistent with the diffusion-dominant limit. The largest microsphere requires about 27 days for release of the drug and has nearly spatially uniform drug concentrations over time. The decrease in the duration of the drug release for the largest microsphere might be attributable to its effective diffusivity profile, which is larger in magnitude and more spatially uniform than the effective diffusivity profiles for the other two

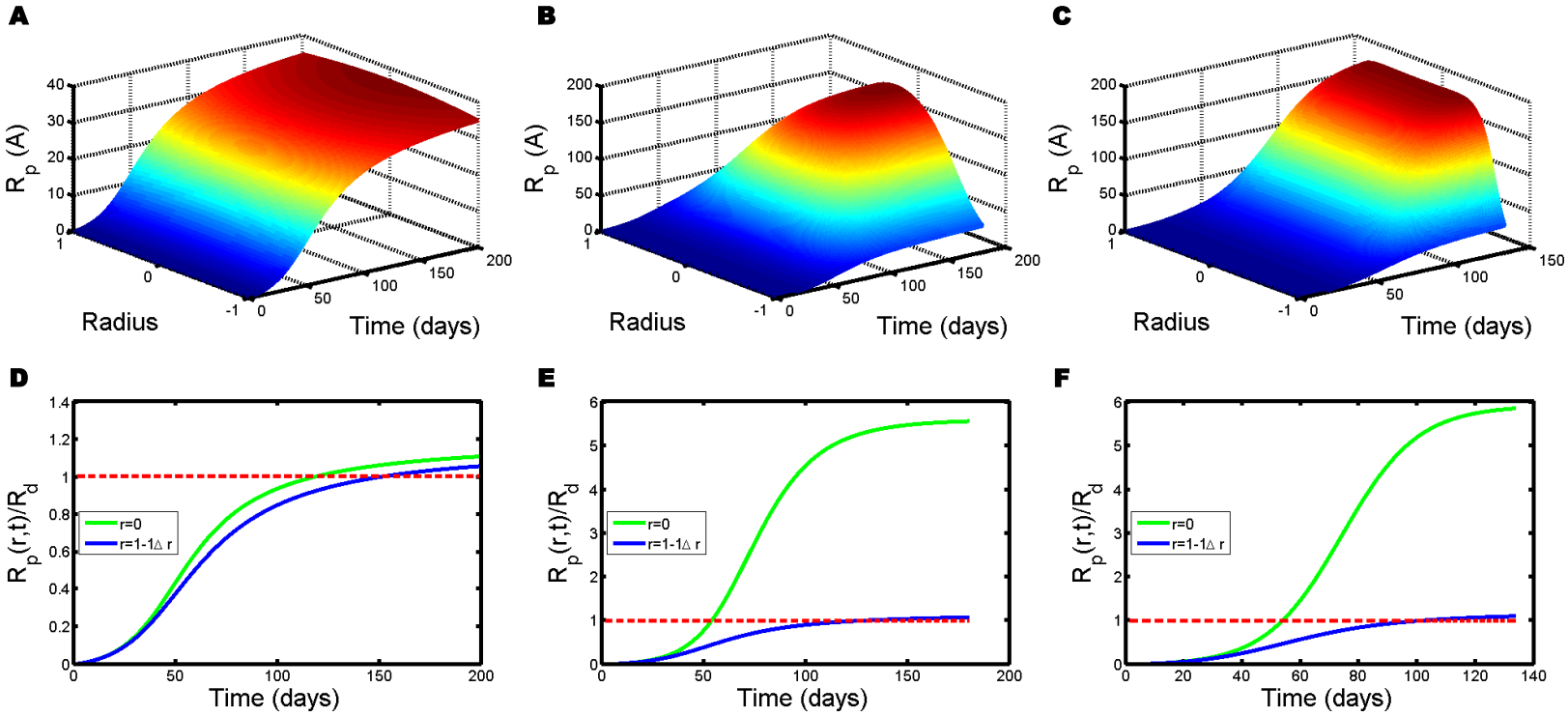

Figure 11.3: Pore radius profiles with microsphere radius $R = 5$ μm (Panels A and D), $R = 25$ μm (Panels B and E) and $R = 50$ μm (Panels C and F). Panels A, B, and C show the profiles of the average pore radius, and Panels D, E, and F show the pore radius scaled by the drug solute radius, R_d, at $r = 0$.

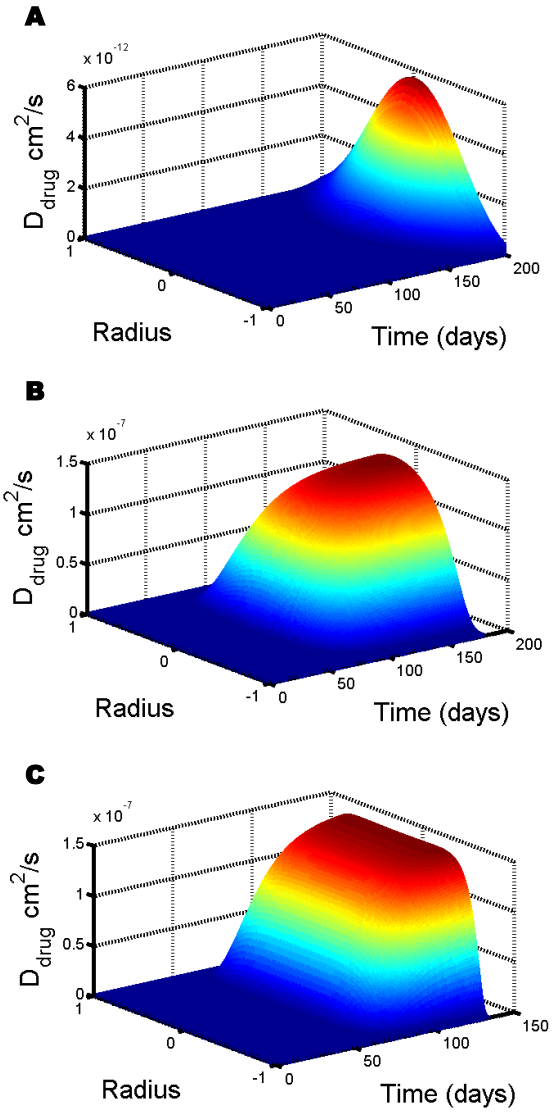

Figure 11.4: Effective diffusivity of drug profiles for microsphere radius A) $R = 5$ μm, B) $R = 25$ μm, and C) $R = 50$ μm.

microspheres sizes.

11.1.6 Drug Release Profiles

Figure 11.6 shows the effects of microsphere radius on the cumulative release profiles of the drug. Unlike the trends for the diffusion-dominant limit with smaller microspheres reaching 100% release before larger microspheres, larger microspheres are shown to start releasing drug earlier than smaller microspheres with effective diffusivity of the drug dependent on the pore evolution of the autocatalytically degrading and eroding polymer microsphere, with the assumption of no diffusion through the polymer bulk. The duration of the release processes vary nonmonotonically with microsphere size as discussed in Section 11.1.5. The release intervals are scaled by the time required for release with t_0 defined as the time when the cumulative release grows larger than the error tolerance and t_{100} defined as the time when the cumulative release is within the error tolerance of 100%. The scaled curves show that the shapes of the cumulative release profiles with variable effective diffusivity are quite different from the shape of the curve with constant effective diffusivity, which is the same for all radii with cumulative release scaled in this manner. The slight differences between the curves for the three microsphere radii may be due to the differences in their effective diffusivity profiles, so the curves do not collapse onto a single curve as the dynamics of the drug release vary.

11.2 Initial Distribution of Drug

The default initial distribution of the drug is uniform throughout the polymer microsphere. Due to burst effects or uneven loading, the drug may be distributed nonuniformly. The model can treat these distributions (and likewise alternative distributions of other species) by supplying the initial solution vector to the code through the input file restart_data.dat and using the $restart = 1$ option. Diffusion

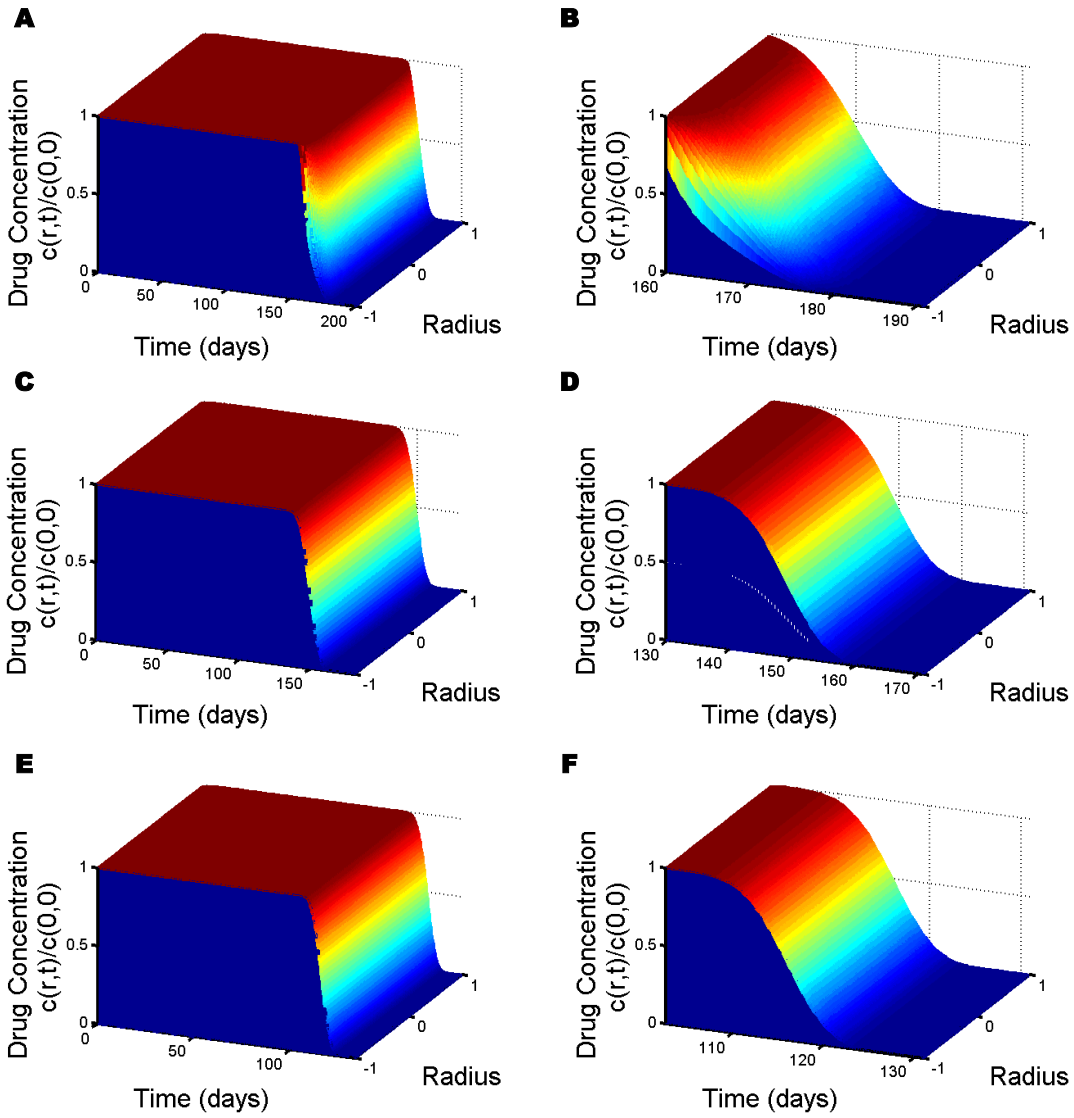

Figure 11.5: Drug concentration profiles for microsphere radius $R = 5$ μm (Panels A and B), $R = 25$ μm (Panels C and D), and $R = 50$ μm (Panels E and F). Panels A, C, and E show the entire simulation time, and Panels B, D, and F focus on the interval when drug release occurs.

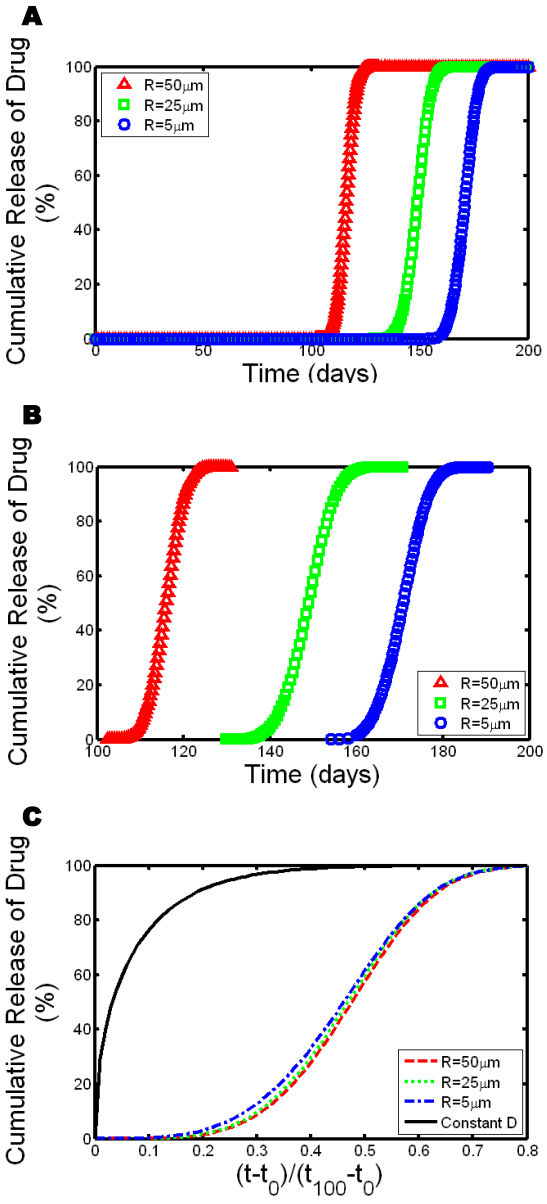

Figure 11.6: Cumulative release profiles for microsphere radius $R = 5$, 25, and 50 μm for A) the entire simulation time, B) the interval when cumulative release is between 0 and 1, and C) the interval when cumulative release is between 0 and 1 with dimensionless time scaled by the endpoints of the drug release interval, t_0 and t_{100}.

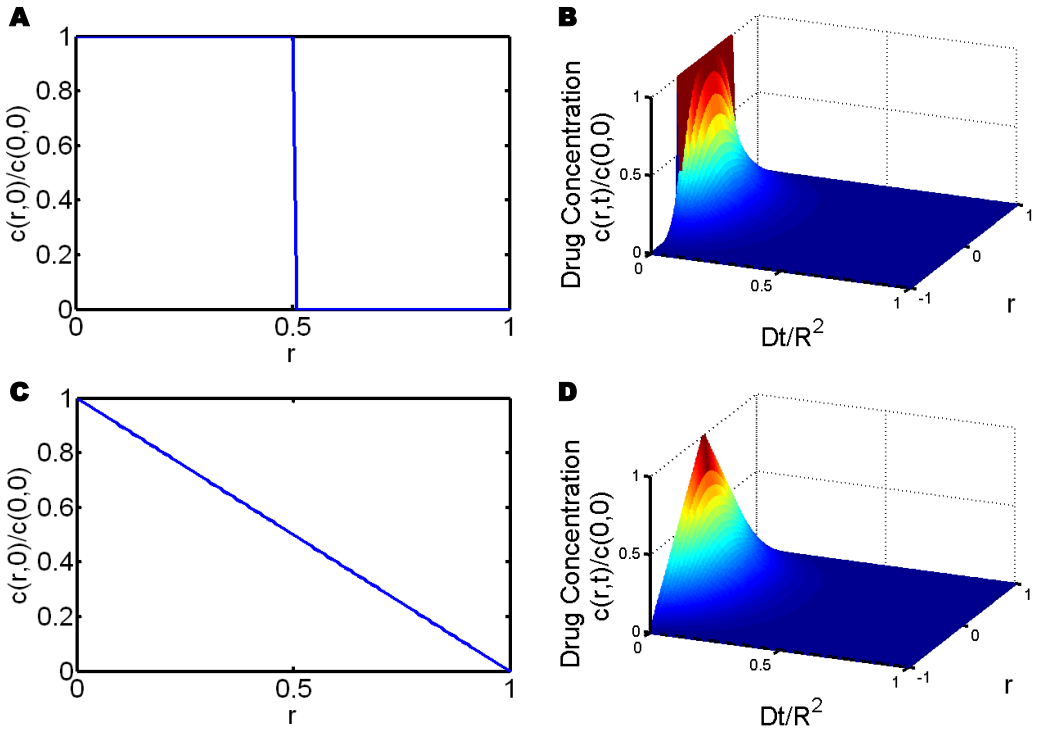

Figure 11.7: Nonuniform drug concentration profiles. Panels A and C show the initial drug distributions, and Panels B and D show the drug concentration profiles in the diffusion-dominant limit as a function of position and time. Panels A and B show the profiles for the step-function initial distribution of drug with uniform concentration of 1 along the inner half of the radius. Panels C and D show the profiles for the linear initial distribution of drug.

of the drug from two sample nonuniform profiles are shown in Figure 11.7.

11.3 Limitations of the Model

All the results presented here are for 50:50 PLGA. The model can accommodate other copolymer fractions of PLGA or pure PLA or PGA, if the appropriate rate constant and molecular weight are supplied. Changing G only adjusts the average monomer size, pKa, and monomer molecular weight.

The concentrations are all scaled either by [drug]$(0,0)$ for the drug or by $[\mathrm{COOH}]_{t0}$ for the polymeric species. pH can be calculated from the output data based on [COOH](r,t). Effects of the medium pH on the reaction rates cancel from the model, except for in the rate constant of the 1.5th-order rate law for

autocatalytic hydrolysis. If the initial carboxylic acid end group concentration can be defined explicitly throughout the polymer interior, perhaps the 1.5th-order rate law would be suitable for treating external pH modulation with the model. External pH is known to have complex influences on the release of drugs from PLGA microspheres, and the PLGA hydrolysis kinetics have been shown not to be significantly impacted by external pH with slight variations in degradation rate constants for the pseudo-first-order rate law reported over a wide range of pH values [14].

The model considers "drug" molecules as unreactive with no charged or electrostatic interactions with the polymer. Actual drugs may be hydrophobic or hydrophilic, charged, small molecules or macromolecules, insoluble, linear or branched or globular, or may possess other nonideal interaction attributes. Some allowance for the relative partitioning of the drug for the polymer phase versus the aqueous phase to quantify the propensity to resist diffusion through the bulk or to favor dissolution can be made by adjusting the minimum and maximum effective diffusivity values used by the model for the drug, $D_{\text{drug},b}$ and $D_{\text{drug},\infty}$, respectively.

The use of the deterministic reaction-diffusion model assumes that all species react and diffuse according to straightforward mathematical equations. The predictions shown here must be taken as average behavior rather than actual behavior in all cases. The pore size distribution also is merely an estimate that allows for coupling the effective diffusivity to the reaction in a quantitative way. The model approach to the pore size distribution allows for more spatial refinement than the model proposed by [55], which uses a particle-average pore size, and less than the three-dimensional spatial variation detail allowed in a stochastic cellular automata method. The information captured with this model seems sufficient to characterize regions where the pore growth should be significant.

Chapter 12

Conclusions

In this dissertation, a model was developed, verified for limiting cases, and used to predict behavior for diffusive drug release from PLGA microspheres undergoing autocatalytic degradation and erosion in aqueous media. The work was motivated by experimental studies in the literature demonstrating size-dependent polymer erosion and variations in drug release profiles that have been attributed to autocatalysis of PLGA. The reaction-diffusion model with pore evolution coupled to hydrolysis and related to the effective diffusivity through hindered diffusion theory was proposed to fill the gap in the modeling literature for the simultaneous treatment of polymer degradation and erosion and drug release with autocatalytic effects and nonconstant effective diffusivity of the drug. The system of partial differential equations comprising the model was solved numerically using the method of lines with the finite difference method and the RADAU5 ordinary differential equation solver. The numerical methods and the computational implementation of the model were described in detail. Three limiting cases for the model were presented with the derivations of the analytical solutions and comparison between the solutions and the model predictions. The model performance for the case of drug release from microspheres of different sizes was presented to highlight the capability of the model for predicting size-dependent, autocatalytic effects on the polymer and the drug release. Limitations of the model were also discussed.

The model presented in this dissertation can be used to investigate the dynamic behavior of the PLGA and drug system under different physical

conditions. The model may also be extended to apply to other drug delivery systems for similar types of polymers and other device geometries such as microcapsules and microspheres composed of layers of different microspheres. Drug characteristics like hydrophobicity and pH sensitivity also can be incorporated with knowledge of effects of the drug-polymer interactions on the physical parameters of the model. Further utilization of the model developed in this work could aid in the development of a database that could include the predictions of the effects of many possible polymer microparticle fabrication designs under a range of conditions. The optimum design for producing a desired drug release profile could be determined, which would be important for manufacturers making microparticles for medical therapeutic use in patients.

Appendix A

Multi-Scale Modeling of PLGA Microparticle Drug Delivery Systems[1]

Abstract

A mechanistic reaction-diffusion model is proposed for the simulation of drug delivery from PLGA microspheres. The model considers the effects of autocatalytic hydrolysis kinetics and the evolution of the pore network on microsphere-size-dependent drug release. Spatial and temporal variations in the intraparticle pH and the void fraction are reported.

Keywords

Multi-scale modeling, drug delivery, PLGA microspheres, polymer degradation, biomedical engineering.

A.1 Introduction

Controlled-release drug delivery systems are being developed as alternatives to conventional medical drug therapy regimens that require frequent administrations due to short pharmaceutical *in vivo* half-life or poor oral bioavailability. Controlled-release systems have the potential to provide better control of drug concentrations, reduce side effects, and improve compliance as compared to

[1]This appendix includes the text and figures reproduced in entirety from the proceedings paper [35] with the references, headings, figures, and pages numbered according to the scheme of this dissertation. Elsevier, the copyright owner, allows the authors to include the article in full or in part in a dissertation. The first author of this publication was responsible for all content and figures, while the other authors were responsible for initial paper idea and text revisions.

conventional regimens. Proteins, pharmaceuticals, and DNA can be encapsulated into biodegradable polymer microparticles of controlled size including microspheres, core-shell microparticles, and microcapsules. Microparticles also enable the encapsulation of drugs for delivery in a multi-stage pulsatile release and for the protection of proteins from being deactivated.

The model-based design of controlled-release devices, such as biodegradable poly(lactic-co-glycolic acid) (PLGA) polymer microspheres, is challenging because of incomplete understanding of the mechanisms that regulate the release of drug molecules. This paper describes the multi-scale modeling of autocatalytic polymer degradation and release of dispersed drug molecules from PLGA microspheres to capture size-dependent degradation observed experimentally. Researchers have suggested that autocatalytic polymer degradation is the primary mechanism by which the diffusive drug release is accelerated, and this process should depend strongly on particle size [25, 27, 41]. Mathematical models that are sufficiently predictive for design purposes must describe all of the important length scales, which range from (1) the nanometer length scales of embedded molecules that are initially smaller than the size of pores in the microspheres but later are larger than the smallest pores and (2) the sub-nanometer to micro-scale pores that span the pore dimensions that are evolving in time as the polymer degrades to (3) the overall radius of the microspheres (up to a millimeter). The underlying phenomena are tightly coupled dynamically, requiring the simultaneous dynamic simulation of drug diffusion, autocatalytic polymer degradation reactions, and pore formation and evolution.

A.2 Model

Autocatalytic PLGA Degradation

The equation for the acid-catalyzed hydrolysis reaction is

$$\mathrm{P}_n + \mathrm{H_2O} + \mathrm{H}^+ \rightleftharpoons \mathrm{P}_r + \mathrm{P}_{n-r} + \mathrm{H}^+ \tag{A.1}$$

where P_n is a PLGA polymer chain of length n and H^+ is the acid catalyst that can be from an external source such as strongly acidic medium or an internal source such as the carboxylic acid end groups, denoted COOH, of the polymer chains. If the catalyst is only from a strong acid external source, there is no net generation of acid as the catalytic terms cancel. PLGA microparticles for drug delivery applications are typically degraded in aqueous media *in vivo* or *in vitro*, so strong acid external catalyst sources are not considered here. With autocatalysis, the carboxylic acid end groups accelerate the reaction by serving as proton donors that enable the acid-catalyzed reaction mechanism. A variety of kinetic models have been proposed for the polymer hydrolysis, including uncatalyzed kinetics [102], pseudo-first-order kinetics [103], quadratic-order kinetics [91], and 1.5-order kinetics with partial dissociation of COOH [104]. The kinetic models for the catalyzed hydrolysis reaction treat the carboxylic acid end groups as the catalyst source but differ by the terms that are considered constant and by whether the end groups are assumed to be fully or partially dissociated. Here the kinetic treatment assumes full dissociation of carboxylic acid end groups and constant concentration of water as it is in excess for PLGA, which is hydrated on a time scale much faster than the diffusion or degradation time scales. The species are not assumed to be well-mixed, and the reactions occur throughout the polymer microsphere volume. The concentrations of reacting species are functions of space and time and are coupled to diffusion. Previous drug release models that simultaneously incorporate reaction

and diffusion do not consider autocatalytic effects. The kinetic model is used in conjunction with Fickian diffusion to simulate controlled-release drug delivery from PLGA microspheres that are known to exhibit autocatalytic, size-dependent degradation behavior.

Reaction-Diffusion Equations

The combined reaction-diffusion equations for the water-soluble small oligomer chains of PLGA that are capable of diffusing out of the system are

$$\begin{aligned}\frac{\partial[\mathrm{P}_n](r,t)}{\partial t} =& \frac{1}{r^2}\frac{\partial}{\partial r}\left(r^2\frac{D_{\mathrm{P}_n}(r,t)}{R^2}\frac{\partial[\mathrm{P}_n](r,t)}{\partial r}\right) \\ &+ 2k[\mathrm{COOH}](r,t)\sum_{i=n+1}^{\infty}[\mathrm{P}_i](r,t) - (n-1)k[\mathrm{COOH}](r,t)[\mathrm{P}_n](r,t)\end{aligned} \tag{A.2}$$

where $D_{\mathrm{P}_n}(r,t)$ is the effective diffusivity of the polymer chains P_n and r is the radial position within a microsphere. The boundary conditions are a constant surface concentration of zero and symmetry at $r = 0$. Here small oligomers are considered to be those with 9 or fewer monomeric units as lactic oligomers with number-average molecular weight smaller than 830 Da are known to be soluble in buffer at pH 7.4 [148].

The drug species is assumed to not react with the polymer, so the differential equation for the drug concentration is

$$\frac{\partial[\mathrm{Drug}](r,t)}{\partial t} = \frac{1}{r^2}\frac{\partial}{\partial r}\left(r^2\frac{D_{\mathrm{Drug}}(r,t)}{R^2}\frac{\partial[\mathrm{Drug}](r,t)}{\partial r}\right) \tag{A.3}$$

where D_{Drug} is the effective diffusivity of the drug.

Each polymer chain has a single carboxylic acid end group that can serve as a proton donor to catalyze the polymer hydrolysis. The carboxylic acid

concentration is then

$$[\mathrm{COOH}](r,t) = \sum_{n=1}^{\infty} [\mathrm{P}_n](r,t) \tag{A.4}$$

The reaction-diffusion equation for carboxylic acid can be written in terms of the soluble polymer chain lengths that diffuse and the quadratic-order reaction using the total ester bond concentration,$[\mathrm{E}](r,t)$, which is related to the carboxyl end group concentration through $[\mathrm{E}](r,t) = [\mathrm{E}](r,0) + [\mathrm{COOH}](r,0) - [\mathrm{COOH}](r,t)$. The carboxylic acid reaction-diffusion equation is

$$\begin{aligned} \frac{\partial [\mathrm{COOH}](r,t)}{\partial t} =& \sum_{n=1}^{s} \frac{1}{r^2} \frac{\partial}{\partial r} \left(r^2 \frac{D_{\mathrm{P}_n}(r,t)}{R^2} \frac{\partial [\mathrm{P}_n](r,t)}{\partial r} \right) \\ &+ k[\mathrm{COOH}](r,t) \left([\mathrm{E}](r,0) + [\mathrm{COOH}](r,0) - [\mathrm{COOH}](r,t) \right) \end{aligned} \tag{A.5}$$

where s is the chain length of the largest oligomer that is capable of diffusing out of the microsphere. For this work, s was taken to be 9, as explained above. The distribution of large oligomers at each radial position is not needed explicitly at each time as the small oligomers depend only on the sum of the large oligomers in (A.2). To increase the computational efficiency by reducing the number of species with reaction-diffusion equations to be solved, (A.5) is used to determine $[\mathrm{COOH}](r,t)$ and (A.2) is used to determine $[\mathrm{P}_n](r,t)$ for $n \in [1,s]$. The sum of the large oligomers is updated at each radial position and time by using (A.4) to relate the concentrations of the small oligomers to the carboxylic acid concentration. The polymer degradation reaction and catalyst concentration are coupled to the diffusion of drug and small oligomers through the effective diffusivity. The functional form for the effective diffusivity for diffusing species i is

$$D_i(r,t) = D_i(r,0) + \Phi_i(r,t) \left(D_{\mathrm{H_2O},i} - D_i(r,0) \right) \tag{A.6}$$

where $D_i(r,0)$ is the effective diffusivity of the species in the bulk polymer at the initial porosity, $D_{\mathrm{H_2O},i}$ is the effective diffusivity of the species in aqueous solution,

and $\Phi_i(r,t)$ is the void fraction in the polymer. The void fraction is the ratio of the mass of soluble polymers to the mass of the entire polymer microsphere. The void fraction couples the evolution of the pore network to the effective diffusivity.

Model Summary and Solution Method

The developed model tracks the acid catalyst concentration as a function of space and time with a system of nonlinear partial differential equations while modeling acid-catalyzed degradation kinetics, molecular weight distribution variation, and drug transport with varying diffusivity coupled to the concentrations of other reacting species. The chemical reaction mechanism including autocatalytic effects is coupled to a diffusion model and pore evolution model to incorporate spatial variations in degradation rate for all species within the microspheres. The parameters used for the simulations are $[\text{COOH}](r,0) = [\text{COOH}]_0 = 0.173$ M and $[\text{Drug}](r,0) = [\text{Drug}]_0 = 3.25$ mM for $0 \leq r \leq 1$, $k = 0.001$ day$^{-1}/[\text{COOH}]_0$, and $D_i(r,0) = 10^{-14}$ cm^2/s and $D_{\text{H}_2\text{O},i} = 10^{-12}$ cm^2/s for all diffusing species i. The stiff system of ordinary differential equations resulting from the spatial discretization of the partial differential equations is solved using an implicit Runge-Kutta solver of order 5 (RADAU5 [142]) to capture an entire release profile. The simulation of the coupling between reaction and diffusion describes an interaction observed in experiments that cannot be modeled with the models in the literature that have simpler numerical solution but do not take the dynamic coupling into account. The intraparticle pH as a function of position and time is another unique contribution of this modeling effort.

A.3 Results and Discussion

The cumulative release of drug from a microsphere with a constant effective diffusivity without coupling to PLGA hydrolysis is shown in Figure A.1a. With the

time scale normalized by the time required for 90% of the total drug concentration to be released, the curves for different ratios of $D_{\text{Drug}}(r,t)/R^2$ collapse onto a single curve. Upon coupling the diffusion to the polymer hydrolysis reaction, the drug release curves no longer collapse onto a single curve and instead exhibit size-dependent behavior (see Figure A.1b). Size-dependent release profiles for PLGA microspheres, which are observed in experiments [27], cannot be described by the pure-diffusion model (Figure A.1a) but are observed in simulations that couple reaction and diffusion (Figure A.1b).

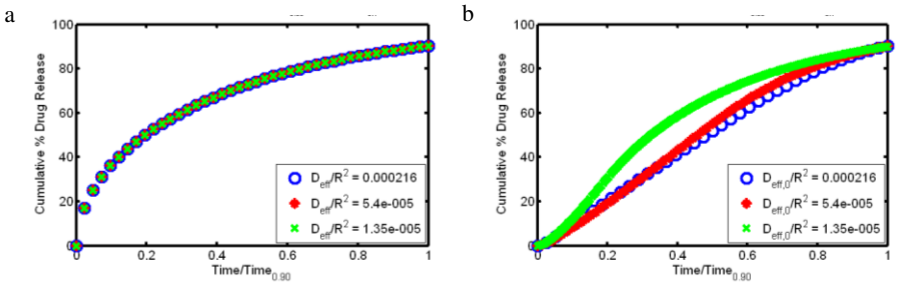

Figure A.1: Cumulative % drug release vs. time, scaled by the time required for 90% of the drug to be released, for (a) constant and (b) variable effective drug diffusivity arising from the coupling of autocatalytic polymer degradation reactions and diffusion.

The intraparticle pH is difficult to measure experimentally [149] but is a key variable in the autocatalysis reaction and is important to quantify for drug species that become biologically inactive when the local environment is sufficiently acidic. For a large microsphere, the pH can become very acidic in the microsphere, with a significantly more acidic environment in its center (see Figure A.2a). The center can become sufficiently acidic to hollow out the microsphere, to create a cavity surrounded by a highly porous polymer shell (see Figure A.2b). Such particles have been observed experimentally [18, 27, 38].

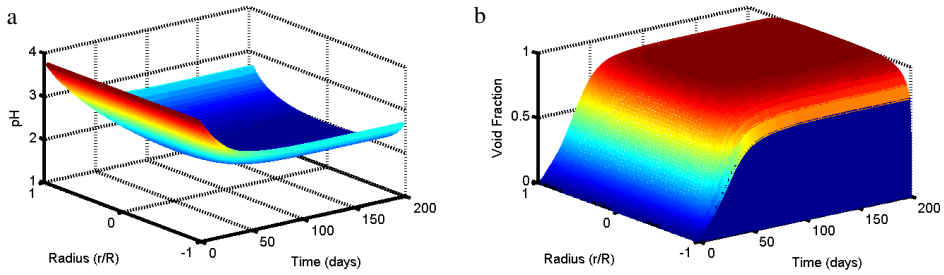

Figure A.2: Spatiotemporal profiles of (a) intraparticle pH and (b) void fraction for a multiscale model for a microsphere with initial effective drug diffusivity of $D_{\text{eff},0}/R^2 = 5.4 \times 10^{-5}$.

A.4 Conclusions

A mechanistic reaction-diffusion model with quadratic, autocatalytic hydrolysis kinetics and variable effective diffusivity to account for pore evolution has been proposed. Size-dependent cumulative drug release profiles and spatiotemporal profiles of intraparticle pH and void fraction are generated by simulations using the reaction-diffusion model. The results are consistent with experimental observations. The model is currently being extended to account for hydrophobic/hydrophilic interactions between drug molecules, polymer chains, and aqueous pores.

A.5 Acknowledgments

Support is acknowledged from the Department of Energy CSGF (Grant #DE-FG02-97ER25308), the National Institutes of Health (NIBIB 5RO1EB005181), and the National Science Foundation (Grant #0426328).

Appendix B

Fortran Code

The published ODE solver RADAU5 [142] is used to solve the system of ODEs that result when the system of PDEs for the model given in Chapter 7 is discretized in space using the methods of Chapter 8. The authors of RADAU5 have the code freely available for download from the website http://www.unige.ch/~hairer/software.html. The Fortran 77 routines *radau5.f* for the solver and *decsol.f* and *dc_decsol.f* for the linear algebra were downloaded and used without modification. The routine *driver_radau5.f* was derived from the driver files available for different example problems and was modified significantly for solving the model system of this dissertation. The routine *driver_radau5.f* and the other routines developed during this dissertation work to solve the model system of equations are given in this Appendix and are available in the supplemental files. A example script file, *kraken.deck*, used to specify parameters and to submit runs to the Kraken Cray XT5 supercomputer at the National Institute for Computational Sciences (a resource of the Extreme Science and Engineering Discovery Environment) and the *makefile* for linking and compiling the executable from the subroutines are also included in this Appendix and the supplemental files.

B.1 *driver_radau5.f*

The code used for the *driver_radau5.f* routine described in this thesis may be found in a supplemental file named driver_radau5.f.

```
C * * * * * * * * * * * * * * * * * * * * * * * * * * * * * * * * * * * * * * * * * * * * * * *
C --- Description ---
C     Main file for numerical solution of system of reaction-diffusion PDEs
C     for drug delivery from spherical polymer particles. The PDEs for the
C     concentrations of the drug, carboxylic acid end groups, ester bonds,
C     small soluble polymer oligomers, and large polymer oligomers,
C     average pore radius, and effective diffusivities of species within
C     a sphere as functions of radial position and time comprise the system
C     of PDEs. The PDEs are discretized radially to form a system of ODEs
C     solved by the numerical integrator RADAU5. The output data from
C     this main file are the simulation parameters, concentration profiles of
C     the species, the average pore radius, and the effective diffusivities
C     of the species at each radial position as functions of time for external
C     calculation of pH and cumulative drug release and visualizations.
C --- Author ---
C     Ashlee N. Ford Versypt
C     Ph.D. Dissertation 2012
C     Department of Chemical and Biomolecular Engineering
C     University of Illinois at Urbana-Champaign
C     600 S. Mathews Ave., MC-712, Urbana, IL 61801, USA
C --- Numerical Integrator Source ---
C     This file serves as the driver for the RADAU5 subroutine and its
C     subsidiary subroutines, which are used directly from the book:
C        E. Hairer and G. Wanner, Solving Ordinary Differential Equations II.
C        Stiff and Differential-Algebraic Problems. Springer Series in
C        Computational Mathematics 14, Springer-Verlag 1991,
C        Second Edition 1996.
C     The numerical integrator calculates the numerical solution of a stiff
C     (or differential algebraic) system of first order ordinary differential
C     equations M*u' = F(t,u). The system can be (linearly) implicit
C     (mass-matrix M .NE. I) or explict (M = I). The method used is an implicit
C     Runge-Kutta Method (RADAU IIA) of order 5 with step size control and
C     continuous output (Section IV.8 of the reference).
C --- Parameters ---
C  MAX_NE      Maximum dimension of the system (number of equations):
C              integer parameter declared before the initialization code
C              (intpar subroutine) is called to specify the number of
C              equations for a specific simulation.
C  MAX_NS      Maximum number of species in the system:
C              integer parameter declared before the initialization code
```

```
C               (intpar subroutine) is called to specify the number of
C               species for a specific simulation.
C  MAX_NR       Maximum number of radial discretization points:
C               integer parameter declared before the initialization code
C               (intpar subroutine) is called to specify the number of
C               radial discretizations for a specific simulation.
C  t            Time in days. Input parameter for RADAU5 subroutine:
C               Initial t-value.
C               Output parameter from RADAU5 subroutine:
C               t-value for which the solution has been computed (after
C               successful return, t=tend).
C  tend         Final t-value for call to RADAU5 subroutine
C               (tend-t may be positive or negative).
C  u(NE)        Input parameter for RADAU5 subroutine:
C               Initial values for u.
C               Output parameter from RADAU5 subroutine:
C               Numerical solution at t.
C               u(NE) is comprised of the concentrations of the species, [i],
C               the average pore radius, Rp, and the effective diffusivities of
C               the species, Deff_i. The spatial discretizations for each
C               variable are adjacent in the vector. The vector is indexed
C               as u(NR*(nn-1)+r), where r is the spatial discretization index
C               r=1:NR and nn is the index of the variables:
C               [small oligomers] 1:s (nn=1:NS-4), [E] (nn=NS-3),
C               sum [large oligomer] (nn=NS-2), [COOH] (nn=NS-1),
C               [drug] (nn=NS), Rp (nn=NS+1), Deff_i (nn=NS+1+i=NS+2:2*NS+1)
C               with i corresponding to nn for the species concentrations
C  ut(NE)       Derivative vector of u. ut(NE) is comprised of the
C               derivatives of the concentrations of the species, [i],
C               the average pore radius, Rp, and the effective diffusivities of
C               the species, Deff_i. The spatial discretizations for each
C               variable are adjacent in the vector. The vector is indexed
C               as ut(NR*(nn-1)+r) in the same manner as u(NE).
C  NE           Dimension of the ODE system (number of equations):
C               integer calculated as NE=NR*(2*NS+1) by intpar subroutine.
C  NS           Number of species: integer output parameter from intpar
C               subroutine.
C  NR           Number of radial discretization points: integer output
C               parameter from intpar subroutine.
C  NT           Number of time points including t=0. NT-1 is number of calls to
```

```
C              RADAU5 and writes to file (time output points): integer output
C              parameter from intpar subroutine.
C  h           Input parameter for RADAU5 subroutine:
C              Initial step size guess:
C              If h=0.d0, the RADAU5 code uses h=1.D-6.
C              Output parameter from RADAU5 subroutine:
C              Predicted step size of the last accepted step.
C  RPAR, IPAR  Double precision and integer parameter arrays which are used
C              to communicate parameter values between the main file and
C              the Fderiv subroutine through RADAU5.
C  intpar      Name (external) of subroutine that reads a script file with
C              input parameters for the physical properties and simulation
C              options and calculates other parameter initial values:
C  Fderiv      Name (external) of subroutine that computes the value of F(t,u),
C              the ODE function of u
C  Jderiv      Name (external) of subroutine that computes the partial
C              derivatives of F(t,u) with respect to u:
C              this routine is only called if IJAC=1; supply a dummy routine
C              in the case IJAC=0.
C  LWORK       Length of array WORK for RADAU5 subroutine:
C              declared as a parameter.
C  WORK        Array of working space of length LWORK for RADAU5 subroutine:
C              WORK(1), WORK(2),..., WORK(20) serve as as parameters for the
C              RADAU5 subroutine code. For standard use of the code,
C              WORK(1),...,WORK(20) must be set to zero before calling.
C              Full details of the more sophisticated use of WORK are
C              available in the RADAU5 source. WORK(21),...,WORK(LWORK)
C              serve as worksing space for all vectors and matrices.
C              In the usual case (used here) where the Jacobian is full
C              and the mass-matrix is the identity matrix (IMAX=0),
C              the minimum storage requirement is LWORK=4*NE*NE+12*NE+20.
C  LIWORK      Length of array IWORK for RADAU5 subroutine:
C              declared as a parameter.
C  IWORK       Integer working space of length LIWORK for RADAU5 subroutine:
C              IWORK(1),IWORK(2),...,IWORK(20) serve as parameters for the
C              RADAU5 subroutine code. For standard use of the code,
C              IWORK(1),.., IWORK(20) must be set to zero before calling.
C              Full details of the more sophisticated use of IWORK are
C              available in the RADAU5 source code.
C              IWORK(21),...,IWORK(LIWORK) serve as working area.
```

```
C               LIWORK must be at least 3*NE+20.
C  IWORK(14)    NFCN output parameter from RADAU5 subroutine:
C               number of function evaluations (those for numerical
C               evaluation of the Jacobian are not counted).
C  IWORK(15)    NJAC output parameter from RADAU5 subroutine:
C               number of Jacobian evaluations (either analytically
C               or numerically).
C  IWORK(16)    NSTEP output parameter from RADAU5 subroutine:
C               number of computed steps.
C  IWORK(17)    NACCPT output parameter from RADAU5 subroutine:
C               number of accepted steps.
C  IWORK(18)    NREJCT output parameter from RADAU5 subroutine:
C               number of rejected steps (due to error test; step rejections
C               in the first step are not counted).
C  IWORK(19)    NDEC output parameter from RADAU5 subroutine:
C               number of LU-decompositions of both matrices.
C  IWORK(20)    NSOL output parameter from RADAU5 subroutine:
C               number of forward-backward substitutions of both systems;
C               the NSTEP forward-backward substitutions, needed for step
C               size selection, are not counted.
C  IJAC         Switch for the computation of the Jacobian for RADAU5 subroutine:
C               IJAC=0: Jacobian is computed internally by finite
C               differences; the subroutine Jderiv is never called,
C               IJAC=1: Jacobian is supplied by subroutine Jderiv.
C  MLJAC        Switch for the banded structure of the Jacobian:
C               MLJAC=NE: Jacobian is a full matrix. The linear
C               algebra is done by full-matrix Gauss-elimination.
C               0<=MLJAC<NE: MLJAC is the lower bandwith of Jacobian
C               matrix (>= number of non-zero diagonals below
C               the main diagonal).
C  MUJAC        Upper bandwidth of Jacobian matrix (>= number of non-zero
C               diagonals above the main diagonal).
C               Need not be defined if MLJAC=NE.
C  MAS          Name (external) of subroutine computing the mass-matrix M.
C               If IMAS=0, this matrix is assumed to be the identity
C               matrix and needs not to be defined.
C  IMAS         Gives information on the mass-matrix:
C               IMAS=0: M is supposed to be the identity
C               matrix, MAS is never called.
C               IMAS=1: Mass-matrix is supplied.
```

```
C  MLMAS       Switch for the banded structure of the mass-matrix:
C              MLMAS=NE: the full matrix case. The linear
C              algebra is done by full-matrix Gauss-elimination.
C              0<=MLMAS<NE: MLMAS is the lower bandwidth of the
C              matrix (>= number of non-zero diagonals below
C              the main diagonal).
C              MLMAS is supposed to be .LE. MLJAC.
C  MUMAS       Upper bandwidth of mass-matrix (>= number of non-
C              zero diagonals above the main diagonal).
C              Need not be defined if MLMAS=NE.
C              MUMAS is supposed to be .LE. MUJAC.
C  SOLOUT      Name (external) of subroutine providing the
C              numerical solution during integration.
C              If IOUT=1, it is called after every successful step.
C              Supply a dummy subroutine is IOUT=0. Instead of using
C              SOLOUT, output is written after each call to RADAU5 rather
C              than each successful step.
C  IOUT        Switch for calling the subroutine SOLOUT:
C              IOUT=0: subroutine is never called,
C              IOUT=1: subroutine is available for output.
C  RTOL, ATOL  Relative and absolute error tolerances for RADAU5 subroutine:
C              both can be scalars or else both vectors of length NE.
C  TOL         Specified TOL=RTOL=ATOL: output parameter from
C              intpar subroutine.
C  ITOL        Switch for RTOL and ATOL for RADAU5 subroutine:
C              ITOL=0: both RTOL and ATOL are scalars. The code keeps, roughly,
C              the local error of u(i) below RTOL*ABS(u(i))+ATOL,
C              ITOL=1: both RTOL and ATOL are vectors. The code keeps the local
C              error of u(i) below RTOL(i)*ABS(u(i))+ATOL(i).
C  IDID        Reports on successfulness upon return from RADAU5 subroutine:
C              IDID= 1: computation successful,
C              IDID= 2: computation successful (interrupted by SOLOUT)
C              IDID=-1: input is not consistent,
C              IDID=-2: larger NMAX is needed,
C              IDID=-3: step size becomes too small,
C              IDID=-4: matrix is repeatedly singular.
C * * * * * * * * * * * * * * * * * * * * * * * * * * * * * * * * * * * * * *
      implicit double precision (A-H,O-Z)
C --- Parameters for system size initialization ---
      integer MAX_NE, MAX_NS,MAX_NR
```

```
      parameter (MAX_NE=5427,MAX_NS=13,MAX_NR=201)
C --- Parameters for RADAU5 ---
      parameter (LWORK=4*MAX_NE*MAX_NE+12*MAX_NE+20,LIWORK=3*MAX_NE+20)
      dimension WORK(LWORK),IWORK(LIWORK),ISTAT(20)
C --- Arrays and other variables ---
      integer IPAR(2),NE,NR,NS,NT,tt,ii,ee,ss
      integer out,restart,diffn_on,rxn_on
      double precision RPAR(MAX_NS+7),t,u(MAX_NE),tend,tp,h,Ri(MAX_NS)
      double precision dr,R,t0,tf,tfinal,k,Xrxn
      double precision COOH0,E0,drug0,Rp0,Rd,lave,G,beta
      double precision tau,alphaH,alphaD,DH,DD,TOL
      common/param/NS,NR
C --- Array for DTIME function ---
      real*4 TARRAY(2)
C --- External subroutines ---
      external intpar,initial,Fderiv,Jderiv,SOLOUT
C --- Initialization of tokens, constants, and parameters ---
      call intpar(NE,NR,NS,NT,restart,diffn_on,rxn_on,
     &    dr,R,t0,tf,tfinal,k,Xrxn,COOH0,E0,drug0,Rp0,Rd,lave,G,beta,
     &    tau,alphaH,alphaD,DH,DD,alpha0H,alpha0D,TOL)
C --- Open output file ---
      out = 12
      if (restart.eq.0) then
         open(out,file='simulation.out')
      elseif (restart.ge.1) then
         open(out,file='simulation_restart.out')
      endif
C --- Write parameters to simulation output file ---
      write(out,50) NR,NS,NT,NE,R,k,
     &    DH,DD,COOH0,rxn_on,diffn_on,E0,Xrxn,tau
50    format(i3,/,i2,/,i4,/,i5,/,d24.17,/,d24.17,/,d24.17,/,d24.17,
     &    /,d24.17,/,i1,/,i1,/,d24.17,/,d24.17,/,d24.17)
C --- Initial and boundary conditions ---
      call initial(restart,NR,NS,NE,NT,E0,COOH0,drug0,Rp0,
     &    Rd,lave,alphaD,alphaH,alpha0H,alpha0D,t0,tf,
     &    tfinal,Ri(1:NS),u(1:NE))
C --- Allocation of parameter values to IPAR and RPAR for passing to Fderiv
C     subroutine through RADAU5 ---
      IPAR(1) = diffn_on
      IPAR(2) = rxn_on
```

```
      RPAR(1) = dr
      RPAR(2) = k
      RPAR(3) = E0
      RPAR(4) = G
      RPAR(5) = beta
      RPAR(6) = alphaH
      RPAR(7) = alphaD
      RPAR(8:(NS+7)) = Ri(1:NS)
C --- Output time for calls to integrator ---
      tp = tf
      write(*,*) 'tp = ', tp
      t = t0
      tend = tp+t
      write(*,*) 'tend = ', tend
C --- Write initial time and ODE vector to simulation output file ---
      write(out,20) t
 20   format(d24.17)
      do 30 ee = 1,NE
         write(out,22) u(ee)
 22      format(d24.17)
 30   continue
      close(out)
C --- Compute the Jacobian analytically (1) or numerically (0) ---
      IJAC = 0
C --- Jacobian is full ---
      MLJAC = NE
C --- Differential equation is in explicit form ---
      IMAS = 0
C --- Output routine is (1) or is not (0) used during integration ---
      IOUT = 0
C --- Error tolerances ---
      RTOL = TOL
      ATOL = RTOL
      ITOL = 0
C --- Initial step size ---
      h = 1.0d-6
C --- Call of the subroutine RADAU5 ---
C --- Set default RADAU5 parameter values ---
      do I = 1,20
         WORK(I) = 0.d0
```

```
            IWORK(I) = 0
            ISTAT(I) = 0
         end do
C --- Loop over NT ---
         do tt = 1,NT-1
            call DTIME(TARRAY)
            call RADAU5(NE, Fderiv, t, u, tend, h,
     &              RTOL,ATOL,ITOL,
     &               Jderiv, IJAC, MLJAC, MUJAC,
     &               Fderiv, IMAS, MLMAS, MUMAS,
     &               SOLOUT, IOUT,
     &               WORK,LWORK,IWORK,LIWORK,RPAR,IPAR, IDID)
C --- Print statistics ---
            do J = 14,20
               ISTAT(J) = ISTAT(J)+IWORK(J)
            end do
            write(6,*)' ***** TOL=',RTOL,'  ELAPSED TIME=',TARRAY(1),' ****'
            write (6,91) (ISTAT(J),J=14,20)
 91         format(' fcn=',I10,' jac=',I10,' step=',I10,
     &       ' accpt=',I10,' rejct=',I10,' dec=',I10,
     &       ' sol=',I10)
            write(*,*) 'current h = ',h
            write(*,*) 'IDID = ', IDID
C --- Print solution ---
            call DTIME(TARRAY)
C --- Write time and ODE vector to simulation output file ---
            if (restart.eq.0) then
               open(out,file='simulation.out',access='append',status='old')
            elseif (restart.ge.1) then
               open(out,file='simulation_restart.out',access='append',
     &            status='old')
            endif
            write(out,23) tend
 23         format(d24.17)
            do 31 ee = 1,NE
               write(out,24) u(ee)
 24            format(d24.17)
 31         continue
C --- Close simulation output file to ensure that full output is saved
C      at the end of each call to RADAU5---
```

```
         close(out)
C --- Advance solution ---
         t = tend
         tend = tend+tp
C --- To next output ---
      enddo
C --- Write final totals for statistics ---
      write(*,*) 'total fcn', ISTAT(14)
      write(*,*) 'total jac', ISTAT(15)
      write(*,*) 'total steps', ISTAT(16)
      write(*,*) 'total accpt', ISTAT(17)
      write(*,*) 'total rejct', ISTAT(18)
      write(*,*) 'total dec', ISTAT(19)
      write(*,*) 'total sol', ISTAT(20)
      write(*,*) 'final h',h
C --- End of driver_radau5.f ---
   end
C
   subroutine SOLOUT (nr,XOLD,t,u,CONT,LRC,NE,RPAR,IPAR,IRTRN)
C --- Required by RADAU5, but not used here as output is written after each
C     call to RADAU5 instead of each successful step---
      implicit real*8 (A-H,O-Z)
      dimension u(NE),CONT(LRC)
C --- dummy routine ---
   return
   end
```

B.2 *intpar.f*

The code used for the *intpar.f* routine described in this thesis may be found in a supplemental file named intpar.f.

```
C * * * * * * * * * * * * * * * * * * * * * * * * * * * * * * * * * * * * * * * * * * * *
C --- Description ---
C     Reads input tokens and parameters from command line or the script file
C     kraken.deck. Calculates constant quantities.
C --- Output ---
C  NE        integer  Number of first order ODEs
C  NR        integer  Number of spatial discretizations
```

```
C  NS        integer  Number of species
C  NT        integer  Number of time points including t=0 for output; NT-1 is
C                     number of calls to RADAU5
C  restart   integer  0 to start from t=0, 1 to finish an incomplete run, and
C                     2 to refine an interval
C  diffn_on  integer  0 for diffn off, 1 for constD, 2 for drug varD,
C                     3 for all species varD
C  rxn_on    integer  0 for rxn off, 1 for uncat, 2 for pseudo,
C                     3 for quad, 4 for half
C  dr        double   Spatial discretization size
C  R         double   Particle radius
C  t0        double   Initial time with restart=0
C  tf        double   Elapsed time for each call to RADAU5 with restart=0
C  tfinal    double   Final simulation time after NT-1 calls to RADAU5
C  k         double   Reaction rate constant
C  Xrxn      double   Extent of reaction
C  COOH0     double   Initial COOH concentration
C  E0        double   Initial E concentration
C  drug0     double   Initial drug concentration
C  Rp0       double   Initial pore radius
C  Rd        double   Stokes-Einstein radius of drug
C  lave      double   Average monomer length in Angstroms
C  G         double   Glycolic acid fraction of the polymer
C  beta      double   Constant prefactor for pore radius calculation
C  tau       double   Tortuosity
C  alphaD    double   D_{\infty}/R^2/tau for the drug
C  alphaH    double   D_{\infty}/R^2/tau for the soluble oligomers
C  DH        double   D_{\infty}/tau of the monomers in cm^2/day
C  DD        double   D_{\infty}/tau of the drug in cm^2/day
C  alpha0H   double   D_bulk/R^2 for the drug
C  alpha0D   double   D_bulk/R^2 for the soluble oligomers
C  TOL       double   Error tolerance TOL=RTOL=ATOL
C * * * * * * * * * * * * * * * * * * * * * * * * * * * * * * * * * * * * * * *
      subroutine intpar(NE,NR,NS,NT,restart,diffn_on,rxn_on,
     &    dr,R,t0,tf,tfinal,k,Xrxn,COOH0,E0,drug0,Rp0,Rd,lave,G,beta,
     &    tau,alphaH,alphaD,DH,DD,alpha0H,alpha0D,TOL)
        implicit none
C --- Parameters ---
        integer NE,NR,NS,NT
        integer restart,diffn_on,rxn_on,kscale_on
```

```
      double precision dr,R,t0,tf,tfinal,k,Xrxn
      double precision COOH0,E0,drug0,Rp0,Rd,lave,G,beta
      double precision tau,alphaH,alphaD,DH,DD,alpha0H,alpha0D,TOL
      double precision PDI,Mw,Mn,M0,EoverCOOH
      double precision tfinal_rxn,tfinal_diffn
      double precision tfinal_override,k_unscaled,Psi
      double precision mw_glycolide,mw_lactide,pKa,Ka,a,b,c,DH0,DD0
      double precision l_lactide,l_glycolide,T,pi,mu,kB,trxn
C --- Read values from input stream ---
C --- Tokens for simulation options ---
      print*, 'Enter 0 to start from t=0, 1 to finish an incomplete run, and
     &     2 to refine an interval:'
      read*, restart
      print*, 'Enter 0 no diffn, 1 constD, 2 drug varD, 3 drug & olig varD:'
      read*, diffn_on
      print*, 'Enter 0 rxn off, 1 uncat, 2 pseudo, 3 quad, 4 half:'
      read*, rxn_on
      print*, 'Enter 0 k given, 1 scale to find ku and kc:'
      read*, kscale_on
C --- Number of spatial discretization points ---
      print*, 'Enter number of spatial discretizations:'
      read*, NR
      dr = (1.0d0)/dfloat(NR-1)
C --- Number of species: s+4 ---
      print*, 'Enter number of species:'
      read*, NS
C --- Number of equations: each variable has NR spatial discretizations
C     and the variables are species concentrations (1:NS), average pore
C     radius (NS+1), and species effective diffusivities (NS+2:2*NS+1) ---
      NE = NR*(2*NS+1)
C --- Microsphere radius ---
      print*, 'Enter radius in cm:'
      read*, R
C --- Tortuosity ---
      print*, 'Enter tortuosity:'
      read*, tau
C --- Diffusivity at infinite dilution ---
      print*, 'Enter diffusivity at inf. dilution of the drug in cm^2/s:'
      read*, DD
      print*, 'Enter diffusivity at inf. dilution of the oligomers in cm^2/s:'
```

```
      read*, DH
C --- Temperature ---
      T = 310.0d0
      pi = 3.14159265358979324D0
      kB = 1.3806503d-23
C --- Viscosity of water (kg/m/s) at 37C interpolated from values at 35 & 40C
      mu = (719.1d0+(652.71d0-719.1d0)*(37.0d0-35.0d0)/(40.0d0-35.0d0))
     &    *1.0d-6
C --- Stokes-Einstein drug radius ---
      Rd = (kB)*T/(6.0d0*pi*mu*DD*1.0d-14)
C --- Convert to cm^2/day hindered by tortuosity ---
      DD = DD*3600.0d0*24.0d0/tau
      DH = DH*3600.0d0*24.0d0/tau
C --- Rate constant for hydrolysis reaction ---
      print*, 'Enter hydrolysis rate constant with time units of day^-1:'
      read*, k_unscaled
C --- Polymer molecular weight ---
      print*, 'Enter polydispersity index:'
      read*, PDI
      print*, 'Enter M_w wt-avg molecular weight of the polymer:'
      read*, Mw
C --- Number avg molecular weight of polymer ---
      Mn = Mw/PDI
C --- Polymer drug loading information ---
      print*, 'Enter dimensionless initial drug concentration:'
      read*, drug0
C --- Scaled drug concentration ---
      print*, 'Enter dimensionless initial COOH concentration:'
      read*, COOH0
C --- Extent of hydrolysis reaction in reaction-dominant limit ---
      print*, 'Enter extent of reaction:'
      read*, Xrxn
C --- Number of calls to the ODE solver and time output points ---
      print*, 'Enter desired number of output points including t=0:'
      read*, NT
C --- Initial pore radius ---
      print*, 'Enter initial pore radius in Angstroms:'
      read*, Rp0
C --- Optional tfinal override ---
      print*, 'Enter optional tfinal override time in days (0.0=>off):'
```

```
      read*, tfinal_override
C --- Glycolic acid content ---
      print*, 'Enter glycolic acid fraction of the polymer: '
      read*, G
      if (rxn_on.eq.4) then
         pKa = (1.0d0-G)*3.86d0+G*3.83d0
         Ka = 10.0d0**(-pKa)
         write(*,*) 'Ka', Ka
      endif
C --- Error tolerances ---
      print*, 'Enter error tolerance TOL=RTOL=ATOL: '
      read*, TOL
C --- Average monomer molecular weight ---
      mw_lactide = 72.06266d0
      mw_glycolide = 58.03608d0
      M0 = (1.0d0-G)*mw_lactide+G*mw_glycolide
C --- Average monomer length in Angstroms ---
      l_lactide = 3.517d0
      l_glycolide = 3.510d0
      lave = (1.0d0-G)*l_lactide+G*l_glycolide
C --- E0/COOH0 ---
      EoverCOOH = Mn/M0-1.0d0
      E0 = EoverCOOH*COOH0
C --- Constant prefactor for rate of pore growth ---
      beta = lave*dfloat(NS-3)*dfloat(NS-3+1)/2.0d0/(E0+COOH0)
C --- Units of k--uncat: 1/time; pseudo: 1/time; quad: 1/time/conc;
C     half: 1/time/conc^0.5 ---
      if (kscale_on.eq.0) then
C --- Assume the given rate constant is k for the specified kinetic case ---
         k = k_unscaled
C --- If kscale_on.gt.0, assume given k=k1'. Scale rate constant based on
C     RvCOOH(0) equal and find ku and kc for dimensionless conservation
C     equation when kscale_on.eq.1. ---
      elseif (kscale_on.eq.1) then
         if (rxn_on.eq.1) then
            k = k_unscaled/EoverCOOH
         elseif (rxn_on.eq.2) then
            k = k_unscaled
         elseif (rxn_on.eq.3) then
            k = k_unscaled/EoverCOOH
```

```
         elseif (rxn_on.eq.4) then
            k = k_unscaled/dsqrt(COOH0)/EoverCOOH
         endif
      endif
C --- Calculate D\infty/R^2/tau (day^-1) ---
      alphaH = DH/(R*R)
      alphaD = DD/(R*R)
      write(*,*) 'alphaH = ', alphaH
      write(*,*) 'alphaD = ', alphaD
      write(*,*) 'DH = ', DH
C --- Diffusivity through bulk dense polymer ---
      print*, 'Enter diffusivity of the drug in cm^2/s in the
     &   dense polymer:'
      read*, DD0
      print*, 'Enter diffusivity of the oligomers in cm^2/s in the
     &   dense polymer:'
      read*, DH0
C --- Calculate D_bulk/R^2 (day^-1) ---
      alpha0H = DH0*3600.0d0*24.0d0/(R*R)
      alpha0D = DD0*3600.0d0*24.0d0/(R*R)
C --- Calculate the tfinal needed by the simulation ---
C --- Initialize all tfinal to zero ---
      tfinal_diffn = 0.0d0
      tfinal_rxn = 0.0d0
C --- tfinal=tfinal_diffn=diffn time constant if rxn_on=0; for rxn_on.gt.0,
C     tfinal=tfinal_rxn=time required for Xrxn extent of reaction ---
C --- Diffusion contribution: tfinal_diffn is R^2/D for the smaller non-zero D
C --- In diffusion-dominant limit, drug is only diffusing species since
C     no small oligomers are generated ---
      if (diffn_on.gt.0) then
         tfinal_diffn = R*R/DD
         if ((rxn_on.gt.0).and.(DH.gt.0).and.(DH.lt.DD)) then
            tfinal_diffn = R*R/DH
         endif
      endif
      write(*,*) 'tfinal_diffn = ', tfinal_diffn
C --- Reaction contribution: each hydrolysis case has a different
C     tfinal_rxn=t_{Xrxn} ---
      if (rxn_on.eq.1) then
         tfinal_rxn = -dlog(1.0d0-Xrxn)/k
```

```
      elseif (rxn_on.eq.2) then
         tfinal_rxn = dlog(1.0d0+Xrxn*EoverCOOH)/k
      elseif (rxn_on.eq.3) then
         tfinal_rxn = 1.0d0/k/(E0+COOH0)*
     &       dlog((EoverCOOH*Xrxn+1.0d0)/(1.0d0-Xrxn))
      elseif (rxn_on.eq.4) then
         a = (EoverCOOH+1.0d0)
         b = 1.0d0+EoverCOOH*Xrxn
         c = (dsqrt(a)+1.0d0)/(dsqrt(a)-1.0d0)
         tfinal_rxn = 1.0d0/k/dsqrt(a*Ka)*
     &       dlog((dsqrt(a)+dsqrt(b))/((dsqrt(a)-dsqrt(b))*c))
      endif
      write(*,*) 'tfinal_rxn = ', tfinal_rxn
      if (rxn_on.eq.0) then
C --- Diffusion-dominant limit ---
         tfinal = tfinal_diffn
      else
C --- With reaction and diffusion, the simulation time of interest occurs
C     while the polymer is still reacting ---
         tfinal = tfinal_rxn
      endif
C --- Limiting tfinal for desired maximum duration ---
      if (tfinal_override.gt.0.0d0) then
         tfinal = tfinal_override
      endif
      write(*,*) 'tfinal = ', tfinal
C --- Initial, final values of time in the first call to the integrator ---
      t0 = 0.0d0
      tf = tfinal/dfloat(NT-1)
      write(*,*) 'tf = ', tf
C --- End of intpar.f ---
   return
   end
```

B.3 *initial.f*

The code used for the *initial.f* routine described in this thesis may be found in a supplemental file named initial.f.

```
C * * * * * * * * * * * * * * * * * * * * * * * * * * * * * * * * * * * * * * * * * * * * * * *
C --- Description ---
C     Sets the initial conditions for u(NE) and species radius Ri(NS).
C --- Input ---
C  restart  integer  0 to start from t=0, 1 to finish an incomplete run, and
C                    2 to refine an interval
C  NR       integer  Number of spatial discretizations
C  NS       integer  Number of species
C  NE       integer  Number of first order ODEs
C  NT       integer  Number of time points including t=0 for output with
C                    restart=0; NT-1 is number of calls to RADAU5
C  E0       double   Initial E concentration
C  COOH0    double   Initial COOH concentration
C  drug0    double   Initial drug concentration
C  Rp0      double   Initial pore radius
C  Rd       double   Stokes-Einstein radius of drug
C  lave     double   Average monomer length in Angstroms
C  alphaD   double   D_{\infty}/R^2/tau for the drug
C  alphaH   double   D_{\infty}/R^2/tau for the soluble oligomers
C  alpha0H  double   D_bulk/R^2 for the drug
C  alpha0D  double   D_bulk/R^2 for the soluble oligomers
C  t0       double   Initial time with restart=0
C  tf       double   Elapsed time for each call to RADAU5 with restart=0
C  tfinal   double   Final simulation time after NT-1 calls to RADAU5
C --- Output ---
C  Ri(NS)   double   Radius of each species
C  u0(NE)   double   ODE solution vector initial condition
C  t0       double   Initial time with updated with restart.ge.1
C  NT       integer  Number of time points including t=0 for output with
C                    restart=1; NT-1 is number of calls to RADAU5
C  tf       double   Elapsed time for each call to RADAU5 upated with
C                    restart=2
C * * * * * * * * * * * * * * * * * * * * * * * * * * * * * * * * * * * * * * * * * * * * * * *
      subroutine initial(restart,NR,NS,NE,NT,E0,COOH0,drug0,Rp0,
     &    Rd,lave,alphaD,alphaH,alpha0H,alpha0D,t0,tf,tfinal,Ri,u0)
        implicit none
C --- Parameters ---
        integer NR,NS,NE,NT,nn,rr,ss,restart,ee
        double precision u0(NE),E0,COOH0,drug0,Rp0,Rd,lave,Ri(NS),lambda
        double precision alphaH,alphaD,H,pi,num,denom,t0,tf,tfinal
```

```
      double precision alpha0H,alpha0D
      pi = 3.14159265358979324D0
C --- Species radius ---
C --- Small oligomers ---
         do nn = 1,NS-4
            Ri(nn) = dfloat(nn)*lave
         enddo
C --- Ester bonds and large oligomers and COOH ---
         do nn = NS-3,NS-1
            Ri(nn) = 0.0d0
         enddo
C --- Drug ---
         nn = NS
            Ri(nn) = Rd
C --- When restart.eq.0, assume that the initial conditions and
C     simulation time are determined using parameters from intpar.f ---
      if (restart.eq.0) then
C --- Initial conditions ---
         do rr = 1,NR-1
C --- Small oligomers ---
            do nn = 1, NS-4
               u0(NR*(nn-1)+rr) = 0.0d0
            enddo
C --- Ester bonds ---
            nn = NS-3
               u0(NR*(nn-1)+rr) = E0
C --- Large oligomer sum and COOH ---
            nn = NS-2
               u0(NR*(nn-1)+rr) = COOH0
            nn = NS-1
               u0(NR*(nn-1)+rr) = COOH0
C --- Drug ---
            nn = NS
               u0(NR*(nn-1)+rr) = drug0
C --- Rp ---
            nn = NS+1
               u0(NR*(nn-1)+rr) = Rp0
C --- Deff ---
            do ss = 1,NS
               nn = NS+1+ss
```

```
C ---- Lambda(r)=Ri/Rp for each species ----
                lambda = Ri(ss)/u0(NR*(NS+1-1)+rr)
                H = 0.0d0
                if (lambda.le.1) then
                   if (lambda.gt.0) then
C ---- Calculate hindrance factor ----
                      num = 6.0d0*pi*(1.0d0-lambda)**2.0d0
                      denom = 2.25d0*pi**2.0d0*dsqrt(2.0d0)
     &                    *(1.0d0-lambda)**(-2.5d0)*(1.0d0-73.0d0/60.0d0
     &                    *(1.0d0-lambda)+77293.0d0/50400.0d0
     &                    *(1.0d0-lambda)**2.0d0)-22.5083d0-5.6117d0*lambda
     &                    -0.3363d0*lambda**2.0d0-1.216d0*lambda**3.0d0
     &                    +1.647d0*lambda**4.0d0
                      H = num/denom
                   endif
                endif
C ---- Calculate effective diffusivities ----
                if (ss.lt.NS-2) then
                   u0(NR*(nn-1)+rr) = alphaH*H+alpha0H
                endif
                if ((ss.eq.(NS-2)).or.(ss.eq.(NS-1))) then
                   u0(NR*(nn-1)+rr) = 0.0d0
                endif
                if (ss.eq.NS) then
                   u0(NR*(nn-1)+rr) = alphaD*H+alpha0D
                endif
             enddo
          end do
C ---- When restart.ge.1, assume that the initial conditions is given by
C      restart_data.dat and the simulation time should be determined here ---
          else
C ---- Read restart data for initial time t0 and ODE vector u0(NE) ----
          open(9,file='restart_data.dat')
C ---- Initial time ---
          read(9,*) t0
          write(*,*) 't0_restart = ', t0
C ---- Initial & boundary conditions from restart_data.dat ----
          do ee = 1,NE
             read(9,*) u0(ee)
          enddo
```

```
C --- Simulation time calculations ---
         write(*,*) 'tfinal_restart = ', tfinal
C --- Restart the simulation from t0 with the remaining function calls from the
C     original NT with the same tfinal and tf ---
         if (restart.eq.1) then
            write(*,*) 'tf_restart = ', tf
            NT = int((tfinal-t0)/tf)+1
            write(*,*) 'NT_restart = ', NT
C --- Restart the simulation from t0 to tfinal with NT function calls and
C     updated tf ---
         elseif (restart.eq.2) then
            write(*,*) 'NT_restart = ', NT
            tf = (tfinal-t0)/dfloat(NT-1)
            write(*,*) 'tf_restart = ', tf
         endif
      endif
C --- Boundary condition at r=1 ---
      do nn = 1,2*NS+1
         u0(NR*(nn-1)+NR) = 0.0d0
      enddo
C --- End of initial.f ---
   return
   end
```

B.4 *Jderiv.f*

The code used for the *Jderiv.f* routine described in this thesis may be found in a supplemental file named Jderiv.f.

```
C * * * * * * * * * * * * * * * * * * * * * * * * * * * * * * * * * * * * * * * * * * * *
C --- Description ---
C     Dummy routine for computation of the Jacobian matrix.
C --- Input ---
C  NE        integer  Number of first order ODEs
C  t         double   Time
C  u(NE)     double   ODE solution vector
C  DFU(i,j)  double    Partial ut(i) / partial u(j) where ut is the
C                      derivative vector
C  LDFU      double   Column-length of the array
```

```
C ---- Output ----
C  This routine is never called as IJAC=0 in driver_radau5.f
C * * * * * * * * * * * * * * * * * * * * * * * * * * * * * * * * * * * * * * * * * *
      subroutine Jderiv(NE,t,u,DFU,LDFU,RPAR,IPAR)
         implicit none
C ---- Parameters ----
      integer NE,LDFU,IPAR(2)
      double precision t,u(NE),DFU(LDFU,NE)
      double precision RPAR(13+12)
C ---- dummy routine ----
C ---- End of Jderiv.f ----
      return
      end
```

B.5 *Fderiv.f*

The code used for the *Fderiv.f* routine described in this thesis may be found in a supplemental file named Fderiv.f.

```
C * * * * * * * * * * * * * * * * * * * * * * * * * * * * * * * * * * * * * * * * * *
C ---- Description ----
C     Passes the IPAR and RPAR parameters to deriv.f for computing the
C     derivative vector ut with reaction, diffusion, pore growth,
C     and effective diffusivity growth.
C ---- Input ----
C  NE        integer  Number of first order ODEs
C  t         double   Time
C  u(NE)     double   ODE solution vector
C  ut(NE)    double   ODE derivative vector
C  RPAR, IPAR         Double precision and integer parameter arrays which are
C                     used tocommunicate parameter values between main file
C                     driver_radau5.f and the Fderiv subroutine through RADAU5
C ---- Output ----
C  ut(NE)    double   ODE derivative vector updated
C * * * * * * * * * * * * * * * * * * * * * * * * * * * * * * * * * * * * * * * * * *
      subroutine Fderiv(NE,t,u,ut,RPAR,IPAR)
         implicit none
C ---- Parameters ----
         integer NE,NR,NS,rxn_on,diffn_on,IPAR(2)
```

```
      double precision t,u(NE),ut(NE),dr,k
      double precision COOH0,E0,drug0,G,beta,Ri(NS)
      double precision alphaH,alphaD,RPAR(NS+8)
      common/param/NS,NR
C --- Parameter values ---
      diffn_on = IPAR(1)
      rxn_on = IPAR(2)
      dr = RPAR(1)
      k = RPAR(2)
      E0 = RPAR(3)
      G = RPAR(4)
      beta = RPAR(5)
      alphaH= RPAR(6)
      alphaD = RPAR(7)
      Ri(1:NS) = RPAR(8:(NS+7))
C --- Pass parameter values to deriv.f ---
      call deriv(NE,NR,NS,u,ut,diffn_on,rxn_on,
     &    dr,k,E0,G,beta,alphaH,alphaD,Ri)
C --- End of Fderiv.f ---
    return
    end
```

B.6 *deriv.f*

The code used for the *deriv.f* routine described in this thesis may be found in a supplemental file named deriv.f.

```
C * * * * * * * * * * * * * * * * * * * * * * * * * * * * * * * * * * * * * * * * * * * *
C --- Description ---
C     Computes the derivative vector ut with reaction, diffusion,
C     pore growth, and effective diffusivity growth.
C --- Input ---
C  NE        integer  Number of first order ODEs
C  NR        integer  Number of spatial discretizations
C  NS        integer  Number of species
C  u(NE)     double   ODE solution vector
C  ut(NE)    double   ODE derivative vector
C  diffn_on  integer  0 for diffn off, 1 for constD, 2 for drug varD,
C                     3 for all species varD
```

```
C  rxn_on    integer  0 for rxn off, 1 for uncat, 2 for pseudo,
C                     3 for quad, 4 for half
C  dr        double   Spatial discretization size
C  k         double   Reaction rate constant
C  E0        double   Initial E concentration
C  G         double   Glycolic acid fraction of the polymer
C  beta      double   Constant prefactor for pore radius calculation
C  alphaD    double   D_{\infty}/R^2/tau for the drug
C  alphaH    double   D_{\infty}/R^2/tau for the soluble oligomers
C  Ri(NS)    double   Radius of each species
C --- Output ---
C  ut(NE)    double   ODE derivative vector updated
C * * * * * * * * * * * * * * * * * * * * * * * * * * * * * * * * * * * * * * * *
      subroutine deriv(NE,NR,NS,u,ut,diffn_on,rxn_on,
     &    dr,k,E0,G,beta,alphaH,alphaD,Ri)
        implicit none
C --- Parameters ---
        integer NE,NR,NS,rr,ss,nn,diffn_on,rxn_on
        double precision u(NE),ut(NE),dr,k,E0,G,beta
        double precision alphaH,alphaD,Ri(NS)
C --- Compute derivative ut ---
C --- Initialize all ut to zero ---
        do nn = 1,2*NS+1
           do rr = 1,NR
              ut(NR*(nn-1)+rr) = 0.0d0
           enddo
        enddo
C --- Hydrolysis reaction ---
C --- Call rxn for small oligomers and drug, update ester and COOH with
C     reaction contributions ---
        if (rxn_on.gt.0) then
           call rxn(NE,NR,NS,u,ut,k,E0,alphaH,alphaD,
     &    G,beta,Ri,rxn_on)
        endif
C --- Maintain BC constant at r=1 ---
        do nn = 1,2*NS+1
           ut(NR*(nn-1)+NR) = 0.0d0
        enddo
C --- Diffusion ---
C --- Call diffn for updating small oligomers, drug, ester, and COOH with
```

```
C      diffusion contributions ---
       if (diffn_on.gt.0) then
          call diffn(NE,NR,NS,u,ut,alphaH,alphaD,dr,diffn_on)
       endif
C --- Maintain BC constant at r=1 ---
       do nn = 1,2*NS+1
          ut(NR*(nn-1)+NR) = 0.0d0
       enddo
C --- End of deriv.f ---
    return
    end
```

B.7 *rxn.f*

The code used for the *rxn.f* routine described in this thesis may be found in a supplemental file named rxn.f.

```
C * * * * * * * * * * * * * * * * * * * * * * * * * * * * * * * * * * * * * * * * * * * *
C --- Description ---
C      Computes the reaction dependent-terms when rxn_on.gt.0.
C --- Input ---
C  NE        integer  Number of first order ODEs
C  NR        integer  Number of spatial discretizations
C  NS        integer  Number of species
C  u(NE)     double   ODE solution vector
C  ut(NE)    double   ODE derivative vector
C  k         double   Reaction rate constant
C  E0        double   Initial E concentration
C  alphaD    double   D_{\infty}/R^2/tau for the drug
C  alphaH    double   D_{\infty}/R^2/tau for the soluble oligomers
C  G         double   Glycolic acid fraction of the polymer
C  beta      double   Constant prefactor for pore radius calculation
C  Ri(NS)    double   Radius of each species
C  rxn_on    integer  0 for rxn off, 1 for uncat, 2 for pseudo,
C                     3 for quad, 4 for half
C --- Output ---
C  ut(NE)    double   ODE derivative vector updated with reaction contribution
C * * * * * * * * * * * * * * * * * * * * * * * * * * * * * * * * * * * * * * * * * * * *
    subroutine rxn(NE,NR,NS,u,ut,k,E0,alphaH,alphaD,G,beta,Ri,rxn_on)
```

```
      implicit none
C --- Parameters ---
      integer NE,NR,NS,rr,nn,rxn_on
      double precision u(NE),ut(NE),k,smallolig_dtsum
      double precision E0,G,RvCOOH,beta,Ri(NS)
      double precision alphaH,alphaD,Rp,dRpdt,lambda
C --- rxn_on=0 no reaction, rxn_on=1 uncatalyzed hydrolysis, rxn_on=2 pseudo-
C     first-order hydrolysis, rxn_on=3 quadratic-order hydrolysis, rxn_on=4
C     1.5th-order hydrolysis ---
C --- Update Rvi for COOH, E, and small oligomers ---
      if (rxn_on.eq.1) then
         call rxn_uncat(NE,NR,NS,u,ut,k)
      elseif (rxn_on.eq.2) then
         call rxn_pseudo(NE,NR,NS,u,ut,k,E0)
      elseif (rxn_on.eq.3) then
         call rxn_quad(NE,NR,NS,u,ut,k)
      elseif (rxn_on.eq.4) then
         call rxn_half(NE,NR,NS,u,ut,k,G)
      endif
C --- Update large oligomer derivative, Rp derivative, and Deff derivative
C     for each species based on reaction update ---'
      do rr = 1,NR-1
         smallolig_dtsum = 0.0d0
C --- Local variable for RvCOOH ---
         nn = NS-1
            RvCOOH = ut(NR*(nn-1)+rr)
C --- Upate pore radius Rp: Rate of pore radius growth due to ester
C     bond cleavage or end group generation=dRp/dt=beta*RvCOOH ---
         nn = NS+1
            ut(NR*(nn-1)+rr) = beta*RvCOOH
            dRpdt = ut(NR*(nn-1)+rr)
            Rp = u(NR*(nn-1)+rr)
         do nn = 1,NS-4
C --- Calculate lambda ---
            lambda = Ri(nn)/Rp
C --- Calculate sum of Rvi for small oligomers ---
            smallolig_dtsum = smallolig_dtsum+ut(NR*(nn-1)+rr)
C --- Test 0<lambda<1: lambda between 0 and 1 gives H>0 ---
            if (lambda.lt.1.0d0) then
               if (lambda.gt.0.0d0) then
```

```
C ---- Update Deff(r) for small oligomers based on pore growth ----
                  call derivDeff(ut(NR*(NS+1+nn-1)+rr),Rp,dRpdt,
     &                 alphaH,lambda)
               endif
            endif
         enddo
C ---- Update large oligomers using the RvCOOH and sum of Rvi for small
C      oligomers----
         nn = NS-2
            ut(NR*(nn-1)+rr) = RvCOOH - smallolig_dtsum
C ---- Update Deff(r) for drug based on pore growth ----
         nn = NS
C ---- Calculate lambda ----
            lambda = Ri(nn)/Rp
C ---- Test 0<lambda<1: lambda between 0 and 1 gives H>0 ----
            if (lambda.lt.1.0d0) then
               if (lambda.gt.0.0d0) then
C ---- Update Deff(r) for drug based on pore growth ----
                  call derivDeff(ut(NR*(NS+1+nn-1)+rr),Rp,dRpdt,
     &                 alphaD,lambda)
               endif
            endif
       enddo
C ---- End of rxn.f ----
   return
   end
```

B.8 *rxn_uncat.f*

The code used for the *rxn_uncat.f* routine described in this thesis may be found in a supplemental file named rxn_uncat.f.

```
C * * * * * * * * * * * * * * * * * * * * * * * * * * * * * * * * * * * * * * * * * * * *
C ---- Description ----
C      Computes the Rvi terms for the uncatalyzed hydrolysis model
C      when rxn_on.eq.1.
C ---- Input ----
C  NE        integer  Number of first order ODEs
C  NR        integer  Number of spatial discretizations
```

```
C  NS        integer  Number of species
C  u(NE)     double   ODE solution vector
C  ut(NE)    double   ODE derivative vector
C  k         double   Reaction rate constant
C --- Output ---
C  ut(NE)    double   ODE derivative vector updated with Rvi contribution
C * * * * * * * * * * * * * * * * * * * * * * * * * * * * * * * * * * * * * * *
      subroutine rxn_uncat(NE,NR,NS,u,ut,k)
        implicit none
C --- Parameters ---
        integer NR,NE,NS,nn,rr
        double precision u(NE),ut(NE),k,smallolig_sum,largeolig_sum
C --- Loop over all interior spatial discretizations ---
        do rr = 1,NR-1
C --- Large oligomer sum, [P_{n>s}](r,t) ---
          nn = NS-2
            largeolig_sum = u(NR*(nn-1)+rr)
C --- Sum of small oligomers, sum_{i=1}^s [P_i](r,t) ---
          smallolig_sum = 0.0d0
          do nn = 1,NS-4
            smallolig_sum = smallolig_sum+u(NR*(nn-1)+rr)
          enddo
C --- Small oligomers ---
          do nn = 1,NS-4
C --- Reduce sum of small oligomers to sum_{i=n+1}^s ---
            smallolig_sum = smallolig_sum-u(NR*(nn-1)+rr)
            ut(NR*(nn-1)+rr) = ut(NR*(nn-1)+rr)
     &          +2.0d0*k*(smallolig_sum+largeolig_sum)
     &          -dfloat(nn-1)*k*u(NR*(nn-1)+rr)
          enddo
C --- Ester ---
          nn = NS-3
            ut(NR*(nn-1)+rr) = ut(NR*(nn-1)+rr)
     &          -k*u(NR*(nn-1)+rr)
C --- COOH ---
          nn = NS-1
            ut(NR*(nn-1)+rr) = ut(NR*(nn-1)+rr)
     &          +k*u(NR*(NS-3-1)+rr)
        enddo
C --- End of rxn_uncat.f ---
```

```
      return
      end
```

B.9 *rxn_pseudo.f*

The code used for the *rxn_pseudo.f* routine described in this thesis may be found in a supplemental file named rxn_pseudo.f.

```
C * * * * * * * * * * * * * * * * * * * * * * * * * * * * * * * * * * * * * * * * * * * * * * * *
C --- Description ---
C     Computes the Rvi terms for the pseudo-first-order hydrolysis model
C     when rxn_on.eq.2.
C --- Input ---
C  NE        integer  Number of first order ODEs
C  NR        integer  Number of spatial discretizations
C  NS        integer  Number of species
C  u(NE)     double   ODE solution vector
C  ut(NE)    double   ODE derivative vector
C  k         double   Reaction rate constant
C  E0        double   Initial E concentration
C --- Output ---
C  ut(NE)    double   ODE derivative vector updated with Rvi contribution
C * * * * * * * * * * * * * * * * * * * * * * * * * * * * * * * * * * * * * * * * * * * * * * * *
      subroutine rxn_pseudo(NE,NR,NS,u,ut,k,E0)
        implicit none
C --- Parameters ---
        integer NR,NE,NS,nn,rr
        double precision u(NE),ut(NE),smallolig_sum,largeolig_sum,COOH
        double precision k,E0,reactingolig_sum
C --- Loop over all interior spatial discretizations ---
        do rr = 1,NR-1
C --- Large oligomer sum, [P_{n>s}](r,t) ---
          nn = NS-2
            largeolig_sum = u(NR*(nn-1)+rr)
C --- Sum of small oligomers, sum_{i=1}^s [P_i](r,t) ---
          smallolig_sum = 0.0d0
          do nn = 1,NS-4
            smallolig_sum = smallolig_sum+u(NR*(nn-1)+rr)
          enddo
```

```
C ---- Reacting oligomers: sum_{n=2}^\infty Pn = small + large - P1 ----
          reactingolig_sum = largeolig_sum+smallolig_sum-u(NR*(1-1)+rr)
C ---- Update reaction only if E.gt.0.
C      E is not updated for pseudo, so use reactingolig_sum.gt.0 ----
          nn = NS-1
             COOH = u(NR*(nn-1)+rr)
          if (reactingolig_sum.gt.0.0d0) then
C ---- Small oligomers ----
             do nn = 1,NS-4
C ---- Reduce sum of small oligomers to sum_{i=n+1}^s ----
                smallolig_sum = smallolig_sum-u(NR*(nn-1)+rr)
C ---- Divide k k1' by E0 for the RvPn term; keep for RvCOOH ----
                ut(NR*(nn-1)+rr) = ut(NR*(nn-1)+rr)
     &             +2.0d0*k*COOH/E0*(smallolig_sum+largeolig_sum)
     &             -dfloat(nn-1)*k*COOH/E0*u(NR*(nn-1)+rr)
             enddo
C ---- COOH ----
             nn = NS-1
                ut(NR*(nn-1)+rr) = ut(NR*(nn-1)+rr)
     &             +k*u(NR*(nn-1)+rr)
          endif
        enddo
C ---- End of rxn_pseudo.f ----
    return
    end
```

B.10 *rxn_quad.f*

The code used for the *rxn_quad.f* routine described in this thesis may be found in a supplemental file named rxn_quad.f.

```
C * * * * * * * * * * * * * * * * * * * * * * * * * * * * * * * * * * * * * * * * * * * *
C ---- Description ----
C      Computes the Rvi terms for the quadratic-order hydrolysis model
C      when rxn_on.eq.3.
C ---- Input ----
C  NE        integer  Number of first order ODEs
C  NR        integer  Number of spatial discretizations
C  NS        integer  Number of species
```

```
C  u(NE)     double   ODE solution vector
C  ut(NE)    double   ODE derivative vector
C  rateconstdouble    Reaction rate constant
C --- Output ---
C  ut(NE)    double   ODE derivative vector updated with Rvi contribution
C * * * * * * * * * * * * * * * * * * * * * * * * * * * * * * * * * * * * * * *
      subroutine rxn_quad(NE,NR,NS,u,ut,rateconst)
          implicit none
C --- Parameters ---
          integer NR,NE,NS,nn,rr,ss
          double precision u(NE),ut(NE),smallolig_sum,largeolig_sum
          double precision rateconst,COOH
C --- Loop over all interior spatial discretizations ---
          do rr = 1,NR-1
C --- Large oligomer sum, [P_{n>s}](r,t) ---
             nn = NS-2
                largeolig_sum = u(NR*(nn-1)+rr)
C --- Sum of small oligomers, sum_{i=1}^s [P_i](r,t) ---
             smallolig_sum = 0.0d0
             do nn = 1,NS-4
                smallolig_sum = smallolig_sum+u(NR*(nn-1)+rr)
             enddo
C --- Small oligomers ---
             do nn = 1,NS-4
C --- Reduce sum of small oligomers to sum_{i=n+1}^s ---
                smallolig_sum = smallolig_sum-u(NR*(nn-1)+rr)
                ss = NS-1
                   COOH = u(NR*(ss-1)+rr)
                ut(NR*(nn-1)+rr) = ut(NR*(nn-1)+rr)
     &             +2.0d0*rateconst*COOH*(smallolig_sum+largeolig_sum)
     &             -dfloat(nn-1)*rateconst*COOH*u(NR*(nn-1)+rr)
             enddo
C --- Ester ---
             nn = NS-3
                ut(NR*(nn-1)+rr) = ut(NR*(nn-1)+rr)
     &             -rateconst*u(NR*(nn-1)+rr)*u(NR*(NS-1-1)+rr)
C --- COOH ---
             nn = NS-1
                ut(NR*(nn-1)+rr) = ut(NR*(nn-1)+rr)
     &             +rateconst*u(NR*(nn-1)+rr)*u(NR*(NS-3-1)+rr)
```

```
      enddo
C --- End of rxn_quad.f ---
   return
   end
```

B.11 *rxn_half.f*

The code used for the *rxn_half.f* routine described in this thesis may be found in a supplemental file named rxn_half.f.

```
C * * * * * * * * * * * * * * * * * * * * * * * * * * * * * * * * * * * * * * * * * * * *
C --- Description ---
C     Computes the Rvi terms for the 1.5th-order hydrolysis model
C     when rxn_on.eq.4.
C --- Input ---
C  NE       integer  Number of first order ODEs
C  NR       integer  Number of spatial discretizations
C  NS       integer  Number of species
C  u(NE)    double   ODE solution vector
C  ut(NE)   double   ODE derivative vector
C  k        double   Reaction rate constant
C  G        double   Glycolic acid fraction of the polymer
C --- Output ---
C  ut(NE)   double   ODE derivative vector updated with reaction contribution
C * * * * * * * * * * * * * * * * * * * * * * * * * * * * * * * * * * * * * * * * * * * *
   subroutine rxn_half(NE,NR,NS,u,ut,k,G)
      implicit none
C --- Parameters ---
      integer NR,NE,NS,nn,rr,ss
      double precision u(NE),ut(NE),smallolig_sum,pKa,Ka,G
      double precision k,largeolig_sum,COOH
      pKa = (1.0d0-G)*3.86d0+G*3.83d0;
      Ka = 10d0**(-pKa);
C --- Loop over all interior spatial discretizations ---
      do rr = 1,NR-1
C --- Large oligomer sum, [P_{n>s}](r,t) ---
         nn=NS-2
            largeolig_sum=u(NR*(nn-1)+rr)
C --- Sum of small oligomers, sum_{i=1}^s [P_i](r,t) ---
```

```
            smallolig_sum=0.0d0
            do nn=1,NS-4
               smallolig_sum=smallolig_sum+u(NR*(nn-1)+rr)
            enddo
C --- Small oligomers ---
            do nn = 1,NS-4
C --- Reduce sum of small oligomers to sum_{i=nn+1}^s ---
               smallolig_sum = smallolig_sum - u(NR*(nn-1)+rr)
               ss = NS-1
                  COOH = u(NR*(ss-1)+rr)
               ut(NR*(nn-1)+rr) = ut(NR*(nn-1)+rr)
     &            +2.0d0*k*dsqrt(Ka*COOH)*(smallolig_sum+largeolig_sum)
     &            -dfloat(nn-1)*k*dsqrt(Ka*COOH)*u(NR*(nn-1)+rr)
            enddo
C --- Ester ---
            nn=NS-3
               ut(NR*(nn-1)+rr) = ut(NR*(nn-1)+rr)
     &            -k*u(NR*(nn-1)+rr)*dsqrt(u(NR*(NS-1-1)+rr)*Ka)
C --- COOH ---
            nn = NS-1
               ut(NR*(nn-1)+rr) = ut(NR*(nn-1)+rr)
     &            +k*u(NR*(NS-3-1)+rr)
     &            *dsqrt(u(NR*(nn-1)+rr)*Ka)
          enddo
C --- End of rxn_half.f ---
      return
      end
```

B.12 *derivDeff.f*

The code used for the *derivDeff.f* routine described in this thesis may be found in a supplemental file named derivDeff.f.

```
C * * * * * * * * * * * * * * * * * * * * * * * * * * * * * * * * * * * * * * * * * * * * * * * *
C --- Description ---
C     Computes the derivative of the effective diffusivity.
C --- Input ---
C  dDeffdt  double   ODE derivative for Deff for a single species
C  Rp       double   Pore radius
```

```
C  dRpdt     double   ODE derivative for Rp for a single species
C  Dinf      double   D_{\infty}/R^2/tau for the species
C  lambda    double   Ri/Rp
C --- Output ---
C  dDeffdt   double   ODE derivative for Deff for a single species updated
C * * * * * * * * * * * * * * * * * * * * * * * * * * * * * * * * * * * * * *
      subroutine derivDeff(dDeffdt,Rp,dRpdt,Dinf,lambda)
          implicit none
C --- Parameters ---
          double precision dDeffdt,Rp,dRpdt,Dinf,lambda,dHdt
C --- H from Bungay & Brenner 1973; Deen 1987 ---
                call derivH(Rp,dRpdt,lambda,dHdt)
C --- dDeff/dt ---
                dDeffdt = Dinf*dHdt
C --- End of derivDeff.f ---
      return
      end
```

B.13 *derivH.f*

The code used for the *derivH.f* routine described in this thesis may be found in a supplemental file named derivH.f.

```
C * * * * * * * * * * * * * * * * * * * * * * * * * * * * * * * * * * * * * *
C --- Description ---
C     Computes the derivative of the hindered diffusion coefficient
C     with H from
C        P. M. Bungay and H. Brenner. The Motion of a Closely-Fitting Sphere
C        in a Fluid-Filled Tube. International Journal of Multiphase Flow,
C        1(1):25-56, 1973
C        and
C        W. M. Deen. Hindered Transport of Large Molecules in Liquid-Filled
C        Pores. AIChE Journal, 33(9):1409-1425, 1987.
C --- Input ---
C  dDeffdt   double   ODE derivative for Deff for a single species
C  Rp        double   Pore radius
C  dRpdt     double   ODE derivative for Rp for a single species
C  Ri        double   Radius of the species
C  Dinf      double   D_{\infty}/R^2/tau for the species
```

```
C --- Output ---
C  dDeffdt  double  ODE derivative for Deff for a single species updated
C * * * * * * * * * * * * * * * * * * * * * * * * * * * * * * * * * * * * * * * * * * * *
      subroutine derivH(Rp,dRpdt,lambda,dHdt)
          implicit none
C --- Parameters ---
          double precision Rp,dRpdt,lambda,dHdt,lambdaprime
          double precision num,denom,numprime,denomprime,pi
          pi = 3.14159265358979324d0
C --- Calculate the derivative of lambda ---
          lambdaprime = -lambda/Rp*dRpdt
C --- Calculate the numerator of H ---
          num = 6.0d0*pi*(1.0d0-lambda)**2.0d0
C --- Calculate the numerator of H ---
          denom = 2.25d0*pi**2.0d0*dsqrt(2.0d0)
     &    *(1.0d0-lambda)**(-2.5d0)*(1.0d0-73.0d0/60.0d0
     &    *(1.0d0-lambda)+77293.0d0/50400.0d0
     &    *(1.0d0-lambda)**2.0d0)-22.5083d0-5.6117d0*lambda
     &    -0.3363d0*lambda**2.0d0-1.216d0*lambda**3.0d0
     &    +1.647d0*lambda**4.0d0
C --- Calculate the derivative of the numerator of H ---
          numprime = -12.0d0*pi*(1.0d0-lambda)
C --- Calculate the derivative of the denominator of H ---
          denomprime = 45.0d0/8.0d0*pi**2.0d0*dsqrt(2.0d0)
     &    *(1.0d0-lambda)**(-3.5d0)*(1.0d0-73.0d0/60.0d0*(1.0d0-lambda)
     &    +77293.0d0/50400.0d0*(1.0d0-lambda)**2.0d0)
     &    +2.25d0*pi**2.0d0*dsqrt(2.0d0)*(1.0d0-lambda)**(-2.5d0)*
     &    (73.0d0/60.0d0-2.0d0*77293.0d0/50400.0d0
     &    *(1.0d0-lambda))-5.6117d0-2.0d0*0.3363d0*lambda
     &    -3.0d0*1.216d0*lambda**2.0d0+4.0d0*1.647d0*lambda**3.0d0
C --- Calculate the derivative of H ---
          dHdt = lambdaprime*(denom*numprime-num*denomprime)/denom**2.0d0
C --- End of derivH.f ---
      return
      end
```

B.14 *diffn.f*

The code used for the *diffn.f* routine described in this thesis may be found in a supplemental file named diffn.f.

```
C * * * * * * * * * * * * * * * * * * * * * * * * * * * * * * * * * * * * * * * * * * * * * * * *
C --- Description ---
C     Computes the diffusion-dependent terms when diffn_on.gt.0.
C --- Input ---
C  NE        integer  Number of first order ODEs
C  NR        integer  Number of spatial discretizations
C  NS        integer  Number of species
C  u(NE)     double   ODE solution vector
C  ut(NE)    double   ODE derivative vector
C  alphaD    double   D_{\infty}/R^2/tau for the drug
C  alphaH    double   D_{\infty}/R^2/tau for the soluble oligomers
C  dr        double   Spatial discretization size
C  diffn_on  integer  0 for diffn off, 1 for constD, 2 for drug varD,
C                     3 for all species varD
C --- Output ---
C  ut(NE)    double   ODE derivative vector updated with diffusion contribution
C * * * * * * * * * * * * * * * * * * * * * * * * * * * * * * * * * * * * * * * * * * * * * * * *
   subroutine diffn(NE,NR,NS,u,ut,alphaH,alphaD,dr,diffn_on)
      implicit none
C --- Parameters ---
      integer NR,NE,NS,nn,rr,diffn_on
      double precision u(NE),ut(NE),dr,alphaH,alphaD,largeolig_dtsum
      double precision udiffn(NR),utdiffn(NR),Ddiffn(NR),smallolig_dtsum(NR)
      double precision Deff(NS*NR),smallolig_diffnsum(NR)
C --- Populate Deff vector for each species according to diffn_on value ---
      if (diffn_on.eq.1) then
C --- Constant diffusivity for small oligomers and drug ---
         do rr = 1,NR
            do nn = 1,NS-4
               Deff(NR*(nn-1)+rr) = alphaH
            enddo
            do nn = NS-3, NS-1
               Deff(NR*(nn-1)+rr) = 0.0d0
            enddo
            nn = NS
               Deff(NR*(nn-1)+rr) = alphaD
```

```
          enddo
        elseif (diffn_on.eq.2) then
C ---- Constant diffusivity for small oligomers and variable
C       diffusivity for drug ----
          do rr = 1,NR
             do nn = 1,NS-4
                Deff(NR*(nn-1)+rr) = alphaH
             enddo
             do nn = NS-3,NS-1
                Deff(NR*(nn-1)+rr) = 0.0d0
             enddo
             nn = NS
                Deff(NR*(nn-1)+rr) = u(NR*(NS+1+nn-1)+rr)
          enddo
        elseif (diffn_on.eq.3) then
C ---- Variable diffusivity for small oligomers and drug
          do rr = 1,NR
             do nn = 1,NS-4
                Deff(NR*(nn-1)+rr) = u(NR*(NS+1+nn-1)+rr)
             enddo
             do nn = NS-3,NS-1
                Deff(NR*(nn-1)+rr) = 0.0d0
             enddo
             nn = NS
                Deff(NR*(nn-1)+rr) = u(NR*(NS+1+nn-1)+rr)
          enddo
        endif
C ---- Initialize sum of small oligomers for ester and COOH updates ----
        do rr = 1,NR
           smallolig_diffnsum(rr) = 0.0d0
           smallolig_dtsum(rr) = 0.0d0
        enddo
C ---- Diffusion of small oligomers ----
        do nn = 1,NS-4
C ---- Initialize input vectors ----
          do rr = 1,NR
             udiffn(rr) = u(NR*(nn-1)+rr)
             utdiffn(rr) = 0.0d0
             Ddiffn(rr) = Deff(NR*(nn-1)+rr)
          enddo
```

```
C ---- Diffusion terms at r = 0 ----
          call diffn_ctr(utdiffn(1),Ddiffn(1),Ddiffn(2),
     &       dr,udiffn(1),udiffn(2))
C ---- Diffusion terms 0 < r < 1 ----
          call diffn_int(utdiffn(1:NR),Ddiffn(1:NR),dr,udiffn(1:NR),NR)
C ---- Assign output vectors to appropriate derivative values ----
          do rr = 1,NR-1
             smallolig_diffnsum(rr) = smallolig_diffnsum(rr)+(nn-1)*utdiffn(rr)
             ut(NR*(nn-1)+rr) = ut(NR*(nn-1)+rr)+utdiffn(rr)
             smallolig_dtsum(rr) = smallolig_dtsum(rr)+ut(NR*(nn-1)+rr)
          enddo
       enddo
       do rr = 1,NR-1
C ---- Update ester with small oligomer diffusion ----
          nn = NS-3
             ut(NR*(nn-1)+rr) = ut(NR*(nn-1)+rr)+smallolig_diffnsum(rr)
C ---- Update COOH with small oligomer diffusion: the calculation includes
C      rxn and diffn contributions to small oligomer and rxn contribution
C      to large oligomers ----
          nn = NS-2
             largeolig_dtsum = ut(NR*(nn-1)+rr)
          nn = NS-1
             ut(NR*(nn-1)+rr)=smallolig_dtsum(rr)+largeolig_dtsum
       enddo
C ---- Diffusion of drug ----
       nn = NS
C ---- Make input vectors ----
          do rr = 1,NR
             udiffn(rr) = u(NR*(nn-1)+rr)
             utdiffn(rr) = ut(NR*(nn-1)+rr)
             Ddiffn(rr) = Deff(NR*(nn-1)+rr)
          enddo
C ---- Diffusion terms at r = 0 ----
          call diffn_ctr(utdiffn(1),Ddiffn(1),Ddiffn(2),
     &       dr,udiffn(1),udiffn(2))
C ---- Diffusion terms 0 < r < 1 ----
          call diffn_int(utdiffn(1:NR),Ddiffn(1:NR),dr,udiffn(1:NR),NR)
C ---- Assign output vectors to appropriate derivative values ----
          do rr = 1,NR-1
             ut(NR*(nn-1)+rr) = utdiffn(rr)
```

```
          enddo
C --- End of diffn.f ---
      return
      end
```

B.15 *diffn_ctr.f*

The code used for the *diffn_ctr.f* routine described in this thesis may be found in a supplemental file named diffn_ctr.f.

```
C * * * * * * * * * * * * * * * * * * * * * * * * * * * * * * * * * * * * * * * * * * * *
C --- Description ---
C     Computes the diffusion terms at r=0 for a single species
C     when diffn_on.gt.0.
C --- Input ---
C  ut        double   ODE derivative at r=0
C  Deff1     double    Effective diffusivity of the species at r=0
C  Deff2     double    Effective diffusivity of the species at r=dr
C  dr        double    Spatial discretization size
C  u1        double   ODE solution at r=0
C  u2        double   ODE solution at r=dr
C --- Output ---
C  ut        double   ODE derivative at r=0 updated with diffusion contribution
C * * * * * * * * * * * * * * * * * * * * * * * * * * * * * * * * * * * * * * * * * * * *
      subroutine diffn_ctr(ut,Deff1,Deff2,dr,u1,u2)
          implicit none
C --- Parameters ---
          double precision ut,Deff1,Deff2,dr,u1,u2,diffnterm
C --- Compute value at r=0
          diffnterm = 3.0d0*(Deff1+Deff2)*(u2-u1)/dr/dr
          ut = ut+diffnterm
C --- End of diffn_ctr.f ---
      return
      end
```

B.16 *diffn_int.f*

The code used for the *diffn_int.f* routine described in this thesis may be found in a supplemental file named diffn_int.f.

```
C * * * * * * * * * * * * * * * * * * * * * * * * * * * * * * * * * * * * * * * * * * * * * * * *
C --- Description ---
C     Computes the diffusion terms at 0<r<1 for a single species
C     when diffn_on.gt.0.
C --- Input ---
C  ut(NR)    double   ODE derivative vector
C  Deff(NR)  double    Effective diffusivity of the species
C  dr        double    Spatial discretization size
C  u(NR)     double   ODE solution vector
C  NR        integer  Number of spatial discretizations
C --- Output ---
C  ut(NR)    double   ODE derivative vector updated with diffusion contribution
C * * * * * * * * * * * * * * * * * * * * * * * * * * * * * * * * * * * * * * * * * * * * * * * *
   subroutine diffn_int(ut,Deff,dr,u,NR)
      implicit none
C --- Parameters ---
      integer rr,jj,NR
      double precision ut(NR),Deff(NR),dr,u(NR)
      double precision diffnterm
C --- Loop over all interior spatial discretizations 0<r<1 ---
      do rr = 2,NR-1
         jj = rr-1
         diffnterm = Deff(rr)/dfloat(jj)/2.0d0/dr/dr*
     &      (dfloat(jj+2)*u(rr+1)-2.0d0*dfloat(jj)*u(rr)+dfloat(jj-2)
     &      *u(rr-1))+1.0d0/2.0d0/dr/dr*
     &      (Deff(rr+1)*(u(rr+1)-u(rr))+Deff(rr-1)*(u(rr-1)-u(rr)))
         ut(rr) = ut(rr)+diffnterm
      enddo
C --- End of diffn_int.f ---
   return
   end
```

B.17 *kraken.deck*

The code used for the *kraken.deck* parameter input file described in this thesis may be found in a supplemental file named kraken.deck.

```
#!/bin/csh
# ================================================================
#PBS -l walltime=2:00:00
#PBS -A account number
#PBS -l size=12
#PBS -q small
#PBS -N radau
#PBS -o rad_pbsout.out
#PBS -e rad_pbsout.err
# ================================================================
echo -n ``$user job starting at ''; date
unlimit
date
# Run the program, reading input data between the EOF lines below.
# This batch job will create files 'rad_pbsout.out' and 'rad_pbs.err' in the
# directory from which you submit the job (``qsub sphdiscrkraken.deck'').
# As set up below, the output is stored in 'radau.out'.
# The executable name is 'radau'.
time
aprun -n 1 ./radau << EOF >! radau.out
0                       restart
2                       diffn_on
3                       rxn_on
1                       kscale_on
101                     NR
13                      NS
25.0d-4                 R
3.0d0                   tau
1.0d-6                  DD
1.0d-15                 DH
0.0773d0                k
1.0d0                   PDI
2.0d4                   Mw
1.0d0                   drug0
1.0d0                   COOH0
0.99d0                  Xrxn
```

```
101                     NT
0.0d0                   Rp0
0.0d0                   tfinal_override
0.5d0                   G
1.0d-6                  TOL
1.0d-15                 DD0
0.0d0                   DH0
EOF
echo ' '
date
echo ' '
echo -n ''$user job finished at ''; date
```

B.18 *makefile*

The code used for the *makefile* used to link and compile the routines described in this thesis into the executable *radau* may be found in a supplemental file named makefile.

```
#
# Makefile for driver_radau5.
# First line is default, so typing ''make'' makes executable named radau.
# The executable has its name, then all dependencies (object files).
# Beneath that is the statement to link them and create the program.
# The last statements say how to turn .f files into .o files: compiling.
# Use -O for usual optimization.
#
F90   = ftn
OPTS  = -O
OBJS =   driver_radau5.o radau5.o decsol.o dc_decsol.o intpar.o\
         deriv.o initial.o diffn.o diffn_ctr.o diffn_int.o \
         rxn.o rxn_half.o rxn_uncat.o rxn_pseudo.o rxn_quad.o\
         Fderiv.o Jderiv.o derivH.o derivDeff.o
radau:   $(OBJS)
   $(F90) $(OPTS) -o radau $(OBJS)
.f.o:
   $(F90) -c $*.f
clean:
   rm -f *.o radau
```

References

[1] R. D. Braatz, A. N. Ford Versypt, and L. M. Goh. *Nanoscale Drug Delivery Module: Teacher's Edition*. Materials World Modules, Northwestern University, Evanston, Illinois, 2012.

[2] R. D. Braatz, A. N. Ford Versypt, and L. M. Goh. *Nanoscale Drug Delivery Module: Student's Edition*. Materials World Modules, Northwestern University, Evanston, Illinois, 2012.

[3] U. Edlund and A. C. Albertsson. Degradable Polymer Microspheres for Controlled Drug Delivery. *Advances in Polymer Science*, 157:67–112, 2002.

[4] N. K. Varde and D. W. Pack. Microspheres for Controlled Release Drug Delivery. *Expert Opinion on Biological Therapy*, 4(1):35–51, 2004.

[5] S. Freiberg and X. X. Zhu. Polymer Microspheres for Controlled Drug Release. *International Journal of Pharmaceutics*, 282(1-2):1–18, 2004.

[6] V. R. Sinha and A. Trehan. Biodegradable Microspheres for Protein Delivery. *Journal of Controlled Release*, 90(3):261–280, 2003.

[7] J. W. Haefner. *Modeling Biological Systems: Principles and Applications*. Springer, New York, 2nd edition, 2005.

[8] A. Gopferich. Mechanisms of Polymer Degradation and Erosion. *Biomaterials*, 17(2):103–114, 1996.

[9] J. M. Anderson and M. S. Shive. Biodegradation and Biocompatibility of PLA and PLGA Microspheres. *Advanced Drug Delivery Reviews*, 28(1):5–24, 1997.

[10] R. Lipsa, N. Tudorachi, and C. Vasile. Poly(α-Hydroxyacids) in Biomedical Applications: Synthesis and Properties of Lactic Acid Polymers. *e-Polymers*, (87):1–43, 2010.

[11] F. Alexis. Factors Affecting the Degradation and Drug-Release Mechanism of Poly(Lactic Acid) and Poly[(Lactic Acid)-co-(Glycolic Acid)]. *Polymer International*, 54(1):36–46, 2005.

[12] D. Klose, F. Siepmann, K. Elkharraz, S. Krenzlin, and J. Siepmann. How Porosity and Size Affect the Drug Release Mechanisms from PLGA-Based Microparticles. *International Journal of Pharmaceutics*, 314(2):198–206, 2006.

[13] N. Faisant, J. Siepmann, and J. P. Benoit. PLGA-Based Microparticles: Elucidation of Mechanisms and a New, Simple Mathematical Model Quantifying Drug Release. *European Journal of Pharmaceutical Sciences*, 15(4):355–366, 2002.

[14] N. Faisant, J. Akiki, F. Siepmann, J. P. Benoit, and J. Siepmann. Effects of the Type of Release Medium on Drug Release from PLGA-Based Microparticles: Experiment and Theory. *International Journal of Pharmaceutics*, 314(2):189–197, 2006.

[15] J. C. Kang and S. P. Schwendeman. Determination of Diffusion Coefficient of a Small Hydrophobic Probe in Poly(Lactide-co-Glycolide) Microparticles by Laser Scanning Confocal Microscopy. *Macromolecules*, 36(4):1324–1330, 2003.

[16] R. Langer and N. Peppas. Chemical and Physical Structure of Polymers as Carriers for Controlled Release of Bioactive Agents: A Review. *Journal of Macromolecular Science: Reviews in Macromolecular Chemistry and Physics*, C23(1):61–126, 1983.

[17] R. A. Kenley, M. O. Lee, T. R. Mahoney, and L. M. Sanders. Poly(Lactide-co-Glycolide) Decomposition Kinetics *In Vivo* and *In Vitro*. *Macromolecules*, 20(10):2398–2403, 1987.

[18] K. Fu, D. W. Pack, A. M. Klibanov, and R. Langer. Visual Evidence of Acidic Environment within Degrading Poly(Lactic-co-Glycolic Acid) (PLGA) Microspheres. *Pharmaceutical Research*, 17(1):100–106, 2000.

[19] L. Li and S. P. Schwendeman. Mapping Neutral Microclimate pH in PLGA Microspheres. *Journal of Controlled Release*, 101(1-3):163–173, 2005.

[20] B. S. Zolnik and D. J. Burgess. Effect of Acidic pH on PLGA Microsphere Degradation and Release. *Journal of Controlled Release*, 122(3):338–344, 2007.

[21] J. Siepmann, N. Faisant, J. Akiki, J. Richard, and J. P. Benoit. Effect of the Size of Biodegradable Microparticles on Drug Release: Experiment and Theory. *Journal of Controlled Release*, 96(1):123–134, 2004.

[22] C. Berkland, K. Kim, and D. W. Pack. PLG Microsphere Size Controls Drug Release Rate through Several Competing Factors. *Pharmaceutical Research*, 20(7):1055–1062, 2003.

[23] S. M. Li. Hydrolytic Degradation Characteristics of Aliphatic Polyesters Derived from Lactic and Glycolic Acids. *Journal of Biomedical Materials Research*, 48(3):342–353, 1999.

[24] I. Grizzi, H. Garreau, S. Li, and M. Vert. Hydrolytic Degradation of Devices Based on Poly(DL-Lactic Acid) Size-Dependence. *Biomaterials*, 16(4):305–311, 1995.

[25] J. Siepmann, K. Elkharraz, F. Siepmann, and D. Klose. How Autocatalysis Accelerates Drug Release from PLGA-Based Microparticles: A Quantitative Treatment. *Biomacromolecules*, 6(4):2312–2319, 2005.

[26] D. Klose, F. Siepmann, K. Elkharraz, and J. Siepmann. PLGA-Based Drug Delivery Systems: Importance of the Type of Drug and Device Geometry. *International Journal of Pharmaceutics*, 354(1-2):95–103, 2008.

[27] C. Berkland, E. Pollauf, C. Raman, R. Silverman, K. Kim, and D. W. Pack. Macromolecule Release from Monodisperse PLG Microspheres: Control of Release Rates and Investigation of Release Mechanism. *Journal of Pharmaceutical Sciences*, 96(5):1176–1191, 2007.

[28] C. Berkland, E. Pollauf, N. Varde, D. W. Pack, and K. Kim. Monodisperse Liquid-Filled Biodegradable Microcapsules. *Pharmaceutical Research*, 24(5):1007–1013, 2007.

[29] C. Berkland, E. Pollauf, D. W. Pack, and K. Kim. Uniform Double-Walled Polymer Microspheres of Controllable Shell Thickness. *Journal of Controlled Release*, 96(1):101–111, 2004.

[30] E. Pollauf and D. W. Pack. Use of Thermodynamic Parameters for Design of Double-Walled Microsphere Fabrication Methods. *Biomaterials*, 27(14):2898–2906, 2006.

[31] K. J. Pekarek, J. S. Jacob, and E. Mathiowitz. Double-Walled Polymer Microspheres for Controlled Drug Release. *Nature*, 367(6460):258–260, 1994.

[32] C. Berkland, M. King, A. Cox, K. Kim, and D. W. Pack. Precise Control of PLG Microsphere Size Provides Enhanced Control of Drug Release Rate. *Journal of Controlled Release*, 82(1):137–147, 2002.

[33] W. Lee, M. E. Wiseman, N. J. Cho, J. S. Glenn, and C. W. Frank. The reliable targeting of specific drug release profiles by integrating arrays of different albumin-encapsulated microsphere types. *Biomaterials*, 30(34):6648–6654, 2009.

[34] N. S. Berchane, F. F. Jebrail, and M. J. Andrews. Optimization of PLG Microspheres for Tailored Drug Release. *International Journal of Pharmaceutics*, 383(1-2):81–88, 2010.

[35] A. N. Ford, D. W. Pack, and R. D. Braatz. Multi-Scale Modeling of PLGA Microparticle Drug Delivery Systems. In E. N. Pistikopoulos, M. C. Georgiadis, and A. C. Kokossis, editors, *21st European Symposium on Computer Aided Process Engineering: Part B*, pages 1475–1479. Interscience, New York, 2011.

[36] L. L. Lao, N. A. Peppas, F. Y. C. Boey, and S. S. Venkatraman. Modeling of Drug Release from Bulk-Degrading Polymers. *International Journal of Pharmaceutics*, 418(1):28–41, 2011.

[37] M. Vert, S. Li, H. Garreau, J. Mauduit, M. Boustta, G. Schwach, R. Engel, and J. Coudane. Complexity of the Hydrolytic Degradation of Aliphatic Polyesters. *Die Angewandte Makromolekulare Chemie*, 247:239–253, 1997.

[38] A. Shenderova, A. G. Ding, and S. P. Schwendeman. Potentiometric Method for Determination of Microclimate pH in Poly(Lactic-co-Glycolic Acid) Films. *Macromolecules*, 37(26):10052–10058, 2004.

[39] A. Ding and S. P. Schwendeman. Acidic Microclimate pH Distribution in PLGA Microspheres Monitored by Confocal Laser Scanning Microscopy. *Pharmaceutical Research*, 25(9):2041–2052, 2008.

[40] A. Brunner, K. Mader, and A. Gopferich. pH and Osmotic Pressure inside Biodegradable Microspheres during Erosion. *Pharmaceutical Research*, 16(6):847–853, 1999.

[41] A. C. R. Grayson, M. J. Cima, and R. Langer. Size and Temperature Effects on Poly(Lactic-co-Glycolic Acid) Degradation and Microreservoir Device Performance. *Biomaterials*, 26(14):2137–2145, 2005.

[42] T. H. Lowry and K. S. Richardson. *Mechanism and Theory in Organic Chemistry*. Harper and Row, New York, 2nd edition, 1981.

[43] M. L. Houchin and E. M. Topp. Chemical Degradation of Peptides and Proteins in PLGA: A Review of Reactions and Mechanisms. *Journal of Pharmaceutical Sciences*, 97(7):2395–2404, 2008.

[44] C. F. van Nostrum, T. F. J. Veldhuis, G. W. Bos, and W. E. Hennink. Hydrolytic Degradation of Oligo(Lactic Acid): A Kinetic and Mechanistic Study. *Polymer*, 45(20):6779–6787, 2004.

[45] R. P. Batycky, J. Hanes, R. Langer, and D. A. Edwards. A Theoretical Model of Erosion and Macromolecular Drug Release from Biodegrading Microspheres. *Journal of Pharmaceutical Sciences*, 86(12):1464–1477, 1997.

[46] R. A. Siegel and M. J. Rathbone. Overview of Controlled Release Mechanisms. In J. Siepmann, R. A. Siegel, and M. J. Rathbone, editors, *Fundamentals and Applications of Controlled Release Drug Delivery*, pages 19–43. Springer, New York, 2012.

[47] J. Siepmann and A. Gopferich. Mathematical Modeling of Bioerodible, Polymeric Drug Delivery Systems. *Advanced Drug Delivery Reviews*, 48(2-3):229–247, 2001.

[48] R. Wada, S. H. Hyon, and Y. Ikada. Kinetics of Diffusion-Mediated Drug Release Enhanced by Matrix Degradation. *Journal of Controlled Release*, 37(1-2):151–160, 1995.

[49] P. Arosio, V. Busini, G. Perale, D. Moscatelli, and M. Masi. A New Model of Resorbable Device Degradation and Drug Release - Part I: Zero Order Model. *Polymer International*, 57(7):912–920, 2008.

[50] E. K. Euranto. Esterification and Ester Hydrolysis. In S. Patai, editor, *The Chemistry of Carboxylic Acids and Esters*, pages 505–588. Interscience, New York, 1969.

[51] C. K. Sackett and B. Narasimhan. Mathematical Modeling of Polymer Erosion: Consequences for Drug Delivery. *International Journal of Pharmaceutics*, 418(1):104–114, 2011.

[52] G. Perale, P. Arosio, D. Moscatelli, V. Barri, M. Mller, S. Maccagnan, and M. Masi. A New Model of Resorbable Device Degradation and Drug Release: Transient 1-Dimension Diffusional Model. *Journal of Controlled Release*, 136(3):196205, 2009.

[53] S. J Siegel, J. B. Kahn, K. Metzger, K. I. Winey, K. Werner, and N. Dan. Effect of Drug Type on Degradation Rate of PLGA Matrices. *European Journal of Pharmaceutics and Biopharmaceutics*, 64(7):287–293, 2006.

[54] A. Kulkarni, J. Reiche, and A. Lendlein. Hydrolytic Degradation of Poly(*rac*-Lactide) and Poly[(*rac*-Lactide)-co-Glycolide] at the Air-Water Interface. *Surface and Interface Analysis*, 39(9):740–746, 2007.

[55] A. Zhao, S. K. Hunter, and V. G. J. Rodgers. Theoretical Prediction of Induction Period from Transient Pore Evolvement in Polyester-Based Microparticles. *Journal of Pharmaceutical Sciences*, 99(11):4477–4487, 2010.

[56] S. M. Li, H. Garreau, and M. Vert. Structure-Property Relationships in the Case of the Degradation of Massive Aliphatic Poly-(α-Hydroxy Acids) in Aqueous Media—Part 1: Poly(D,L-Lactic Acid). *Journal of Materials Science: Materials in Medicine*, 1(3):123–130, 1990.

[57] F. von Burkersroda, L. Schedl, and A. Gopferich. Why Degradable Polymers Undergo Surface Erosion or Bulk Erosion. *Biomaterials*, 23(21):4221–4231, 2002.

[58] S. Fredenberg, M. Wahlgren, M. Reslow, and A. Axelsson. The Mechanisms of Drug Release in Poly(Lactic-co-Glycolic Acid)-Based Drug Delivery Systems—A Review. *International Journal of Pharmaceutics*, 415(1-2):34–52, 2011.

[59] C. Raman, C. Berkland, K. Kim, and D. W. Pack. Modeling Small-Molecule Release from PLG Microspheres: Effects of Polymer Degradation and Nonuniform Drug Distribution. *Journal of Controlled Release*, 103(1):149–158, 2005.

[60] S. Fredenberg, M. Jonsson, T. Laakso, M. Wahlgren, M. Reslow, and A. Axelsson. Development of Mass Transport Resistance in Poly(Lactide-co-Glycolide) Films and Particles—A Mechanistic Study. *International Journal of Pharmaceutics*, 409(1-2):194–202, 2011.

[61] J. Siepmann, R. A. Siegel, and F. Siepmann. Diffusion Controlled Drug Delivery Systems. In J. Siepmann, R. A. Siegel, and M. J. Rathbone, editors, *Fundamentals and Applications of Controlled Release Drug Delivery*, pages 127–152. Springer, New York, 2012.

[62] K. C. Wong-Moon, X. Sun, X. C. Nguyen, B. P. Quan, K. Shen, and P. A. Burke. NMR Spectroscopic Evaluation of the Internal Environment of PLGA Microspheres. *Molecular Pharmaceutics*, 5(4):654–664, 2008.

[63] E. Vey, C. Roger, L. Meehan, J. Booth, M. Claybourn, A. F. Miller, and A. Saiani. Degradation Mechanism of Poly(Lactic-co-Glycolic) Acid Block Copolymer Cast Films in Phosphate Buffer Solution. *Polymer Degradation and Stability*, 93(10):1869–1876, 2008.

[64] M. Dunne, O. I. Corrigan, and Z. Ramtoola. Influence of Particle Size and Dissolution Conditions on the Degradation Properties of Polylactide-co-glycolide Particles. *Journal of Materials Science: Materials in Medicine*, 1(3):123–130, 1990.

[65] X. S. Wu. Synthesis and Properties of Biodegradable Lactic/Glycolic Acid Polymers. In D. L. Wise, D. J. Trantolo, D. E. Altobelli, M. J. Yaszemski, J. D. Gresser, and E. R. Schwartz, editors, *Encyclopedic Handbook of Biomaterials and Bioengineering Part A: Biomaterials*, volume 2, pages 1015–1054. Marcel Dekker, New York, 1995.

[66] S. D. Allison. Analysis of Initial Burst in PLGA Microparticles. *Expert Opinion on Drug Delivery*, 5(6):615–628, 2008.

[67] D. Y. Arifin, L. Y. Lee, and C. H. Wang. Mathematical Modeling and Simulation of Drug Release from Microspheres: Implications to Drug Delivery Systems. *Advanced Drug Delivery Reviews*, 58(12-13):1274–1325, 2006.

[68] J. Siepmann and F. Siepmann. Mathematical Modeling of Drug Delivery. *International Journal of Pharmaceutics*, 364(2):328–343, 2008.

[69] J. T. He, C. L. Zhong, and J. G. Mi. Modeling of Drug Release from Bioerodible Polymer Matrices. *Drug Delivery*, 12(5):251–259, 2005.

[70] A. Charlier, B. Leclerc, and G. Couarraze. Release of Mifepristone from Biodegradable Matrices: Experimental and Theoretical Evaluations. *International Journal of Pharmaceutics*, 200(1):115–120, 2000.

[71] N. S. Berchane, K. H. Carson, A. C. Rice-Ficht, and M. J. Andrews. Effect of Mean Diameter and Polydispersity of PLG Microspheres on Drug Release: Experiment and Theory. *International Journal of Pharmaceutics*, 337(1-2):118–126, 2007.

[72] J. Siepmann, N. Faisant, and J. P. Benoit. A New Mathematical Model Quantifying Drug Release from Bioerodible Microparticles Using Monte Carlo Simulations. *Pharmaceutical Research*, 19(12):1885–1893, 2002.

[73] D. A. Eavarone, V. Soundararajan, T. Haller, and R. Sasisekharan. A Voxel-Based Monte Carlo Model of Drug Release from Bulk Eroding Nanoparticles. *Journal of Nanoscience and Nanotechnology*, 10(9):5903–5907, 2010.

[74] A. Gopferich. Polymer Bulk Erosion. *Macromolecules*, 30(9):2598–2604, 1997.

[75] A. Gopferich and R. Langer. Modeling of Polymer Erosion in Three Dimensions: Rotationally Symmetric Devices. *AIChE Journal*, 41(10):2292–2299, 1995.

[76] A. Barat, M. Crane, and H. J. Ruskin. Quantitative Multi-Agent Models for Simulating Protein Release from PLGA Bioerodible Nano- and Microspheres. *Journal of Pharmaceutical and Biomedical Analysis*, 48(2):361–368, 2008.

[77] A. G. Thombre and K. J. Himmelstein. A Simultaneous Transport-Reaction Model for Controlled Drug Delivery from Catalyzed Bioerodible Polymer Matrices. *AIChE Journal*, 31(5):759–766, 1985.

[78] F. Mollica, M. Biondi, S. Muzzi, F. Ungaro, F. Quaglia, M. I. La Rotonda, and P. A. Netti. Mathematical Modelling of the Evolution of Protein Distribution within Single PLGA Microspheres: Prediction of Local Concentration Profiles and Release Kinetics. *Journal of Materials Science: Materials in Medicine*, 19(4):1587–1593, 2008.

[79] S. N. Rothstein, W. J. Federspiel, and S. R. Little. A Simple Model Framework for the Prediction of Controlled Release from Bulk Eroding Polymer Matrices. *Journal of Materials Chemistry*, 18(16):1873–1880, 2008.

[80] Y. Wang, J. Pan, X. Han, C. Sinka, and L. Ding. A Phenomenological Model for the Degradation of Biodegradable Polymers. *Biomaterials*, 29(23):3393–3401, 2008.

[81] H. Antheunis, J. C. van der Meer, M. de Geus, W. Kingma, and C. E. Koning. Improved Mathematical Model for the Hydrolytic Degradation of Aliphatic Polyesters. *Macromolecules*, 42(7):2462–2471, 2009.

[82] M. Zilberman and A. Malka. Drug Controlled Release from Structured Bioresorbable Films Used in Medical Devices–A Mathematical Model. *Journal of Biomedical Materials Research Part B: Applied Biomaterials*, 89(1):155–164, 2009.

[83] A. G. Ding, A. Shenderova, and S. P. Schwendeman. Prediction of Microclimate pH in Poly(Lactic-co-Glycolic Acid) Films. *Journal of the American Chemical Society*, 128(16):5384–5390, 2006.

[84] M. P. Zhang, Z. C. Yang, L. L. Chow, and C. H. Wang. Simulation of Drug Release from Biodegradable Polymeric Microspheres with Bulk and Surface Erosions. *Journal of Pharmaceutical Sciences*, 92(10):2040–2056, 2003.

[85] L. Zhang, C. Long, J. Pan, and Y. Qian. A Dissolution-Diffusion Model and Quantitative Analysis of Drug Controlled Release from Biodegradable Polymer Microspheres. *The Canadian Journal of Chemical Engineering*, 84(5):558–566, 2004.

[86] M. I. Cabrera and R. J. A. Grau. A Generalized Integral Method for Solving the Design Equations of Dissolution/Diffusion-Controlled Drug Release from Planar, Cylindrical and Spherical Matrix Devices. *Journal of Membrane Science*, 293(1-2):1–14, 2007.

[87] J. Pan, Y. Zhang, and Y. Qian. Structure-Property Relationships and Models of Controlled Drug Delivery of Biodegradable Poly (D,L-Lactic Acid) Microspheres. *Chinese Journal of Chemical Engineering*, 12(6):869–876, 2004.

[88] V. Lemaire, J. Belair, and P. Hildgen. Structural Modeling of Drug Release from Biodegradable Porous Matrices Based on a Combined Diffusion/Erosion Process. *International Journal of Pharmaceutics*, 258(1-2):95–107, 2003.

[89] A. Gopferich and R. Langer. Modeling Monomer Release from Bioerodible Polymers. *Journal of Controlled Release*, 33(1):55–69, 1995.

[90] J. E. J. Staggs. Discrete Bond-Weighted Random Scission of Linear Polymers. *Polymer*, 47(3):897–906, 2006.

[91] H. Antheunis, J. C. van der Meer, M. de Geus, A. Heise, and C. E. Koning. Autocatalytic Equation Describing the Change in Molecular Weight during Hydrolytic Degradation of Aliphatic Polyesters. *Biomacromolecules*, 11(4):1118–1124, 2010.

[92] H. Nishida, M. Yamashita, M. Nagashima, N. Hattori, T. Endo, and Y. Tokiwa. Theoretical Prediction of Molecular Weight on Autocatalytic Random Hydrolysis of Aliphatic Polyesters. *Macromolecules*, 33(17):6595–6601, 2000.

[93] G. L. Siparsky, K. J. Voorhees, and F. D. Miao. Hydrolysis of Polylactic Acid (PLA) and Polycaprolactone (PCL) in Aqueous Acetonitrile Solutions: Autocatalysis. *Journal of Environmental Polymer Degradation*, 6(1):31–41, 1998.

[94] S. Lyu, R. Sparer, and D. Untereker. Analytical Solutions to Mathematical Models of the Surface and Bulk Erosion of Solid Polymers. *Journal of Polymer Science Part B: Polymer Physics*, 43(4):383–397, 2005.

[95] S. Lyu and D. Untereker. Degradability of Polymers for Implantable Biomedical Devices. *International Journal of Molecular Sciences*, 10(9):4033–4065, 2009.

[96] P. Sansdrap and A. J. Moes. *In Vitro* Evaluation of the Hydrolytic Degradation of Dispersed and Aggregated Poly(DL-Lactide-co-Glycolide) Microspheres. *Journal of Controlled Release*, 43(1):47–58, 1997.

[97] R. M. Ziff and E. D. McGrady. The Kinetics of Cluster Fragmentation and Depolymerization. *Journal of Physics A: Mathematical and General*, 18(15):3027–3037, 1985.

[98] W. M. Deen. *Analysis of Transport Phenomena*. Oxford University Press, New York, 1998.

[99] C. V. Pao. *Nonlinear Parabolic and Elliptic Equations*. Plenum Press, New York, 1992.

[100] J. Crank. *The Mathematics of Diffusion*. Clarendon Press, Oxford, 1st edition, 1956.

[101] J. R. Wiley, C. E. Wicks, R. E. Wilson, and G. L. Rorrer. *Fundamentals of Momentum, Heat, and Mass Transfer*. John Wiley & Sons, New York, 4th edition, 2001.

[102] J. S. Yoon, I. J. Chin, M. N. Kim, and C. Kim. Degradation of Microbial Polyesters: A Theoretical Prediction of Molecular Weight and Polydispersity. *Macromolecules*, 29(9):3303–3307, 1996.

[103] C. G. Pitt, F. I. Chasalow, Y. M. Hibionada, D. M. Klimas, and A. Schindler. Aliphatic Polyesters I. The Degradation of Poly(ϵ-Caprolactone) *In Vivo*. *Journal of Applied Polymer Science*, 26(11):3779–3787, 1981.

[104] S. P. Lyu, J. Schley, B. Loy, D. Lind, C. Hobot, R. Sparer, and D. Untereker. Kinetics and Time-Temperature Equivalence of Polymer Degradation. *Biomacromolecules*, 8(7):2301–2310, 2007.

[105] S. Fredenberg, M. Reslow, and A. Axelsson. Measurement of Protein Diffusion Through Poly(D,L-Lactide-co-Glycolide). *Pharmaceutical Development and Technology*, 10(2):299–307, 2005.

[106] L. K. Chiu, W. J. Chiu, and Y. L. Cheng. Effects of Polymer Degradation on Drug Release—A Mechanistic Study of Morphology and Transport Properties in 50:50 Poly(D,L-Lactide-co-Glycolide). *International Journal of Pharmaceutics*, 126(1-2):169–178, 1995.

[107] B. Ertl, P. Platzer, M. Wirth, and F. Gabor. Poly(D,L-Lactic-co-Glycolic Acid) Microspheres for Sustained Delivery and Stabilization of Camptothecin. *Journal of Controlled Release*, 61(3):305–317, 1999.

[108] H. K. Kim and T. G. Park. Comparative Study on Sustained Release of Human Growth Hormone from Semi-Crystalline Poly(L-Lactic Acid) and Amorphous Poly(D,L-Lactic-co-Glycolic Acid) Microspheres: Morphological Effect on Protein Release. *Journal of Controlled Release*, 98(1):115–125, 2004.

[109] G. A. Truskey, F. Yuan, and D. F. Katz. *Transport Phenomena in Biological Systems*. Prentice Hall, Upper Saddle River, New Jersey, 2004.

[110] J. C. Kang and S. P. Schwendeman. Pore Closing and Opening in Biodegradable Polymers and Their Effect on the Controlled Release of Proteins. *Molecular Pharmaceutics*, 4(1):104–118, 2007.

[111] S. R. Mao, J. Xu, C. F. Cai, O. Germershaus, A. Schaper, and T. Kissel. Effect of WOW Process Parameters on Morphology and Burst Release of FITC-Dextran Loaded PLGA Microspheres. *International Journal of Pharmaceutics*, 334(1-2):137–148, 2007.

[112] S. Fredenberg, M. Wahlgren, M. Reslow, and A. Axelsson. Pore Formation and Pore Closure in Poly(D,L-Lactide-co-Glycolide) Films. *Journal of Controlled Release*, 150(2):142–149, 2011.

[113] H. S. Fogler. *Elements of Chemical Reaction Engineering*. Prentice Hall, Upper Saddle River, New Jersey, 3rd edition, 1999.

[114] E. E. Petersen. Diffusion in a Pore of Varying Cross Section. *AIChE Journal*, 4(3):343–345, 1958.

[115] R. Aris. *The Mathematical Theory of Diffusion and Reaction in Permeable Catalysts*, volume 1. Clarendon Press, New York, 1975.

[116] C. N. Satterfield. *Mass Transfer in Heterogeneous Catalysis*. MIT Press, Cambridge, Massachusetts, 1970.

[117] C. N. Satterfield, C. K. Colton, , and W. H. Pitcher Jr. Restricted Diffusion in Liquids within Fine Pores. *AIChE Journal*, 19(3):628–635, 1973.

[118] J. Siepmann and N. A. Peppas. Higuchi Equation: Derivation, Applications, Use and Misuse. *International Journal of Pharmaceutics*, 418(1):6–12, 2011.

[119] E. L. Cussler. *Diffusion: Mass Transfer in Fluid Systems*. Cambridge University Press, Cambridge, 2nd edition, 1997.

[120] C. L. Yaw. *Yaws' Handbook of Thermodynamic and Physical Properties of Chemical Compounds*. Knovel, 2003.

[121] W. J. Albery, A. R. Greenwood, and R. F. Kibble. Diffusion Coefficients of Carboxylic Acids. *Transactions of the Faraday Society*, 63(530P):360–368, 1967.

[122] P. E. Liley, R. C. Reid, and E. Buck. Physical and Chemical Data. In R. H. Perry, D. W. Green, and J. O. Maloney, editors, *Perry's Chemical Engineers' Handbook*, pages 3.1–3.291. McGraw Hill, New York, 6th edition, 1973.

[123] C. Tanford. *Physical Chemistry of Macromolecules*. John Wiley & Sons, New York, 1961.

[124] M. H. Smith. Molecular Weights of Proteins and Some Other Materials Including Sedimentation, Diffusion and Frictional Coefficients and Partial Specific Volumes. In H. A. Sorber, editor, *Handbook of Biochemistry: Selected Data for Molecular Biology*, pages C3–C35. CRC, Cleveland, Ohio, 2nd edition, 1970.

[125] J. Benitez. *Principles and Modern Applications of Mass Transfer Operations*. John Wiley & Sons, Hoboken, New Jersey, 2nd edition, 2009.

[126] W. M. Deen. Hindered Transport of Large Molecules in Liquid-Filled Pores. *AIChE Journal*, 33(9):1409–1425, 1987.

[127] P. Dechadilok and W. M. Deen. Hindrance Factors for Diffusion and Convection in Pores. *Industrial and Engineering Chemistry Research*, 45(21):6953–6959, 2006.

[128] E. M. Renkin. Filtration, Diffusion, and Molecular Sieving through Porous Cellulose Membranes. *Journal of General Physiology*, 38(2):225–243, 1954.

[129] B. D. Prasher and Y. H. Ma. Liquid Diffusion in Microporous Alumina Pellets. *AIChE Journal*, 23(3):303–311, 1977.

[130] S. Nakao. Determination of Pore Size and Pore Size Distribution: 3. Filtration Membranes. *Journal of Membrane Science*, 96(1-2):131–165, 1994.

[131] H. Faxen. The Motion of a Rigid Sphere Along the Axis of One Pipe Filled with Viscous Fluid (in German). *Arkiv for Matematik, Astronomi och Fysik*, 17(27):1–28, 1923.

[132] L. R. Bacon. Measurement of Absolute Viscosity by the Falling Sphere Method. *Journal of the Franklin Institute*, 221(1322-18):251–273, 1936.

[133] P. M. Bungay and H. Brenner. The Motion of a Closely-Fitting Sphere in a Fluid-Filled Tube. *International Journal of Multiphase Flow*, 1(1):25–56, 1973.

[134] G. M. Mavrovouniotis and H. Brenner. Hindered Sedimentation, Diffusion, and Dispersion Coefficients for Brownian Spheres in Circular Cylindrical Pores. *Journal of Colloid Interface Science*, 124(1):269–283, 1988.

[135] J. J. L. Higdon and G. P. Muldowney. Resistance Functions for Spherical Particles, Droplets, and Bubbles in Cylindrical Tubes. *Journal of Fluid Mechanics*, 298:193–210, 1995.

[136] W. F. Ames. *Numerical Methods for Partial Differential Equations* . Academic Press, New York, 3rd edition, 1992.

[137] D. R. Durran. *Numerical Methods for Wave Equations in Geophysical Fluid Dynamics*. Springer-Verlag, New York, 1999.

[138] R. J. LeVeque. *Finite Difference Methods for Ordinary and Partial Differential Equations: Steady-State and Time-Dependent Problems*. SIAM, Philadelphia, 2007.

[139] J. Peiro and S. Sherwin. Finite Difference, Finite Element, and Finite Volume Methods for Partial Differential Equations. In S. Yip, editor, *Handbook of Materials Modeling: Part A. Methods*, pages 2415–2446. Springer, New York, 2005.

[140] K. W. Morton and D. F. Mayers. *Numerical Solution of Partial Differential Equations*. Cambridge University Press, New York, 2nd edition, 2005.

[141] H. J. Lee and W. E. Schiesser. *Ordinary and Partial Differential Equation Routines in C, C++, Fortran, Java, Maple, and MATLAB*. Chapman and Hall, New York, 2004.

[142] E. Hairer and G. Wanner. *Solving Ordinary Differential Equations II: Stiff and Differential-Algebraic Problems*. Springer, New York, 2nd edition, 1996.

[143] P. Deuflhard and F. Bornemann. *Scientific Computing with Ordinary Differential Equations*. Springer, New York, 2002.

[144] H. S. Carslaw and J. C. Jaeger. *Conduction of Heat in Solids*. Oxford University Press, New York, 2nd edition, 1986.

[145] P. J. Roache. *Verification and Validation in Computational Science and Engineering*. Hermosa Publishers, Albuquerque, New Mexico, 1998.

[146] F. M. Hemez and J. R. Kamm. A Brief Overview of the State-of-the-Practice and Current Challenges in Solution Verification. In F. Graziani, editor, *Computational Methods in Transport: Verification and Validation*, pages 229–250. Springer, New York, 2008.

[147] R. Haberman. *Applied Partial Differential Equations: with Fourier Series and Boundary Value Problems*. Prentice Hall, Upper Saddle River, New Jersey, 4th edition, 2004.

[148] G. Schliecker, C. Schmidt, S. Fuchs, and T. Kissel. Characterization of a Homologous Series of D,L-Lactic Acid Oligomers: A Mechanistic Study on the Degradation Kinetics *In Vitro*. *Biomaterials*, 24(21):3835–3844, 2003.

[149] K. D. Stovall. *Investigation of Properties Affecting Controlled Release of Macromolecules from PLGA Microspheres*. Ph.D. Dissertation, University of Illinois at Urbana-Champaign, Urbana, IL, 2009.